ANL-79-29

ANL-79-29

CHEMICAL ENGINEERING DIVISION

FUEL CYCLE PROGRAMS QUARTERLY PROGRESS REPORT

October—December 1978

by

M. J. Steindler, Milton Ader, R. E. Barletta, J. K. Bates, C. H. Bean, R. A. Couture, E. D. Creamer, K. F. Flynn, T. J. Gerding, L. J. Jardine, D. K. Kroeck, Michael Krumpelt, B. J. Kullen, O. C. Linhart, W. J. Mecham, K. M. Myles, R. H. Pelto, B. B. Saunders, W. B. Seefeldt, M. G. Seitz, L. E. Trevorrow, Seymour Vogler, and Jacqueline Williams

ARGONNE NATIONAL LABORATORY, ARGONNE, ILLINOIS

Prepared for the U. S. DEPARTMENT OF ENERGY under Contract W-31-109-Eng-38

DISCLAIMER

The facilities of Argonne National Laboratory are owned by the United States Government. Under the terms of a contract (W-31-109-Eng-38) among the U. S. Department of Energy, Argonne Universities Association and The University of Chicago, the University employs the staff and operates the Laboratory in accordance with policies and programs formulated, approved and reviewed by the Association.

MEMBERS OF ARGONNE UNIVERSITIES ASSOCIATION

The University of Arizona
Carnegie-Mellon University
Case Western Reserve University
The University of Chicago
University of Cincinnati
Illinois Institute of Technology
University of Illinois
Indiana University
The University of Iowa
Iowa State University
The University of Kansas
Kansas State University
Loyola University of Chicago
Marquette University
The University of Michigan
Michigan State University
University of Minnesota
University of Missouri
Northwestern University
University of Notre Dame
The Ohio State University
Ohio University
The Pennsylvania State University
Purdue University
Saint Louis University
Southern Illinois University
The University of Texas at Austin
Washington University
Wayne State University
The University of Wisconsin-Madison

Printed in the United States of America
Available from
National Technical Information Service
U. S. Department of Commerce
5285 Port Royal Road
Springfield, VA 22161

NTIS price codes
Printed copy: A10
Microfiche copy: A01

Distribution Categories:
Nuclear Waste Management (UC-70)

ANL-79-29

ARGONNE NATIONAL LABORATORY
9700 South Cass Avenue
Argonne, Illinois 60439

Chemical Engineering Division

FUEL CYCLE PROGRAMS QUARTERLY PROGRESS REPORT October-December 1978

by

M. J. Steindler, Milton Ader, R. E. Barletta, J. K. Bates, C. H. Bean, R. A. Couture, E. D. Creamer, K. F. Flynn, T. J. Gerding, L. J. Jardine, D. K. Kroeck, Michael Krumpelt, B. J. Kullen, O. C. Linhart, W. J. Mecham, K. M. Myles, R. H. Pelto, B. B. Saunders, W. B. Seefeldt, M. G. Seitz, L. E. Trevorrow, Seymour Vogler, and Jacqueline Williams

January 1980

Previous reports in this series

ANL-78-37
ANL-78-68
ANL-78-76
ANL-79-6

THIS PAGE

WAS INTENTIONALLY

LEFT BLANK

TABLE OF CONTENTS

TABLE OF CONTENTS (contd)

LIST OF FIGURES

LIST OF FIGURES (contd)

LIST OF FIGURES (contd)

LIST OF TABLES

LIST OF TABLES (contd)

LIST OF TABLES (contd)

CHEMICAL ENGINEERING DIVISION

FUEL CYCLE PROGRAMS QUARTERLY PROGRESS REPORT

October-December 1978

by

M. J. Steindler, Milton Ader, R. E. Barletta, J. K. Bates, C. H. Bean, R. A. Couture, E. D. Creamer, K. F. Flynn, T. J. Gerding, L. J. Jardine, D. K. Kroeck, Michael Krumpelt, B. J. Kullen, O. C. Linhart, W. J. Mecham, K. M. Myles, R. H. Pelto, B. B. Saunders, W. B. Seefeldt, M. G. Seitz, L. E. Trevorrow, Seymour Vogler, and Jacqueline Williams

ABSTRACT

In the program on pyrochemical and dry processing methods (PDPM) for nuclear fuel, tungsten crucibles have been successfully spun (by Schwarzkopf Development Corporation) for use in laboratory-scale experiments and in addition, two tungsten crucibles (12.7-cm ID, 27.9 cm long, 0.51-cm wall) were spun at Rocky Flats. Corrosion testing of refractory metals and alloys in PDPM environments was done, and ceramic substrates were successfully coated with tungsten. Laboratory equipment to test the feasibility of dissolving actinide monocarbide in molten chlorides has been set up and tested in a shakedown run. Solubility measurements have been made to determine Cd/Mg alloy composition and temperature at which dissolved thorium will precipitate. Experiments have been started to study the reduction of high-fired ThO_2 with calcium in a molten metal-molten salt system. Work on the fused salt electrolysis of CaO has started. A description of the coprocessing of uranium and plutonium by a salt transport process has been prepared. Equipment for determining phase diagrams for the uranium-copper-magnesium system has been set up. The reaction of uranium dioxide with molten equimolar sodium nitrate-potassium nitrate was studied as part of a project to identify chemically feasible nonaqueous fuel reprocessing methods. Work was continued on the development of a flowsheet for reprocessing actinide oxides by extracting the actinides into ammonium chloroaluminate (and alternative salts) from a bismuth solution; preparation of thorium, uranium, and plutonium nitrides after dissolution of spent fuel elements in molten tin is being studied; and in a project to provide engineering support for the PDPM program, several engineering aspects of the zinc distillation process were studied.

In work on the encapsulation of radioactive waste in metal, leach rates of glass beads, pulverized beads, and beads encapsulated in a lead matrix with no protective envelope have been studied. Also, a method (employing no pressure or vacuum systems) of encapsulating various solid wastes in a lead metal matrix has been developed and tested. A preliminary integration has been made of earlier data on the effects of impacts on metal-matrix waste forms.

In work on the transport properties of nuclear waste in geologic media, leach migration experiments were compared with conventional infiltration experiments as methods of evaluating geologic formations as barriers to nuclide migration. The effect of the streaming potential on the rates of transport of radioactive I^- and Na^+ through kaolinite columns was measured, as well as adsorption of iodide and iodate by several compounds; implications of the results upon the disposal of radioactive iodine were discussed.

SUMMARY

Pyrochemical and Dry Processing Methods Program

Materials Development for PDPM. A report of an investigation of potential materials problems for various candidate PDPM processes has been prepared by R. J. Teitel Associates. Conclusions, recommendations, and suggested candidates are presented.

The PDPM Environmental Test Facility has been successfully operated for 100 continuous hours at 800°C. However, bearing problems have prevented consistently good tests. Work is under way to correct these problems and to ensure reliability of further experiments.

Six tungsten crucibles were successfully spun by Metallwerk Plansee for use in laboratory-scale experiments. The sales agent, Schwarzkopf Development, appears to be a reliable source for moderate-sized hardware.

Corrosion tests were performed on a series of refractory metals and alloys in a molten zinc-salt system. All alloys tested showed reasonably low corrosion rates.

Work on the application of a tungsten coating on 9 $Al_2O_3 \cdot 3\%\ Y_2O_3$ ceramic substrates has been very successful. Despite problems of occasional entrainment of ceramic material in the tungsten coating, the coating is consistently dense and the metallic phase is continuous, appearing to provide an impervious barrier to potential corrosive agents.

Molten Bismuth Reprocessing. Laboratory experiments have been delayed due to continuing laboratory renovations. The fabrication of an apparatus for testing the three phase separation required by the bismuth flowsheet has been completed.

The first three chapters of a report on the structure and reactivity of carbides have been issued as a series of memos. A search of the literature pertinent to carbide reprocessing has been completed. This review will also be included in the carbide report. Work on the remaining chapters of the report is continuing.

Dissolution of spent carbide fuels in molten chloride salts is being considered as a head-end step for introducing such fuels into various pyroprocesses. Equipment to investigate this concept has been constructed, installed, and tested in a shakedown run. Flowsheet experiments will be undertaken next.

Uranium-Plutonium Salt Transport Processing. In the reprocessing of LWR and FBR by the salt transport process, it has been decided to focus on coprocessing of uranium and plutonium.

Preliminary design criteria and a proliferation analysis of the Pyro-Civex Process for coprocessing spent FBR fuel were provided to ORNL as requested by ANL. Specific operational design criteria, flowsheets with sequence of operation, conceptual equipment design, and material balances for the salt transport option were also included.

The computer model of the salt transport process is now operating and has provided much data for mass balances. The program is being expanded and will be rewritten in FORTRAN IV for use with other computers.

Equipment for the uranium-copper-magnesium ternary studies at the Colorado School of Mines has been obtained and set up. Experimentation will begin early in the second quarter of FY 1979.

Fabrication of Process-Size Refractory Metal Vessels. The topical report summarizing the literature search on tungsten fabrication is complete and is being reviewed before distribution. Two tungsten crucibles, 12.7-cm ID, 27.9-cm long, and 0.51-cm wall (5" by 11" by 1/5"), have been successfully spun. In addition, tungsten sheet was bent by a three-roll bender into a 5-in.-diameter by 10 1/4 in.-high cylinder which was brazed to a drawn tungsten bottom cup to form a crucible.

Molten Nitrate Salt Oxidation Processes. Studies of the reaction of uranium dioxide with equimolar sodium nitrate-potassium nitrate were continued. The sodium to uranium atomic ratio of the product is one. The X-ray powder diffraction patterns indicate only the presence of sodium diuranate, $Na_2U_2O_7$ in the solid. These and other results indicate that carbonate ion has no effect on the reaction.

A glove box has been modified for plutonium chemistry studies.

Molten Salt Processes Applied to Ceramic Fuels. Ammonium chlorogallate, ammonium chloroferrate, zinc chloride, and lead chloride all appear to be acceptable substitutes for ammonium chloroaluminate in the extraction of uranium and thorium from bismuth, if the need of a substitute for the latter salt should develop sometime in the future. Ammonium chloroaluminate still appears to be the best salt for the recovery of the actinides from bismuth, however.

For a head-end step to process ceramic fuels in molten salt, the initial rate of chlorination and dissolution of thorium oxide microspheres in the $LiAlCl_4/AlCl_3$ eutectic at 220°C was shown to fit the equation, $d[Th]/dt = const[Th]^{0.27}$, under the conditions employed. This equation implies that the dissolution is self-catalyzing at the temperature and acidity of lithium chloroaluminate used.

Molten Tin Processes. Analysis of the literature data indicates that fission products dissolved in tin at 1900 K have a volatility higher by about 2 to 3 orders of magnitude than earlier estimates. Consequently, the flowsheet for the molten tin process has been revised to reflect this and to provide for the removal of essentially all of the As, Cs, Rb, Cd, Se, and Te and a substantial portion of the Sb, Sr, Ba, Eu, and Sm by distillation from the tin solvent.

Laboratory experimentation has established that cobalt is an effective catalyst in accelerating the carbothermic reduction of UO_2 to form a solution of uranium in molten tin. The reaction requires about 2 h at 1900 K. Iron and nickel may also be effective catalysts for this reaction.

Calcium has been found to be an effective additive for catalyzing the nitriding of uranium for uranium dissolved in molten tin. At 1900 K, the catalyst reduces the reaction time from 2.6 h to 1.3 h.

Engineering Support for the PDPM Program. A study of the zinc distillation process indicated that the amount of unrecoverable uranium collecting on the side walls of the zinc still pot is best controlled either by preventing the formation of zinc vapor bubbles in the melt or by redissolving the uranium in a zinc wash.

Data from various mass transfer unit operations were examined, and correlations were sought using dimensionless numbers such as the Sherwood number and the Reynolds number.

Encapsulation of Radioactive Waste in Metal

Leach testing of various waste forms using a variety of leaching media are continuing. Neutron activation analysis techniques based on the radioisotopes ^{124}Sb and ^{134}Cs have been used to study the leaching characteristics of Pyrex (borosilicate) glass. Comparative measurements of the leach rate using three different physical forms of the glass have been made. These forms were: intact beads (4-mm), pulverized beads, and beads encapsulated in a lead matrix with no protective envelope. These studies indicated that pulverizing the glass beads for the purpose of using Soxhlet extraction techniques significantly affects the leaching characteristics of this waste form. It was also observed that incorporation of the Pyrex beads into a very small-scale metal matrix with no protective envelope had little if any effect on reducing the apparent surface area exposed to the leaching medium. However, this effect is believed due to the particular laboratory-scale fabrication technique used and will be examined further.

A general method of encapsulating various solid wastes in a lead metal matrix which does not require pressure and/or vacuum systems has been developed and tested by producing 3 1/8-in.-OD by 24-in.-long castings. Pyrex glass beads and Al_2O_3 pellets were used as simulated waste forms. This encapsulation method is proposed to be a versatile packaging method for various waste types (i.e., HLW, TRU, fractionated cesium and strontium, etc.) since the method can improve the dispersibility attributes of the unencapsulated waste forms.

Evaluations have been made of information from impact studies of waste forms. This information was summarized in the literature review presented in the preceding quarterly report. Although the literature disclosed no comprehensive theory capable of yielding quantitative results of a practical kind nor any empirical data on composite bodies of the type of greatest concern in this study, various methodologies, quantitative theories, and empirical test data were relevant and mutually confirmatory as a basis of a systematic analysis of the effects of impacts of metal-matrix waste forms. A preliminary integration of this reference material has been the chief accomplishment of this quarter.

For materials and conditions of specific interest to the present study, impact deformations of both ductile and brittle materials show dependence on energy but do not show strain-rate sensitivity. Therefore, empirical measurements can probably be made with small-scale models and these results generalized to any size of waste package or to any impact velocity within the range of practical interest. Critical review of experimental data and of solid-state structures of materials also lends support to these preliminary findings.

The chief quantitative determinations of impact consequences are (1) the energy input and (2) the threshold stresses for inelastic deformation of the component materials. A body of mass, M (kg), falling a distance H (m) with a normal gravitational acceleration, g (9.8 m/s^2), will attain a velocity, u (m/s), just before ground impact, and the energy 1/2 Mu^2 (J) will be available to cause deformation, which is measured quantitatively as a displacement volume ΔV (m^3) for plastic deformation, and as generation of surface area ΔS (m^2) of the fragments formed in brittle fracture. The impact deformation of a composite body of brittle and ductile material can be summarized by the energy equation

$$gMH = 1/2\ Mu^2$$

$$= \sigma_D \Delta V + K_F \Delta S,$$

where σ_D is the dynamic flow stress (Pa) of the ductile material and K_F is the energy coefficient per unit surface energy (J/m^2) in brittle fracture. In general, σ_D and K_F must be determined empirically for a given material and impact configuration. For the purposes of the present study, calculational models of idealized cylindrical bodies were used to estimate values of σ_D and K_F in terms of the elastic properties usually known or measurable.

The minimum value of the threshold compressive stress associated with K_F was similarly estimated. In addition to the total surface area of fragmentation, the particle size distribution is important for characterizing brittle fracture; application of the lognormal probability function was made to relate (1) the two parameters of this distribution function to (2) the ratio of total particle surface area to total particle mass. In adjusting the two parameters of the lognormal distribution, namely, the geometric mean diameter, D_g, and the geometric mean standard deviation, σ_g, to empirical size distributions, it was found that σ_g does not change much for impacts of various energies; therefore, surface areas can be predicted from mean particle size determinations, and vice versa, to a degree of approximation depending on impact conditions and materials.

Transport Properties of Nuclear Waste in Geologic Media

A geologic formation might retard radionuclides transported by flowing water if a future nuclear-waste repository should be breached. To evaluate geologic formations as barriers to nuclide migration, we have conducted leach-migration experiments, which treat leaching and migration phenomena collectively. The results of these experiments and of more conventional infiltration experiments indicate that the migration of cesium in oolitic limestone depends on the method of applying the cesium to the rock column; this raises questions about experimental methodology.

Other work was done to determine whether cesium was associated with finely divided residues of leached glass or other colloidal material. In filtration and dialysis studies, no cesium was observed in colloids or particulates larger than 0.0014 μm. Whatever the mechanism responsible for the observed migration behavior of cesium, the leach-migration experiments are thought to simulate migration of radionuclides from a breached waste repository more closely than conventional infiltration methods and may be preferable for evaluating the safety of a waste repository.

Trace-Element Transport in Lithic Material by Fluid at High Temperature

During late 1978, two separate subjects were investigated. First, in order to determine the effect of the streaming potential on the migration rates of ions through kaolinite columns, the rates of transport of radioactive I^- and Na^+ relative to that of tritiated water were measured. Second, adsorption of iodide and iodate by several compounds was studied; some implications of the results for disposal of radioactive iodine are discussed. This work may have practical value in relation to the disposal of iodine-129 from irradiated nuclear fuel.

The rates of transport of trace quantities of radioactive I^-, Na^+, and tritiated water in 0.1M $NaHCO_3$ solution through packed columns of kaolinite [$Al_2Si_2O_5(OH)_4$] were determined in successive experiments. Iodide was eluted at about 115% the rate of water, in qualitative agreement with theory. Na^+ moved about 30% faster than expected from the ion-exchange capacity of the clay. Thus, the measurement of the ion-exchange capacity may be in error. From these two measured rates of transport, the effect of the streaming potential on Cs-Na selectivity coefficients is determined to be fairly small at an ionic strength of 0.1.

In the part of our work on removal of iodine species from aqueous solutions, it was observed that iodate, at low concentrations, is strongly adsorbed by submicron hematite (Fe_2O_3) particles in a $NaHCO_3$ solution of about 0.001M. The reagent grade hematite used has an anion exchange capacity slightly in excess of 10 μmol/g. Little iodide was adsorbed on hematite, $Fe(OH)_3$, Al_2O_3, $Al(OH)_3$, or kaolinite. Of these adsorbents, only Fe_2O_3 and $Fe(OH)_3$ adsorb iodate.

Sorption of iodate by one or more iron oxides appears to be a practical method of retaining radioactive iodine-129 in the vicinity of a leaking waste repository. A practical existing method for disposal involves encapsulating slightly soluble $Ba(IO_3)_2$ in Portland cement, but this waste form has a finite leach rate. Iron oxide emplaced around the concrete could adsorb a large fraction of the iodine. It is estimated that 200 Mg of Fe_2O_3 could adsorb as much as 98% of 2000 moles of iodate--the amount in 1500 tons of nuclear fuel. Iron oxides present in some geologic formations may also form a usable barrier.

Disposal of iodate on land requires an oxidizing or dry environment with low dissolved-sulfate concentrations. Deep-sea disposal may be feasible.

An alternative strategy for disposal of iodate might be coprecipitation of iodate with $Fe(OH)_3$ or with a calcium or barium salt. This might produce a waste form that is less leachable than $Ba(IO_3)_2$.

I. PYROCHEMICAL AND DRY PROCESSING METHODS PROGRAM
(C. H. Bean, K. M. Myles, and M. J. Steindler)

A. Introduction

A Pyrochemical and Dry Processing Methods (PDPM) Program was established at the beginning of FY 1978 within the Chemical Engineering Division, Fuel Cycle Section at Argonne National Laboratory (ANL). Upon redirection of the Fuel Cycle Development Program by DOE for FY 1979, the technical lead for all fuel reprocessing was established at Oak Ridge Operations/Oak Ridge National Laboratory (ORO/ORNL). The PDPM work plan prepared by ANL for FY 1979 is coordinated by the Chicago Operations Office with ORO/ORNL. Under this plan, ANL continues technical direction of the PDPM Program. The PDPM Program is an expansion of the National Fuel Cycle Program for reprocessing fuel by processes that will reduce the risk of proliferation of nuclear weapons. Work on this program is being performed at ANL, at other DOE laboratories, and by industrial contractors.

The program for FY 1979 has been administratively divided into individual work packages, five of which are being done at ANL. Purchase orders have been placed for six work packages and subcontracts have been placed for three additional work packages. A list of work packages is included in Table 1. The purchase order for Work Package 11 and the subcontract for Work Package 06 are for effort needed to terminate work supported in FY 1978 and to complete the required documentation and reporting of processes investigated in FY 1978.

Each work package is being managed for conformance to established statements of work, program objectives, a cost plan, a milestone plan, and a management plan in accordance with the Uniform Contractor Reporting System, DOE/CR-0001/1 dated February, 1978, as required by DOE.

B. Management
(C. H. Bean, K. M. Myles, and Seymour Vogler)

1. Evaluation of PDPM Processing

The ANL PDPM Program management is providing assistance to Oak Ridge National Laboratory (ORNL) in conducting a study to analyze the potential for PDPM reprocessing meeting the requirements for an "exportable technology" *vis a vis* comparable aqueous methods. Meetings were held at ANL on October 9 and 17, 1978, with Rockwell International, Rocky Flats, consultants to the study, and at ORNL on October 18 and 19, 1978, with Rocky Flats, General Electric Company, San Jose (GE), and Bechtel consultants to the study.

At the ANL meetings, the details of the conceptual design and proliferation analysis for a reference proliferation-resistant pyrochemical process were determined. The reference flowsheet included unit operations for decladding, oxide reduction, FP-3 decontamination, alternative zinc distillation and salt-transport enrichment, and product conversion and refabrication. Data on mass balances, operating parameters, and process streams were identified.

At the meeting at ORNL on October 18 and 19, ANL and Rocky Flats (RF) submitted information to ORNL, GE, and Bechtel that would be used in the Exportable Pyro Reprocessing Study. This included an overview of the Pyro-Civex type evaluation by ANL; descriptions of proliferation-resistant

Table 1. PDPM Work Packages

Work Package	ANL Activity	Work Package Title	Location
00	00	Management Planning, Reporting, Costing, and QA	ANL
01	AO	Materials Development for PDPM	ANL
02	BO	Carbide Fuel Processing	ANL
03	CO	Thorium-Uranium Salt-Transport Processing	ANL
04	DO	Uranium-Plutonium Salt-Transport Processing	RI-RF[a]
05	EO	Fabrication of Process-Size Refractory Metal Vessels	RI-RF
06	FO	Aluminum-Alloy Processing of Thorium- and Uranium-Based Fuels	IRT[b]
07	GO	Chloride Volatility Processing of Thorium-Based Fuels	B&W[c]
08	HO	Material Characterization and Process Analysis	RI-AI[d]
09	JO	Molten Nitrate Salt Oxidation Processes	PNL[e]
10	KO	Molten Salt Processes Applied to Ceramic Fuels	ORNL[f]
11	LO	Reprocessing of Thoria-Urania Fuel in Molten Salts Containing $ThCl_4$	AMES[g]
12	MO	Molten-Tin Process for Reactor Fuels	LLL[h]
13	NO	Engineering Support for PDPM Processes	ANL

[a]Rockwell International-Rocky Flats.

[b]IRT Corporation.

[c]Babcock & Wilcox.

[d]Rockwell International-Atomics International.

[e]Pacific Northwest Laboratory.

[f]Oak Ridge National Laboratory.

[g]Ames Laboratory.

[h]Lawrence Livermore Laboratory.

flowsheets, the salt-transport process, and the zinc-distillation process; and an engineering analysis of the reference pyrochemical flowsheet. Lines of communication were established so that ANL and RF can provide input to the proliferation analysis by GE and provide technology needed by Bechtel for a conceptual design.

Additional information was sent to Bechtel and GE giving details of process chemistry, proliferation resistance of the pyrolytic zinc process, the fission products in spent fuel, and fission product distribution in fuel reprocessing steps.

Updated flowsheets, process descriptions, and mass balance data were provided, in support of the ORNL study of PDPM reprocessing. The data covered three process options. These options are (1) two core elements, including axial blanket, (2) one core element with axial blanket plus one radial blanket element, and (3) two radial blanket elements. Additional meetings were held with ORNL staff on December 13 and 14, 1978, to review the proliferation analysis for the reference Pyro-Civex zinc distillation process and to provide additional input to this analysis as requested by ORNL.

It is expected that the ORNL report will show an assessment of technology requirements and needs, key areas of concern, and identification of problem areas for pyro processes. The report will emphasize the positive side of the pyro program, particularly the nonproliferation advantages, although there may be other advantages.

2. Program Management

Meetings were held at ANL with contractor representatives from IRT, Babcock & Wilcox (B&W), and Atomic International (AI) on October 2, 5, and 20, respectively, to discuss program redirection, revised scope of work, and funding for FY 1979. The redirection of effort applies to Work Packages 06, 07, and 08 and is consistent with the specific programmatic guidance [BAUER].

The revised contract for Work Package 07 at B&W in FY 1979 was approved, and work was resumed per Revision III of Statement of Work C0030-0065, Chloride Volatility Processing of Thorium-Based Fuels. The contract for Work Package 08 at Atomics International was executed on December 22, 1978. All other contracts for PDPM work packages were completed in October and November. With the completion of these contracts, information will be supplied by the contractors that is needed to complete the PDPM Program Management Plan for FY 1979. The PDPM logic network, reference scenario, key milestones, milestone schedule, and cost plan are being revised to be consistent with the change in scope, program direction, and funding for FY 1979. These changes will be shown in the FY 1979 Management Plan, now scheduled for completion in January 1979.

The second scheduled PDPM Program technical information exchange meeting was held at ANL on November 7 and 8, 1978. Contractor and ANL personnel responsible for ten of the twelve work packages supported in FY 1978 were present to describe the status and progress of work performed since the previous meeting held in May 1978. Progress on the remaining two work

packages, which are being terminated, was not reported. Work that was reported included the status of engineering analysis, separations processes, and materials development in support of the PDPM Program. A review of the Fuel Refabrication and Development (FRAD) Program was presented by John Carrell, PNL, for the purpose of interfacing that work with the PDPM Program. The information exchange meeting provided information from which DOE representatives, contractor personnel, consultants, and program managers are able to assess program progress and to critique the program goals and objectives.

A DOE-CH quality assurance audit of the PDPM Program was performed on October 4, 1978. The procedures were described that are applied to ANL and contractor work packages for conformance to the requirements of AQR-002, Quality Assurance Program Description. No findings were reported by the audit committee.

The Nuclear Fuel Cycle Division of the American Nuclear Society is being assisted by PDPM personnel with program planning for a special session on pyrochemical reprocessing of nuclear fuel at the ANS Annual Meeting in Atlanta, Georgia, June 3 to 8, 1979. Mr. Bean attended the NFCD Program Committee Meeting in Washington on November 12, 1978. A program outline consisting of five invited papers, subjects, speakers, and authors was presented and was approved by the committee.

C. Engineering Analysis and Separations Processes

In the engineering analysis, prior work will be examined and evaluated. From these evaluations, a flowsheet will be devised for each of the reprocessing techniques. Gaps in the data (which must be filled to obtain operable flowsheets) will be filled by experimental work carried out under separations process subtasks.

1. Materials Development for PDPM

(R. M. Arons* and J. Y. N. Wang*)

The project objectives are to anticipate, identify, and scope potential materials or materials fabrication problems that may limit the practical realization of candidate processes in the PDPM Program; to devise (by analytical and experimental methods) means to resolve these problems; to assess the refabricability of the fuel after reprocessing; and to provide program support to the PDPM Program Office by coordinating materials activities and lending technical assistance within the program.

a. Engineering Analysis

(1) R. J. Teitel Associates Subcontract

The final report on the subcontract of R. J. Teitel Associates to assist ANL in the determination of materials requirements for various candidate PDPM Processes was received on November 21, 1978. This

---

*Materials Science Division, Argonne National Laboratory.

report [TEITEL] presents a discussion of the rationale used in the selection of materials for selected processes. Process containment conditions, materials selection, and recommended container studies are discussed for each of the processes being considered. Conclusions and recommendations are presented and discussed. A common bibliography, referenced to each process, is presented in the last section of the report.

Suggested candidate materials for process containment are summarized in Table 2. The rationale for these selections is outlined in the report.

Table 2. Candidate Container Materials

AIROX, RAHYD Processes

304, 310, 347 stainless steels

CARBOX

Not much information available

Molten Salts for Ceramic Fuel Process

Chlorination Step: consult Chloride Volatility (below)
Bi-Salt Extractions: consult ThO_2-UO_2 in ThF_4 Salt Process (below)
Volatilization of NH_4AlCl_4: consult Chloride Volatility (below)

ThO_2-UO_2 in ThF_4 Salt Process

Pyro-carbon coated graphite
Oxides: ThO_2, BeO, ZrO_2, Al_2O_3 all stabilized
SiO_2
Metals: W, W-Re

Chloride Volatility

Chlorination Volatilization Steps: Pyro-carbon coated graphite, tungsten alloys, nickel-aluminum (12% Al) alloys
Coatings on nickel and nickel superalloys
Pyrohydrolysis: SiO_2 or stabilized Al_2O_3

Nitrate Salt Process

Pyro-carbon coated graphite, fused SiO_2, stabilized BeO, ZrO_2, and Al_2O_3.

Molten Tin

Pyro-carbon or carbide-coated graphite

(2) Reports and Deliverables

During this quarter, we submitted the following documents:

- Management and Program Plan for Work Package 01
- Statement of Work for Work Package 01
- Quality Assurance Plan for the PDPM Materials Investigation Program

In addition, a 50-min oral presentation was prepared for the PDPM Program Technical Information Exchange Meeting held November 7 and 8, 1978, at ANL.

(3) Publications

R. M. Arons, J. T. Dusek, and J. W. Hafstrom, Development of Tungsten Coatings for the Corrosion Protection of Alumina-Based Ceramics, abstract submitted to the International Conference on Metallurgical Coatings at the Sixth International Vacuum Metallurgy conference, to be held April 23 to 27, 1979, San Diego, California (October, 1978).

R. M. Arons and J. W. Hafstrom, Ceramic Hardware for Use in the Pyrochemical Reprocessing of Nuclear Fuels, abstract submitted to the American Ceramic Society Nuclear Division, annual meeting to be held April 28 to May 2, 1979, Cincinnati, Ohio (November, 1978).

b. Experimental

(1) PDPM Environmental Test Facility (PETF)
(R. M. Arons* and D. J. Dorman*)

Two "dry runs" of a PETF test cell (shown in the preceding quarterly report) were made with dummy tantalum and stainless steel specimens in an environment of pure zinc and a eutectic salt of $CaCl_2$-KCl. Plans were to run for 100 h at 800°C under an argon atmosphere. The purpose of these tests was to indicate any deficiencies in design, construction materials, or experimental procedure.

The first experiment did indicate certain weaknesses in design. One problem encountered was gradual failure of the measuring thermocouple (TC) which was located in a thermowell immersed in the zinc bath. The insulation on the TC wires degraded and the TC shorted. This problem was rectified easily by use of an alumina insulator on the wires within the thermowell.

*Materials Science Division, Argonne National Laboratory.

The second and more serious problem was seizure of the lower graphite bearing in the pump after roughly 5 h of operation. This bearing, which was a simple thrust type bearing, consisted of a cylindrical hole in graphite in which a tantalum shaft could spin. The bearing was redesigned as a conical bearing which could allow for dimensional changes in the graphite or tantalum, and could clear any particulate matter which happens to work into the bearing seat. This modification seemed to alleviate the problem, and the second experiment ran the full 100 h. In subsequent testing [reported below in Section (2)], bearing seizure was also observed in the middle pump bearing. These seizures were evidently caused by fretting of tantalum at the graphite-tantalum bearing interface. We are currently modifying the design of this bearing and will use a polished alumina sleeve on the rotating shaft which will bear against either graphite or boron nitride (pending results of a static corrosion test of boron nitride).

It should be noted that no dissolution of any of the tantalum components or specimens was observed. The tantalum was embrittled, however, as evidenced by the brittle fracture of various components upon disassembly of the pump. Slight cracking was observed in the pump tube, indicating possible stress corrosion cracking initiated at machined holes. Although these cracks do not inhibit successful operation of the pump, we attempted to avoid them by fully annealing parts after machining to eliminate residual stresses. This procedure was found to have no beneficial effect and is being discontinued.

(2) Tungsten Crucibles

Six tungsten crucibles have been received from Schwarzkopf Development Corporation, Holliston, MA. These crucibles were spin formed by the Schwarzkopf parent company Metallwerk Plansee, Tyrol, Austria. They are approximately 10.2 cm × 20.3 cm (4 in. × 8 in.) and are of excellent quality. (A drawing showing their shape and dimensions is given in Fig. 1.) Original cost was $1322 per crucible plus a nonrecurring tooling charge of $737. This tooling is the property of ANL and is being retained in the contractor's plant for use in processing any subsequent orders.*

Service testing of the tungsten crucibles will be conducted in the ANL PETF in the coming quarter.

(3) Metallic Materials

(J. Y. N. Wang,† R. M. Arons,† D. H. Dorman,† and L. J. Marek‡)

Tungsten and molybdenum have low solubilities in molten zinc [MARTIN-1961, LAWROSKI]. Data on the Ta-Zn system have not been well established. New and old alloys (tungsten, molybdenum, and tantalum-base)

*Any PDPM subcontractor requiring tungsten or other refractory metal crucibles of the configuration shown in Fig. 1 should contact K. M. Myles or R. M. Arons at ANL for details.

†Materials Science Division, Argonne National Laboratory.

‡Accelerator Research Facilities, Argonne National Laboratory.

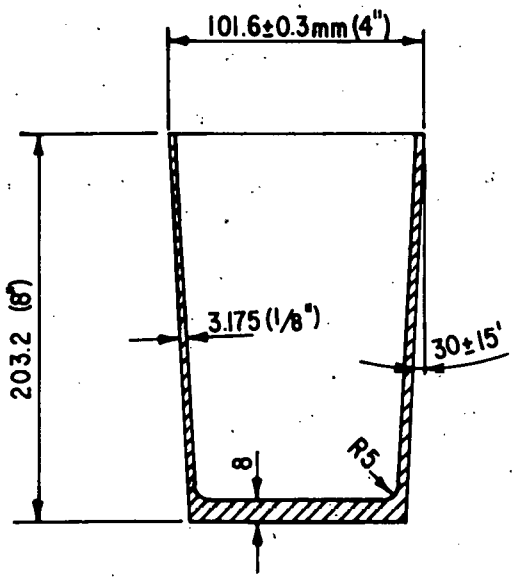

Fig. 1. Schematic of Tungsten Crucibles Supplied by Schwarzkopf Development Corp. (dimensions are in mm)

with high-temperature strength and low-temperature ductility have been developed [KLOPP, COOPER] and may be of use as containment materials, pending verification of corrosion resistance in PDPM environments.

In conjunction with the Materials Science Division corrosion test program in PETF, three refractory alloys (W-25Re, Mo-30W, and Ta-10W) and their respective pure metals were chosen for the first test run. These materials were prepared in accordance with standard corrosion test specimen preparation procedures. The weights and dimensional measurements were taken. Specimens were characterized by metallographic and chemical analyses.

Pretest microexamination indicated that all materials except molybdenum and Ta-10W showed fibered microstructure in the as-rolled condition. The molybdenum and Ta-10W had been recrystallized. Chemical analyses of alloying constituents revealed that the W-25Re contained 25.26% Re, Mo-30W contained 28.00% W, and Ta-10W contained 9.73% W. All pure metals were commercial grades with purities >99.95%.

Corrosion testing of these alloys was conducted in a molten zinc-molten $CaCl_2$-KCl mixture (50 wt % $CaCl_2$-50 wt % KCl, a eutectic composition at about 800°C under inert atmospheric conditions). The planned exposure time was 100 h of continuous operation. However, because of unexpected failure of rotation bearings of the PETF system, the test was terminated at about 61 h. Temperature for the first 16 h was about 875°C and was about 800°C for the remaining 48 h of exposure.

No change was apparent visually in the post-test specimens. Except for the molybdenum and Mo-30W specimens, which showed corrosion rates of 0.816 and 0.005 mil/y, respectively, there was no significant weight change of the specimens. The corrosion rates observed are tentative and may include an effect of the cleaning procedures. A second run for a longer period of exposure is now in preparation. Microexamination of the first run specimens is in progress.

(4) Tungsten Metallization

(R. M. Arons* and J. T. Dusek*)

Work on the application of a tungsten coating to Al_2O_3-$3Y_2O_3$ ceramic substrates has been very successful. In the current investigation, small crucibles (6.5-cm height by 5.6-cm OD) of alumina-3 wt % yttria were prepared by slip casting from a slurry of mixed 20- and 0.3-μm alumina powders, yttria powder, a distilled water vehicle, an ammonium alginate suspending agent, and ammonium hydroxide for pH adjustment. These were then brush-coated in the green state with a slurry of mixed 5.0- and 1.45-μm tungsten powder, distilled water, ammonium alginate, and ammonium hydroxide. The alumina and tungsten particle sizes selected are critical for matching the shrinkage of substrate and coating upon subsequent firing. The composite is then fired in vacuum or dry hydrogen at about 1780°C for 4 h. The resultant products are very dense ceramic crucibles with adherent, crack-free, about 65-μm-thick tungsten coatings. SEM micrographs show the coatings to be free of interconnected porosity and suggest that they will protect the substrate from corrosion by liquid species. These coatings show good thermal shock resistance and have survived heating rates of 85°C-min^{-1} with no substrate or coating degradation and with no spallation of the coating.

Previous investigations with alumina-yttria metallization have suggested that tungsten adherence is promoted by an yttrium-rich phase at the coating-substrate interface. Existence of such a phase in our crucibles was verified by energy-dispersive X-ray analysis.

A potential problem which still remains is volatilization of alumina and yttria at the high temperatures required to sinter tungsten. This volatilized ceramic has been occasionally observed to recondense on the exterior surface of the tungsten coating and has also been found entrained in the coating. A new firing schedule or different atmosphere is being sought that would avoid this phenomenon. However, the migrated alumina-yttria is not expected to impair the corrosion resistance of these crucibles since there is no continuous path through the continuous, albeit occasionally inhomogeneous tungsten layer.

(5) Plasma-Sprayed Tungsten

(R. M. Arons*)

Three tungsten crucibles and one tungsten tube formed by plasma spraying on graphite substrate were shipped to Rocky Flats on November 28, 1978, for infiltration and heat treating with a nickel nitrate

*Materials Science Division, Argonne National Laboratory.

sintering aid. Treated parts will be compared with an untreated control sample for density, dimensional changes, chemical composition, and corrosion resistance. The objective of this work is to evaluate the usefulness of plasma spraying followed by activated sintering as a means of fabricating tungsten.

2. Carbide Fuel Reprocessing
(Michael Krumpelt, B. B. Saunders, Milton Ader, R. E. Barletta, and D. K. Kroeck)

In this program, potential reprocessing methods for carbide fuels are studied. In principle, carbides can be burned to oxides and then reprocessed like oxide fuel. A direct reduction of the carbides into a metal solvent or an oxidation into a salt phase is more attractive for pyrochemical processes.

Two alternatives are presently considered. In the first, carbides are dissolved and partially separated in liquid bismuth. In the second, carbides are oxidized into a salt phase using zinc chloride or cadmium chloride. The salt phase would then be contacted with a liquid metal to partially separate the actinides from the fission products. This is an independent new process for carbides. The second alternative is a head-end step for salt transport processing being studied in other segments of the PDPM Program.

(a) Molten Bismuth Reprocessing
(R. E. Barletta, B. B. Saunders, and D. K. Kroeck)

The start of laboratory experiments has been delayed due to continuing laboratory renovations. The glovebox has been modified to permit repurification of the glovebox atmosphere during recirculation of the gas. Apparatus has been designed and has been fabricated for testing (on a laboratory scale) the three phase separation required by the bismuth flowsheet (presented in [STEINDLER-1978D]). The intent is to test the separation of a finely divided powder on the surface by displacing the liquid phase so that the top solid phase, along with some of the liquid phase, overflows into a secondary container. Complete phase separation of the three phases can then be accomplished by filtration. It is expected that this principle will be tested by using mercury as the liquid metal phase and powdered silicon carbide and tungsten as the upper and lower solid phases, respectively.

Work on the report concerning the structure and reactivity of the carbides is continuing. Chapter I, "Structure and Physical Properties of the Carbides," Chapter II, "The Preparation of the Carbides," and Chapter III, "Carbide Reactivity With Water and Oxygen," have been written, and Chapter IV, "Reactivity of Carbides with Metals," has been completed [BARLETTA]. A review of the literature pertinent to the reprocessing of carbide fuels has been undertaken. This review is to be included as a part of the report and will include a summary of both aqueous and nonaqueous reprocessing methods. Chapter VI on the reprocessing of carbide fuels in bismuth is partially complete.

(b) Flowsheets Utilizing Immiscible Molten Metals and Molten Salts
(Milton Ader)

Dissolution of spent carbide fuels in molten chloride salts is being considered as a head-end step for introducing such fuels into various pyroprocesses. One such concept involves oxidation of actinide and fission product carbides to salt-soluble chlorides by reaction with $CdCl_2$ dissolved in $MgCl_2$-NaCl-KCl eutectic (mp, 396°C). The salt phase, in the case of a Pu-^{238}U fuel, could then be reduced with a copper-magnesium alloy in a salt-transport operation designed to coprocess uranium, plutonium, and rare earth fission products in a diversion-resistant manner. In the case of thorium-containing fuels, the salt phase could be reduced with the requisite amount of Cd-50 wt % Mg that would partition thorium between (soluble) plutonium and (insoluble) uranium.

Laboratory equipment has been set up to test the feasibility of dissolving actinide monocarbide in molten chloride media. Experiments will be carried out in a glove box equipped with a helium recirculation-purification system so as to minimize exposure of the reactants to moisture and oxygen. The equipment and its operation are described in a safety review [ADER]. Recently, the solubility of thorium in several cadmium-rich magnesium alloys was measured under a helium atmosphere between 550 and 650°C in a shakedown test of the equipment. Overall operational behavior was satisfactory, and it is expected that flowsheet experimentation will be started during the next quarter.

3. Thorium-Uranium Salt-Transport Processing
(Michael Krumpelt, L. J. Jardine, J. K. Bates, and T. J. Gerding)

The objective of this program is to examine concepts for the selective transfer of spent fuel constitutents between molten alloys and/or molten salts and to develop process flowsheets for the thorium-based oxides and metal fuels. Initial flowsheets will be constructed based upon published data and thermodynamic evaluations. These flowsheets will be analyzed in more detail. Potential problem areas and missing data will be identified as portions of an engineering analysis subtask. Laboratory-scale experiments will be instituted as a separations processes subtask in order to generate data required to establish the feasibility of selected flowsheets.

a. Thorium Salt Transport
(J. K. Bates)

Pyrochemical processes involving salt-transport and metal precipitation steps are currently being investigated for use in projected thorium-based fuel cycles. The reference flowsheet (Fig. 2) republished here, has been designed to meet proliferation standards and is applicable to plutonium-thorium transmuter and undenatured thorium-uranium breeder fuels. The necessary criteria are that the fissile streams be coprocessed (Th:Pu/U ratio of 4:1) and be diversion-resistant as a result of the inclusion of some fission products. A description of the flowsheet, together with supporting experimental data, was presented at the PDPM contractor meeting (at ANL, November 7 and 8, 1978).

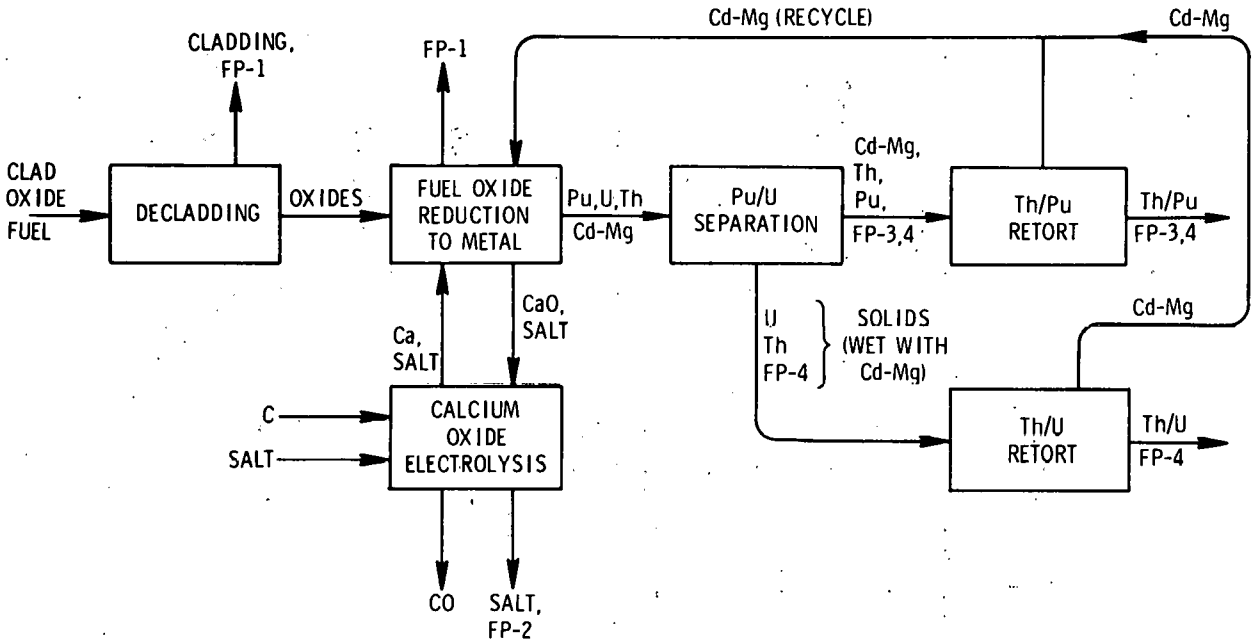

Fig. 2. Conceptual Flowsheet for Thorium-Based Fuels - ANL. FP-1: Xe, Kr, ^{3}H; FP-2: I, Br, Cs, Rb, Ba, Sr, Sm, Eu, Se, Te; FP-3: trivalent rare earths, Y; FP-4: Zn, Nb, Mo, Tc, Ru, Rh, Pd, Hg, Cd, In, Sn, Sb.

(1) Solubility of Thorium in Cadmium/Magnesium Alloys

The main process separation step requires that thorium be partitioned between (1) the plutonium, which is soluble in Cd/Mg alloys and (2) the uranium which is insoluble in Cd/Mg alloys. The solubility of thorium in Cd/Mg alloys (0 to 42 wt % Mg) has been determined at 550, 600, and 650°C by preparing saturated solutions and analyzing the filtered samples of the liquidus.

Three series of experiments were done. In the first two, thorium was added to magnesium to make a Mg-45 wt % Th alloy. According to the thorium-magnesium phase diagram [YAMAMOTO], a eutectic Mg-42 wt % Th forms having a melting point of 582°C. At 650°C, the solubility of thorium in magnesium is about 45 wt %. Thus, the initial thorium-magnesium alloy should be saturated with thorium at temperatures below 650°C. Incremental amounts of cadmium were added to the alloy, and samples of the melt were taken at 650, 600, and 550°C; in some cases, the freezing point of the melt was determined. Two experiments were done because the results from the initial run (Table 3) indicated that at 650°C the melt was not saturated with thorium.

Table 3. Liquidus Determination--Thorium/Cadmium/Magnesium System. Expt. Series 1. Initial Charge: 148.13 g Mg, 122.22 g Th (45 wt % Th)

Sample No.	Temp, °C	Composition of Melt			Equilibration, h	Quantity of Cd Added after Preced. Equilibrat., g
		Th, wt %	Mg, wt %	Cd, wt %		
1-1	650.0	33.1	64.1	3.59	18	
1-2	650.4	31.3	61.4	8.9	3	12.75
1-3	650.3	29.8	57.6	14.6	3	16.31
1-4	650.2	28.2	53.6	21.4	19	23.55
1-5	652.3	26.6	48.4	27.3	3	22.59
1-6	651.5	24.5	45.3	32.6	3	21.42
1-7	649.7	24.1	41.1	36.7	22	20.51
1-8	658.2	22.2	36.8	42.3	3	33.80
1-9	551.2	16.6	42.5	42.1	19	
1-10	649.2	19.5	36.2	46.7	4	30.66
1-11	549.0	15.3	39.8	46.5	19	
1-12	532.9	14.6	40.8	46.1	1	
1-13	649.7	19.4	31.9	50.5	3	30.47
1-14	552.0	14.6	37.0	49.7	1	
1-15	549.5	14.2	38.2	49.4	19	
1-16	529.0	13.4	38.6	49.7	1 1/2	
1-17	650.0	18.6	32.2	50.8	3	30.2
1-18	550.0	13.9	34.9	51.4	21	

In the third series of experiments, an initial alloy, Cd-12.5 wt % Th, was prepared and sampled at 600, 575, and 550°C. These data points represent the solubility of thorium in cadmium. Magnesium was added incrementally, and samples were taken at temperatures between 650 and 550°C. No samples were taken at the freezing points as these temperatures are difficult to determine. The results of these experiments are presented in Tables 3-5 and Fig. 3. Also presented in Fig. 3 are the results of Amecke [AMECKE] who has measured the solubility of thorium in Cd-Mg (0 to 40 wt %) alloys. The present data indicate a higher thorium solubility than obtained by Amecke, but the solubility of thorium in cadmium compares very well with the data of [MARTIN-1959].

The results of runs 1 and 3 at 550°C form a continuous curve which suggests that the experiments are consistent. Results at 650°C are inconclusive; there is evidence that the melts were not saturated. In run 1, the initial thorium-magnesium sample which should have been Mg-45 wt % Th was analyzed to be Mg-33 wt % Th-3.5 wt % Cd.

However, worthwhile process information can be obtained from the 550°C and 600°C curves which indicate that the desired thorium solubility (10 to 20 wt %) can be achieved by using a Cd-50 wt % Mg alloy to 550°C.

(2) Equilibrium Solid Phase in Cadmium/Magnesium/Thorium System

It is also necessary to determine the equilibrium solid phase to make the solubility experiments more meaningful. From a process standpoint, although uranium is known to precipitate from cadmium-magnesium alloys as solid uranium [JOHNSON-1960] such data have not been obtained for thorium. If thorium precipitates from the cadmium-magnesium alloy as an intermetallic compound, there may also be simultaneous plutonium precipitation via coprecipitation. This would result in incomplete separation.

Three separate experiments were done in which a melt (cadmium-magnesium) was equilibrated with a known amount of thorium metal. The melt was then sampled and quenched. The experimental conditions are listed in Table 6. Rapid quenching was done by removing the crucible containing the molten metal from the furnace tube. Under these conditions, the melt solidified within 60 s. Slow quenching was achieved by simply turning off the furnace. The experiments were done in stainless steel crucibles, and one alloy sample (JKB-51) was submitted for spectrochemical analysis of iron, chromium, and nickel with the result given in the JKB-51 comment (Table 6).

The alloys were sectioned and submitted for analysis by electron microprobe and X-ray diffraction. SEM was investigated as a method of determining whether separate phases exist, but apparently it is not possible to distinguish between thorium and cadmium with this technique.

Table 4. Liquidus Determination--Thorium/Cadmium/Magnesium System.
Expt. Series 2. Initial Charge: 110.37 g Mg, 89.83 g Th

Sample No.	Temp, °C	Composition of Melt			Equilibration, h	Quantity of Cd Added after Preced. Equilibrat., g
		Th, wt %	Mg, wt %	Cd, wt %		
2-1	600	38.7	62.4	0.57	15	
2-2	600	35.6	57.9	7.3	1 1/2	10.89
2-3	600	32.9	55.9	12.5	1 1/2	9.65
2-4	601	29.0	53.0	19.6	1 1/2	13.93
2-5	605	29.8	51.9	19.2	16[a]	
2-6	600	25.3	47.7	29.0	1 1/2	19.42
2-7	599	21.3	42.5	38.8	1	22.95
2-8	598	21.4	43.7	36.6	24[a]	
2-9	598	17.9	36.8	46.0	1 1/2	32.95
2-10	600	16.6	31.8	52.9	2	32.39

[a]Overnight.

Table 5. Liquidus Determination--Thorium/Cadmium/Magnesium System. Expt. Series 3. Initial Charge: 57.33 g Th, 402.36 g Cd (12.47 wt % Th)

Sample No.	Temp, °C	Composition of Melt			Equilibration, h	Quantity of Mg Added after Preced. Equilibrat., g
		Th, wt %	Mg, wt %	Cd, wt %		
3-1a	575	6.05		93.0	2 1/4	
3-1b[a]	550	5.91		94.9	24	
3-2a	550	5.48		95.9	2	
3-2b[a]	600	8.76		93.1	2 1/2	
3-3	600	8.60	4.73	88.0	2	20.01
3-4	550	7.73	5.09	89.0	1	
3-5	600	10.8	8.21	82.2	2	21.19
3-6	550	9.19	9.69	82.7	2	
3-7	650	9.81	16.4	77.1	2	39.97
3-8a	600	9.98	16.1	76.7	2	same melt
3-8b	600	10.7	16.0	76.4	2	at same time
3-9	550	10.2	16.7	76.5	3	
3-10	550	11.2	22.4	70.0	2	40.21
3-11	650	9.25	22.8	71.4	2	Th saturation 9.7 wt %
3-12	600	8.40	24.2	70.3	2	24.15

[a]This was a separate experiment with an initial charge of 74.81 g Th, 400.81 g Cd rather than a resampling of an experiment at another temperature. This experiment was discontinued due to sampling difficulties.

Table 6. Experimental Conditions for Phase-Determination Studies

Sample	Initial Alloy Composition			Equilibration Procedure	Sampling Temp., °C	Measured Solution Composition, wt %			Quenching Rate
	Th	Cd	Mg			Th	Cd	Mg	
JKB-51	31.38 g (37.62 wt %)		52.04 g (62.38 wt %)	stir at 675°C for 1 h, cool to 600°C with stirring, then hold at 600°C for 5 h while sampling	602	30.0[a] 29.8[a] 29.2[a]	0.08	64.6	
JKB-52	31.1 g	54.32 g	51.5 g	add Cd at 600°C and cool to 550°C with stirring; equilibrate at 550°C for 1 1/2 h.	550	18.7	42.7	39.5	Rapid
JKB-53	40.08 g (50.8 wt %)		38.87 g (49.2 wt %)	stir at 700°C for 1 h, cool to 620°C, and equilibrate for 1/2 h.	619	37.6	0.02	62.9	
JKB-54	39.6 g	156.85 g	38.1 g	add Cd and equilibrate at 625°C for 3 h with stirring.	621	11.1	73.8	18.4	Rapid
JKB-55	40.04 g		38.56 g	stir at 775°C for 1 h, cool to 625°C.	625	35.5	0.06	65.5	
JKB-56	39.7 g	156.19 g	37.9 g	add Cd and equilibrate at 625°C for 2 1/2 h.	627	8.5	74.0	19.3	Slow
JKB-57					627	14.2	70.7	17.2	

Comments

JKB-51 SS-crucible--mass balance of 94.7%. Th double-checked and the alloy sample was checked for impurities spectrochemically. Cd-0.03 wt %, Cr-<0.001 wt %, Fe-FT,[b] Ni-0.004 wt %, Cu-0.002 wt %

JKB-52 a filtered sample could not be obtained, and so a drop on the end of the sampling tube was submitted for analysis--these results can be compared with results for sample JKB 2-9,[c] and it is suggested that unfiltered samples are about 2 wt % high in Th concentration

JKB-53 at 700°C, the Th should be completely dissolved in the Mg, while at 625°C the alloy composition should be Mg-43 wt % Th.

JKB-54 No filtered sample could be obtained and so a drop on the end of the sampling tube was submitted for analysis--again the Th percentage appears greater than expected--a sample was also submitted for spectrochemical analysis which indicated Cr-0.001 wt %, Fe-FT,[b] Ni-<0.001 wt %

JKB-56 JKB-56 is a filtered sample, and JKB-57 is a small drop at the tip of the sampling tube

[a]Replicate measurements.

[b]FT--faint trace.

[c][BATES]:

	Th, wt %	Mg, wt %	Cd, wt %
JKB 2-9	16.6	42.5	42.1
JKB-52	18.7	39.5	42.7

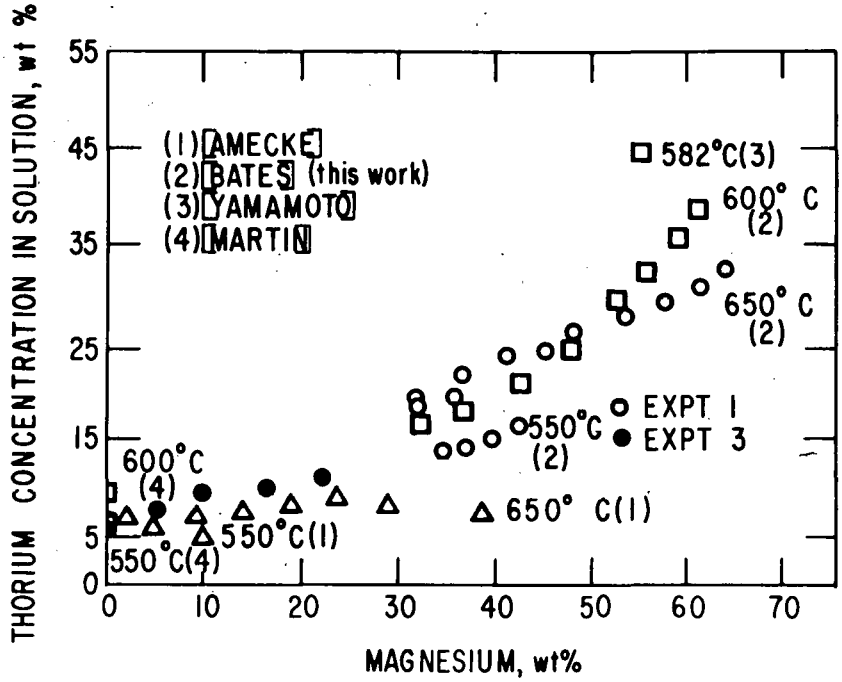

Fig. 3. Solubility of Thorium in Cadmium-Magnesium Alloys

Electron microprobe examination indicated that Sample JKB-52 (with nominally equal weight fractions of Cd and Mg) had five areas which can be distinguished visually. These areas consisted of regions for which the cadmium:magnesium:thorium ratios have been determined by electron microprobe measurements (accurate to about 25 relative percent). One region which consisted of 100% thorium appeared to be an undissolved piece of thorium metal, uniformly surrounded by a region which was composed of cadmium-magnesium-thorium with an atom ratio of 1.5:1.7:1.

Regions of similar composition were found interdispersed throughout the melt in the form of islands or crystals. These features were more concentrated at the bottom of the melt. The area between these crystals had a composition which was 60 wt % Mg and 40 wt % Cd. Very little thorium was found in this region. The insoluble crystals seem to be settling near the bottom of the crucible. The remainder of the melt, somewhat depleted in cadmium, contained very little thorium.

A large anomalous region was also identified near the top of the melt. This region contained essentially no cadmium and consisted of a 100% magnesium background with thorium-magnesium regions having an atom ratio of 1:3.

Samples JKB-54 and JKB-56 resulted from an alloy (thorium in nominal Cd-20 wt % Mg), one of which was quenched rapidly (JKB-54) and the other slowly (JKB-56). Both samples consisted of background, crystals or

islands, and small particles near the bottom of the melt. The background was cadmium-magnesium with a weight ratio of 80:19 and essentially no thorium. The crystals, which were about five times larger in sample JKB-56, were cadmium:magnesium:thorium with an atom ratio of 6.9:4:1. The small particles, which were the same size in both melts, are of higher thorium content, perhaps being undissolved ThO_2.

From the above data, an identification of the precipitated phase cannot be made at this time. However, it does appear that the intermetallic which forms in a Cd-50 wt % Mg alloy is different from that which forms in a Cd-20 wt % Mg alloy.

b. Reduction of High-Fired Thoria
(J. K. Bates and D. K. Kroeck)

A preliminary experiment designed to demonstrate the reduction of high-fired thoria by calcium was completed. Samples of both the salt and the alloy phases were taken at 2-h intervals. However, the results indicate that during sampling, the two phases had not separated and the samples submitted contained no alloy. The entire salt-alloy mixture has been dissolved and further analyses of the mixture are in progress. Extensive reduction experiments are planned for the near future.

c. Molten Salt Recycle, Electrolysis of CaO in Molten Salt
(L. J. Jardine, T. J. Gerding, and D. K. Kroeck)

Several flowsheets for reprocessing oxide fuels under development in the PDPM Progam include a reduction step utilizing calcium metal, a solvent alloy of cadmium, zinc, or copper and a cover salt containing $CaCl_2$. The current "reference" salt transport flowsheet for thorium oxide fuels (Fig. 2) is an example. The basic reduction reaction is:

$$MO(alloy/salt) + Ca(salt/alloy) \rightarrow CaO(salt) + M(alloy) \quad (1)$$

where M = uranium, thorium, plutonium, fission products, etc.

As the salt is reused in the reduction step, the concentration of CaO can increase to near the saturation point. At this point, it becomes necessary either to remove some of the accumulated oxide or to discard the salt as a high-level waste. If the salt is discarded, the volume of solid waste is about 850 L for each megagram of oxide fuel reduced.

The preceding quarterly report [STEINDLER-1979] summarized schemes in the literature designed to treat the salt and discussed their inherent disadvantages. A new electrochemical concept for treating the salt was introduced that is aimed at significantly reducing the waste volume. This electrochemical concept is based on fused salt ($CaCl_2 \cdot CaF_2$) electrolysis of CaO. This salt has the same composition as that used in the reduction step and serves as the electrolyte of the cell. The cathode reaction generatess calcium metal for recycle. The anode reaction yields

oxygen, which presumably reacts in situ with the carbon anode to yield CO/CO_2.* The latter gas can be cleaned and released to the atmosphere as a common gas, not as a large-volume solid waste. The net cell reaction proposed is

$$CaO(salt) + C(anode) \xrightarrow{700°C} Ca(alloy/salt)_{cathode} + CO(g) \qquad (2)$$

To evaluate the concept, an electrochemical cell for operation in the furnace tube of an inert-atmosphere (argon) dry box has been constructed (Fig. 4). The cell has a liquid metal cathode that is more dense than the salt electrolyte and can also serve as the collector for newly formed

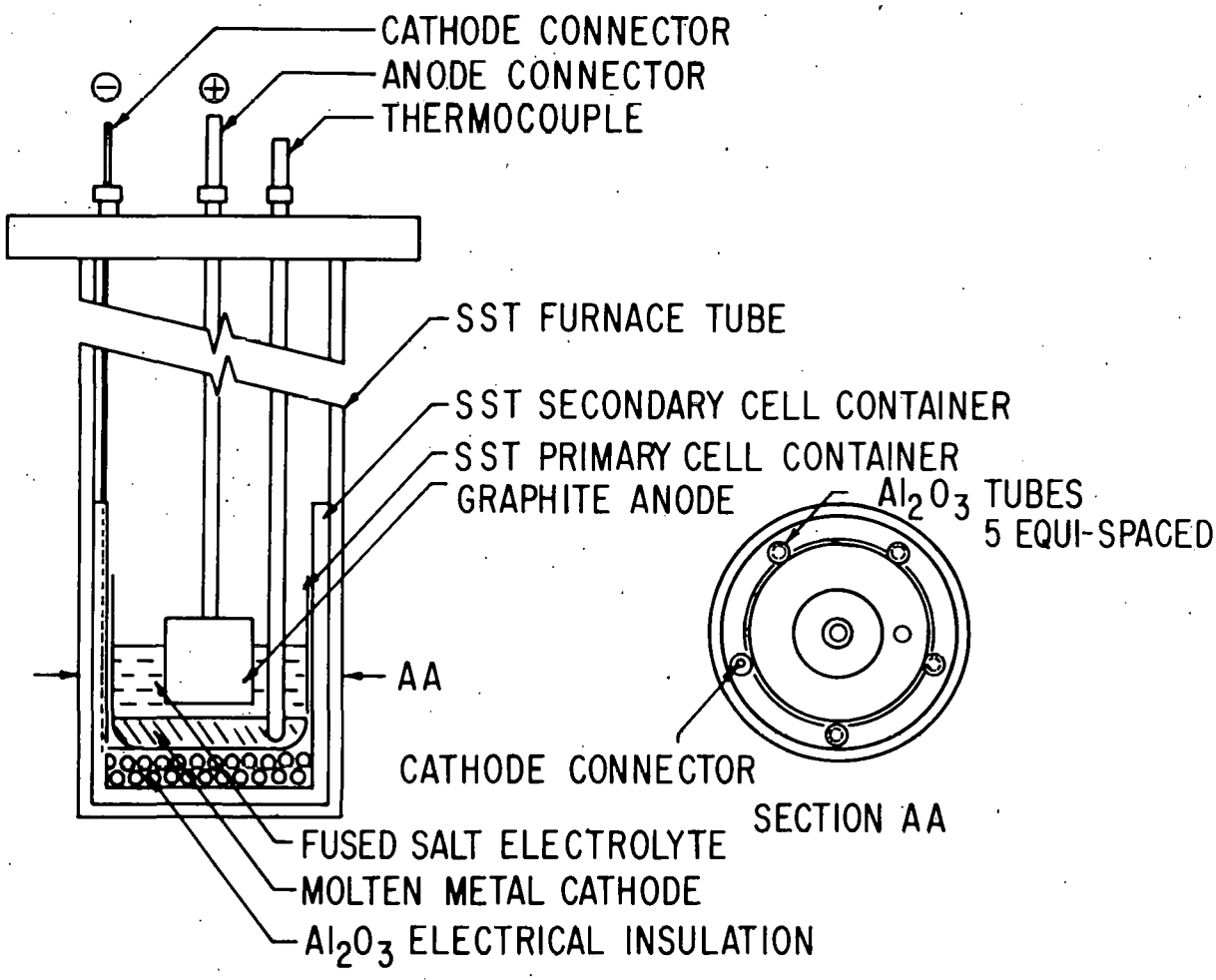

Fig. 4. Electrolytic Cell for Initial CaO Electrolysis Study

*The relative amounts of CO and CO_2 may depend upon the specific electrolyzing conditions of the cell. For discussion purposes, only CO is assumed to be formed.

calcium metal. The initial cathode alloys were selected to be compatible with the oxide fuel reduction alloys (i.e., cadmium and copper alloys), but the concept is not limited to these. Removal of the regenerated calcium from the cell for direct reuse in the reduction step should be possible.

The initial electrolysis experiment utilized 208 g $CaCl_2$, 38 g CaF_2, and 5 g CaO in the starting electrolyte and 370 g of cadmium as the cathode. The loaded cell was heated to about 690°C, a cylindrical graphite* anode was lowered into the salt about 1/2 in. from the molten cathode layer, and power was applied. The cell operated smoothly in a constant (4-A) current mode for about 220 min. During the initial about 105 min, the cell operated at an approximately constant voltage of 1.75 to 1.80, which is in reasonable agreement with the theoretical voltage for Eq. 2. The time to deplete the entire 5 g CaO in the salt at 100% cell efficiency was calculated to be 72 min. After 105 min, the cell voltage (still at constant current) drifted slowly but regularly to about 2.6 V and the experiment was manually terminated.

Filtered samples of the molten cadmium cathode alloy and salt were taken for analysis--initially and at the termination of the experiment--to confirm Reaction 2. However, the analytical determinations gave inconclusive results with respect to the calcium content of the cadmium, due to the low concentration of calcium in the cadmium alloy. Also, with the analytical procedures used, the alloy was subject to contamination by the salt phase. Thus, although the cell operated in a manner consistent with the proposed concept, the initial experiment did not confirm Eq. 2.

To circumvent the problems of the initial run, experiments will be carried out with an improved sampling technique which should show higher concentrations of calcium in the cathode alloy. In these subsequent experiments, the off gas from the cell will be sampled and other cathode alloys (copper-magnesium) will be evaluated.

4. Uranium-Plutonium Salt-Transport Processing

(J. B. Knighton,† C. Baldwin,† W. A. Averill,† M. F. Boyle,† J. E. Hicks,† T. D. Santa Cruz,† S. P. Sontag,† and J. L. Zoellner†)

a. Introduction

The purpose of this work package is to develop pyrochemical processes and associated hardware for coprocessing uranium and plutonium contained in spent FBR reactor fuels. The primary objective is to develop a process capable of producing a proliferation-resistant product suitable for reactor use. This proliferation resistance can be accomplished by coprocessing and/or by producing fission product-contaminated plutonium. In addition, waste management of by-products, for both interim and ultimate disposal, will be explored.

---

*The graphite was kindly supplied free of charge by Great Lakes Carbon Corporation and was their grade HLM.

†Rockwell International-Rocky Flats.

The technical goals of this work package are (a) to develop a viable flowsheet for producing, by pyrochemical means through coprocessing, a proliferation-resistant product suitable for reactor use; (b) to identify key problems and conduct early proof-of-principle experiments on key problems that challenge the feasibility of the flowsheet; (c) to prepare a process description and design criteria for a conceptual Pyrochemical Processing Facility (PPF); (d) to examine and integrate design concepts for the unit operations of the salt transport process; and (e) to evaluate containment of fission products and management of waste products.

b. Engineering Analysis

(1) Salt Transport Process Description (See Fig. 5)

The salt transport process for coprocessing uranium and plutonium may offer unique advantages over more conventional processing methods with respect to meeting nonproliferation requirements. Some pyrochemical processes developed in the past were rejected because they did not yield a completely decontaminated product. Under current nonproliferation policies, some residual fission product contamination of coprocessed plutonium and uranium is desirable for diversion resistance and proliferation resistance.

The major objectives of the salt transport process are: (1) to process spent FBR fuel and obtain a plutonium-uranium-fission product oxide product suitable for fabrication into new fuel and (2) to produce a product from which the recovery of plutonium for subsequent use in weapons would require a major detectable effort by a foreign nation.

Objectives to be met in processing include: (1) keep uranium and plutonium together, (2) provide for the removal of part or all of the fission products, (3) repair radiation damage, (4) restore fuel reactivity, (5) contain all of the fission products, (6) minimize the size of waste product streams, and (7) produce waste streams that require minimum treatment prior to interim and long-term storage.

Potential advantages of the salt transport process include the following:

1. The process can accommodate fuels after short cooling times.
2. Out-of-reactor fuel inventories are small.
3. Process solvents (molten salts and metals) are resistant to radiation damage.
4. Process wastes are solids and may require minimum treatment for packaging, shipment, and storage.
5. Iodine is contained in a solid waste stream.
6. The critical mass restriction is reduced.
7. Mechanical disassembly of the fuel assembly is avoided.
8. Pyrochemical processes are compact.

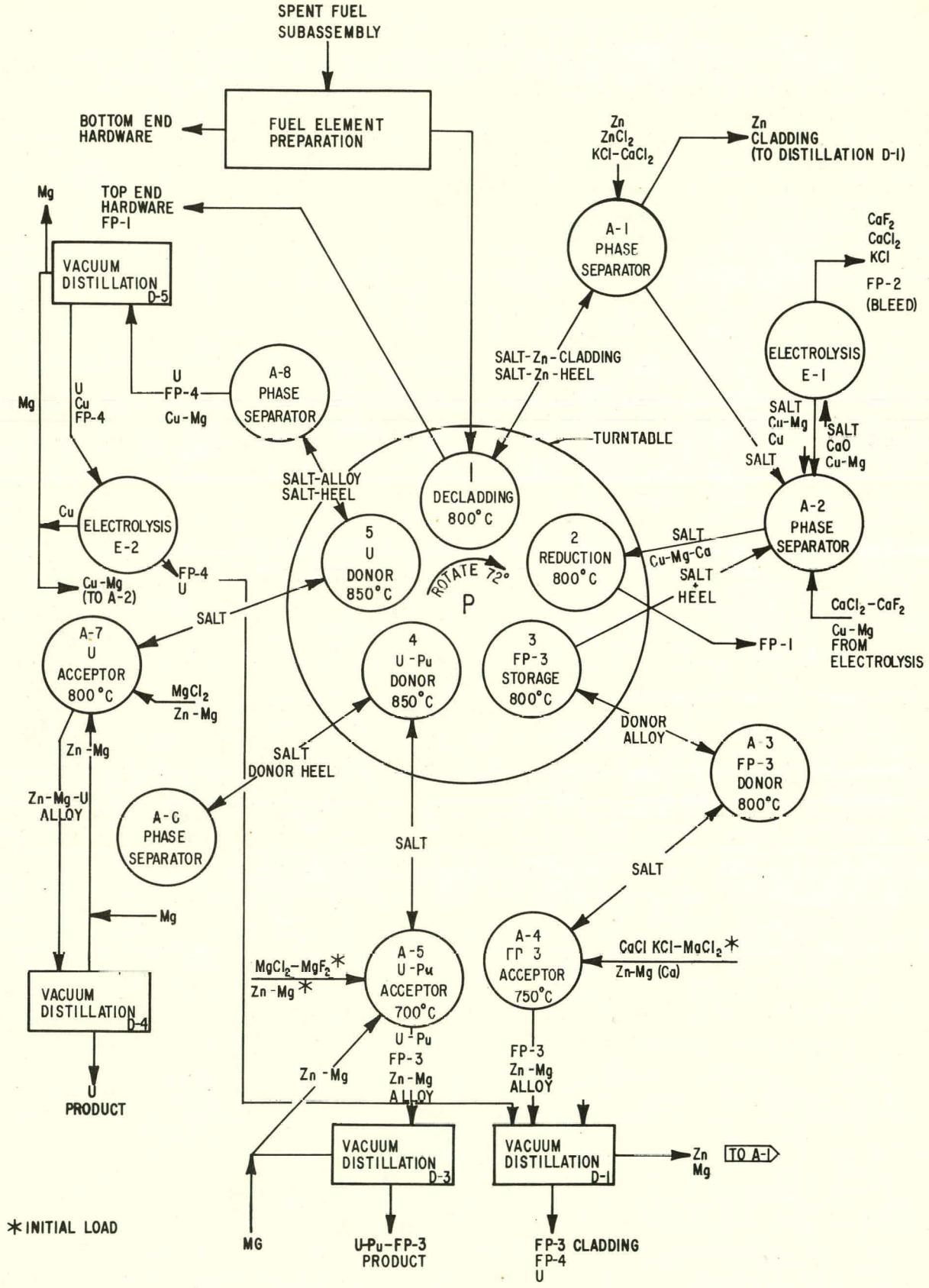

Fig. 5. Process Flow Diagram for Coprocessing Spent FBR Fuel by the Salt Transport Process

The major disadvantages are: (1) this is a new technology that has not reached the technical maturity of the Purex process and (2) development work is required to demonstrate the feasibility of the proposed salt transport process.

(a) Description of Process Chemistry

The chemical basis for the various separations used in this pyrochemical process is the difference in the partitioning of uranium-plutonium and the fission product elements between molten salt and liquid alloy phases. This difference in partitioning is largely determined by the values of the standard free energy of formation (ΔG_f°) of the chlorides of uranium, plutonium, and the fission products.

Table 7 lists the chlorides of selected elements in the order of decreasing values of free energy of formation at 1000 K. For convenience, the fission product elements are divided into four groups: FP-1, FP-2, FP-3, and FP-4. FP-1 fission products are volatile and consist of tritium, Xe, and Kr. FP-2 fission products are I, Br, Cs, Rb, Ba, Sr, Sm, Eu, Se, and Te. FP-3 fission products are yttrium and the rare earth elements which form +3 chlorides, Y, La, Ce, Pr, Nd, Pm, Gd, and Tb. FP-4 fission products are the refractory and noble metal elements, Zr, Nb, Mo, Tc, Ru, Rh, Pd, Ag, Cd, In, Sn, and Sb. In structuring the process, the separations occur in the numerical sequence of the above fission product groups.

Two separate oxidation-reduction couples ($CaCl_2$-Ca and $MgCl_2$-Mg) are used to "buffer" the partitioning of elements between molten salt and liquid metal phases. The FP-2 elements lie above $CaCl_2$ in the free energy scale. The FP-3 elements lie between $CaCl_2$ and $MgCl_2$, and the FP-4 elements lie below $MgCl_2$.

In general, the distribution coefficients of various elements fall in the same order as the free energies of formation of their chlorides. However, large differences occur in the distribution coefficients because of solvent effects.

The term "salt transport" has been applied to a purification technique whereby a metallic solute is transferred selectively from one liquid alloy (donor) to another liquid alloy (acceptor) by circulating a molten salt between the two alloys. The transfer takes place by oxidation of the solute by the salt at the donor alloy and its subsequent reduction by the acceptor alloy.

(b) Block Diagram

Figure 6 gives the conceptual flowsheet for the salt transport process for coprocessing uranium and plutonium. The steps in this process (Table 8) are discussed in the following portions of the process description.

Table 7. Standard Free Energies of Formation of Chlorides at 1000 K

MCl_n	$-\Delta G_f^\circ$, kcal/g-equiv Cl	Reference
$BaCl_2$	83.6	[CHASE-1975]
CsCl	82.6	[STULL]
RbCl	82.5	[GLASSNER]
LiCl	78.8	[STULL]
KCl	81.6	[STULL]
$SrCl_2$	80.8	[CHASE-1975]
$SmCl_2$	80.0	[WICKS]
$EuCl_2$	79.0	[WICKS]
$CaCl_2$	76.8	[STULL]
NaCl	76.2	[STULL]
$LaCl_3$	67.0	[WICKS]
$PrCl_3$	66.3	[WICKS]
$CeCl_3$	66.3	[WICKS]
$NdCl_3$	64.2	[WICKS]
YCl_3	61.2	[WICKS]
$PuCl_3$	58.4	[OETTING]
$MgCl_2$	57.7	[STULL]
UCl_3	54.0	[RAND]
$MnCl_2$	42.2	[WICKS]
$ZrCl_2$	34.2	[STULL]
$ZnCl_2$	35.0	[WICKS]
$CrCl_2$	32.8	[WICKS]
$CdCl_2$	30.4	[WICKS]
$FeCl_2$	26.3	[CHASE-1974]
CuCl	22.0	[STULL]
$NiCl_2$	18.6	[WICKS]
$NbCl_5$	11.4	[GLASSNER]
$MoCl_2$	8.0	[WICKS]
$TcCl_3$	7.4	[GLASSNER]
$PdCl_2$	5.3	[GLASSNER]
RhCl	1.4	[GLASSNER]
$RuCl_3$	0.3	[GLASSNER]

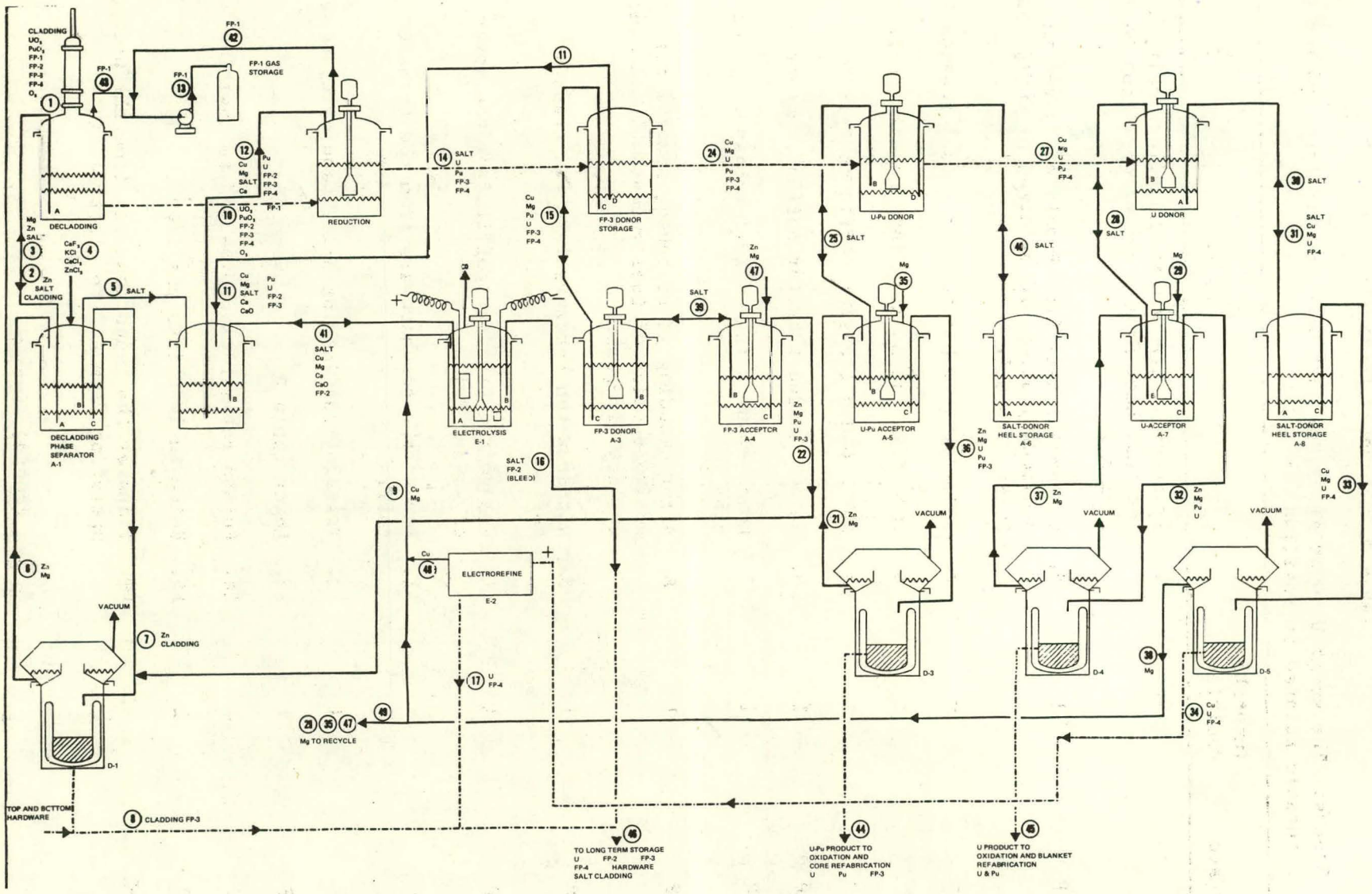

Fig. 6. Process Flow Diagram

Table 8. Sequence of Events

Status: The spent U donor alloy has just been removed from P-5 and the turntable rotated to position, P-1, 1.

Furnace	Turntable Position		Event
		1.	Transfer molten decladding alloy, salt, and residual heel from previous operation to P-1 from A-1
P	1	2.	U in metal heel from P-5 is dissolved in decladding alloy and oxidized by $ZnCl_2$ and taken into salt
-	-	3.	Remove bottom hardware from fuel subassembly
-	-	4.	Load fuel subassembly into transfer coffin
-	-	5.	Move loaded transfer coffin to P-1
P	1	6.	Attach loaded transfer coffin to cover of P-1
P	1	7.	Lower about 2 in. of fuel subassembly into zinc
P	1	8.	After cladding is breached, immerse the active section of fuel subassembly in zinc. Collect off-gases
P	1	9.	Withdraw top hardware into the transfer coffin
P	1	10.	Remove the transfer coffin from the cover of vessel P-1
-	-	11.	Remove the top hardware from the transfer coffin
P	1	12.	Transfer Zn-cladding alloy (and salt) to A-1
P	1	13.	Lower table P
P	1	14.	Rotate table P clockwise 72° to position 2
P	2	15.	Raise table P into position
A-2	-	16.	Transfer the reduction salt from the previous operation from A-2 to electrolysis

(contd)

Table 8. (contd)

Furnace	Turntable Position	Event
A-1	-	17. Transfer the Zn-cladding alloy to vacuum distillation, D-1, leaving salt in A-1 by making a phase separation
A-1	-	18. Transfer salt in A-1 (containing released iodine) into A-2
A-1	-	19. Add Zn and salt to A-1, and melt
A-2	2	20. Transfer new molten salt, Cu-Mg-Ca alloy, decladding cover salt, and alloy heel from previous reduction from A-2 to P-2
P	2	21. Mix system and reduce oxide fuel
P	2	22. At the end of reduction, the salt is not removed, but carried with the vessel to P-3
P	2	23. Lower table
P	2	24. Rotate table P clockwise 72° to position 3
P	3	25. Raise table P into position
A-4	-	26. Transfer a small portion (about 1/5) FP-3 acceptor alloy (from the previous FP-3 transport operation) from A-4 to vacuum distillation, leaving a large acceptor alloy heel in A-4
A-4	-	27. Add Zn-Mg to A-4 for new acceptor alloy makeup
P	3	28. Transfer 10% of alloy from P-3 to A-3
A-3	-	29. Transfer salt from A-4 to A-3 (leaving a salt heel in A-4
A-3	-	30. Equilibrate A-3 by mixing; stop the mixing, allowing phase disengagement
A-3	-	31. Return salt from A-3 to A-4, leaving a small salt heel in A-3
A-4	-	32. Equilibrate A-4 by mixing; stop the mixing, allowing phase disengagement

(contd)

Table 8. (contd)

Furnace	Turntable Position	Event
A-3	-	33. Transfer donor heel from A-3 to P-3
P	3	34. Transfer salt and a small amount of metal from P-3 to A-2
P	3	35. Lower table P
P	3	36. Rotate table P clockwise 72° to position 4
P	4	37. Raise table P into position
A-5	-	38. Transfer U-Pu acceptor alloy from previous U-Pu transport operation from A-5 to vacuum distillation (leaving a small acceptor alloy heel in A-5)
A-5	-	39. Add Zn-Mg to A-5 for new acceptor alloy
A-6	-	40. Return donor heel and salt from A-6 to P-4
P	4	41. Equilibrate by mixing; stop the mixing, allowing phase disengagement
P	4	42. Transfer salt (leaving a small salt heel in P-4) from P-4 to A-5
A-5	-	43. Equilibrate by mixing; stop the mixing, allowing phase disengagement
A-5	-	44. Transfer salt (leaving small heel in A-5) from A-5 to P-4
P-4, A-5	-	45. Repeat steps 41-44 as required to achieve desired Pu enrichment
P	4	46. Transfer salt and a small donor alloy heel from P-4 to A-6
P	4	47. Lower table P
P	4	48. Rotate table P clockwise 72° to position 5
P	5	49. Raise table P into position
A-7	-	50. Transfer U acceptor alloy from U transport operation from A-7 to vacuum distillation, leaving a small acceptor alloy heel in A-7

(contd)

Table 8. (contd)

Furnace	Turntable Position	Event
A-7	-	51. Add Zn-Mg to A-7 for new acceptor alloy
P	5	52. Transfer donor alloy heel and salt from A-8 to P-5
P	5	53. Equilibrate by mixing
P	5	54. Stop the mixing, and allow phases to disengage
A	7	55. Transfer salt from P-5 to A-7
A	7	56. Equilibrate by mixing
A	7	57. Stop the mixing, and allow phases to disengage
P	5	58. Transfer salt from A-7 to P-5
P-5 & A-7		59. Repeat steps 53 through 59 to achieve the desired U transfer
P	5	60. Transfer salt and alloy from P-5 to A-8, minimizing remaining heel
P	5	61. Transfer spent U-donor alloy from A-8 to vacuum distillation D-5
P	1	62. Transfer Zn-cladding alloy (and salt) from previous decladding operation from P-1 to A-1
P	5	63. Lower table P
P	5	64. Rotate table P clockwise 72° to position 1
P	1	65. Raise table P into position
P	1	66. Go to step 1

To provide a basis for a plant design study, spent core and radial blanket fuel from a conceptual 1000-MW(e) Fast Breeder Reactor was selected as the feed to the process. The process will handle one fuel assembly (either core or radial blanket) at a time. The core and the associated axial blanket are processed together without prior mechanical separation. The hardware below the active section of the subassembly is removed prior to processing. The hardware above the active section does not enter the process streams.

In this low-decontamination process, the spent fuel is selectively dissolved in molten metals and molten salts and coprocessing of uranium and plutonium and separation from fission products is achieved. Near-quantitative separation of FP-1, FP-2, and FP-4 fission product elements from uranium and plutonium is accomplished during the process.

The salt transport process uses five basic operations to coprocess uranium and plutonium (Fig. 7):

1. Decladding
2. Oxide reduction
3. Partial FP-3 decontamination
4. Plutonium enrichment and FP-4 decontamination
5. Heavy metals concentration

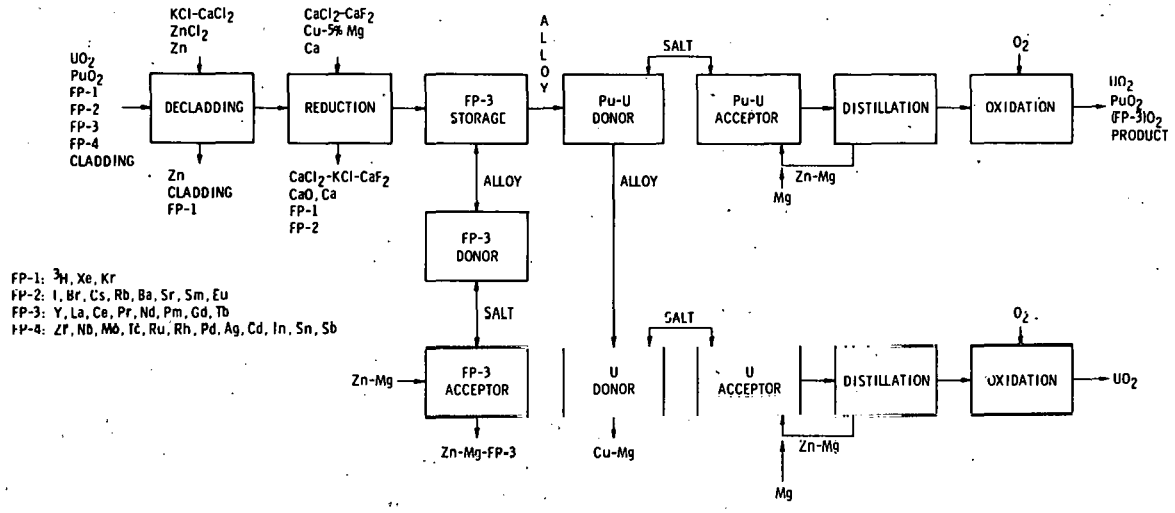

Fig. 7. Conceptual Salt Transport Process for UO_2-PuO_2 Fuel

The feed to the process is assumed to be (1) one core assembly which has an axial blanket above and below the core fuel section or (2) one radial blanket assembly. The core and axial blanket are processed together without prior mechanical separation. The subassembly hardware below the active section is removed prior to processing. The hardware above the active section is not taken into the process streams.

To avoid the necessity of handling solids (declad mixed-oxide fuel and solid UCu_5 compound), the primary process operations are conducted sequentially in the same tungsten crucible. These primary operations are conducted in a circular processing assembly with operating stations dedicated for each operation. Decladding is conducted at the first station. Oxide reduction is conducted at the second station, removal

of FP-3 is conducted at the third station. Separation of U-Pu from U is conducted at the fourth station, and U purification is conducted at the fifth station. Each station has the necessary apparatus to conduct the desired operations (such as introduction of a fuel subassembly, stirring, and transfer of molten salt and metal phases into and out of the crucible).

At each of these operating stations, a furnace (with an open bottom) is suspended from the cover of the processing assembly. At each of the operating stations, a tungsten crucible is located on a rotatable platform. After each operation is completed, the platform (and crucibles) must be lowered about seven feet so that the stirrers and transfer tubes will not obstruct the rotation of the crucibles. The platform is then rotated for the next operation. After rotation, the crucibles are raised back to the operating level at new operating positions. The mechanisms and seals for raising, lowering, and rotating the platform are located below the heated zone of the furnace.

To facilitate the flow of molten material into and out of the main process vessels and to achieve separation of the salt and metal phases, auxiliary furnaces are positioned around the circular processing assembly. These auxiliary furnaces are stationary. Molten salt and metal phases are pressure-siphoned through heated transfer tubes between the furnaces.

For recycle, volatile metal process solvents (zinc and magnesium) are separated from waste and product streams by vacuum distillation. In the salt transport process, copper is recovered for recycle by electrorefining. By these recycle processes, the waste produced by the process is held to an absolute minimum.

(c) Decladding

Zinc and cover salt are transferred from the decladding phase separator (A-1, Fig. 6) to the decladding crucible prior to decladding. After the bottom hardware is removed from the fuel subassembly, the fuel is placed in a transfer coffin which is then introduced into the process bay area. The transfer coffin is equipped with: (1) provisions for raising and lowering the fuel subassembly, (2) provisions for cooling to remove fission product decay heat, and (3) a gate-flange assembly. The coffin is secured to a second gate-flange assembly located on the cover of the circular processing assembly at the decladding position. Both gates (on the coffin and on the cover) are opened, and the fuel is lowered to immerse the bottom of the fuel pins through the cover salt and a few inches into the molten zinc at 800°C.

When the cladding is breached, the FP-1 gases (^3H, Xe, Kr) are vented and collected in the cell cover gas. These gases are confined for fission product decay. Splashing of molten zinc and salt may occur as a result of release of high-pressure gases in the fuel pins. An iron shroud (which will dissolve in zinc) may be placed around the fuel subassembly to contain the splashing. A molten $CaCl_2$-KCl-$ZnCl_2$ cover salt is maintained on top of the zinc to prevent vaporization of zinc. Elemental iodine that may be released during decladding reacts with zinc to form ZnI_2

which is taken up by the cover salt. Alkali or alkaline earth iodine salts that may be released during decladding will also be taken up by the cover salt. Potassium chloride in the cover salt complexes with volatile halides ($ZnCl_2$, ZnI_2, etc.) and keeps them in the salt phase.

Zinc chloride in the cover salt reacts with any residual uranium, plutonium, and magnesium in the crucible from the prior operations and with any sodium metal associated with the fuel assembly. The resultant UCL_3, $PuCl_3$, $MgCl_2$, and NaCl salts are taken up by the cover salt. The zinc reaction product is taken up by the metal. Part of the more noble FP-4 elements (Ru, Rh, Pd, and Ag) may be exposed to zinc during decladding and will be taken up by dissolution in zinc.

The active section of the fuel subassembly is fully immersed in the zinc, and the cladding and hardware associated with it are removed from the oxide fuel by dissolution in molten zinc at 800°C. Table 9 gives the single-element solubility of iron, chromium, and nickel in molten zinc. Investigators at ANL have determined that stainless steel loadings of between 15 and 20 wt % in zinc are obtainable at 800°C and that the resultant zinc-stainless steel alloy is sufficiently fluid that it can be transferred out of a reaction vessel through a heated transfer line [WEBSTER-1970]. At these stainless steel loadings, iron is present in excess of its solubility limit. Small metallic iron grains are in suspension in the iron-saturated zinc solution. Because the densities of iron and zinc are very similar, these iron grains do not segregate to any appreciable extent. Zinc dissolution of nickel at the grain boundary was found to be the controlling mechanism in the destruction of stainless steel cladding.

Table 9. Solubility (Wt %) of Fe, Cr, and Ni in Zn

Temp, °C	Fe[a]	Cr[b]	Ni[a]
500	0.11	0.59	0.85
600	0.82	0.86	2.3
700	3.85	1.29	5.0
800	7.90	1.85	10.6

[a] Fe, Ni [JOHNSON-1965].

[b] Cr [VOGEL]

After decladding is complete, the upper hardware is raised into the transfer coffin, the gates are closed, and the coffin is removed from the decladding position and returned to the area where the bottom hardware was removed from the fuel assembly. The upper hardware is removed from the transfer coffin, a new fuel subassembly is loaded into the transfer coffin, and the decladding operation is repeated.

After decladding is complete, the zinc-stainless steel slurry and the salt are transferred to the decladding phase separator A-1. The crucible which contains the mixed oxide fuel and a very small metal heel is ready for rotation to the reduction position.

(d) Decladding Phase Separation--A-1, Fig. 6

1. In the decladding phase separator, the salt and metal phases are separated. The zinc-cladding slurry and the cover salt from the decladding vessel are received in the phase separator vessel. The salt and metal phases are allowed to disengage. The salt cover is transferred to the reduction phase separator tank A-2 leaving a small salt heel in A-1. No metal should be removed with the salt. New cover salt is added to vessel A-1. The liquid metal slurry is transferred to distillation, D-1, leaving a small metal heel behind. No salt should be transferred to D-1. Fresh zinc is transferred into A-1 and along with the remaining salt and metal heels including the new salt addition, is returned to decladding.

(e) Oxide Reduction

The crucible containing the declad mixed-oxide fuel is rotated to the reduction position and the oxide reduction step is performed in the same crucible used in decladding to avoid handling of the solid oxide fuel. To carry out oxide reduction, $CaCl_2$-CaF_2 reduction salt, decladding cover salt ($CaCl_2$-KCl-$ZnCl_2$-etc.), and copper-magnesium-calcium alloy are added to the crucible from the reduction phase separator A-2.

The salt and metal phases are vigorously contacted with the oxide fuel at about 800°C.

Because the mixed-oxide fuel is solid, provisions must be made to start with the mixing blade shallow in the melt and to lower it deep into the melt as reduction proceeds. If deep mixing were attempted initially, the stirrer would jam upon contact with the solid oxide fuel.

Calcium metal reduces the oxide fuel by the following reactions:

$$UO_2 + 2Ca \rightarrow U + 2CaO \quad (1)$$

$$PuO_2 + 2Ca \rightarrow Pu + 2CaO \quad (2)$$

The CaO reaction product and the FP-2 elements are taken up by the reduction salt. Figure 8 gives the $CaCl_2$ corner for the $CaCl_2$-CaF_2-CaO ternary salt system [WENZ]. Calcium oxide is shown in Fig. 8 to be soluble in the salt. This solubility provides a mechanism for removal of the calcium oxide from the reaction site. At the end of reduction, calcium oxide will be present below its solubility limit in the reduction salt.

The calcium metal reductant is slightly soluble in calcium chloride [WADE]. This solubility of calcium in calcium chloride provides a mechanism for transfer of calcium metal to the reaction site.

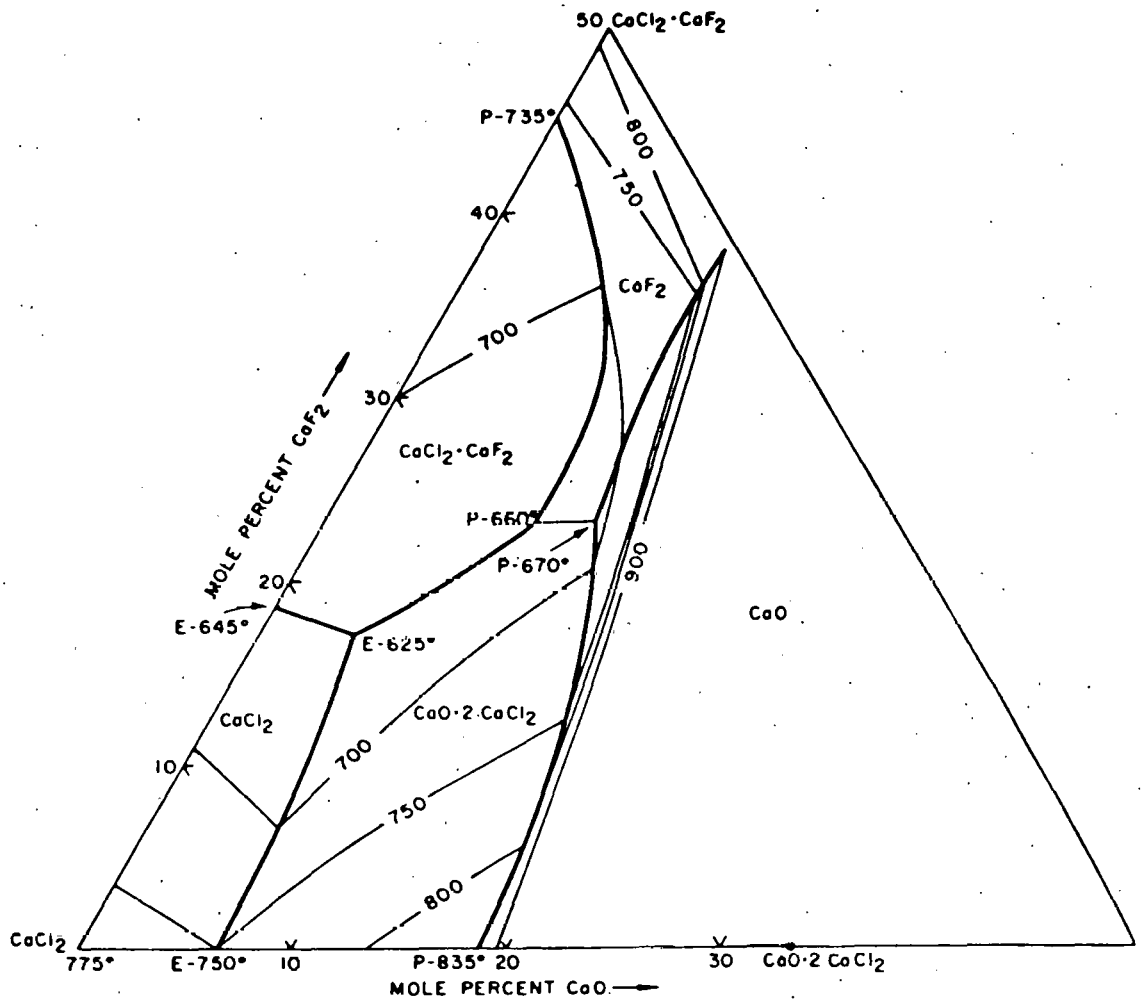

Fig. 8. Partial Phase Diagram of the $CaCl_2$-CaF_2-CaO System [WENZ]

The reduced metals (uranium, plutonium, FP-3, and FP-4) are taken up by the zinc or copper-magnesium reduction alloy. Uranium and plutonium are completely soluble in the molten zinc. The single-element solubilities of uranium and plutonium in zinc are shown in Tables 10 and 11. Uranium is present in the copper-magnesium alloy in excess of its solubility limit. The uranium in excess of its solubility precipitates as UCu_5 intermetallic compound. Plutonium, FP-3, and most of the FP-4 elements are soluble in the molten zinc or copper-magnesium alloy. A detailed discussion of the copper-magnesium alloy is presented later in this report.

During reduction of the fuel oxide, the remaining FP-1 elements in the oxide fuel are released from the oxide matrix and are taken up by the cover gas. The cover gas is handled in the same manner as in the decladding step.

Table 10. Calculated Solubility[a] of Uranium in Liquid Zinc

t, °C	1000/T, °K	Uranium, wt %	Uranium, at %
950	0.818	26.2	8.67
900	0.852	15.8	4.55
850	0.890	8.47	2.59
800	0.932	5.47	1.58
750	0.977	2.62	0.753
700	1.028	1.19	0.342
650	1.083	0.495	0.142
600	1.145	0.187	0.0533
550	1.215	0.0624	0.0178
500	1.293	0.0181	0.00537
450	1.383	0.00443	0.00125

[a]Calculated from the following empirical equations [JOHNSON-1965]:

800°C < t < 957°C

$$\log (\text{at \% U}) = 21.771 - 42250T^{-1} + 2.051 \times 10^{7}T^{-2};$$

$$\log (\text{wt \% U}) = 21.860 - 41780T^{-1} + 2.052 \times 10^{7}T^{-2}.$$

419°C < t < 800°C

$$\log (\text{at \% U}) = 6.579 - 6857T^{-1};$$

$$\log (\text{wt \% U}) = 7.101 - 6837T^{-1};$$

To minimize the quantity of waste generated by the process, the waste reduction salt is fed to an electrolysis process for electrowinning of calcium oxide. Calcium metal formed at the cathode is taken up by the zinc or copper-magnesium reduction alloy. The oxygen collected at the anode reacts with the carbon anode and is vented as carbon monoxide and carbon dioxide. The purified reduction salt is recycled to the next oxide reduction operation.

To provide a bleed for the FP-2 elements, a small amount of the reduction salt is sent to discard. The FP-2 content of this bleed stream is equal to the quantity of FP-2 elements introduced into the salt during the prior oxide reduction step. With this mode of operation, a large residual loading of FP-2 elements will be present in recycle salt sent to oxide reduction.

Table 11. Calculated Solubility[a] of Plutonium in Liquid Zinc

t, °C	1000/T, °K	Plutonium, wt %	Plutonium, at %
850	0.890	17.44	4.83[b]
800	0.932	9.29	2.56[b]
750	0.977	4.66	1.281
700	1.028	2.18	0.594
650	1.083	0.937	0.254
600	1.145	0.366	0.0984
550	1.215	0.127	0.0340
500	1.293	0.0387	0.0102
450	1.383	0.00996	0.00261

[a]Calculated from empirical equation [JOHNSON-1965]:

$450°C < t < 750°C$

$$\log (\text{at \% Pu}) = 6.594 - 6637^{-1};$$

$$\log (\text{wt \% Pu}) = 7.108 - 6588^{-1}.$$

[b]Estimated with above equations for 800 and 850°C.

After reduction is complete, the crucible containing the reduction alloy and reduction salt is ready for rotation to the FP-3 donor storage position.

(f) Reduction Phase Separator--A-2

1. Salt from electrolysis, reduction step cover salt, and new reduction alloy containing calcium are received into the reduction phase separator, A-2. All of this material except a small metal heel is transferred to the crucible in Reduction Position P-2. The spent salt from A-1 and the reduction salt and a small amount of FP-3 donor heel from the FP-3 donor storage vessel are next received into A-2. The salt and metal phases are allowed to disengage. The salt, with the exception of a small heel is transferred to electrolysis.

The crucible transferred to the FP-3 donor storage position contains the salt and the metal products from oxide reduction. The reduction salt layer on the metal is retained to prevent distillation of volatile metals, zinc, or magnesium, depending on the process option.

(g) FP-3 Removal

Because of the chemical similarity of plutonium and the FP-3 elements in pyrochemical systems, the separation of FP-3 elements from plutonium is a key step in the process.

As has been reported previously [STEINDLER-1979], in the salt transport process, salt transport is used to separate FP-3 elements from plutonium. The Cu-16 at % Mg alloy used in oxide reduction is a FP-3 donor alloy. The FP-3 elements are oxidized by $MgCl_2$ by the reaction:

$$FP\text{-}3 + 3/2\ MgCl_2 \rightarrow (FP\text{-}3)Cl_3 + 3/2\ Mg \qquad (3)$$

and are taken up by a molten salt at 800°C. Uranium, plutonium, and FP-4 elements remain in the donor alloy. The salt is subsequently equilibrated with a Zn-20 at % Mg acceptor alloy at 750°C. The FP-3 elements are reduced by magnesium by the reaction:

$$(FP\text{-}3)Cl_3 + 3/2\ Mg \rightarrow FP\text{-}3 + 3/2\ MgCl_2 \qquad (4)$$

The reduced FP-3 metals are taken up by the acceptor alloy. The $MgCl_2$ reaction product is taken up by the salt. Magnesium chloride consumed at the donor alloy is regenerated at the acceptor alloy. The overall salt composition remains constant, and the salt may be reused indefinitely.

Figure 9 gives the estimated values for the cerium, plutonium, and uranium distribution coefficients for these elements partitioning between a $CaCl_2$-KCl-$MgCl_2$ salt of various $MgCl_2$ contents and Cu-16 at % Mg donor alloy at 800°C. For our application, a $MgCl_2$ content in the extraction salt of 11 mol % was selected. Figure 10 gives the estimated values for the cerium, plutonium, and uranium distribution coefficients for these elements partitioning between a $CaCl_2$-KCl-$MgCl_2$ salt of various $MgCl_2$ contents and the Zn-20 at % Mg acceptor alloy at 750°C. Cerium is used as a stand-in for the FP-3 elements. These values of the distribution coefficients were estimated from existing data by a relationship derived by [JOHNSON-1967] at ANL:

$$D = C(x\ MgCl_2)^{3/2} \qquad (5)$$

$$\text{where } D = \frac{\text{mol \% solute in salt}}{\text{at. \% solute in metal}}$$

$$C = \text{constant}$$

$$x\ MgCl_2 = \text{mole fraction } MgCl_2 \text{ in salt}$$

The estimated values of D in Figs. 9 and 10 need to be experimentally verified.

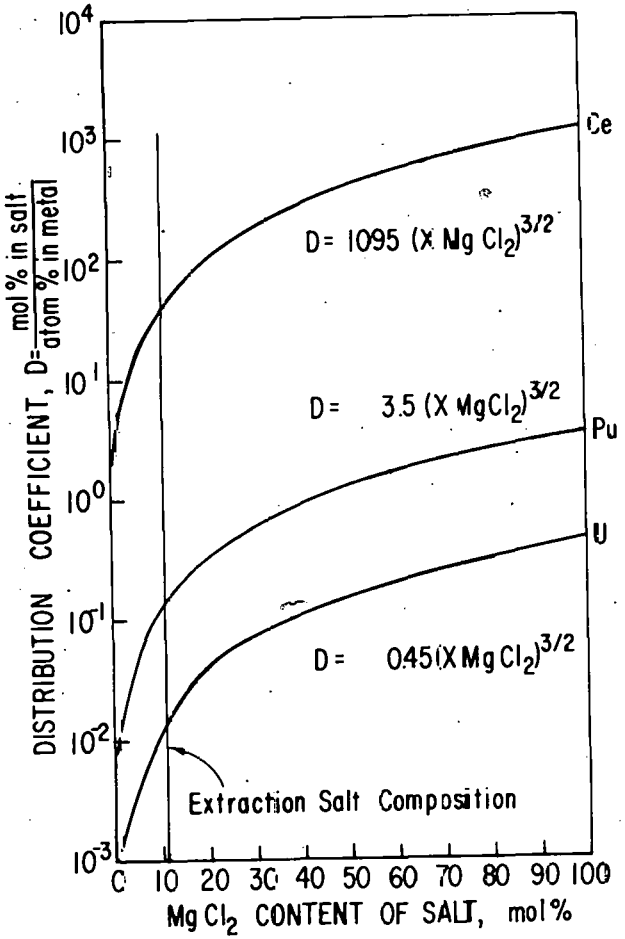

Fig. 9. Estimated Distributions of Cerium, Plutonium, and Uranium between $CaCl_2$-KCl-$MgCl_2$ Salt and Cu-16 at. % Mg Alloy at 800°C

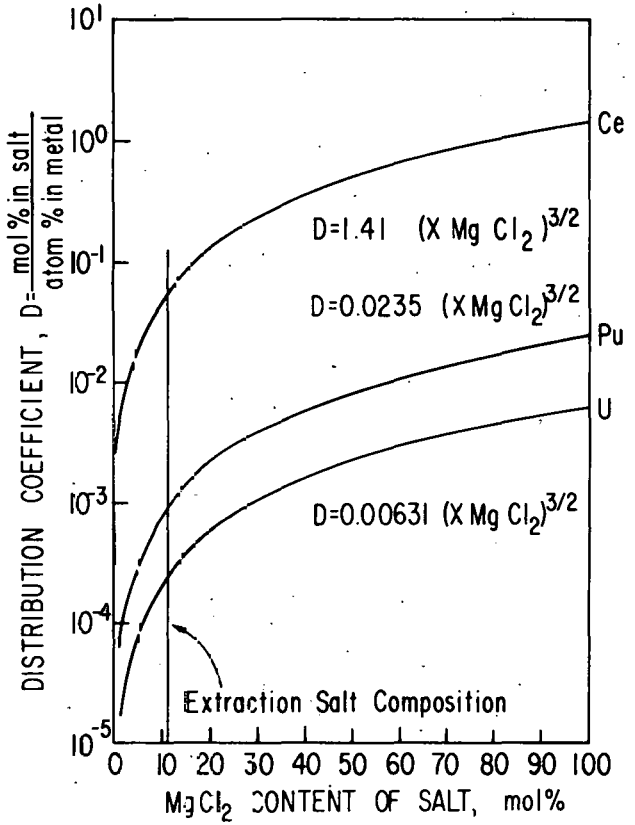

Fig. 10. Estimated Distributions of Cerium, Plutonium, and Uranium between $CaCl_2$-KCl-$MgCl_2$ Salt and Zn-20 at. % Mg Alloy at 750°C

A fairly high removal of FP-3 elements can be achieved with multiple contacting--especially if high recovery of plutonium is not a requirement. To enhance diversion resistance and proliferation resistance, about 10% of the FP-3 elements are removed. The remaining 90% of the FP-3 elements follow plutonium through subsequent process steps. This mode of operation imposes a significant recycle of FP-3 to the reactor. The 10% of FP-3 elements removed must equal the amount of FP-3 elements generated as fission products in each pass through the reactor.

To ensure that FP-3 removals are not excessive, the process operation is modified by transferring a small amount (11%) of the donor alloy to the FP-3 donor alloy crucible A-3. At this point, the extraction salt is transferred to the donor alloy crucible A-3 and equilibrated with the donor alloy. Repeated cycling of the extraction salt may result in a fairly high removal of FP-3 elements from this small amount of donor alloy. However, when the donor alloy is returned to the remaining 89% of the alloy in vessel P-3, it is immediately recontaminated.

Repeated transfers of donor alloy to the FP-3 donor alloy crucible for FP-3 removal would be possible. However, because of backmixing of the cleaned donor alloy with FP-3-contaminated donor alloy, it would be difficult to remove sufficient FP-3 elements to make the plutonium product attractive for diversion and/or proliferation.

Just prior to rotation of the crucible from the FP-3 donor position to the next position, the oxide reduction salt and a small amount of donor alloy are transferred to reduction phase separator A-2. The crucible, now free of salt, is rotated to the next position.

(h) FP-3 Removal Step

Donor metal from the FP-3 donor storage position is transferred to A-3. Extraction salt from A-4 is transferred to A-3. During equilibration of the phases by mixing, the FP-3 elements are taken up by the extraction salt. Plutonium, uranium, and the FP-4 elements remain in the donor alloy. After equilibration is complete, the extraction salt is transferred back to A-4 and the donor alloy is returned to FP-3 donor storage. Salt and metal heels are maintained in A-3 to facilitate clean separations of salt and metal phases.

(i) FP-3 Acceptor Vessel

Extraction salt from FP-3 donor A-3 is transferred to FP-3 acceptor A-4. The acceptor alloy is transferred from vacuum distillation to A-4. Makeup magnesium or calcium is added directly to A-4. During equilibration of the salt and metal phases by mixing, the FP-3 chlorides in the salt are reduced by calcium for the zinc distillation option or by magnesium for the salt transport option. The reduced FP-3 elements are taken up by the acceptor alloy, and the $CaCl_2$ or $MgCl_2$ reaction product is taken up by the salt. After equilibration is complete, the salt and metal phases are allowed to disengage. Acceptor alloy is transferred to vacuum distillation D-1. To facilitate phase separations, salt and metal heels are maintained in A-4.

(j) U-Donor and U-Pu Donor Theory

Coprocessing of Uranium and Plutonium by the Salt Transport Process. Uranium, plutonium, and FP-3 elements are separated from the FP-4 elements in the donor alloy by the salt transport process.

A salt transport procedure for uranium is illustrated schematically in Fig. 11. Metallic uranium, which is initially present in the donor alloy, is oxidized and extracted into the transport salt. The FP-4 and structural metals remain in the donor alloy:

$$U(\text{donor alloy}) + 3/2\ MgCl_2(\text{salt}) \rightarrow UCl_3(\text{salt}) + 3/2\ Mg(\text{donor alloy}) \quad (6)$$

When the transport salt containing the UCl_3 is contacted with the acceptor alloy, the reverse reaction takes place:

$$UCl_3(\text{salt}) + 3/2\ Mg(\text{acceptor alloy}) \rightarrow U(\text{acceptor alloy}) + 3/2\ MgCl_2(\text{salt}) \quad (7)$$

Therefore, the net reaction is:

$$U(\text{donor alloy}) + 3/2\ Mg(\text{acceptor alloy}) \rightarrow U(\text{acceptor alloy}) + 3/2\ Mg\ (\text{donor alloy}) \quad (8)$$

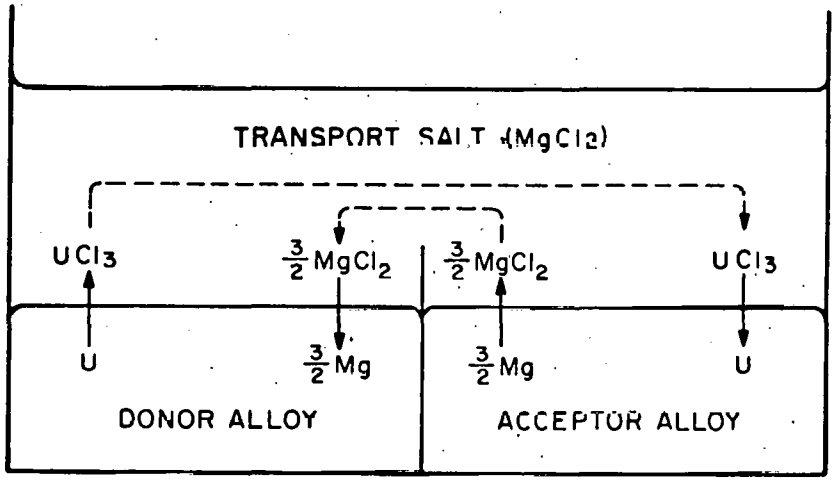

Fig. 11. Schematic Representation of the Salt Transport Process

Magnesium chloride consumed at the donor alloy by the oxidation of uranium and plutonium is regenerated at the acceptor alloy by magnesium reduction of UCl_3 or $PuCl_3$. Thus, in the salt transport operation the beginning and end salt compositions are constant and the salt may be reused indefinitely. For each mole of uranium transferred from the donor alloy to the acceptor alloy, 1.5 mol of magnesium are transferred in the

opposite direction. The increasing concentration of magnesium in the donor alloy and the magnesium depletion in the acceptor alloy must be taken into account in the design of a practical process.

When reaction 8 has reached equilibrium, both alloys are in equilibrium with the transport salt, and the ratio, R, of uranium in solution in the acceptor and donor alloys is equal to the ratio of the distribution coefficients of uranium for each alloy and the salt:

$$R = \frac{\text{at. \% U in acceptor alloy}}{\text{at. \% U in donor alloy}} = \frac{D(\text{donor alloy})}{D(\text{acceptor alloy})} \qquad (9)$$

The transfer of a solute (e.g., uranium or plutonium) from the donor alloy to the acceptor alloy is achieved by circulating the transport salt between the two liquid alloys. Uranium and plutonium have limited solubilities in several usable alloys. If not all of the uranium present in the transport salt-donor alloy system is in solution, the fraction of the total uranium present that is transferred to the acceptor alloy during each cycle of the transport salt is less than would be the case if all uranium present was in solution. Therefore, the limited solubility of uranium in the donor alloy increases the number of cycles of transport salt required to transfer a given fraction of the uranium to the acceptor alloy. The quantity of uranium transferred from the donor alloy to the acceptor alloy during each cycle will be constant (assuming that equilibrium is established in the acceptor alloy) until sufficient uranium has been transferred so that the amount of uranium remaining in the donor alloy is completely in solution.

If the uranium has a limited solubility in the acceptor alloy, the acceptor alloy will become saturated after a few cycles of the transport salt and the amount of uranium back-transferred to the donor alloy will reach a constant value. This constant value is lower with a saturated acceptor alloy than it would be if the amount of uranium in solution in the acceptor increased with each cycle of the transport salt. The overall effect of limited solubility in the acceptor alloy is to decrease the number of transport salt cycles needed to transfer a given fraction of uranium. The maximum possible fraction transferred may also be increased by limiting the uranium solubility in the acceptor alloy. A low solubility of uranium in the acceptor alloy can be used to compensate for a large value of the distribution coefficient.

The fraction of the uranium initially present in the transport salt-donor alloy system that may be transferred to the acceptor alloy may be increased if the uranium present initially exceeds the solubility. The principles that govern the rate of transfer of uranium also apply to the rate of transfer of plutonium and the impurity elements (FP-3 and FP-4) present in the donor alloy.

Molten Salt-Liquid Alloy Systems for the Salt Transport of Uranium and Plutonium. The rate of uranium or plutonium transport from a donor alloy to an acceptor alloy depends upon (1) their distribution

coefficients betweeen each alloy and the transport salt and (2) their solubilities in the two alloys. Therefore, distribution coefficients and solubilities of uranium and plutonium in various systems of process interest were investigated experimentally [KNIGHTON-1969B]. The distribution coefficients of uranium and plutonium between molten $MgCl_2$ and liquid Cu-Mg and Zn-Mg alloys at 800°C are shown in Fig. 12. To provide operational flexibility, the 78 mol % $MgCl_2$ - 22 mol % MgF_2 eutectic, which melts at 628°C (Fig. 13) is used rather than pure $MgCl_2$. Distribution coefficients are assumed to be the same for both salts.

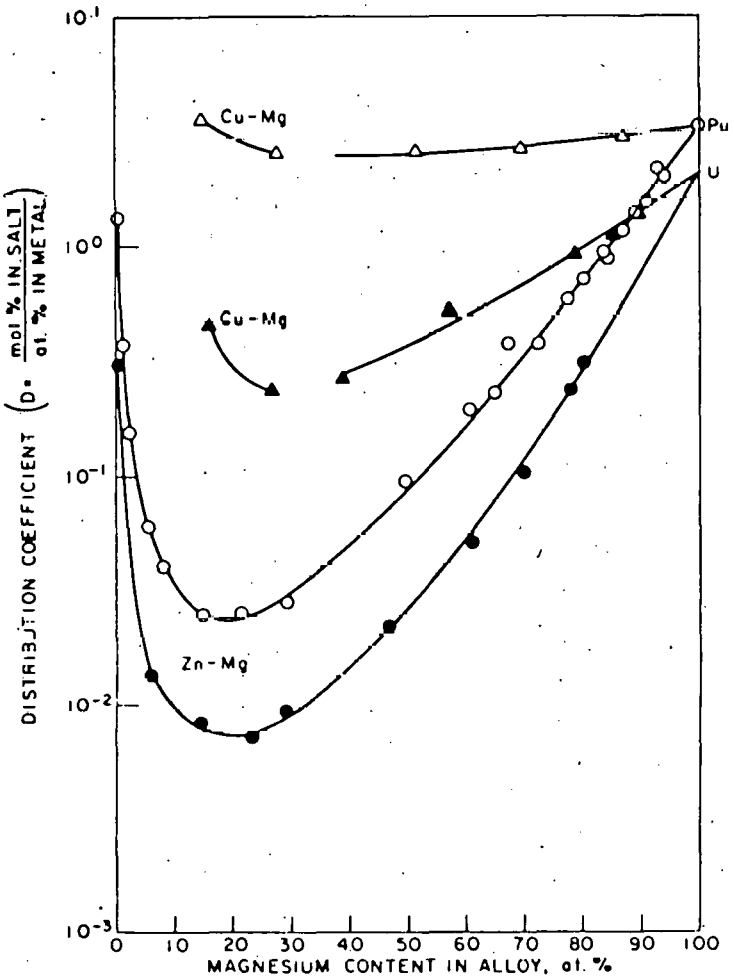

Fig. 12. Distribution of U and Pu between $MgCl_2$ Salt and Cu-Mg and Zn-Mg Alloys at 800°C [KNIGHTON-1969B]

In general, as the magnesium content of the alloy is increased from a near-zero initial value, the distribution coefficients decrease at first, pass through a minimum, and then increase (Fig. 12). The values of the distribution coefficients shown in Fig. 12 are nearly independent of the plutonium or uranium concentration in the alloy.

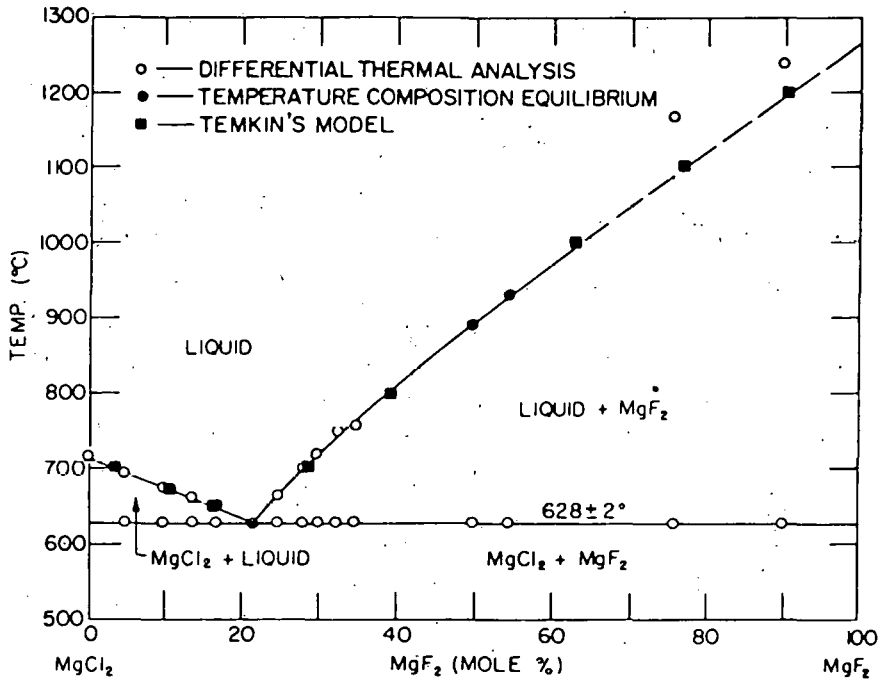

Fig. 13. Liquidus-Temperature Diagram of the $MgCl_2$-MgF_2 Binary System [SHARMA]

The solubilities of uranium in liquid Cu-Mg and Zn-Mg alloys and of plutonium in liquid Zn-Mg alloys at 800°C are shown as a function of the magnesium content of the liquid alloy in Fig. 14. Values of the solubility of plutonium in liquid Cu-Mg alloys [KNOCH] are so large that solubility is not an important factor in limiting the use of Cu-Mg alloy as a donor for plutonium. The discontinuties of the distribution coefficient and solubility curves for the Cu-Mg alloy system in Figs. 12 and 15 represent regions where liquids of these compositions do not exist at 800°C.

The amount of uranium or plutonium that can be transferred in each cycle of the transport salt between the donor and acceptor alloys depends upon the amount of salt transferred and the uranium or plutonium content of the salt. At equilibrium, the uranium or plutonium content of the transport salt is the product of the uranium or plutonium content of the alloy and the distribution coefficient.

$$\text{mol \% M(salt)} = \text{at. \% M(metal)} \times D \qquad (10)$$

To obtain a large quantity of uranium or plutonium in the salt equilibrated with the donor alloy, both the solubility and distribution coefficients in the donor alloy-salt system should have large values. Conversely, to obtain a small uranium or plutonium content in salt that has been equilibrated with the acceptor alloy, both the solubility and distribution coefficients in the acceptor alloy-salt system should have small values. Mass transfer of uranium or plutonium and magnesium between the

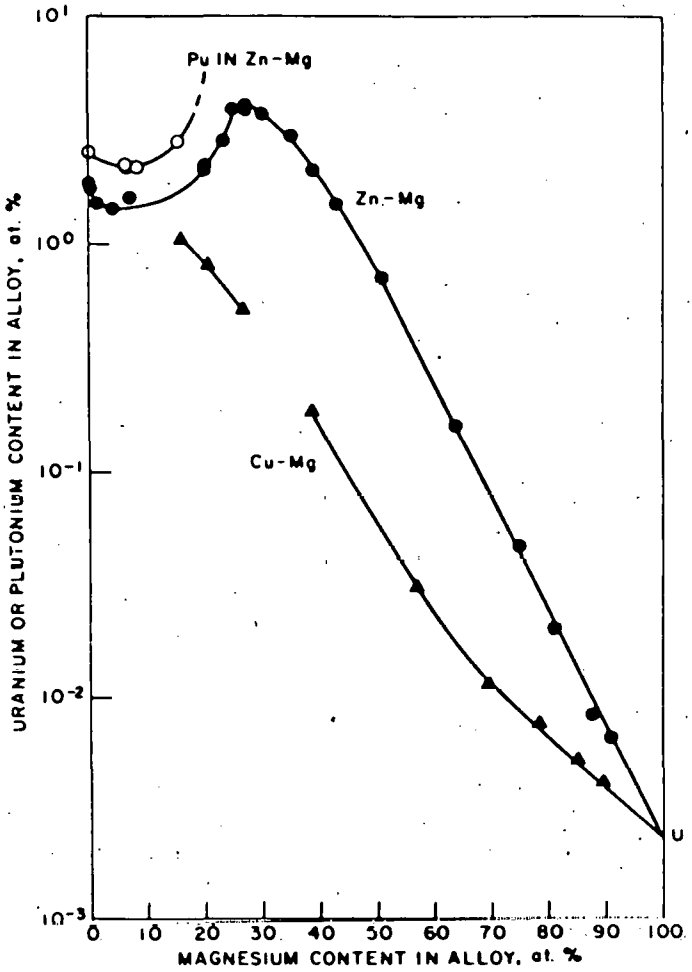

Fig. 14. Solubility of U and Pu in Cu-Mg and Zn-Mg Alloys at 800°C [KNIGHTON-1969B]

donor and acceptor alloys stops when the equilibrium uranium or plutonium content of the transport salt is the same above both alloys.

The maximum uranium and plutonium contents of molten $MgCl_2$ in equilibrium with saturated liquid Cu-Mg and Zn-Mg alloys at 800°C are given in Fig. 15. These curves may be used to determine the compositions of donor and acceptor alloys for uranium and plutonium. For example, at 800°C, only a low-magnesium-content (about 16 at. %) Cu-Mg alloy would be a practical donor for uranium, while Zn-Mg alloys with either low (about 15 at. %) or high (>60 at. %) magnesium contents would be practical acceptor alloys for uranium. The compositions of the most promising donor and acceptor alloys of those studies for uranium and plutonium are summarized in Table 16. At 800°C the Cu-16 at. % Mg alloy is a donor for both uranium and plutonium, while the Zn-10 at. % Mg alloy is an acceptor for both uranium and

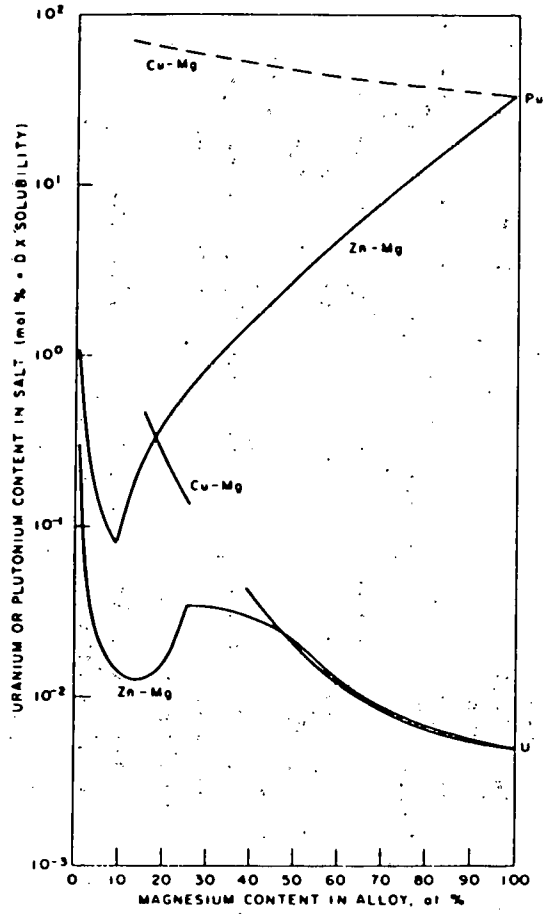

Fig. 15. Maximum Concentration of U and Pu in $MgCl_2$ Salt in Equilibrium with U- or Pu-Saturated Cu-Mg and Zn-Mg Alloys at 800°C [KNIGHTON-1969B]

plutonium. It is also evident from Table 12 that the Cu-16 at. % Mg donor alloy is a more effective donor for plutonium than for uranium because of the relatively low solubility of uranium.

Uranium transfers at a lower rate than plutonium because (1) uranium has a lower solubility than plutonium in the donor alloy and (2) uranium has a lower distribution coefficient than plutonium in the donor alloy-salt system. This difference in the rate of transfer is very desirable because it provides a means of enriching the plutonium content of the product by terminating the circulation of the transport salt before complete uranium transfer has occurred.

Table 12. Composition of Donor and Acceptor Alloys for Uranium and Plutonium Salt Transport Using $MgCl_2$ at 800°C. Maximum Conten:

Alloy	D		Solubility, at. %		In Salt, mol %		Classification[a]	
	Pu	U	Pu	U	$PuCl_3$	UCl_3	Pu	U
Cu-16 at. % Mg	3.5	0.45	high	1.05	high	0.46	Donor[b]	Donor
Zn-10 at. % Mg	0.035	0.0094	2.3	1.5	0.080	0.014	Acceptor	Acceptor

[a]All of the salt-alloy systems shown are acceptors for the FP-4 metals.

[b]When there is high plutonium solubility, the distribution coefficients provide the basis for evaluating the relative donor properties of the alloys.

Uranium and plutonium are separated from the FP-4 metal fission product elements by the use of a Cu-16 at. % Mg donor alloy, a molten $MgCl_2$ transport salt, and a Zn-10 at. % Mg acceptor alloy at a temperature of 800 to 900°C [KNIGHTON-1969A, 1969B]. The operation of this donor alloy may be illustrated by referring to the copper-rich region of the Cu-Mg-U system shown in Fig. 16. This representation must be regarded as tentative because it was constructed from the Cu-U and Cu-Mg binary diagrams and from limited data from the Cu-Mg-U ternary system. Point M is a eutectic in the Cu-U binary alloy. Point G is an eutectic in the Cu-Mg binary alloy. Point N is estimated to be the ternary Cu-Mg-U eutectic. Hence, the curve M-C-N describes a eutectic valley. Point D is the composition of the liquidus of the Cu-Mg binary at 800°C. Point C is the 800°C liquidus on the eutectic valley, and C-D is the 800°C liquidus isotherm between the eutectic valley and the Cu-Mg binary. Line A-B is an operating line that is

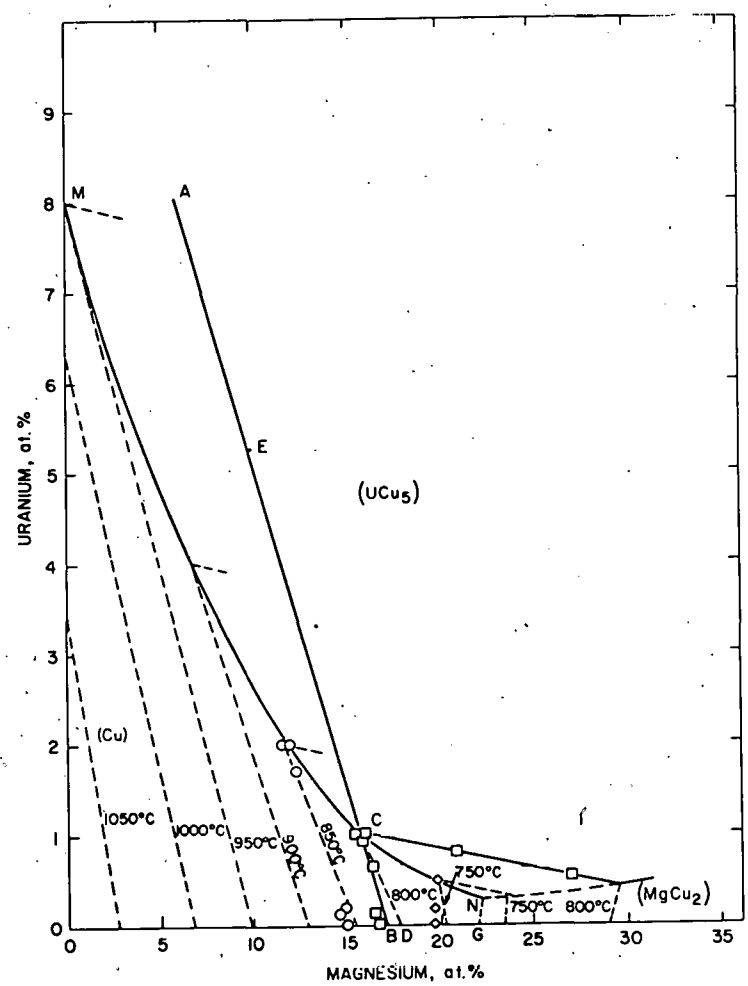

Fig. 16. Tentative Liquidus Surface for the Copper-Rich Region of the Cu-Mg-U Phase Diagram [KNIGHTON-1969B] (see text for discussion of A, B, C, etc.)

the path that the bulk composition of the donor alloy will follow as transport of uranium takes place. The line represents the change in bulk composition that results from depletion of the uranium by $MgCl_2$ oxidation and the resultant buildup of magnesium in the donor alloy. These composition changes are related by the equation:

$$U + 3/2\ MgCl_2 \rightarrow UCl_3 + 3/2\ Mg \qquad (11)$$

which indicates that 1.5 moles of magnesium are introduced into the donor alloy for each mole of uranium removed. Any point, E, lying on the operating line represents an initial bulk composition of the donor alloy.

Point B is the bulk composition of the donor alloy upon completion of uranium transport. At point E, the equilibrium phases present are a solid phase containing uranium, which is believed to be the intermetallic compound, UCu_5 and a liquid phase of composition C. As uranium transport proceeds, the bulk alloy composition moves along the operating line, A-B, from Point E toward Point C. The compound UCu_5 dissolves, replacing the uranium extracted from the liquid donor alloy by the transport salt:

$$UCu_5(solid) \rightarrow U(Cu\text{-}Mg\ liquid) + 5Cu(Cu\text{-}Mg\ liquid) \qquad (12)$$

The copper released by dissolution of UCu_5 combines with the magnesium that is introduced by uranium reduction of $MgCl_2$ to produce additional liquid of the eutectic composition (Point C) at the operating temperature.

Thus, the composition of the liquid phase remains constant as the ratio of liquid to solids increases.

When Point C is reached, all of the solids have been consumed. As transport of uranium continues, the bulk composition follows the operating line from Point C to Point B, and Cu-Mg solid solution is formed. The composition of the liquid phase in equilibrium with the Cu-Mg solid solution is represented by the 800°C liquidus isotherm, C-D. During this last phase of uranium transport, all of the uranium in the donor alloy is in solution.

To control the magnesium buildup in the donor alloy during uranium transport, the operating line should pass through the liquidus on the eutectic valley at the operating temperature. This liquidus composition on the eutectic valley is the composition the liquid phase will have as UCu_5 dissolves. Under the above conditions, the system provides (1) control of magnesium buildup in the donor and (2) operation at optimum donor compositions. The optimum donor compositions provide maximum uranium solubility and the highest uranium distribution coefficient at the specified operating temperature during the transport of uranium.

Because all of the plutonium is in solution in the donor alloy and because the distribution coefficient for plutonium is greater than that for uranium, plutonium transfers at a faster rate than uranium does. Calculations show that after six cycles of an appropriate amount of transport salt between the donor and acceptor alloys, 99+% of the initial

plutonium and 52% of the initial uranium are transferred. About 26 cycles are required for 99% uranium transfer. Thus, plutonium enrichment may be achieved by limiting the number of salt cycles between the Pu-U donor and the Pu-U acceptor; the transport salt may then be diverted to a second acceptor to complete the transfer of uranium.

As UCl_3 and $PuCl_3$ are transferred to the acceptor, both are reduced by magnesium, and the plutonium and uranium metal reduction products are taken up by the acceptor alloy. By proper adjustment of the amount of acceptor alloy, the uranium and plutonium reduced will rapidly exceed their solubility limits and will precipitate as intermetallic compounds--presumably as U_2Zn_{17} and Pu_2Zn_{17}. Some coprecipitation of plutonium with uranium is expected and is desirable. Coprecipitation of plutonium with uranium will lower the plutonium content in solution in the acceptor alloy, which in turn will lower the back-transfer of plutonium via the salt to the donor alloy.

Transfer of uranium and plutonium from the donor to the salt may be enhanced by raising the temperature of the donor-salt system to about 850°C. The subsequent transfer of uranium and plutonium from the salt to the acceptor may be enhanced by lowering the temperature of the acceptor-salt system to about 700°C.

(k) U-Pu Donor Unit Operations--Equipment and Operation

U-Pu Donor. The crucible containing U, Pu, FP-3, and FP-4 elements in the donor alloy is rotated from the FP-3 donor storage position to the U-Pu donor position. Salt and a donor alloy heel are transferred from salt-donor heel storage A-6 to the crucible at the U-Pu donor position. The salt and metal phases are equilibrated by mixing. Plutonium, uranium, and the residual FP-3 fission product elements are oxidized by $MgCl_2$ in the salt. The resultant chlorides of plutonium, uranium, and the FP-3 elements are taken up by the salt. The magnesium metal reaction product is taken up by the donor alloy.

After equilibration is complete, the phases are allowed to disengage. The salt is transferred from the U-Pu donor position to the U-Pu acceptor A-5. To prevent cross-contamination of donor alloy into the acceptor alloy, the transfer line is positioned above the salt metal interface so that only the salt is transferred.

In the salt transport process, the salt is circulated between the donor and acceptor alloys a sufficient number of times to result in proper plutonium enrichment of the coprocessed fuel for recycle of the fuel back to the reactor. After the desired number of salt cycles are completed, the salt and a small donor alloy heel are transferred from U-Pu donor to salt donor heel storage A-6. The crucible is now ready for rotation to the U donor position.

U-Donor. In the prior U-Pu donor salt transport operation, 99+% of the plutonium and FP-3 elements and about one-half of the uranium are removed from the donor alloy. At the U donor position, most of the remaining uranium is separated from the donor alloy containing the FP-4

elements. Salt and donor alloy heel are transferred from salt-donor heel storage A-8 to U donor. The salt and metal phases are equilibrated by mixing. Uranium is oxidized by $MgCl_2$ in the salt. The resultant UCl_3 is taken up by the salt, and the magnesium reaction product is taken up by the donor.

After equilibration is complete, the phases are allowed to disengage. The salt is transferred from the U donor to the U acceptor A-7. The inlet to the transfer line is positioned above the salt-metal interface to avoid transfer of donor alloy with the salt. To accomplish the desired removal of uranium from the donor alloy, the salt must be circulated a number of times between the donor and the acceptor alloys. At completion, the salt and the spent donor alloy are transferred from the U donor position to salt-donor heel storage A-8. The inlet for the transfer line is positioned at the bottom of the crucible to maximize transfer of salt and donor alloy.

U-Pu Acceptor. Salt from U-Pu donor, zinc-magnesium alloy from vacuum distillation D-3, and make-up magnesium metal are fed to U-Pu acceptor A-5. The salt and metal phases are equilibrated by mixing. The chlorides of uranium, plutonium, and the FP-3 elements contained in the salt are reduced by magnesium. The metal products (uranium, plutonium, and FP-3 elements) are taken up by the acceptor alloy. The $MgCl_2$ reaction product is taken up by the salt. After equilibration is complete, the phases are allowed to disengage. The inlet to the transfer line is positioned above the salt-metal interface. The salt is transferred back to the U-Pu donor, leaving a small salt heel on top of the acceptor alloy.

To facilitate plutonium transfer to the acceptor alloy and to minimize plutonium recycle via the salt back to the donor alloy, the temperature of the acceptor alloy is 700°C. After the desired number of salt cycles and after the salt has been transferred back to the U-Pu donor, the temperature of the acceptor alloy is increased to 800°C to dissolve Pu_2Zn_{17} and U_2Zn_{17} intermetallic compounds that were precipitated at 700°C.

The liquid acceptor alloy containing uranium, plutonium, and FP-3 elements is transferred to vacuum distillation D-3. To facilitate phase separation, heels of salt and metal phases are left in the crucible.

U Acceptor. Salt from the U donor position, zinc-magnesium alloy from vacuum distillation D-4, and magnesium metal make-up are fed to U acceptor A-7. The salt and metal phases are equilibrated by mixing. Uranium chloride in the salt is reduced by magnesium in the acceptor. The resultant uranium metal product is taken up by the acceptor alloy and the magnesium chloride reaction product is taken up by the salt. After equilibration is complete, the phases are allowed to disengage. After cycling of salt between the donor and acceptor alloys is completed, the inlet to the transfer line is positioned above the salt-metal interface to avoid transfer of acceptor alloy with the salt, and the salt is returned to the U donor.

Liquid acceptor alloy containing uranium is transferred from U acceptor A-7 to vacuum distillation D-4. To facilitate phase separation, salt and metal heels are maintained in the acceptor crucible.

U-Pu Salt-Donor Heel Storage. To avoid cross-contamination of transport salts, at the end of U-Pu salt transport process the salt and a small metal heel are transferred from U-Pu donor to salt-donor heel storage A-6. The inlet to the transfer line is positioned just below the salt-metal interface. This salt and metal heel are available for transfer back to the U-Pu donor after a new batch of donor alloy is rotated to the U-Pu donor position.

U Salt-Donor Heel Storage. This vessel acts as a storage vessel for transport salt at the end of uranium salt transport. The transport salt and the spent donor containing the FP-4 elements are transferred from the U donor to U salt-donor heel storage. Spent donor alloy is transferred from U salt-donor heel storage A-8 to vacuum distillation D-5. A small metal heel is retained in A-8. The transport salt and small metal heel are available for transfer back to the U donor after a new batch of donor alloy is rotated to the U donor position.

(1) U-Pu Donor Unit Operations--Other Support Operations

Electrolysis. This operation is common to both the zinc distillation and salt transport options. Oxide reduction salt contains CaO which must be removed prior to recycle of the salt back to oxide reduction. Electrolysis is proposed for removal of CaO. Salt from reduction phase separator A-2 is transferred to electrolysis. A consumable graphite anode is used. Oxygen formed at the anode reacts with the graphite, and the resultant CO and CO_2 are vented from the cell. The reduction feed alloy (Cu-Mg) is used as a molten cathode. Calcium metal collects at the cathode and is taken up by the reduction alloy.

At the end of electrolysis, a salt bleed stream for FP-2 elements is transferred from electrolysis to waste disposal. The remainder of the salt and the Cu-Mg-Ca reduction alloy are transferred to reduction phase separator A-2.

To minimize polarization at the electrodes, the salt bath is mixed during electrolysis.

Vacuum Distillation. Vacuum distillation operates to separate volatile process solvents from product and waste streams. The basis for the separation is differences in the vapor pressures of the elements. Table 13 gives vapor pressures of the major elements present in the process (zinc, magnesium, calcium, copper, chromium, plutonium, iron, nickel, and uranium) over the temperature range, 600 to 1400°C.

Feed to vacuum distillation operations is solid or liquid metal. Overhead product from vacuum distillation is removed from the condenser as a liquid on a batch basis. Bottom product from vacuum

Table 13. Vapor Pressure (mm Hg) of Selected Elements at 600-1400°C

	600°C	700°C	800°C	900°C	1000°C	1100°C	1200°C	1300°C	1400°C
Zn[NESHMEYANOV]	1.116×10^{1}	6.52×10^{1}	2.65×10^{2}	8.46×10^{2}	2.25×10^{3}	5.20×10^{3}	1.07×10^{4}	2.02×10^{5}	--
Mg[NESHMEYANOV]	--	7.13×10^{0}	3.75×10^{1}	1.49×10^{2}	4.75×10^{2}	1.23×10^{3}	3.01×10^{3}	6.37×10^{3}	--
Ca[NESHMEYANOV]	--	1.07×10^{-1}	7.01×10^{-1}	3.34×10^{0}	1.24×10^{1}	3.82×10^{2}	1.00×10^{2}	2.35×10^{2}	--
Cu[HONIG]	--	--	--	--	6×10^{-5}	5×10^{-4}	3.5×10^{-3}	2×10^{-2}	8×10^{-2}
Cr[HONIG]	--	--	--	--	1.7×10^{-6}	2.3×10^{-5}	2.3×10^{-4}	2×10^{-3}	1×10^{-2}
Pu[MULFORD]	--	--	3.8×10^{-9}	8.74×10^{-8}	1.28×10^{-6}	1.23×10^{-5}	9.27×10^{-5}	5.24×10^{-4}	2.41×10^{-3}
Fe[HONIG]	--	--	--	--	3×10^{-7}	5×10^{-6}	7×10^{-5}	6×10^{-4}	2.5×10^{-3}
Ni[HONIG]	--	--	--	--	1.3×10^{-7}	2×10^{-6}	2.5×10^{-5}	2.4×10^{-4}	1.5×10^{-3}
U[ACKERMANN]	--	--	--	--	--	--	3.04×10^{-9}	2.57×10^{-8}	3.24×10^{-7}

distillation of decladding alloys will be a stainless steel sponge. The steel crucible for the distillation operation will also be the primary containment vessel of the process wastes. The vessel will be mechanically removed from the furnace. No attempt will be made to remove the stainless steel sponge and reuse the crucible.

There are four materials subjected to vacuum distillation operations in the complete process.

(1) the decladding waste plus the FP-3 acceptor metal
(2) the U-Pu acceptor alloy containing Zn-Mg-U-Pu-FP-3
(3) the uranium acceptor alloy containing Zn-Mg-U-Pu
(4) the spent uranium donor alloy containing Cu-Mg-U-FP-4

A major vacuum distillation operation is separation of zinc from the zinc-stainless steel decladding alloy. The data in Table 13 show that zinc would distill easily at 900°C under vacuum, but that the steel constituents (iron, chromium, and nickel) would not volatilize, but remain behind in the still pot. The acceptor alloy from the FP-3 removal and the FP-4 product from copper electrorefining are added to the stainless steel decladding alloy. By this addition, the FP-3 and FP-4 fission product metals are alloyed with stainless steel during vacuum distillation in a presumably stable matrix for both interim and long-term storage.

The products from the salt transport process are recovered from vacuum distillations (2) and (3) above. Again, the data in Table 27 show that zinc and magnesium will volatilize and be removed overhead, while the uranium and plutonium remain behind. The bottom product from the U-Pu acceptor alloy will be removed as molten U-Pu-FP-3 alloy, and the bottom product from the uranium acceptor alloy will be molten uranium with perhaps trace amounts of plutonium. The bottom product from the vacuum distillation (0-5) of the spent uranium donor alloy will be removed as a liquid Cu-U-FP-4 alloy and will be cast into anodes for electrorefining of feed.

(2) Salt Transport Process Design

(J. E. Hicks* and J. B. Knighton*)

During the first quarter of FY 1979, considerable effort was devoted to advancing the design for a conceptual pyrochemical plant for coprocessing spent FBR fuel by the salt transport method. Much effort was also expended in providing input to the ORNL study for evaluating pyrochemical processing as an acceptable, proliferation-resistant process for coprocessing spent FBR nuclear fuel. During this endeavor, some effort was spent in updating flow diagrams for Argonne's zinc transport option.

The block flow diagram for the salt transport process (Fig. 7) has been defined and will remain as is to serve as a basis for design.

---

*Rockwell International-Rocky Flats.

The design criteria for the Pyrochemical Reprocessing Facility using the salt transport process were expanded and updated to cover proliferation and environmental considerations and to allow flexibility in choosing a baseline process. General design criteria are shown in Table 14. More specific criteria for each unit operation are shown in Table 15.

Table 14. General Design Criteria. Salt Transport Process

1. Uranium and plutonium will be coprocessed for proliferation resistance.
2. Recovery of plutonium must exceed 99%.
3. Plutonium enrichment must be sufficient for fuel cycle (10-20% Pu).
4. Fission product removal incomplete to enhance diversion-resistance (1200 rad at 3 ft).
5. Simple and reliable process operations must be used.
6. Types of process operations minimized.
7. All process operations must be remote and suitable for canyon operations.
8. All fission products must be contained.
9. Generation of process wastes must be minimized.
10. All process materials must be contained at process conditions.
11. Addition of non-fission product impurities avoided.
12. High gamma emitters retained with U-Pu product.
13. Maximize recycle of reagent.
14. The mixed-oxide product must be refabricable.
15. Handling of solids in the process must be avoided. (Keep process streams liquid where possible.)
16. Process must be environmentally acceptable.
17. Feed rate of 1/2 Mg/day of mixed-oxide fuel.
18. Recover plutonium contained in one subassembly (core and associated axial blanket or radial blanket).
19. The process must be critically safe for the designed operation.

(contd)

Table 14. (contd)

20. Process volumes will be established by the maximum subassembly size.

21. Energy use by the facility shall be minimized.

22. The feed to the process will be FBR or FFTF fuel with 1000-MW day burnup and 10-15 day cooldown.

23. The midsection of the fuel bundle, containing fission products and U/PuMOX, shall be reprocessed.

24. Process solvents will be kept with uranium and plutonium product until just prior to refabrication.

25. Wastes will be fixed in a retrievable form suitable for ultimate long-term storage.

26. Capability of determining phase levels and interface is required.

27. Remote maintenance will be provided for but shall not be suitable for performing equipment modifications.

28. Equipment placement must be such that no additional equipment can be installed.

29. The maximum volume of the liquid in any vessel should not exceed 75% of the total volume.

30. Each event within each operation will be programmed to occur in the proper sequence by a hard-wired sequence panel. No built-in provisions shall be available to allow altering the operations on the sequence panel (other than emergency shutdown).

31. Normal operation will be at atmospheric pressure in an inert gas (argon, xenon, krypton). Adequate pressure and vacuum will be required to move liquid metals and molten salts between vessels.

32. Materials of containment, stirrers, and transfer lines must be of a material that is resistant to corrosion by the materials contained at operating conditions.

33. In areas where proliferation capabilities exist, equipment parts shall not be interchangeable with other equipment.

34. Temperature control must be provided.

(contd)

Table 14. (contd)

35. The capability of transferring molten salt and liquid metal phases between vessels must be provided.

36. Phase separation efficiency must be high (though varying in different operations).

37. Accountability of feed, product, waste, and in-process streams must be provided.

38. Reagent specifications must be established.

39. The required utilities shall be specified (steam, electric, fuel, etc.), e.g.: steam - xx lb/h, xxx lb steam
elec. - xxx V, xx A, xxx kW
fuel - lb/h CH_4 equivalent

40. The facility shall be able to withstand the following without major damage or release of radioactive materials to the environment.

    1. 10.0-ton TNT blast (direct)
    2. 1000-y flood
    3. 100-y storm, such as a tornado or hurricane
    4. Worst possible case fire

41. Withstand 100-y or Richter 8.5 earthquake, whichever is greater, without release of contaminants to the environment.

42. Cast-in-place concrete shall have 28-d compressive strength of at least 30,000 psi.

Table 15. Specific Operational Design Criteria
(See also Table 14 and Fig. 7)

A. DECLADDING

1. Hardware below the active section of subassembly removed prior to processing.

2. Dissolve the cladding and hardware associated with the active section. The top hardware (not immersed) is discarded after the active section is dissolved.

3. The cladding is dissolved in liquid zinc. A molten cover salt (1) reduces zinc dusting and (2) captures iodine released during decladding.

4. Maximum stainless steel loading in zinc, 20%.

5. Maximum operation temperature, 800°C.

6. The top and bottom hardware is to be discarded along with the stainless steel (SS) remaining after vacuum distillation of the decladding stream.

7. A phase separation of the zinc and cladding from the oxides will be made.

8. All fission products must be contained. Xenon, krypton, and tritium must be contained in the cover gas. Iodine must be contained in the cover salt.

9. Initial breaching of the cladding must occur in the molten zinc phase.

10. Provisions will be made to avoid splashing due to venting of gases during decladding.

11. Removal of the zinc-cladding must be maximized, i.e., a minimum of heel left.

12. Prior to reduction of oxide fuel, the zinc-cladding heel must not exceed 5% of the total weight.

13. Excess zinc may be required to get good coverage of the subassembly during decladding.

14. Operations that must be provided include:

    a. An overhead lock assembly to interface with a transfer coffin for introduction of a subassembly into the process.

(contd)

Table 15. (contd)

b. Venting and containment of the FP-1 gases.

c. A transfer line with the opening positioned at the bottom of the process vessel for:

(1) removal of liquid zinc and cladding, as well as cover salt.
(2) introduction of cover salt and zinc.

The transfer lines should be of a material that withstands corrosion by liquid zinc at the required operating temperature.

The lines should be adequately heated to maintain the materials being transferred in a fluid state and thus prevent plugging by freezing.

d. Adequate heating capability to achieve the required operating temperatures.

B. REDUCTION

1. Operating temperature of 850°C maximum.

2. An excess of 10 wt % calcium will be added to ensure complete reaction.

3. A cover salt, like that used in decladding, will be provided and used for reduction. Any residual iodine from the fuel oxide must be captured by the cover salt.

4. No phase separation of molten salt from the liquid metal alloy will be made in the reduction stage.

5. The contents must be adequately agitated to effect optimum contact of the salt and metal phases.

6. Because of solids on the vessel bottom when reduction begins, the stirrer must be capable of being raised in order to agitate. The agitator would be lowered during reduction as the solids are reduced.

7. There must be the capability for adding calcium metal to the reduction vessel. (Note: A preliminary melting and transfer pot might be made available between the electrolysis vessel and the reduction vessel to allow liquid transfer of calcium to the reduction vessel.)

(contd)

Table 15. (contd)

8. Operations that must be provided include:

   a. An agitator capable of providing intensive mixing to ensure optimum reduction of the oxides.

      The agitator must be capable of being raised and lowered during mixing while maintaining an adequate seal (1) to prevent loss of fission gases and (2) to allow necessary pressure transfer of molten salts and metals from the reduction vessel.

   b. Transfer lines with openings positioned:

      (1) near the top of the vessel for the addition of liquid calcium. (Note: alternatively, calcium may be added as a solid, although this would be undesirable from an operational standpoint.)

      (2) near the top of the vessel for the addition of molten salt and liquid alloy

      (3) at the top of the vessel for venting of the FP-1 gases

      The transfer lines should be of a material that withstands corrosion by molten salt and liquid metal. The lines should be adequately heated to maintain in a fluid state the materials being transferred and thus prevent plugging by freezing.

   c. Adequate heating to achieve the required operating temperature.

C. FP-3 DONOR STORAGE

1. The reduction salt will be transferred (to separate FP-3 elements from plutonium) with the donor alloy as the material in process moves from stage 2 to stage 3.

2. The operating temperature is 800°C.

3. Operations that must be provided include:

   a. Two transfer lines with openings located:

      (1) below the salt phase to remove only a portion of the alloy (no salt) for transfer to and from the FP-3 donor vessel

(contd)

Table 15. (contd)

(2) just below the salt phase to totally remove the salt and a small alloy heel for transfer to reduction phase storage

The transfer lines should be of a material that withstands corrosion by the liquid alloys and salts at the required operating temperature. The lines should be adequately heated to maintain the materials being transferred in a fluid state and to prevent plugging by freezing.

b. Adequate heating to achieve the required operating temperature

D. U-Pu DONOR

1. The operating temperature is 850°C.

2. The contents must be adequately agitated to effect optimum contact of the salt and metal phases. The duration of mixing must be adequate to reach equilibrium conditions of both the salt and the metal phases. Time with no agitation must be allowed to ensure adequate phase disengagement.

3. Operations that must be provided include:

a. Two transfer lines with openings located:

(1) above the salt-metal interface for transfer of only the salt to and from the U-Pu donor and U-Pu acceptor vessels

(2) below the salt-metal interface for transfer of all of the salt and a small metal heel to the salt-donor heel storage vessel and the return of the same to the new U-Pu donor

The transfer lines should be of a material that withstands corrosion by the liquid alloys and molten salts at the required operating temperature. The lines should be adequately heated to maintain in a fluid state the materials being transferred, thereby preventing plugging by freezing.

b. Adequate heating to achieve the required operating temperature.

c. An agitator capable of providing adequate mixing.

Table 15. (contd)

E. U-DONOR

1. The operating temperature is 850°C.

2. The contents must be adequately agitated to effect optimum contact of the salt and metal phases. The duration of mixing must be adequate to reach equilibrium conditions of both the salt and the metal phases. Time with no agitation must be allowed to ensure adequate phase disengagement.

3. Operations that must be provided include:

   a. Two transfer lines with openings located:

      (1) above the salt-metal interface for transfer of only the salt to and from the U donor and U acceptor vessels

      (2) below the salt-metal interface for transfer of all of the salt and a small metal heel to the salt-donor heel storage vessel and the return of the same to the new U donor

      The transfer lines should be of a material that withstands corrosion by the liquid alloys and salts at the required operating temperature. The lines should be adequately heated to maintain the materials being transferred in a fluid state so as to prevent plugging by freezing.

   b. Adequate heating to achieve required operating temperature.

   c. An agitator capable of providing adequate mixing.

F. DECLADDING PHASE SEPARATOR - A-1[a]

1. The operating temperature is 800°C.

2. Operations that must be provided include:

   a. Transfer lines with openings located:

      (1) near the top of the vessel for return of zinc from the distillation vessel, D-1[a]

      (2) just above the salt-metal interface for transfer of salt from vessel A-1[a] to A-2,[a] leaving a salt heel in A-1

(contd)

Table 15. (contd)

(3) near the top of vessel A-1 for the addition of new cover salt

(4) near the bottom of vessel A-1 for removal of metal to D-1[a]

(5) near the bottom of vessel A-1 for transfer of salt and metal to and from decladding

The transfer lines should be of a material that withstands corrosion by molten salt and liquid metal. The lines should be adequately heated to maintain the materials being transferred in a fluid state, preventing plugging by freezing.

b. A-1[a] is a satellite furnace.

c. Adequate heating to achieve the required operating temperature.

3. In order to maintain an undisrupted vacuum in D-1, the metal feed and product in transfer lines, to and from D-1[a] may have to be solidified.

G. REDUCTION PHASE SEPARATOR - A-2[a]

1. Operations that must be provided include:

a. Transfer lines with the openings positioned:

(1) near the top of the vessel for the addition of spent cover salt from vessel A-1[a]

(2) near the top of the vessel for the addition of Cu-Mg from E-2[a] and D-5[a]

(3) below the salt-metal interface for the transfer of new salt and metal to reduction

(4) above the salt-metal interface for the transfer of new salt to electrolysis, E-1[a]

The transfer lines should be of a material that withstands corrosion by molten salt and liquid metal. The lines should be adequately heated to maintain the materials being transferred in a fluid state and to prevent plugging by freezing.

(contd)

Table 15. (contd)

b. Adequate heating to achieve the required operating temperature.

c. A-2 is a satellite furnace.

H. ELECTROLYSIS - E-1[a]

1. All lines and apparatus (transfer tubes, stirring shaft, and electrodes) shall be electrically insulated from the vessel. The vessel shall be electrically insulated from its surroundings.

2. Provisions shall be made for removal of the calcium from the cell and for ensuring that oxidation of the calcium does not occur.

3. Provisions shall be made for continuously removing CO and/or CO_2 from the cover gas and ensuring complete capture of any fission products exiting with this stream.

4. Adequate mixing is required to ensure optimum circulation of the electrolyte (movement of fresh salt circulating past the electrodes at all times).

5. Operations that must be provided include:

a. An agitator capable of providing adequate mixing to ensure proper circulation of the electrolyte.

b. Transfer lines with their openings positioned

(1) near the bottom of the vessel to transfer fresh salt to A-2[a]

(2) sufficiently beneath the salt to remove an adequate bleed of salt from the vessel prior to electrolysis

(3) venting of CO and CO_2

The transfer lines should be of a material that withstands corrosion by molten salt. The lines should be adequately heated to maintain in a fluid state the materials being transferred, preventing plugging by freezing.

c. Adequate heating to achieve the required operating temperature.

d. The electrolysis vessel is a stationary satellite vessel.

(contd)

Table 15. (contd)

I. FP-3 DONOR - A-3[a]

1. The operating temperature is 800°C.

2. The contents must be adequately agitated to effect optimum contact of the salt and metal phases. The duration of mixing must be adequate to reach equilibrium conditions of both salt and metal phases. Time with no agitation must be allowed to ensure adequate phase disengagement.

3. Operations that must be provided include:

   a. Transfer lines with openings located:

      (1) above the salt-metal interface for transfer of salt to the FP-3 acceptor

      (2) below the salt-metal interface for transfer of metal only from the FP-3 donor to the FP-3 donor storage vessel

      The transfer lines should be of a material that withstands corrosion by the liquid alloys and salts at the required operating temperature. The lines should be adequately heated to maintain the materials being transferred in a fluid state, preventing plugging by freezing.

   b. The FP-3 donor is a satellite furnace in a fixed position.

   c. An agitator capable of providing adequate mixing.

   d. Adequate heating to achieve the required operating temperature.

J. FP-3 ACCEPTOR - A-4[a]

1. The operating temperature is 750°C.

2. The contents must be adequately agitated to effect optimum contact of the salt and metal phases. The duration of mixing must be adequate to reach equilibrium in both the salt and metal phases. Time must be allowed with no agitation to ensure adequate phase disengagement.

3. Operations that must be provided include:

   a. Transfer lines with openings located:

(contd)

Table 15. (contd).

(1) near the top of the vessel for the addition of make-up magnesium

(2) above the salt-metal interface for the transfer of salt to the FP-3 donor vessel

(3) near the top of the vessel for the addition of make-up salt

(4) below the salt-metal interface for the transfer of the acceptor alloy to distillation

The transfer lines should be of a material that withstands corrosion by the liquid alloys and salts at the required operating temperature. The lines should be adequately heated to maintain the materials being transferred in a fluid state, preventing plugging by freezing.

b. The FP-3 acceptor vessel is a satellite furnace in a fixed position.

c. An agitator capable of providing adequate mixing.

d. Adequate heating to achieve the required operating temperature.

K. U-Pu ACCEPTOR - A-5[a]

1. The operating temperature is 700°C.

2. The contents must be adequately agitated to effect optimum contact of the salt and metal phases. The duration of mixing must be adequate to reach equilibrium conditions of both the salt and the metal phases. Time must be allowed to ensure adequate phase disengagement.

3. Operations that must be provided include:

a. Transfer lines with openings located:

(1) near the top of the vessel for the addition of make-up magnesium

(2) near the top of the vessel for the addition of magnesium from distillation

(3) above the salt-metal interface for the transfer of only salt to the U-Pu donor vessel

(contd)

Table 15. (contd)

(4) below the salt-metal interface for the transfer of the acceptor alloy to distillation

The transfer lines should be of a material that withstands corrosion by the liquid alloys and salts at the required operating temperature. The lines should be adequately heated to maintain the materials in a liquid sate, preventing plugging by freezing.

b. The U-Pu acceptor vessel is a satellite furnace in a fixed position.

c. An agitator capable of providing adequate mixing.

d. Adequate heating to achieve the required operating temperature.

L. SALT-DONOR HEEL STORAGE VESSEL - A-6[a]

1. The operating temperature is 800°C.

2. No agitation shall be provided.

3. Operations that must be provided include:

a. A transfer line below the salt-metal interface for transfer of salt and alloy heels to and from the vessel.

b. Adequate heating to achieve the required operating temperature.

c. The salt-donor heel storage vessel is a satellite furnace in a fixed position.

M. U-ACCEPTOR - A-7[a]

1. The operating temperature is 800°C.

2. The contents must be adequately agitated to effect optimum contact of the salt and metal phases. The duration of mixing must be adequate to reach equilibrium conditions of both the salt and metal phases. Time must be allowed to ensure adequate phase disengagement.

3. Operations that must be provided include:

a. Transfer lines with openings located:

(contd)

Table 15. (contd)

(1) near the top of the vessel for the addition of make-up magnesium

(2) near the top of the vessel for the addition of magnesium from distillation

(3) above the salt-metal interface for the transfer of only salt to the U donor vessel

(4) below the salt-metal interface for the transfer of the acceptor alloy to distillation

The transfer lines should be of a material that withstands corrosion by the liquid alloys and salts at the required operating temperature. The lines should be adequately heated to maintain the materials in a liquid state, preventing plugging by freezing.

b. The U acceptor vessel is a satellite furnace.

c. An agitator capable of providing adequate mixing.

d. Adequate heating to achieve the required operating temperature.

N. SALT-DONOR HEEL STORAGE VESSEL - A-8[a]

1. The operating temperature is 800°C.

2. No agitation shall be provided.

3. Operations that must be provided include:

a. Transfer lines with openings located:

(1) below the salt-metal interface for the transfer of salt and alloy heels to and from the vessel.

(2) below the salt-metal interface for the transfer of spent U donor heel to distillation.

b. Adequate heating to achieve the required operating temperature.

c. The salt-donor heel storage vessel is a satellite furnace.

(contd)

Table 15. (contd)

O. ELECTROREFINING - E-2[a]

1. All lines and apparatus (transfer tubes and electrodes) shall be electrically insulated from the vessel. The vessel shall be electrically insulated from its surroundings.

2. Provisions shall be made for the removal of sludges from the vessel.

3. Provisions shall be made for the removal of copper from the vessel.

4. The electrorefining vessel is a stationary vessel.

P. DISTILLATION FURNACES - D-1 through D-5[a]

1. The furnaces must provide adequate capacity to maintain process flow rates.

2. Provisions shall be made to ensure that adequate vacuum is maintained during the distillation process.

3. The condensers shall be capable of receiving and holding in a liquid state sufficient metal for recycle to their appropriate operations.

4. Provisions shall be made for removal of the bottoms from the distillation furnaces. Adequate heating shall be provided to achieve the required operating temperature.

[a]See Fig. 6 and Table 8.

The design approach for salt transport process options has been defined. This approach and some target dates are shown in Tables 16 and 17, respectively.

The baseline process has been conceptualized following the Design Approach and Design Criteria. In this process, the main unit operations take place at successive stations on a rotating turntable. This provides semicontinuous operation in which several (reactor fuel) subassemblies are in various stages of processing at the same time. The turntable process is best depicted by the process diagram (Fig. 6) and the sequence of events (Table 8) taken together. The sequence of events gives the process operations, in chronological order, required to reprocess a fuel subassembly.

It should be noted that in real time, steps 65, 15, 25, 37, and 49 occur simultaneously, and that five different subassemblies are in various stages of processing.

Table 16. General Design Approach

1. Define the Block Flow Diagram (Completed)
2. Define Primary Unit Operations (In Process)
3. Define Peripheral Unit Operations (Feed Preparation and Waste Treatment)
4. Combine Primary and Peripheral Unit Operations into Process Flow Diagram
5. Evaluate the Feasibility of the Concept, Considering
   a. Materials of Construction
   b. Environmental Impact
   c. Energy Consumption
   d. Economics
   e. Availability and Applicability of Transfer Media
   f. Accountability
   g. Proliferation and Diversion Resistance
6. Size the Equipment and Develop the Plant Layout

Table 17. Target Dates for Design of Pyrochemical Reprocessing Facility

Task	Estimated Completion Date
I. Turntable Design	01/05/79
A. Equipment Sizing and Plant Layout	01/05/79
B. Finalize Flowsheets	01/05/79
II. Mixer-Settler or CSTR Technology	02/02/79
A. Concept Defined	01/12/79
B. Flowsheets	01/19/79
C. Sizing and Layout	02/02/79
III. Alternate Undefined Concept(s)	02/28/79
A. Concept(s) Defined	02/02/79
B. Flowsheet	02/16/79
C. Plant Layout	02/28/79

The metals and salts are transferred between the various vessels by pressure siphoning. The amount of each phase transferred and the amounts and types of various heels will be controlled by types of transfer tube used and the positioning of the tubes. The furnaces for use with the turntable would be attached to the roof of the process area, along with the agitators and transfer tubes needed at each position.

Figure 17 is a sketch of a crucible on the turntable in operating position. This sketch shows many of the detailed concepts needed for operation, including agitation, transfer tubes, heating, insulation, and sealing (containment).

Figure 18 is a plan sketch of the turntable itself. Figure 19 shows the operational mode of the process (i.e., after one set of operations is conducted in a furnace, the crucible is lowered out of the furnace, moved, and raised into a new furnace).

The process flow and mass and energy balances based on a reference fuel have been defined. The selection of a reference fuel is described in the literature [ORNL].

The process flow diagram (Fig. 6) is a schematic of the process as it would be if the turntable were laid on its side and unrolled. The top row of vessels represents the five crucibles on the turntable (or the same crucible at each of the five operating stations in sequence) in which the primary unit operations are conducted. The middle row of vessels shows the secondary unit operations, while the bottom row shows purification operations necessary for the recycle of process reagents. The major components of each stream are shown on the flow diagram.

c. Engineering Analysis

(1) Proliferation Study
(J. L. Zoellner*)

Efforts were begun to evaluate the salt transport process for possible avenues of proliferation and for the prevention of proliferation. During the last quarter, at the request of ANL, Rocky Flats assisted ORNL in providing preliminary design criteria and a proliferation analysis of a pyrochemical process (the Pyro-Civex Process) for coprocessing spent FBR fuel. As a result of this analysis, several proliferation-related criteria were developed. These criteria were developed during the October 17-19 meeting with ANL and ORNL and in subsequent communications concerning the Pyro-Civex evaluation. These general criteria were established to form a basis for and definition of proliferability and are shown in Table 18. Since these criteria are applicable to any particular process, they will be used as a basis for the Rocky Flats proliferation analysis. As necessary during the course of the analysis, the criteria may be modified or added to for completeness.

*Rockwell International-Rocky Flats.

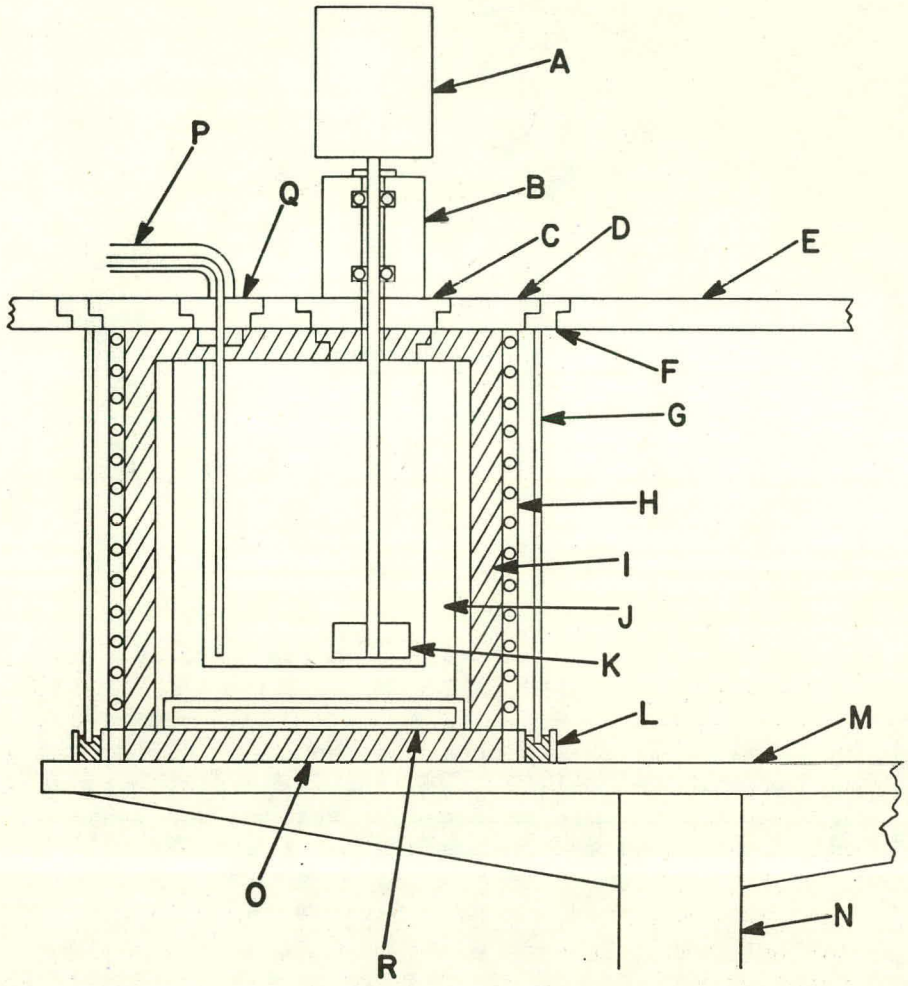

Fig. 17. Crucible Details. A. Drive motor. B. Bearing C. Top-mounting removable seal assembly. Provides seal for shaft and cover assembly. Remotely removable for servicing of motor-bearing-seal-stirrer assembly. D. Cover assembly, removable for maintenance of insulation and induction coils. E. Circular processing assembly. F. Cover ring assembly, removable for maintenance of outside cylindrical enclosure. G. Cylindrical enclosure, pressure of internal inert atmosphere (Ar, Xe, Kr): 10 to 100 psia. H. Induction heating coil. I. Insulation. J. Crucible and susceptor (for induction heating). K. Stirrer shaft. L. Freeze seal for outer cylindrical enclosure. Contains low-melting alloy and a resistance heater to melt the alloy. To break and make the seal each time the rotating turntable is lowered and raised, the alloy is heated, then allowed to cool. M. Rotating turntable. N. Rotating turntable support. O. Insulation, lowers with the rotating turntable. P. Heated transfer line. Q. Removable transfer line seal. R. Transfer pallet.

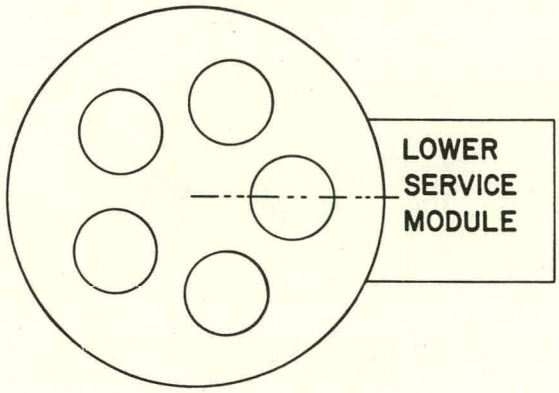

Fig. 18. Top View of Turntable

Table 18. Proliferation-Related Criteria

1.	The fissile materials produced should be sufficiently radioactive and diluted with fertile material to make diversion difficult and easily detected and to make conversion into weapons-usable material difficult.
2.	The process should not be capable of producing, through simple process adjustment or slight equipment modification, highly decontaminated fissile materials.
3.	Any modification of the process equipment should require facilities and components not normally on site and should require plant decontamination or entry into highly radioactive areas.
4.	The length of time required to divert fissile materials should be adequate for appropriate national and/or international responses.
5.	The process must permit real-time accountability of fissile material.
6.	The facility must be operated remotely and must be maintained remotely, utilizing only dedicated equipment.

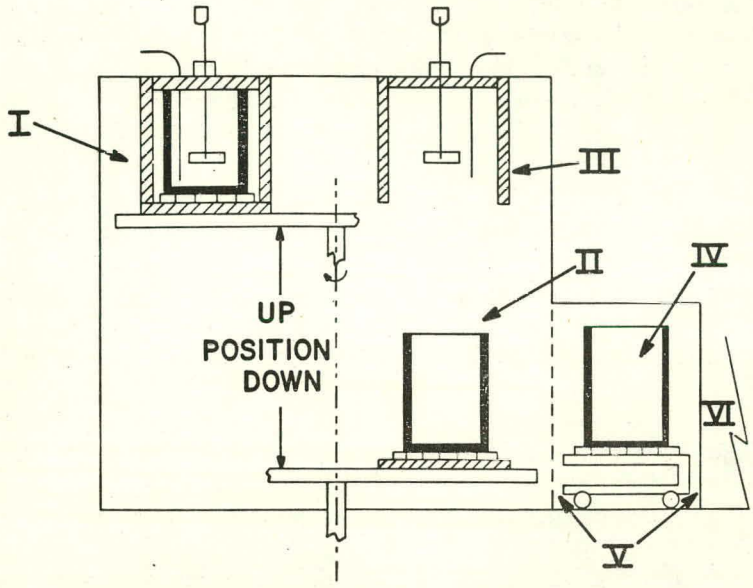

Fig. 19. Side View of Conceptual Turntable. I. One stage is shown in operating (UP) position. Details are seen in Fig. 17. II. One stage is shown in the transfer (DOWN) position. The parts of the stage attached to the movable turntable are: freeze seal (L, Fig. 17), bottom insulation (O, Fig. 17), crucible-susceptor assembly (J, Fig. 17), and transfer pallet (R, Fig. 17). III. The parts of the stage attached to the top of the housing are: stirring motor (A, Fig. 17), bearing housing assembly (B), seal assembly (C), cover assembly (D), cover ring assembly (F), cylindrical enclosure (G), induction heating coil (H), side and top insulation (I), heated transfer line (P), and transfer line seal (Q). IV. A service cart at one turntable position can be used to remove lower stage parts in case of a freeze-up or other problem. The cart is on rails, and doors at V provide atmospheric seals. V. Doors for atmospheric seal. VI. Service bay.

In conjunction with the above-discussed proliferation criteria, some general preliminary process design criteria were also developed, see Section I.B.4.b(2). These also will be used as a starting point for proliferation analysis of the salt transport process. (Since the salt transport process design may incorporate physical characteristics other than a turntable concept, some of these preliminary criteria may or may not apply.

A proliferation analysis outline is being developed and will be completed in January, 1979. This outline will describe the method of analysis to be used during the course of study and will define the areas of proliferability and the corresponding counter-proliferation solutions. These methods will include not only the current rotating turntable concept, but also all concepts developed by process design personnel.

A proliferation study will be closely coordinated with the process design effort. All alternative process design layouts will be evaluated from a proliferation standpoint; conversely, any possible proliferation method will be evaluated for practicality and design application.

An important tool to be used in all analyses is the computer model of the salt transport process, which will be adapted for any physical design scenario evaluated. The initial step in the proliferation study will consist of establishing a base process for the salt transport method, which would include a mass balance (for core and blanket FBR fuels), vessel volumes, heating and radiation, feed and bleed streams, product streams, and heel volumes. The base case and all subsequent cases will then be evaluted for the effects of chemical additions, deletions, substitutions, changes in temperature or time, product or sidestream recycle, operational order change or side stream diversion. Wherever possible proliferation methods exist, a defense against such action will be provided.

For the month of January, 1979, the proliferation analysis outline will be prepared and the proliferation analysis of the base case salt transport process will be prepared.

(2) Salt Studies Literature Search

(T. D. Santa Cruz*)

There exists in the open literature an enormous amount of information dealing with the physical and chemical nature of molten salt systems and particularly those systems of interest to the PDPM program. A proper format for presenting information obtained from the literature would be to prepare topical reports on subjects such as Purification of Molten Salts; Phase Diagrams; Solubilities in Molten Salts; Electrochemistry in Molten Salts; and Spectroscopy in Molten Salts. This list can be altered to include other topics as the situation might warrant, as well as deletion or combination of these topics.

---

*Rockwell International-Rocky Flats.

On the topic of Purification of Molten Salts, three reports are pertinent: one from Argonne National Laboratory [JOHNSON-1969], one from Brookhaven National Laboratory [RASEMAN], and one from Oak Ridge National Laboratory [SHAFFER]. Other methods of producing purified salts on both large and small scales also need evaluation and will be discussed in the future topical report.

(3) Waste Management Studies
(S. P. Sontag*)

In the salt transport process, recycle is important since without recycle the waste volume would be excessive. Most process streams are suited for recycle, although some require purification prior to reuse. The transport salts are recycled almost indefinitely; the cover salts must be processed to remove fission products and calcium oxide. The distillate from the vacuum stills is ideally suited for recycle as is; the still bottoms become product or a concentrated waste source. Purification of process streams will be done in auxiliary furnaces and equipment during approximately the same time period as major salt transport operations. Proper management of nonrecyclable wastes is extremely important to ensure adequate containment for ultimate handling and disposal. A preliminary outline which will be expanded and rearranged as necessary, is given in Table 19.

(4) Analytical Methods
(S. P. Sontag*)

Several meetings have been held to discuss analytical methods which would be suitable and/or available for use on the PDPM program.

The primary purpose of the meetings was to ascertain which analytical techniques had enough resolution to give accurate assays of fission product concentrations expected in FBR fuel when mixed with the alloys and salt used in the salt transport process. Three phases of experimentation were identified. Phase I will involve the use of stable isotopes of fission products to determine if partitioning between molten alloys and molten salts occurs as expected; this is being done in the proof-of-principle experiments. Phase II (experimental studies beyond FY 1979) consists of investigating the possibility of using isotope tracers at Rocky Flats to augment Phase I. Phase III will consist of reprocessing a fuel pin by salt transport in a hot cell facility at some site other than Rocky Flats. The recommendations for each phase are given below.

An additional meeting was held among lab personnel on September 22, 1978, in which representative elements of each fission product group were selected. These representative elements were chosen to allow the lowest possible detection limits with the analytical methods available at Rocky Flats and are:

*Rockwell International-Rocky Flats.

Table 19. Preliminary Recycle and Waste Management Outline

I. Recycle Management

A. Recycle Streams

1. Decladding and Reduction Cover Salt
2. Distillate of Zn-Mg from Cladding/FP-3 Acceptor Still D-1
3. Distillate of Zn-Mg from U-Pu Acceptor Still D-3
4. Distillate of Zn-Mg from U-Acceptor Still D-4
5. Distillate of Mg from Donor Alloy Still D-5
6. Bottoms of Cu & FP-4 from donor Alloy Still D-5
7. Crucible Cover Gas
8. Transport Salts
   a. U-Pu transport salt
   b. U transport salt
9. Products
   a. U-Pu metal with FP-3 from D-3
   b. U metal from D-4

B. Characterize Recycle Streams

1. Composition
2. Radiation Levels
3. Heating Rates and Steady State Temperatures
4. Gas Production Rates
5. Half-Life Effects
6. End of Decay Chain Effects

C. Refining/Separation Methods

1. Chemical Exchange Reactions
2. Electrolysis
3. Zone Refining
4. Salt Transport
5. Electrorefining
6. Gas Separations
7. Other(s)

D. Recycled Material Form

1. Handling Equipment
2. Physical State Change

E. Accountability and Recycle Quality

1. Analytical Techniques
2. Type of Accountability
3. Recycle Quality Limits

(contd)

Table 19. (contd)

II. Waste Management

A. Waste Streams

1. Bottoms of SS and FP-3 from Cladding/FP-3 Acceptor Still D-1
2. Bottoms of Cu, Mg, and FP-4 from Donor Alloy Still D-5
3. Residuals from Refining/Purification Methods
4. Bleeds from Refining/Purification Methods
5. Crucible Cover Gas
6. Condensate on Process Equipment

B. Characterize Waste Streams

1. Composition
2. Radiation Levels
3. Heating Rates and Steady State Temperatures
4. Gas Production Rates
5. Half-Life Effects
6. End of Decay Chain Effects

C. Potential Use

1. Radiation Source
2. Heat Source
3. Isotope Source
4. Other
5. Shape and Packaging

D. Waste Disposal

1. Waste Classification and Acceptability Criteria
   a. WIPP
   b. Other waste facilities
2. Acceptable Physical Forms
   a. Packaging methods
3. Unacceptable Physical Forms
   a. Modification techniques
   b. Packaging methods

E. Accountability

1. Analytical Techniques
   a. Verification of U, Pu, and FP content
   b. Verification of physical properties
2. Type
   a. Real time
   b. Feed to product
   c. Others

Group	Elements
FP-2	Cs, Ba, Te
FP-3	Y, Nd, Ce
FP-4	Mo, Cd, In, Sn

The above elements will be used during Phase I. Detection limits and concentration levels needed for 5% accuracy for atomic adsorption are given for all fission product elements in Table 20. Atomic absorption is agreed to be the most sensitive analytical technique.

Table 20. Atomic Absorption Guidelines (All concentrations given in weight percent)

Group	Element	Concentration needed for 1% absorption	Concentration needed for 5% accuracy
FP-2	Cs	2×10^{-3}	1×10^{-1}
	Rb[a]	1×10^{-3}	5×10^{-2}
	Ba	4×10^{-3}	2×10^{-1}
	Sr[b]	1×10^{-3}	5×10^{-2}
	Sm		1×10^{-1}
	Se	5×10^{-3}	2×10^{-1}
	Te[b]	5×10^{-3}	2×10^{-1}
	Eu		2×10^{-1}
FP-3	Y[b]	2×10^{-2}	1×10^{0}
	La[b]		3×10^{0}
	Pr[b]		3×10^{0}
	Nd[b]		4×10^{-1}
	Gd[b]		3×10^{-1}
	Tb		2×10^{0}
FP-4	Zr	1×10^{-1}	4×10^{0}
	Nb	4×10^{-1}	1×10^{-1}
	Mo[a]	5×10^{-3}	4×10^{-1}
	Tc[a]	3×10^{-2}	3×10^{-1}
	Ru[a]	5×10^{-3}	4×10^{-1}
	Rh[a]	3×10^{-3}	2×10^{-1}
	Pd	3×10^{-4}	1×10^{-1}
	Ag	6×10^{-4}	4×10^{-2}
	Cd	3×10^{-4}	2×10^{-2}
	In	7×10^{-3}	3×10^{-1}
	Sn	4×10^{-2}	2×10^{0}
	Sb	5×10^{-3}	2×10^{-1}

[a] Lamps would need to be purchased. A technetium lamp may be difficult to obtain. Rubidium may require an electrodeless discharge lamp. Lamps cost about $200 each.

[b] Flame emission figures.

The proposed isotopic tracers for use during Phase II are listed in Table 21. These isotopes were selected based on nonmatching gamma ray emissions, half-life, and availability. The quantities used per test will be on the order of 1×10^{-9} g. Preliminary approval for their use is being sought from the Health, Safety, and Environment Department.

Table 21. Proposed Isotopic Tracers

Group	Isotope	Half-Life	Comments
FP-2	^{137}Co	20.2 y	already on plant site
	^{135m}Ba	28 h	make from barium-134 target[a]
	^{123m}Te	119.7 d	make from tellurium-122 target[a]
FP-3	^{91}Y	58.6 d	buy from ORNL
	^{147}Nd	11.0 d	make from neodymium-146 target[a]
	^{141}Ce	32.5 d	make from natural cerium target[a]
FP-4	^{99}Mo	66.0 h	buy from radiopharmaceutical company or make from molybdenum-98[a]
	^{115m}Cd	44.6 d	make from cadmium-114 target[a]
	^{114}In	49.5 d	make from indium-113 target[a]
	^{113}Sn	115.0 d	make from tin-112 target,[a] decays to usable indium-113m isotope tracer

[a]Possibly could be done at the Federal Center in Denver.

Work during this quarter on Phase III has consisted of researching the analytical capabilities of various hot cell facilities. A complete list will be made when all data have been received. This information will be used to recommend to ANL the most capable site for performing the pilot plant reprocessing of an irradiated fuel pin(s). The irradiated fuel reprocessing phase is necessary to identify difficult remote operations and to verify that partitioning occurs as expected when all fission products are present.

(5) Computer Model of Salt Transport Process

(W. A. Averill*)

Extensive progress was made on the computer model of the pyrochemical salt transport reprocessing system. The milestones are as follows:

*Colorado School of Mines.

(1) The model predicts the behavior of uranium, plutonium, FP-1, FP-2, FP-3, and FP-4 groups during the five primary stages of processing: decladding, reduction, FP-3 removal, U-Pu cotransport, and U transport.

(2) The model is capable of demonstrating the effect of process variables, such as the fraction of alloy treated in FP-3 removal, on the number of extraction stages for uranium transport.

(3) The model has the capability of demonstrating the effect of a pyroredox step for the removal of FP-3 from the processing alloy. Complete variability of operational parameters is possible to test all combinations and permutations of this system and the resultant product compositions.

(4) The model calculates the phase volumes at every stage of the process to accurately represent the minimum reactor volume requirements for the process.

(5) Analysis is now possible to determine the possibility of fissile materials of high quality being produced by varying the process parameters, either singly or in combinations. Furthermore, analysis of preventive measures is possible.

(6) The model has been and continues to be used to generate data for the analysis of the ORNL Pyro-Civex Process. These data could not be generated by any other method at the high speed now possible using the model.

(7) The model has the potential for determining the sensitivity of the process to the more subtle parameters of the process, such as the variation of the value of the distribution coefficients as a function of extent of transport in each equilibrium stage.

(8) The model calculates the fraction of plutonium recovered in the U-Pu separation stage as a function of plutonium fed to the process. Additionally, the U-Pu enrichment ratio is calculated and provided by the computer model.

The combined features of the present program allow powerful analysis of many aspects of the process previously neglected through simplifying assumptions. However, other improvements are yet to be implemented. These additions to the model will greatly increase the extent of analysis possible on the process. The improvements, along with estimates of the time of completion, are as follows:

(1) In order to increase the speed of computation and allow the model to be used on other machines, a FORTRAN version will be written. This should be completed before February, 1979.

(2) The model will be extended to include all process vessels and the side and recycle streams to allow calculation of recycle, and to include heels which will alter the complexity of the process. This will be completed by mid-February, 1979.

(3) Regressions will be performed on all distribution coefficient data to obtain relations for these coefficients as a function of alloy composition, salt composition, and temperature. This will give a more complete understanding of process parameters and their effects and should be complete by the end of February, 1979.

(4) Additional information will be printed out by the model to display the contents of all phases employed, including solid precipitate phases present in the salt transport portions of the process. This should be complete by the end of January, 1979.

(5) The printing of all input variable and parameter values will be performed prior to each computer run to establish the conditions for that particular execution. This should be finished by the first week of February, 1979.

(6) The model will be coupled with the ORIGEN Program so that a closed-cycle calculation can be performed between reprocessing and fuel burn-up. This is an extensive algorithm modification which will most likely take until July to complete.

(7) Finally, this model will be inserted in an optimization routine to determine optimum operating levels for all process parameters. This portion is tentatively scheduled for implementation by December, 1979, to February, 1980.

A demonstration of typical output for the model is presented in Table 22, a copy of an actual computer output that shows the present format. This format will be basically the same in the future except for the previously noted modifications.

(6) Training Video Tapes

(W. A. Averill*)

One of the training tapes dealing with the theoretical background of the PDPM effort (see [STEINDLER-1979]) has been completed. It is "Phase Diagrams and Phase Theory." Final editing and copying will be completed and copies made available to project management for approval prior to distribution. The rest of the tapes will be completed as time and funding allow. A tentative target date is December 1979.

(7) Ternary Studies

(W. M. Mueller,* D. L. Olson,* and W. A. Averill*)

At the present time, binary phase diagrams have been determined for the copper-uranium, uranium-magnesium, and copper-magnesium systems. However, no data are available for the copper-uranium-magnesium ternary system.

---

*Colorado School of Mines.

Table 22. Mass Balances Before and After Reduction

I	Component	Feed Oxide	Reduction Alloy	Reduction Salt
		MASS BALANCE PRIOR TO REDUCTION		
1	U	64.464	0	0
2	Pu	10.112	0	0
3	FP-1	0	0	0
4	FP-2	0.963	0	0
5	FP-3	1.122	0	0
6	FP-4	1.66	0	0
7	Mg	0	49.1211	0
8	Zn	0	0	0
9	Ca	0	31.1607	0
10	Cu	0	227.8	0
11	SS	0	0	0
12	XS OXY	1.305	0	0
13	$CaCl_2$	0	0	113.941
14	KCl	0	0	19.7067
15	CaF_2	0	0	29.1479
16	$MgCl_2$	0	0	0
17	MgF_2	0	0	0
18	NaCl	0	0	0
19	$ZnCl_2$	0	0	0.823241
20	CaO	0	0	0
		MASS BALANCE AFTER REDUCTION		
1	U	0	64.464	0
2	Pu	0	10.112	0
3	FP-1	0	0	0
4	FP-2	0	0	0.963
5	FP-3	0	1.122	0
6	FP-4	0	1.66	0
7	Mg	0	49.1211	0
8	Zn	0	0	0
9	Ca	0	2.83276	0
10	Cu	0	277.8	0
11	SS	0	0	0
12	XS OXY	0	0	0
13	$CaCl_2$	0	0	113.941
14	KCl	0	0	19.7067
15	CaF_2	0	0	29.1479
16	$MgCl_2$	0	0	0
17	MgF_2	0	0	0
18	NaCl	0	0	0
19	$ZnCl_2$	0	0	0.823241
20	CaO	0	0	39.636

Copper-uranium-magnesium alloys will be made up, and the alloy composition will be verified with atomic absorption spectroscopy. Initial alloys will be made at increments of 5% compositional variation. After this initial work, other alloys may be needed to more clearly define specific phase reactions.

This research will be conducted in a way to determine the entire extent of this system, with emphasis on the copper-rich region from about 50 wt % magnesium and from about 5 wt % uranium.

It is necessary to determine the solid phases in equilibrium with the melt over the temperature range, 500 to 900°C. This will be accomplished in this research by study of the microstructure and by chemical X-ray analysis of these solid phases or chemical analysis of extracted liquid. The chemical analysis will be done by atomic absorption spectroscopy and X-ray diffraction at the Colorado School of Mines and by analytical scanning electron microscopy at Rocky Flats. This research will also determine the liquidus and solidus profile with respect to temperature over the temperature range 500 to 900°C for the entire ternary system.

Laboratory differential thermal analyses will be performed on alloys to be prepared according to the experimental plan. These experiments will be conducted in an inert atmosphere--a glovebox containing an essentially pure argon environment. Additionally, cooling curves will be obtained under an inert atmosphere. These cooling curves and differential thermal analyses will provide the initial data necessary to begin the plotting procedure for the liquidus and solidus profiles. At the same time, studies will be initiated to determine the nature of solid phases in equilibrium with the melt at the liquidus. This will be accomplished by attempting to quench the phases which are at equilibrium at the temperature of the liquidus down to ambient temperatures and analyzing the microstructure resulting from this quench. At least a 10% check on the data will be performed to ensure that the phases quenched to ambient temperatures are representative of the high-temperature phases in equilibrium with the melt. This check will be performed by analyzing the microstructure using differential thermal analysis, thermal expansion analysis, and possibly hot stage microscopy.

The research effort, to date, has been procurement of the necessary materials and equipment and building and assembly of the experimental arrangements. Depleted uranium has been received from Argonne National Laboratories, and high-purity copper and magnesium have been purchased. Tantalum-sheathed chromel-alumel thermocouples have been special-ordered and received. A two-pen Hewlett-Packard recorder with special amplifier and time-base accessories have been purchased and received. One-inch-high, 3/4-in.-diameter, high-purity aluminum oxide crucibles have been purchased and received.

A clamshell furnace was designed and built to allow the necessary thermal cycles to be used in the differential thermal analysis. Also, a special stainless steel crucible holder has been machined which is designed to guarantee the same thermal experience for the reference crucible (pure copper) as for the crucible with the alloy being investigated (Fig. 20).

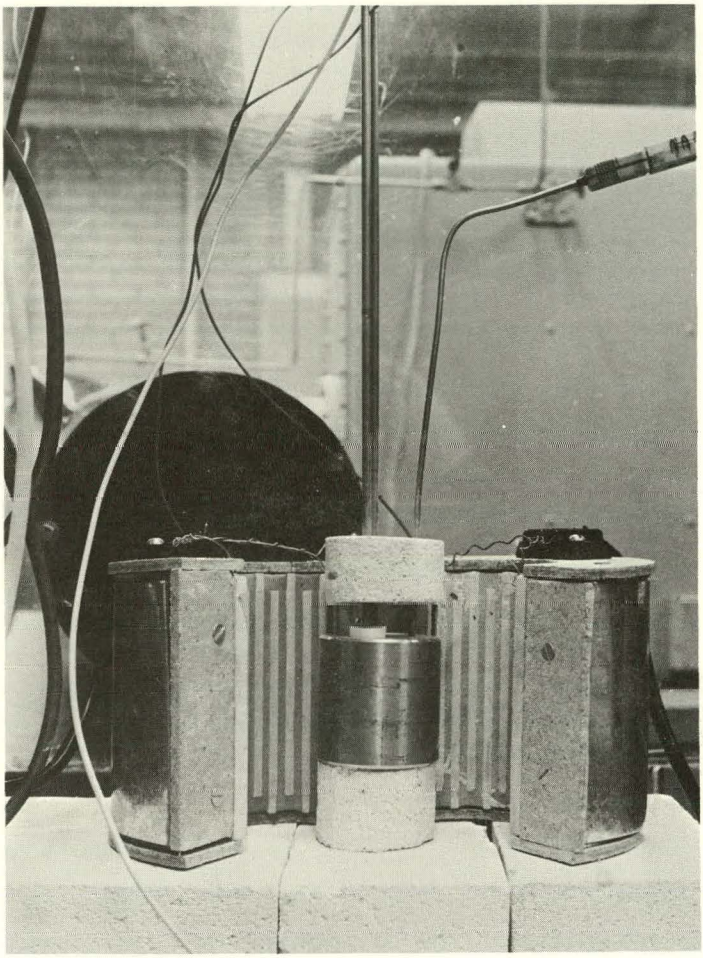

Fig. 20. Crucible Holder in Clamshell Furnace

One protective-atmosphere box has been rebuilt especially for this experiment. A gas purification train has been installed to control the oxygen impurity level. Furnace controls and the data acquisition equipment have been integrated into this protective-atmosphere box system. The box is also hooked up to a gas chromatograph for monitoring the purity of the atmosphere. Figure 21 is a photograph of the experimental chamber with the furnace in place.

The experimental arrangement is nearly complete, and alloy preparation will be initiated during the month of January, 1979. Each alloy will be made individually by melting the necessary weights of pure metal components in the small aluminum oxide crucibles. Chemical analysis will be performed to confirm the alloy composition and to learn whether the alloy is reducing the alumina crucible.

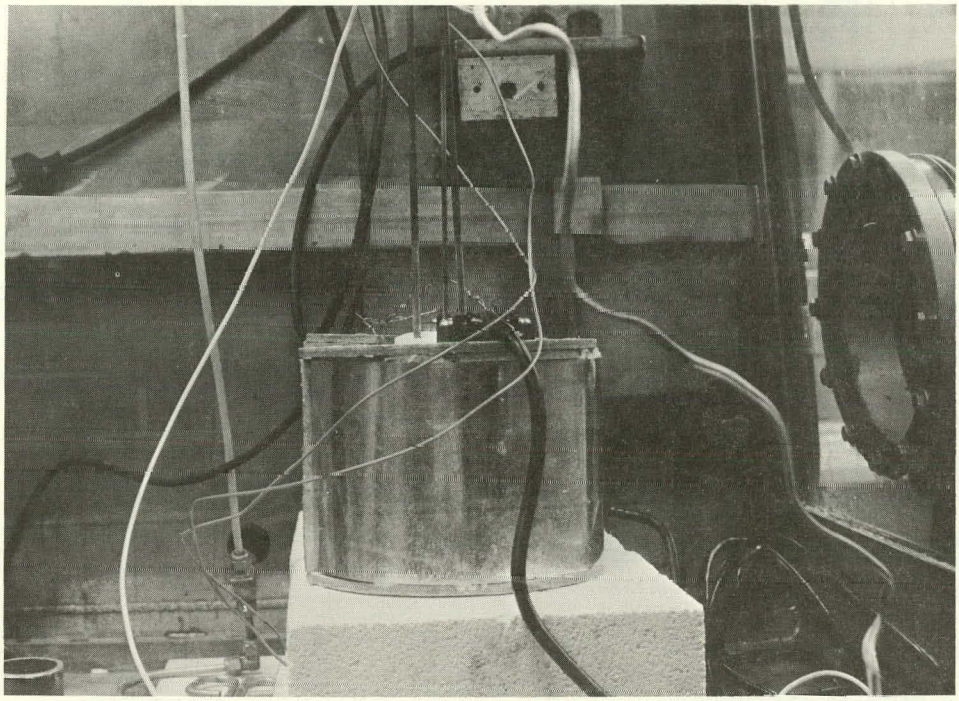

Fig. 21. Controlled-Atmosphere Chamber with Furnace Installed

Also during the month of January, 1979, differential thermal and thermal analysis runs will be made--first on the pure copper and then on several binary alloys in order to calibrate the measuring equipment to known phase equilibria data. The copper-rich region will be determined first in this investigation in order to provide data believed to be useful for immediate application in ongoing programs.

(8) Miscellaneous

Travel. Dr. T. Santa Cruz attended the Second International Symposium on Molten Salts in Pittsburgh from October 15 through 19, 1978. He reported that the majority of the presentations were geared to molten salt batteries and fuel cells. However, numerous papers were presented which examined the fundamental nature of molten salt systems. A paper presented by M. F. Roche is an example: "Theory for Ternary Solutions Dilute in One Component." Another described a method of thermosonimetry for preparing phase diagrams.

S. P. Sontag attended the High-Level R/A Solid Waste Forms Conference held December 19 to 21, 1978, in Denver. The conference had presentations on vitreous forms, encapsulation techniques and failure modes, spent fuel characteristics, and other waste forms. A speech presented by

Senator Harrison Schmitt on the politics and potential of nuclear waste was also attended. Information from this conference will be used to help shape the PDPM waste management.

Program Plan. The updated Program Plan for Work Packages 04 and 05 was submitted to Argonne during this Quarter.

d. Separation Processes

(1) Proof-of-Principle
(M. Boyle*)

(a) Operational Safety Analysis

The Operational Safety Analysis (OSA) for the stationary furnaces in Room 133, Building 779* was approved November 11, 1978. The approval clears the way for the experimental proof-of-principle work except that installation and approval of the vacuum-purge system remain to be done. This system will facilitate sampling of the alloy and salt within the furnaces.

An addendum to the OSA has been written to include the use of a graphite crucible holder. The graphite holder is to be used as a filler to accommodate the smaller MgO crucibles in the stationary furnaces. Small crucibles are favored due to only a limited amount of waste being generated. The graphite crucible holder is of concern because of its potential as a neutron reflector and the potential for criticality. "Nuclear safety" has given their approval for the use and safety of the graphite crucible holder. The addendum to include the graphite has been approved by the responsible supervisor and presently awaits the approval of the Health, Safety and Environment (HS&E) representative.

(b) Stationary Furnaces

Most of the modifications to stationary furnaces have been completed. The modified furnace lids have been fabricated and installed (Fig. 22). Pressure testing of the furnace was delayed in order to upgrade a pressure gauge and to change a faulty regulator valve.

During pressure-testing of the furnace, it was determined that the vessel could hold a pressure up to the limits of the relief value (15 psig). The 15-psig pressure was adequately maintained for two hours. This should be ample time to obtain a liquid metal or molten salt sample.

The sample tubes, thermocouple wells and agitators have been fabricated from tantalum. The sample tubes will be press fitted with porous frits to filter out extraneous materials, as described in the literature [WINSCH].

---

*Rockwell International-Rocky Flats.

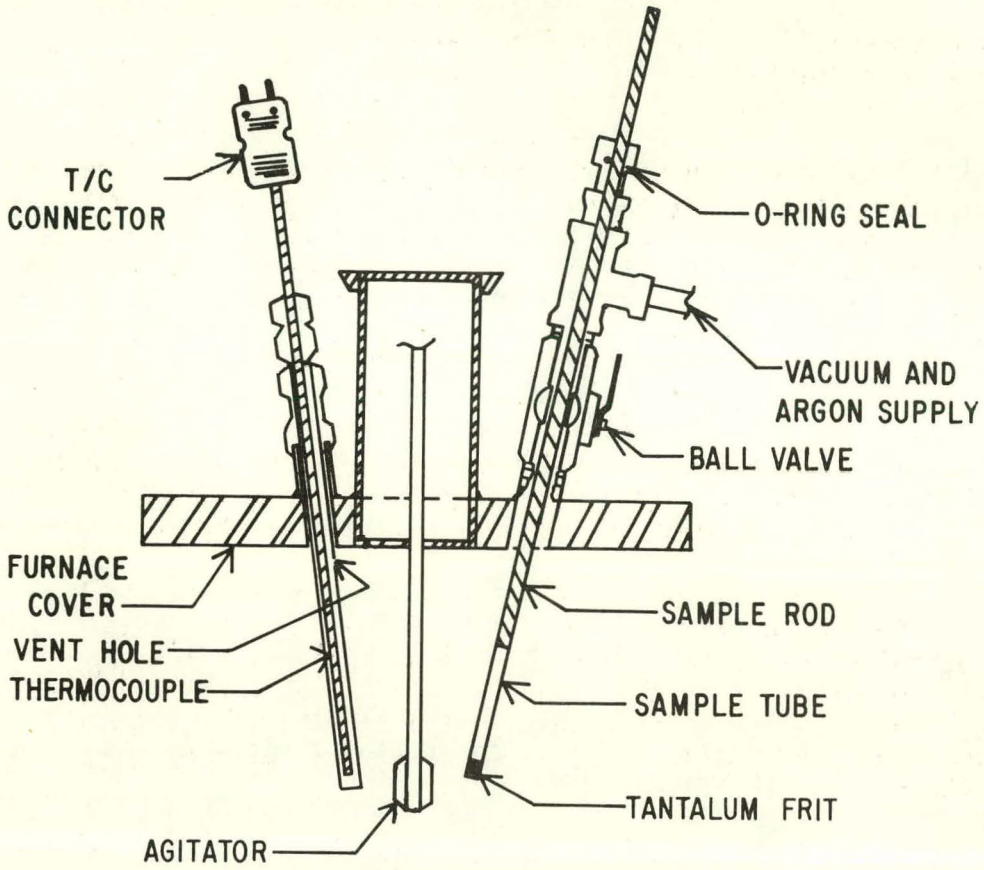

Fig. 22. Furnace Cover Assembly

The graphite crucible holder with a stainless steel liner has been put into the stationary furnace and is ready to be used for the experimental work.

The vacuum-purge system must be installed before experimental studies can begin. Engineering has been completed, and the drawings are now undergoing final review. Upon completion of the review, installation of the system will commence.

A spare stationary furnace resistance heating coil, necessary to avoid extended periods of downtime for the furnace during fabrication of replacement coils, should be ready by January, 1979.

(c) Tilt-Pour Furnace

Furnace modifications have been proposed and submitted for engineering review. Major modifications to the tilt-pour furnace are the insertion of thermocouple ports through the lid and a flange to connect the lower part of the furnace well to the top of the furnace. A flanged furnace well in a contaminated furnace can be replaced with a minimum of effort and time.

Tilt-pour lid modifications are being scheduled. After the drawings for the flanged furnace well are reviewed, this work, also will be scheduled.

The tantalum crucible drawings are complete. The material for construction of the crucibles has arrived, and fabrication will begin as scheduling or maintenance permits. Two stainless steel full-size mockups have been fabricated to the specifications of the drawings. The stainless steel crucibles will serve as working models, along with the drawings, in the fabrication of the tantalum crucibles.

(d) Experimental Procedure

A plant-required formal writeup of the proof-of-principle experiments is being drafted. The writeup will provide better insight on the amount of waste generated during experimentation and help in assessing how to dispose of the waste alloys and salts.

One of the first experiments will be a preliminary run with copper-magnesium alloy and a salt phase to check out the furnace and stirring equipment. Metal and salt will be sampled, using the sample tube assembly, to verify that samples of metal or salt can be obtained at the 15-psig pressure limit. This experiment will also give insight on the time requirement and the degree of phase separation associated with a period of agitation and equilibration.

Samples of the metals to be used in the experiments have been submitted for analysis. Analytical Laboratory personnel have been asked to analyze for Al, Fe, Mn, Si, Zn, C, Mg, Cu, Ni, Sn, Pb, As, Sb, Cd, and Ca.

Also, a sample of depleted uranium metal (D-38) has been sent off for analysis. The random sample (2 g) was taken from a 3-kg lot set aside for the proof-of-principle partitioning studies. The results of the analyses should be available early in January, 1979.

Problems related to storage of the D-38 uranium have been resolved. The initial concern was the potential fire hazard and unwanted oxidation due to the metal having been machined into chips for ease of handling. The metal is presently being stored under an inert atmosphere to protect it against fire and oxidation. Potential oxidation will be evaluated further.

(e) Miscellaneous

Training of technicians "in the gloves" is continuing, to give them expertise in handling nuclear materials and properly filling out required records for the accounting of materials and the storage of nuclear materials.

Acquisition of a small glovebox for immediate wet-chemical analyses of materials generated during experimentation with molten salts and alloys is being pursued. This would not preclude, but would

supplement routine plant analyses and would provide more rapid results for planning future experiments.

(2) Calcium Recycle
(S. P. Sontag*)

An in-stock, Lindberg furnace capable of 1200°C operation has been ordered. A furnace retort to withstand 25 psi at 800°C has been designed. The retort lid has penetrations for thermowells, sampling tubes with or without filters, and a central packing gland for either a stirring shaft or a viscometer probe. Laboratory space for the experiments is being prepared.

A detailed experimental plan for calcium recycle by calcium oxide reduction is being written. The experiments will concentrate on chemical conversion of the calcium oxide to a chloride, followed by electrolysis (see [STEINDLER-1979]). Electrolysis of calcium chloride is the commercial method of producing calcium metal. Direct electrolysis of calcium oxide is being investigated by ANL (see Section I.C.3.c). The proposed experimental outline is given in Table 23.

(3) Salt Purification Laboratory
(T. D. Santa Cruz*)

Work on the Salt Purification Laboratory by the Rocky Flats Plant Facilities and Construction Department was completed December 13, 1978. Construction included the meshing of existing laboratory furniture with new equipment and furniture--i.e., the installation of storage cabinets, a sink, an inert-atmosphere glove box, a spectrophotometer, gas and water utilities to the fume hood, and a vacuum manifold. The overall layout of the Salt Purification Laboratory is illustrated in Fig. 23.

With construction complete, an Operational Safety Analysis (OSA) is being drafted and is due on December 22, 1978. An Operating Procedure is being drafted in conjunction with the OSA. Design criteria can now be established for the design and construction of ancillary hardware (i.e., a furnace for the spectrophotometer, vacuum connections for the vacuum manifold, etc.).

Upon preliminary analysis, a magnesium chloride stock packaged by Research Organic/Inorganic Inc. at a listed purity of 99.9+% was found to contain more oxides and water than another stock packaged by the same vendor at 98+% purity. The latter magnesium chloride was packaged in a better manner. This tends to emphasize the need for better handling and packaging of the salts before, during, and after processing in order to ensure the integrity of the salts.

In the past, some salts have been provided to the Metallurgy Group which is fabricating and testing process vessels. This testing has provided excellent feedback on possible salt problems. In one case, this

*Rockwell International-Rocky Flats.

Table 23. Calcium Recycle Experiments

I. Calcium Oxide Occurrence

A. Solubility in salt phase

1. temperature variation
2. particle size distribution

B. Solubility in metal phase

1. temperature variation
2. particle size distribution

C. Residual metallic calcium distribution coefficient

II. Chlorination of CaO by UCl_4 to $CaCl_2$, i.e., $2CaO + UCl_4 \rightarrow UO_2 + 2CaCl_2$ postulated from $2CaO + UF_4 \rightarrow 2CaF_2 + UO_2$ [GRIMES]

A. Reaction kinetics

B. Optimum operating conditions

C. Minimization of side reactions

III. Regeneration of UCl_4 (i.e., $UO + 2Cl_2 + C \rightarrow UCl_4 + CO_2$ [BENEDICT] and $UO_2 + CCl_4 \xrightarrow{Cl_2} UCl_4 + CO_2$ [SOOD])

A. Kinetics of each reaction

B. Optimum operating conditions

C. Minimization of side reactions

D. Alternative UCl_4 regeneration

1. Formation of UO_2Cl_2 by:
   $UO_2 + Cl_2 \rightarrow UO_2Cl_2$
   $2UO_2 + Cl_2 + CCl_4 \rightarrow UO_2Cl_2 + UCl_4 + CO_2$
2. Thermal degradation of UO_2Cl_2 to UCl_4 [BENEDICT]

group was investigating the corrosion of crucible parts in MgF_2-$MgCl_2$ molten salt and copper-magnesium liquid alloy. They found that in the interfacial region between the alloy and the salt, a zone of "black salt" formed. In the pyrochemical processes at the Rocky Flats Plant, similar black salt zones are found. These zones handicap phase disengagement of the salt and alloy and create an undesirable (undiscardable) byproduct. The Metallurgy Group has provided a specimen of the salt/black salt-alloy system from which samples have been taken for analysis to determine the composition of the black salt.

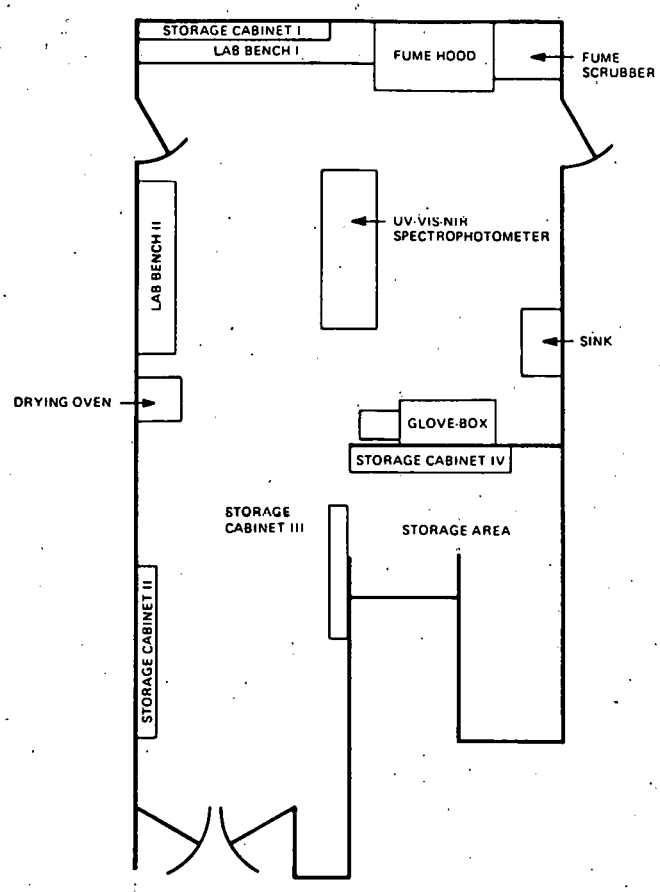

Fig. 23. Floor Plan for Salt Purification Laboratory

During startup, it is planned that the Salt Purification Laboratory will begin providing salts of increasing quality to both the group doing the salt transport studies and the Metallurgy Group. In the phasing-in of equipment, critical pieces of equipment of increasing importance will be operated--that is, the glovebox, the furnaces, and furnace controllers. The procedures for handling molten materials will be checked. In the meantime, the spectrophotometer and vacuum manifold will be brought into operation, the investigation of black salt will be continued and the adequacy of the packaging will be further considered.

5. Fabrication of Process-Size Refractory Metal Vessels

(C. Edstrom,* C. Baldwin,* R. Corle,* L. Johnson,* and A. Phillips*)

a. Introduction

Pyrochemical processing of nuclear fuels requires crucibles, stirrers, and transfer tubing that will withstand the temperature as well as chemical attack from molten salts and metals used in the process. Being able to fabricate the necessary hardware is critical to pyrochemical processing. For economics and safety in the pyrochemical process, a crucible large enough to contain an entire fuel subassembly is needed. Tungsten, a material known to withstand the process temperature and chemical attack, is presently not available in a sheet size large enough to provide the surface area of large crucibles. This dictates development of joining, coating, and/or forming processes to obtain a crucible of the desired shape and size.

b. Engineering Analysis

The topical report of the literature search on tungsten fabrication is complete and is being reviewed by technical writers before distribution. Tungsten fabrication (joining, chemical vapor deposition, plasma spraying, forming, spinning) is the main theme. However, the report also summarizes some literature on molybdenum and on work previously performed at Argonne National Laboratory on other container materials for pyrochemical processing of spent nuclear fuels.

A quotation for the fabrication of riveted tungsten crucibles has been received from Metallwerk Plansee. This crucible consists of two layers of 1.5-mm (0.060-in.) thick tungsten for the wall with one 4-mm (0.200-in.) layer of tungsten on the bottom. The 20-in.-dia by 48-in.-high riveted crucible costs approximately $24,000 plus $1000 for plasma-spraying the inside. A 5-in.-dia by 10 1/2 in.-high crucible costs $2900 plus $260 for plasma spraying.

In December 1978, the possibility of inserting a strip of Palnisil 10 braze between the sheets of the crucible wall and in line with the tungsten rivets was discussed with Fred Bydash, Metallwerk Plansee's U.S. representative. He saw no objection and planned to ask Metallwerk Plansee.

c. Separation Processes

(C. Edstrom,* L. Johnson,* and R. Corle*)

The first successfully spun tungsten crucible was made during the last week in September, 1978, and the second was spun in October, both at Rocky Flats. The assistance of Mr. Dieter Bauer (consultant) made the spinning possible. He contributed several spinning techniques which led to success: First, the drawn tungsten cup must be machined to remove any surface imperfections and to completely radius the lip. Next, and probably the

---

* Rockwell International-Rocky Flats.

most important lesson taught by Mr. Bauer, was to not hurry. Tungsten remains ductile down to 300°C, and as long as the steel mandrel is not hotter than the tungsten there is no chance of cracking during this cooling. In the absence of hurry, the crucible surface can be examined for stress risers after each extrusion spinning pass. Stress risers were removed before the following extrusion pass.

Controlled cool-down made it possible to remove the crucibles from the mandrel. Since neither spun crucible would strip from the mandrel after spinning, the mandrel was cooled with water to approximately 250°C, the crucible was quickly heated to 600-800°C, and the crucible was pulled from the mandrel by hand. Another advantage of stopping between spinning passes was that the spinning rollers cooled, decreasing the quantity of grease melting in the bearings and preventing fire.

Tungsten sheet, 0.040 in. thich by 10 1/4 in. by 15 15/32 in., was rolled into a 5-in.-dia cylinder 10 1/4 in. high, using three passes on a three-roll bender. To bend the sheet, it was heated to 900°C in a furnace; torches maintained this heat during rolling. The cylinder exhibited good roundness, made possible by press breaking a 2 1/2-in. radius on the edge leading into the three-roll bender. The exit edge, however, possessed a 1/2-in.-long flat section. The cylinder also had a slight helix, which left one edge 1/4 in. higher than the other.

This rolled cylinder and a drawn bottom cap were brazed together to form a crucible; however, improved joint soundness is needed. The "Macor" glass fixture broke during the brazing operation, and a gap opened in the longitudinal seam of the cylinder, deteriorating the match of the curvature between the rolled cylinder and an outside strip used to fill the gap at the cylinder seam.

The next brazing attempts will include several modifications. The "Macor" fixture will not be the only support for holding the tungsten in position during the braze. The cylinders will be perfectly round with no helix and with less seam gap. The strip to fill the gap will be placed on the inside of the cylinder to provide a better seal at the crucible bottom.

A material considered in addition to tungsten has been impregnated mullite (ceramic). The impregnated materials tried include:

Sample Type	Chemical Name	Chemical Formula
1	Calcium Chromate	$CaO \cdot 2Cr_2O_3$
2	Magnesium Chromite	$MgCr_2O_4$ or $MgO \cdot Cr_2O_3$
3	Chromium Oxide	Cr_2O_3
4	Zirconia	ZrO_2
5	Cerium Oxide	CeO_2
6	Chromite of Zirconium	$ZrO_2 \cdot Cr_2O_3$
7	Chromite of Cerium	$CeO_2 \cdot Cr_2O_3$
8	Calcium Chromite	$CaO \cdot Cr_2O_3$

Each mullite sample is coated with an aqueous solution containing the densifying material and binder. The binder in most cases is chromic acid. However, the binder for sample 4 was zirconyl chloride and that for sample 5 was cerium nitrate. After each coating, the sample is heat-cured at 430-685°C (1000-1250°F). Coating and heat curing steps are repeated until complete densification is achieved. The samples are then final heat-cured at 945°C (1650°F).

The initial corrosion results for impregnated mullite exposed to copper-magnesium/calcium chloride-calcium fluoride at 800°C for 10 days look good. Untreated mullite (approximately 65% dense) showed complete diffusion by the salt phase. None of the impregnated samples showed any deterioration.

Because of the unresolved corrosion results, a test was performed under more severe conditions. The original salt medium was replaced with magnesium chloride-magnesium fluoride. The temperature was 850°C, and time in the bath was increased to 15 days. In this test, only sample types 5 and 8 showed no signs of attack. However, no conclusions can be drawn from this test because the copper-magnesium did not fully melt.

It has since been demonstrated that melting of the copper-magnesium alloy is achieved by (1) premelting the salt and (2) using the eutectic composition of 9.5 wt % magnesium and 90.5 wt % copper. The practice of premelting and solidifying the salt in the graphite boat and then loading the metal on the salt permits better magnesium-copper contact. The magnesium melts at a lower temperature than the salt and is less dense and so its natural position is on top of the salt. When the magnesium is on the bottom of the boat it is believed that it tends to float on the salt upon melting and to lose contact with the copper.

The corrosion test on impregnated ceramic is to be repeated, using the new copper-magnesium composition.

Linde, a division of Union Carbide, prepared one 5-in.-dia by 10-in.-high tungsten crucible for Rocky Flats by plasma spraying. Linde also supplied Argonne National Laboratory with three 3-in.-dia by 3-in.-high tungsten crucibles. The large crucible was sprayed on a copper mandrel which was removed by dissolving the copper in nitric acid. The small crucibles were made by spraying tungsten onto nickel-coated graphite mandrels. Argonne removed the graphite by machining, and Rocky Flats removed the nickel with nitric acid.

All four crucibles are at Rocky Flats for nickel impregnating. The large crucible has been impregnated. Nickel impregnation is accomplished with a nickel nitrate solution. Mr. Tom Taylor of Linde suggested that we aim for a 0.4% increase in crucible weight as a result of impregnation. In the first attempt to impregnate the crucible, the nickel nitrate solution contained 27 g of nickel per liter of solution. This impregnation increased the weight by 0.04%.

Mr. Taylor recommended a 130 g/L concentration to obtain the desired weight increase. In the preparation of this solution, the desired concentration was overshot. If the nickel pickup was a linear function of

nickel concentration, a 186 g/L solution was used. The net increase in crucible weight was 0.8%. The concentration of nickel nitrate will be reduced when impregnating the Argonne crucible. After impregnation, all tungsten parts will be fired in a furnace at Coor's Porcelain.

Two sintered tungsten crucibles made by GTE Sylvania were received in September. The densities of these crucibles were 96.43% and 96.36% of theoretical. They held acetone and, when X-rayed, one crucible was clear of defects and the other showed some indication of porosity in the bottom and at the crucible lip. These porosities were small and are considered insignificant.

The disadvantage of a sintered tungsten crucible is its weight. A sintered crucible large enough for full-scale nuclear fuel processing would be prohibitively heavy, approximately 2400 lb. The problem is that thick walls are required during sintering if the crucible is to hold its shape and that, after sintering, the tungsten is too brittle to machine by conventional methods. We are therefore attempting to machine a sintered tungsten crucible by stress-free electrochemical machining.

An attempt was made to thin the crucibles by electrochemically machining from the inside out, using a dwell type electrode; however, the surface pitted. The depth and number of pits seemed to increase with increasing machining time. It is thought that the pits are generated by nonuniform metal removal caused by the action of electrolyte removing the unbonded grains of tungsten powder faster than the bonded grains. Because of these pits, electrochemical machining has been discontinued and electrochemical grinding will be tried.

The electrochemical grinding process removes metal by 90% chemical and 10% mechanical action, and the resultant surface is smooth. Because Rocky Flats lacks the equipment to radially grind, Y-12 at Oak Ridge will electrochemically grind the sintered tungsten crucible. Here the metal will be removed from the outside diameter.

Samples coated with chromium oxide and brazed tungsten samples coated with plasma-sprayed tungsten to protect the joint have been subjected to corrosion testing in which the corrosive media used were copper-16 wt % magnesium and calcium chloride-20 wt % calcium fluoride. The temperature was 800°C and the time at temperature 10 days. The metal portion of the corrosive media didn't fully melt because of improper magnesium content and poor magnesium-to-copper contact; however, there was corrosion.

The brazed tungsten sample, plasma-spray coated with tungsten to protect the NIORA* (82% gold, 18% nickel) braze, failed the test. Figure 24 is a metallographic view of that part of the braze which saw the salt phase during the corrosion test. Most of the braze is gone because the plasma spray coating did not seal the joint. Figure 25 shows that part of the braze which saw the metal phase. Here, the plasma spray seal is also broken, but there is less attack on the braze. The problem: the plasma

*Western Gold and Platinum Company, Belmont, California.

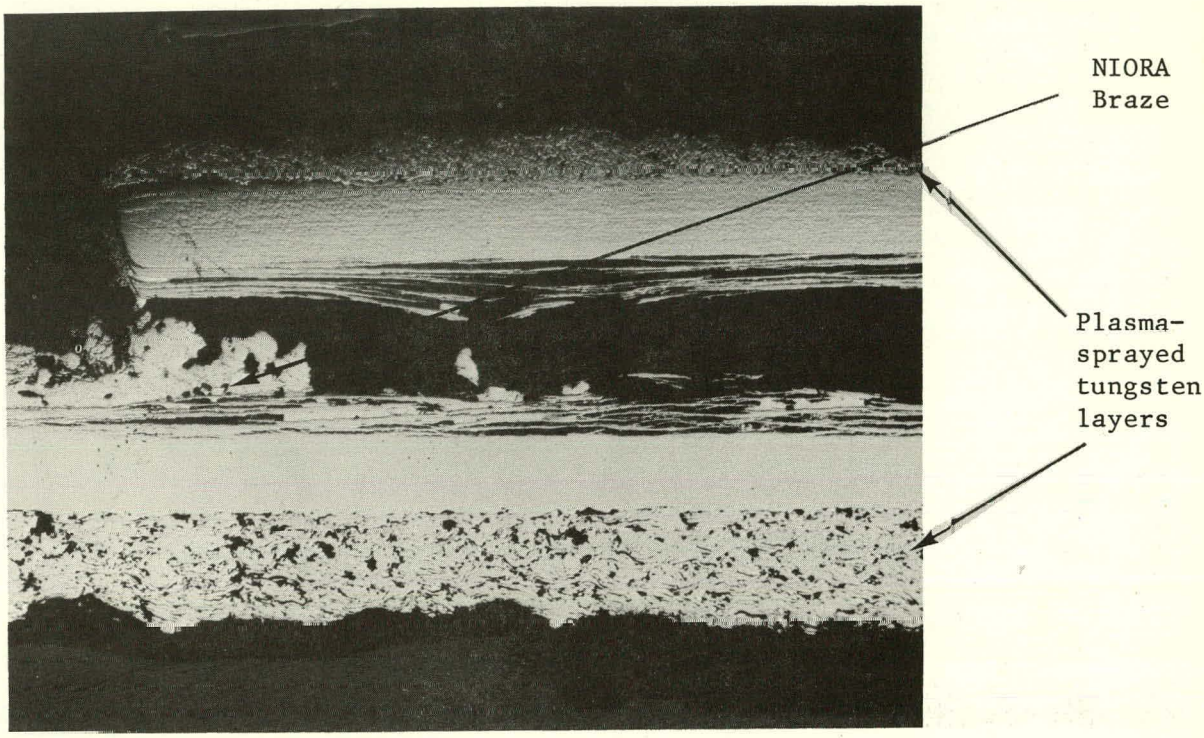

Fig. 24. NIORA Brazed Tungsten with Plasma-Sprayed Tungsten Coating--Attack by Salt Phase. 50X. Notes: 1. Nonuniform thickness of plasma spray. 2. Porous level in plasma spray coating.

spray coating of tungsten did not protect the braze. The quality of the coating has several aspects permitting improvement: the coating thickness was not uniform, and the density was poor.

The plasma-sprayed tungsten samples were shown to and discussed with Mr. Fred Bydash (Metallwerk Plansee representative). The following are his comments: (1) evidence of oxide on the tungsten indicates that there was inadequate atmosphere protection during plasma spraying, (2) Metallwerk Plansee would provide a higher density coating and would improve the bond between the wrought tungsten and the plasma-sprayed tungsten with a thermal post-plasma-spray treatment at 1100°C. A brazed sample using Palnisil* 10 (89.5% silver-0.5% palladium-10% nickel) will be provided to Metallwerk Plansee for plasma spray coating. This braze is a much higher brazing temperature alloy and will not be adversely affected by the post-plasma-spray treatment used by Metallwerk Plansee.

Samples of tungsten and tantalum were coated with chromium oxide with the idea that chromium oxide may be a protective coating on a limited-life vessel. During the corrosion test, these samples lost the

*Western Gold and Platinum Company, Belmont, California.

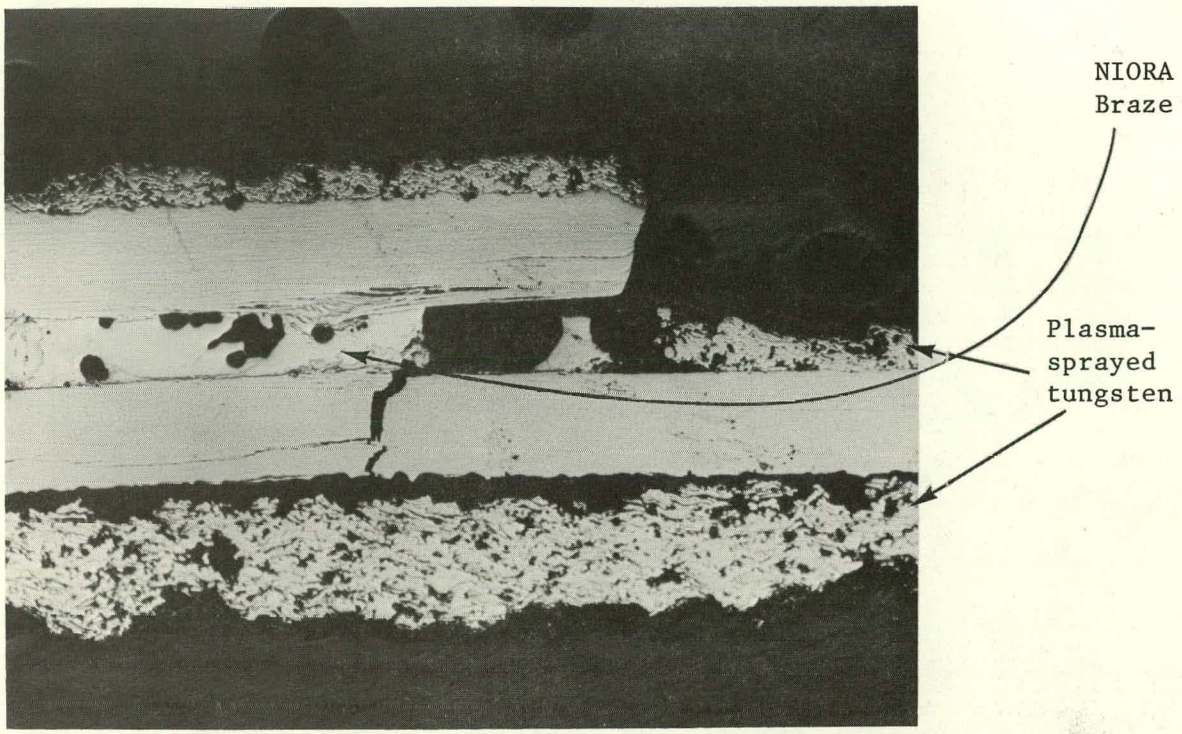

Fig. 25. NIORA Brazed Tungsten with Plasma-Sprayed Tungsten Coating--Attack by Metal Phase. 50X. Note: Lack of bond of plasma-sprayed tungsten to the wrought tungsten sheet.

coating in most areas. The samples were coated by repeated dipping in chromic acid, followed by a thermal firing cycle. The resultant coating was approximately 0.0002 in. thick. The part of the sample in the salt phase lost all of the chromium oxide. The part that had been in the metal phase had some small areas with retained chromium oxide (refer to Fig. 26).

The observations that chromium oxide on the tungsten was attacked and that the chromium oxide-impregnated mullite (sample type 3) showed signs of chemical attack has reduced the emphasis on chromium oxide as the sole protective coating.

Tungsten foil diffusion bonded to molybdenum tubing looks promising. A sample has been prepared by coiling 0.002-in.-thick tungsten foil into a molybdenum tube and then inserting a stainless steel rod. This sample was then heated to 1200°C under 10^{-4} torr vacuum and held for 16 h at temperature. The diameter of the stainless steel rod insert was 0.935 in. (and at 1200°C was 0.952 in.). This forced a 0.011-in. expansion of the inside diameter of the molybdenum tube. Rolling the stainless steel rod in yttria powder prior to inserting it into the tube prevented the tungsten from bonding to the stainless steel. The permanent expansion of the molybdenum plus the ceramic powder interface between tungsten and stainless

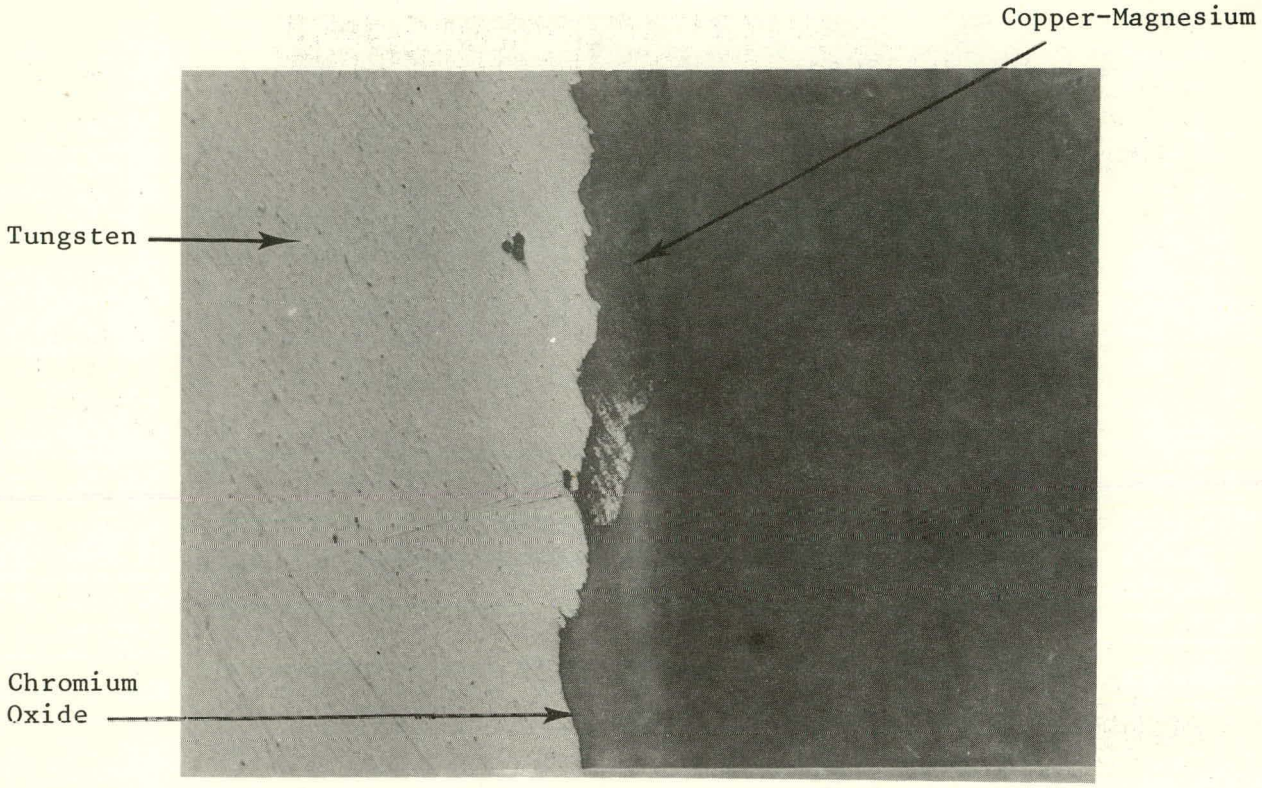

Fig. 26. Chromium Oxide-Coated Tungsten After Corrosion Test--Surface That Had Been Subjected to Metal Phase. 400X.

steel made for easy removal of the stainless rod after bonding. Metallographic examination (see Fig. 27) shows that there is no bond between the tungsten-tungsten interface or the tungsten-molybdenum interface. The most prominent reason for the lack of bond appears to be foreign particles at the interfaces. However, increases in bonding pressure and temperature may also be necessary before a bond is reached.

No further work will be performed in 1979 on bonding of tungsten to molybdenum tubing because of project fund reduction. It is believed that transfer lines of reasonable cost are important for the fuel processing plant and that bonding is the most practical way of lining transfer lines with tungsten.

6. Molten Nitrate Salt Oxidation Processes
(L. L. Burger,* L. G. Morgan,* and R. D. Scheele*)

The objective of this work is to identify chemically feasible nonaqueous reprocessing methods within the framework of nonproliferation. The study examines the treatment of ceramic fuels by molten salts and emphasizes the use of molten nitrate systems. The incorporation of other nonaqueous steps will be considered, where applicable to the development of a conceptual process.

*Pacific Northwest Laboratory.

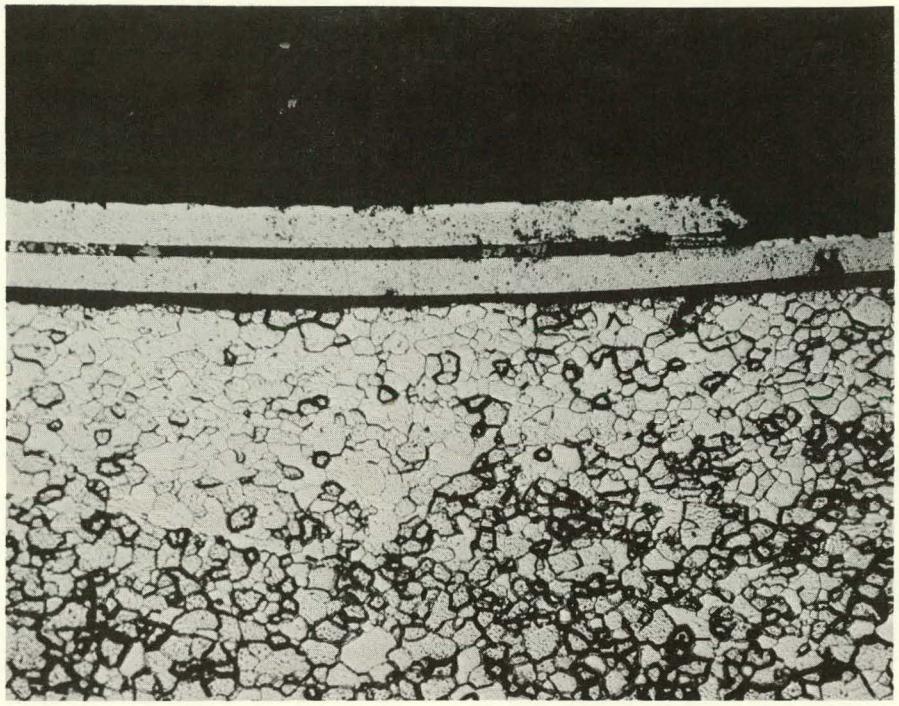

Fig. 27. Tungsten Foil to Molybdenum Tube Bond. 100X. Photograph shows the lapover of the tungsten foil. Note that there is no intermittent tungsten-to-tungsten or tungsten-to-molybdenum contact but rather foreign particles in these interfaces.

a. Engineering Analysis

The engineering analysis phase of our work package for FY 1979 is defined by the following:

- Prepare a preliminary process engineering conceptual design based on studies conducted in FY 1978, flowsheet development, and the experimental work defined under separations processes below. Define material balances and process parameters so that engineering scale-up can be evaluated.

- Identify the nature and composition of waste streams, review waste volumes generated in the process, and study methods of regeneration and recycle of process materials, waste volume reduction, and disposal options.

- Perform a proliferation analysis of the process by reference to criteria to be supplied by ANL.

No engineering analysis studies were scheduled or conducted during this report period.

b. Separations Processes

The separations processes phase of our work package for FY 1979 is defined by the following:

- Perform experiments to determine the actinide behavior and uranate composition in equimolar sodium nitrate-potassium nitrate, as needed to determine uranate stability and to forecast cation behavior in subsequent process steps.
- Determine the optimum conditions for formation of the uranate (i.e., mole ratio of nitrate to uranium, volume of melt, and percent recovery of uranium).
- Continue the studies utilizing 100% nitric acid vapor to determine uranium-plutonium separation and to investigate alternative separation methods--particularly the effects of added anions.
- Investigate each process step for fission product behavior and distribution with respect to the desired actinide recovery.
- Extend the effort to determine uranium-plutonium separation to include the effects of added constituents on the behavior of actinide and fission product compounds in molten nitrates.
- Identify soluble species in molten nitrates and determine whether fission product elements are present as soluble species or solids, also as anionic or cationic species.

Work during this report period is discussed in the following:

(1) Behavior of Plutonium Dioxide in Molten Alkali Metal Nitrates

In preliminary studies conducted in FY 1978 plutonium dioxide did not react with equimolar sodium nitrate-potassium nitrate or form a soluble species upon the addition of 100% nitric acid vapor to the melt. The experimental conditions for adding 100% nitric acid vapor were not, however, identical to those utilized in corresponding studies of the behavior of uranium dioxide. Additional studies are necessary to confirm the FY 1978 results pertaining to plutonium dioxide, to study plutonium-uranium separation, and to determine appropriate further treatment of plutonium dioxide in the process.

An existing glove box, designed and constructed for spectroscopic studies of molten salts, has been readied for our plutonium chemistry studies. A "see-thru" furnace has been installed and tested, the necessary glassware has been designed and constructed, and other apparatus and equipment in support of these studies has been installed and tested. Before the equipment was installed in the glove box, a demonstration run utilizing uranium dioxide was successfully conducted.

Efforts are in progress to obtain a quantity of mixed oxide (PuO_2-UO_2) fuel pellets for project use. Two sources, both at our site, have been identified, and no major problems are anticipated in obtaining this material. As soon as the mixed oxide becomes available, studies of mixed-oxide behavior in molten equimolar sodium-potassium nitrate will be initiated.

(2) Effects of Added Anions in Molten Alkali Metal Nitrates

Studies are continuing on the effects of added anions in equimolar sodium-potassium nitrate. The solubility of sodium carbonate in equimolar sodium-potassium nitrate is, as expected, temperature-dependent. In our preliminary solubility measurements, reproducible results of this solubility were difficult to obtain. The nonreproducible behavior has been determined to be caused by temperature fluctuations during the test period. A method which allows accurate temperature control and measurement, as well as a sampling technique which does not disturb this temperature control, have been developed. No quantitative solubility tests have yet been conducted due to other work having higher priority.

Experiments have been performed to determine the quantitative relationship of added sodium carbonate to the reaction of uranium dioxide in the melt system. Quantitative analyses of the uranium product and determination of carbonate ion remaining in the melt have been conducted.

The reaction of uranium dioxide with equimolar sodium nitrate-potassium nitrate containing sodium carbonate was conducted at four temperatures. The initial reactants were: sodium nitrate (0.13 mol), potassium nitrate (0.13 mol), uranium dioxide (1.85×10^{-3} mol), and sodium carbonate (2.83×10^{-3} mol). The reactants were placed in a Pyrex reaction vessel, which in turn was placed in a controlled-temperature muffle furnace that was allowed to remain at the desired temperature for a period of two to four hours.

The compositions of the solid uranium products from these trials are given in Table 24. The values cited are each averages of three determinations performed on the product from a single experiment. The alkali metal species and content were determined by atomic absorption; uranium content was determined by X-ray fluorescence, utilizing strontium as an internal standard.

Empirical formulas of the products were obtained, it being assumed that oxygen is the other constituent of the compounds. X-ray powder diffraction patterns were also obtained for each sample. Analyses of

Table 24. Alkali Metal Uranate Composition

Temp, °C	Na, wt %	K, wt %	U wt %
300	6.70	3.04	66.4
350	6.65	1.30	70.0
400	6.51	0.55	74.8
450	6.57	0.64	73.0

the total amount of carbonate remaining in the salt phase of each experiment were also conducted. The results are summarized as follows:

- The sodium to uranium atomic ratio is one to one at each temperature.
- The X-ray powder diffraction patterns indicate only the presence of sodium diuranate, $Na_2U_2O_7$, in the solids produced at each temperature. However, the intensities of the lines indicate that noncrystalline material is present as well.
- The oxygen balance, obtained by difference, does not agree particularly well with that of a diuranate compound. This may be due to (1) analytical inaccuracies for the other elements or (2) the presence of the amorphous material (which might have a higher oxygen to uranium ratio than the diuranate).
- The trend of decreasing potassium content in the uranium compound as the temperature increases appears to be both reproducible and real, giving an indication of the relative stability of the alkali metal diuranates as a function of temperature.
- Experimental "blanks" have shown that sodium carbonate does not decompose at the temperatures studied; however, the carbonate analysis technique utilized had approximately a ten percent error.
- Carbonate analyses of the salt phase after reaction indicate that there was no carbonate loss (within the accuracy of the measurements).

These results indicate that carbonate ion has no effect on the reaction of uranium dioxide in molten equimolar sodium-potassium nitrate. The previously postulated reaction of

$$U_2O_7^{2-} + CO_3^{2-} \rightarrow 2\ UO_4^{2-} + CO_2(g)$$

does not occur in our system under the conditions described.

A previous report [STEINDLER-1979] that indicated an enhanced uranium dioxide reaction rate at lower temperatures when carbonate ion was present must be revised in view of the current results. Additional data have shown that the reported temperatures (at which, it was believed, the presence of carbonate ion increased the reaction rate) were in error; the actual temperatures were higher, and it has been shown that increasing the temperature increases the reaction rate.

Experiments to determine the effects of carbonate ion will be discontinued except for a test of its effect on plutonium dioxide under similar experimental conditions.

Selective addition of other anions, whose behavior in our melt system can be interpreted on the basis of the Lux-Flood acid base definition, will be studied, provided that their behavior is predicted to be beneficial to our process.

(3) Development of Analytical Methods

Radioactive tracers will be utilized in the determination of transuranic and fission product behavior in our studies. Counting equipment is available for direct use by our personnel and will therefore aid in reducing the time lag between an experiment and the analytical results.

We have recently acquired the capability of performing cation and anion analyses, utilizing ion chromatography. This relatively new technique will be investigated as a method of studying fission product distributions utilizing nonradioactive materials. If successful, this method would be a valuable supplement to the use of radioactive tracers.

c. General Research Problems

In the course of our studies and review of other work, several problem areas reappear frequently. Because these may be common to several of the projects, commenting on some of them from time to time is worthwhile. Examples are the following:

(1) Nature of Fission Products in Irradiated Fuel

The nature of fission products in irradiated fuel is a fascinating and important problem in the broadest sense. However, for the present, a specific case is considered: How does one synthesize an oxide mixture that simulates the fission product form in the irradiated fuel? The dissolving characteristics and process partitioning cannot be defined or even reproduced unless we know the chemical and physical states of the elements in irradiated fuel elements. At present, all experiments except those performed with "hot" samples are subject to question.

(2) Phase Separation in Salt and Metal Melts

Phase separation is both a scientific and an engineering problem. A typical example is separation of a solid powder from a melt. Solids which separate usually appear as fine powders whose size changes little with time. Why is crystal growth slow? Is there insufficient surface free energy (interfacial surface energy) so that solubility as a function of particle size is not a driving force? Is the solubility so low or the temperature coefficients so small that the kinetics are just impossibly slow?

(3) Thermodynamics

More and better thermodynamic data can help in studying reactions in solutions, as well as in other areas. Very strong interactions are often seen in both the liquid and solid phases (large negative excess free energies). This indicates that chemical species need to be investigated and also implies that care must be exercised in controlling the purity of solutions in thermochemical measurements.

It is recognized that PDPM does not have the goal of gathering fundamental data, but when they can be obtained the information may be a valuable contribution.

(4) Applications of Pyroprocessing

Aside from the goal of nonproliferation, what special features might make pyrochemical methods worthy of future consideration? Discussions at ANL [MYLES] indicated that PDPM might be adaptable in countries that have a relatively small nuclear power program. Close-coupled fuel reprocessing may be one application. Other features that may be important include:

(a) There may be the potential of separating radioactive wastes for more logical packaging than is now planned for waste storage or disposal. No fuel reprocessing scheme has been designed to give waste handling and ultimate waste disposal major emphasis. This concept may prove to be a very important factor in future fuel reprocessing.

(b) A logical extension of item (a) is the separation and isolation of fission products. The following assumptions may be made: (1) nuclear power will continue to expand because there will be no viable alternative for the next 30 y, (2) plutonium will be separated and recycled because power is cheaper with it than without it, (3) the economically and strategically important nuclides produced as byproducts will be recovered because they are a valuable natural resource and, in some cases (e.g., the noble metals) byproducts may be a major source. Improved technology in isotope separation may allow the potential value of these nuclides to be realized. Thus, the next generation of nuclear philosophy may consider the "whole package" which is not politically acceptable at present. A fresh look at the fuel cycle (including new processing methods) offers an opportunity to realize the full potential of uranium fission.

7. Molten Salt Processes Applied to Nuclear Fuels

(D. H. Smith* and E. C. Douglas*)

The purpose of this program is to establish chemical bases for proliferation-resistant methods utilizing molten salts and/or metals for reprocessing nuclear reactor fuels.

a. Progress

(1) Engineering Analysis

The current zero-level flowsheet utilizes ammonium chloroaluminate, NH_4AlCl_4, to recover purified, coprocessed actinides from metallic bismuth. The metallic actinides are oxidized with HCl and dissolve in the solvent salt. The salt and metal phases are then separated, and the solvent salt is distilled off to leave the concentrated actinide chlorides for conversion to fuel [SMITH-1978A].

Although the results of our literature survey and scouting experiments [SMITH-1978A, 1978C] indicate that the use of ammonium chloroaluminate should be successful, we have examined two types of other salts to determine if a better substitute for ammonium chloroaluminate could be found. The two groups of salts examined were (1) compounds with molecular ions which are expected to undergo the reaction $NH_4MCl_4 = HCl + NH_3MCl_3$, characteristic of NH_4AlCl_4, and (2) salts with monatomic ions.

Table 25 summarizes the information found in the literature for two compounds of the first type, NH_4GaCl_4 and NH_4FeCl_4. Less is known about the ferrate compound, but ammonium chlorogallate is a promising backup for ammonium chloroaluminate. As shown by Table 39, the chemistry and phase transition temperatures of the two salts are quite similar. Apparently, nothing is known about the solubilities of actinide chlorides in ammonium chlorogallate or in ammonium chloroferrate.

Table 26 summarizes the melting points, boiling points, and solubility data available for several low-boiling salts with monatomic ions. The chlorides of indium, tin, and zinc melt between 200 and 300°C and have boiling points which are about 400°C higher. The temperature range for lead chloride, which melts at about 500°C and boils near 954°C, is also reasonably favorable.

Some information is available concerning the solubilities of actinide chlorides in these salts. The phase diagram of $UCl_4/PbCl_2$ is known, and shows a very high solubility of the uranium tetrachloride [STERLIN]. The phase diagram of UF_4/SnF_2 is also known [THAMER] and suggests that the solubility of uranium tetrachloride in tin chloride might be sufficiently large for process requirements. No information has been found on the solubilities of uranium trichloride in any of these salts.

---

*Oak Ridge National Laboratory.

Table 25. Physical Constants of NH_4MCl_4 and NH_3MCl_3 Compounds

Compound	Melting Point, °C	"b.p.," °C	Solid Density, mol/L
NH_4AlCl_4	304[a]	380[b]	9.26[c]
NH_4GaCl_4	304,[d] 308[e]	f	9.09[c]
NH_4FeCl_4	295, 297[g]	--	9.09[c]
NH_3AlCl_3	127[h]	418[i]	--
NH_3GaCl_3	124[h]	438[c]	--

[a] [KENDALL]

[b] [LAUGHLIN-1975A]

[c] [FRIEDMAN]

[d] [KRAUS, HAMMOND]

[e] [FEDEROV]

[f] Calculable from data in [FRIEDMAN], if NH_3GaCl_3/NH_4GaCl_4 solutions are ideal.

[g] [HACHMEISTER]

[h] [KLEMM]

[i] [LAUGHLIN-1975B]

Table 26. Physical Constants and Solubility Data for Selected Low-Boiling Salts with Monatomic Ions

Compound	Melting Point, °C	Boiling Point, °C	Binary Phase Diagram	Approx. Solubility, mol %
InCl	225	608	--	--
$InCl_2$	235	560 ± 10	--	--
$SnCl_2$	245	652	--	--
$ZnCl_2$	283	732	--	--
$PbCl_2$	498	954	UCl_4[a]	60(500°C)
SnF_2	200		UF_4[b]	21(600°C)

[a] [STERLIN]

[b] [THAMER]

In conclusion, NH_4GaCl_4, NH_4FeCl_4, $ZnCl_2$, and $PbCl_2$ all appear to be reasonable substitutes for NH_4AlCl_4. However, far less is known for these solvents than is known for ammonium chloroaluminate about solubilities of actinide chlorides, possible volatile complexes with actinide chlorides, etc. Hence, in the continued absence of any difficulties with ammonium chloroaluminate, the latter salt is preferred.

Considerable time was also spent during the first month of FY 1979 on analyses of the proliferation resistance of the PROMEX and the "Pyro-CIVEX" flowsheets [SMITH-1978B].

(2) Separations Processes

A systematic study was begun this quarter of the rates of dissolution of ThO_2 and UO_2 sol-gel microspheres with aluminum trichloride dissolved in lithium chloride, which would be a head-end step for oxide fuel reprocessing. Two series of experiments are planned for each actinide oxide: (1) measurement of the temperature dependence of rate of dissolution in $LiAlCl_4/AlCl_3$ eutectic (40:60 mol % LiCl:$AlCl_3$) and (2) determination of the effect of Lewis acidity on the dissolution rate at 640°C. The initial (up to about 25% consumption of the AnO_2, where An represents an actinide) rates of reaction of unground microspheres will be measured in an excess of molten $LiCl/AlCl_3$, so that the composition and acidity of the solvent salt will be essentially constant during the reaction run. With a full set of these empirical data, it should be possible to predict the rate of fuel dissolution under various typical process conditions of changing temperature and composition. Based on our review of the literature [SMITH-1978C], we assume as a working hypothesis that the net reaction may be written

$$3AnO_2 + 4AlCl_3(\text{salt phase}) = 3AnCl_4(\text{salt phase}) + 2Al_2O_3 \qquad (1)$$

Initial experiments were carried out with thorium oxide, since this has frequently been reported to be the most refractory of the actinide oxides. As shown in Fig. 28, the rate of dissolution of ThO_2 into the $LiAlCl_4/AlCl_3$ eutectic at 220°C has been found in multiple experiments to obey the equation

$$\log [Th] = A \log t + \log B, \qquad (2)$$

where t is the reaction time, [Th] is the concentration of dissolved thorium, and A and B are constants.

Table 27 and Fig. 28 each summarize the results of the three experiments: In two of these, the solvent salt was stirred rapidly with a magnetic stirring bar and the reaction flask was opened periodically for the removal of samples of the salt phase. In the third experiment, the reactants were sealed into evacuated tubes (one tube per reaction time), and only very slight stirring was provided.

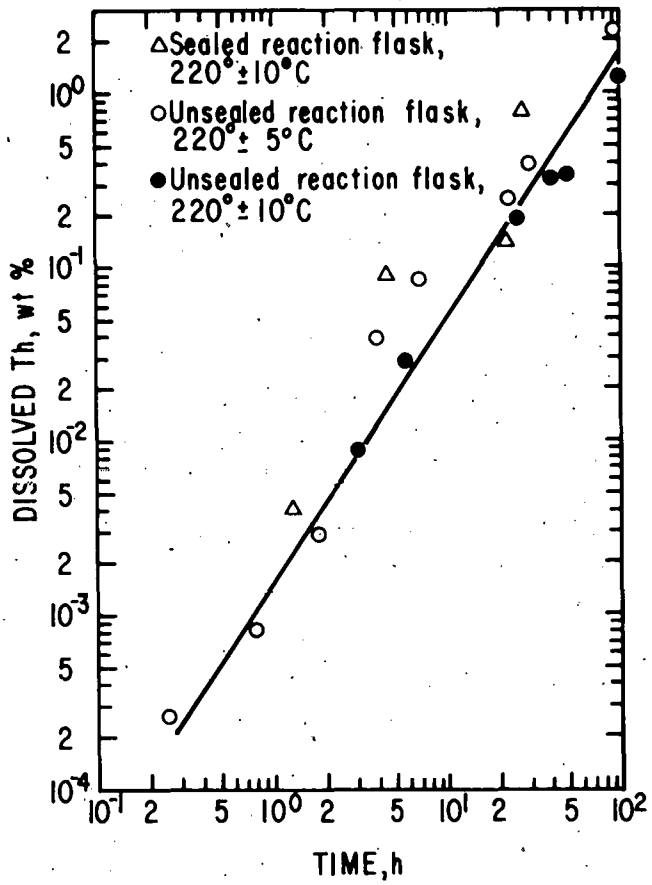

Fig. 28. Rate of Dissolution of ThO_2 Microspheres (12-16 mil) in $LiCl/AlCl_3$ (40/60 mol %) at 220°C from about 0% to about 25% Reaction of the ThO_2. The acidity of the melt was essentially constant during the reaction (initial system composition, 11.59 g salt/g ThO_2) in the three experiments.

The results of all three experiments were in agreement, indicating that the reaction rate was unaffected by atmospheric moisture or oxygen or by the rate of stirring. Scatter in the data of Fig. 28 is believed to be due to (1) fluctuations in the temperature of 5 to 10°C, (2) errors in the chemical analyses, and (3) nonuniformities of the diameters (and possibly other properties) of the microspheres.

Equation 2 may be rewritten as

$$[Th] = Bt^A \qquad (3)$$

hence

$$t = ([Th]/B)^{1/A}$$

Table 27. Initial Rate[a] of Dissolution of ThO_2 Microspheres into $LiAlCl_4/AlCl_3$ Eutectic at 220°C. Three experiments.

[Th], wt %	Reaction time, h
0.000266[b]	0.25
0.000857[b]	0.50
0.004[c]	1.3
0.003[b]	1.75
0.009[d]	3.0
0.04[b]	3.75
0.09[c]	4.5
0.029[d]	6.0
0.088[b]	6.75
0.054[d]	16.0
0.14[c]	22.0
0.25[b]	22.25
0.195[d]	25.0
0.77[c]	27.5
0.40[b]	29.5
0.329[d]	40.0
0.350[d]	49.0
0.503[d]	88.0
2.23[b]	94.5
1.23[d]	97.0

[a] 12 to 16-mil diameter.

[b] Unsealed reaction flask, 220 ± 5°C.

[c] Sealed, evacuated tubes, 220 ± 10°C.

[d] Unsealed reaction flask, 220 ± 10°C.

Differentiation of Eq. 3 gives

$$\frac{d[Th]}{dt} = ABt^{(A-1)} \tag{4}$$

or

$$\frac{d[Th]}{dt} = AB^{1/A}\,[Th]^{(A-1)/A} \tag{5}$$

Inspection of Fig. 28 shows that $A > 1$ or, with reference to Eq. 5, the dissolution of solid ThO_2 was "self-catalyzed" by the thorium in solution.

Previous workers [GIBSON, VANDER WALL] have reported that when the chlorinating agent was Cl_2, the reaction of actinide oxides was catalyzed by the presence of salts with multiple valent cations. However, the catalysis mechanism must differ in the present case, since thorium has only one non-zero oxidation number.

A linear regression fit of Eq. 2 to the data of Fig. 28 gives $A = 1.369$ and $B = 2.83 \times 10^{-3}$(g Th)(100 g salt)$h^{-1.37}$. Hence, at 220°C, the rate of dissolution into the $LiAlCl_4/AlCl_3$ eutectic was $d[Th]/dt$ (g Th/100 g salt h) $= 3.87 \times 10^{-3}[Th]^{0.27}$.

The surface area of the thorium oxide per unit mass was $A_s = 3/\rho\bar{r} = 17.2$ cm^2/g ThO_2, where $\rho = 9.86$ g/cm^3 and $\bar{r} = (0.0178 \pm 0.0030)$cm. The initial salt to thorium oxide ratio was 11.59 g salt/g ThO_2.

b. Plans for Next Quarter

Work on the series of experiments for dissolution of fuel oxides will be continued. Thermodynamic and mass balance analyses of the process flowsheet will be made.

8. Molten Tin Process for Reactor Fuels

(O. Krikorian,* J. Grens,* M. Coops,* and W. Parrish*)

The objective of this work is to identify chemically feasible pyrochemical reprocessing methods within the general frame of nonproliferation. This effort is aimed at decomposition and dissolution of spent fuel elements and the formation of thorium, uranium, and plutonium nitrides in molten tin solutions. Separation of fission product elements and other impurities by the use of various physical and chemical processes is anticipated.

a. Scope of Work Package

Lawrence Livermore Laboratory will provide program management, studies and analyses, fuel reprocessing flowsheet development, and general support for the research and development of molten tin processes for the

*Lawrence Livermore Laboratory.

removal of fission products and other impurities from spent uranium-plutonium and thorium-uranium (plutonium) fuels in oxide, metal, or carbide form. Initial effort is planned to be on oxide fuel, followed by metal and then carbide. For an oxide fuel, a carbothermic reduction reaction is used in which the fuel is introduced directly into tin at about 1900 K in the presence of excess carbon.

More specifically, effort will be directed in FY 1979 to determining the technical feasibility of a selected process flowsheet. Laboratory experiments will be performed with small-scale simulated fuel specimens to refine process parameters and to test process performance. A topical report will be prepared containing a review of thermodynamic and kinetic data relevant to the process, and a proliferation analysis will be made for the process according to guidelines established by Argonne.

b. Engineering Analysis

Based on initial evaluations of the literature data on the thermodynamics of fission products dissolved in molten tin, we estimate that the activity coefficients of fission products in tin solution are generally in the range of 10^{-1} to 10^{-3} at 1900 K. These activity coefficient values are substantially higher than our earlier estimates, and therefore, in most cases, we need to revise our earlier values of fission product volatilities upward by about 2 to 3 orders of magnitude. Lanthanides will have the lowest activity coefficients in tin, with values of about 10^{-3} at 1900 K. This compares with about 10^{-2} for uranium; taking into account the rest of the thermodynamics involved, it indicates that a significant proportion of the lanthanides should remain in solution in liquid tin during the nitriding step in which UN is precipitated out.

The process flow diagram has been revised to reflect the above findings (see Figs. 29 and 30). The principal changes are (1) to volatilize a greater portion of the fission products after the carbothermic reduction step, and (2) to use a second-stage nitriding step at higher nitrogen pressures to remove residual actinides and lanthanides from the spent tin solvent. The estimated degree of removal of fission products in the volatilization step (i.e., evaporation step), is shown for 10% and 25% distillation removal of the tin solvent (Fig. 30). As shown, not only should the usual volatiles be removed, but also significant amounts of Sr, Ba, Sb, Sm, and Eu.

c. Separations Processes

(1) Carbothermic Reduction of UO_2 in a Tin Bath

Two additional experiments (experiments 3 and 4) were conducted this quarter on the carbothermic reduction of UO_2. The reactions were carried out in graphite crucibles, using 50 g of tin and 10 g of UO_2 microspheres (150-210 μm in diameter) for each run. Progress of the reaction was monitored by using a calibrated gas volume (about 10 L) in the system, isolating the system under vacuum, and observing the rate of CO gas generation. The reaction is represented by

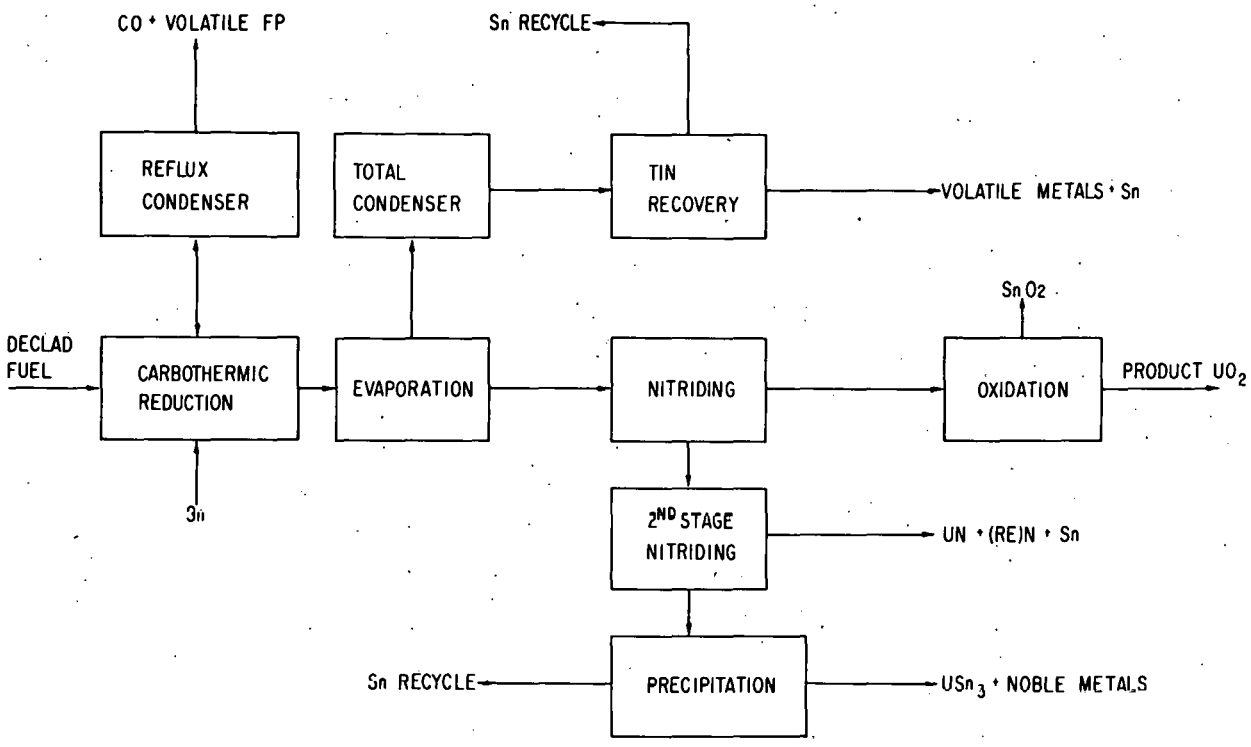

Fig. 29. Flowsheet for the Molten Tin Process. The process has been revised to provide a higher fraction removal of fission products by volatilization in the evaporation step.

$$UO_2(s) + 2C(\text{in Sn soln}) \rightarrow U(\text{in Sn soln}) + 2CO(g).$$

The rate of reaction in experiment 3 (see Fig. 31) was found to be linear and quite slow at 1873 K--the gas generation rate was 4.5 torr/h, corresponding to about 10% reaction in 3 h. In experiment 4, 4.7 g of cobalt was added as a catalyst to a fresh batch of Sn/UO_2 and the experiment was repeated (initially at 1873 K). A catalytic effect of cobalt is postulated on the basis that it promotes the solubility and permeation rate of carbon in the solvent. The reaction rate of the catalyzed mixture was found to be 27 torr/h (or six times the earlier rate) and constant with time. The rates were then checked at 1823 K and 1913 K and were found to be 12 torr/h and 36 torr/h, respectively. Upon returning the temperature to 1873 K, however, a new rate (approximately constant in time) of 65 torr/h or 14.5 times the rate of the uncatalyzed mixture was observed (see Fig. 31). At this latter rate, carbothermic reaction would be complete in 2 h. A possible explanation for the observed increase in rate at 1873 K is that as uranium dissolves in the tin, it as well as cobalt acts as a carrier for carbon in the solvent. In addition to cobalt and uranium, we should also be able to use iron and nickel for promoting carbon solubility and permeation through the melt.

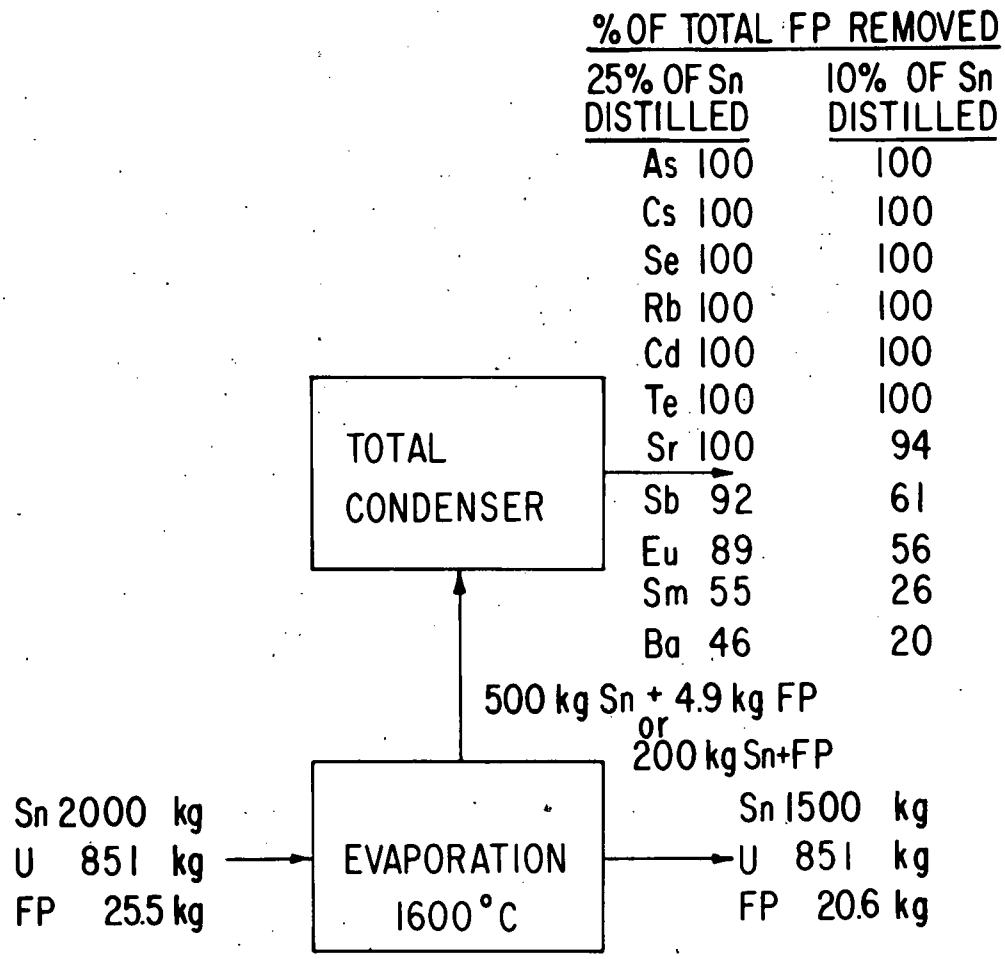

Fig. 30. Portion of Flowsheet showing Mass Flow through the Fission Product Volatilization Step. Estimated percentages of fission products removed are illustrated for the distillation of 25% and 10% of the tin solvent, respectively.

(2) Nitriding of Uranium in Tin

We carried out nine runs (experiments 5 to 13) to evaluate the rates and yields for nitriding uranium dissolved in tin. Results of these runs are summarized in Table 28. Using a sample composed of 9 g of U dissolved in 50 g of Sn and an overpressure of 0.9 atm N_2 (exp. 6), we found the average rate of nitriding of the uranium to be 26%/h over a 2.6-h period. The rate varied somewhat during the run, reaching a peak rate of 35%/h at one point.

Recognizing the low solubility and consequently low permeation rate of nitrogen in molten tin, we reasoned that the addition of certain metals to the melt might improve nitrogen solubility. Metals such as Ca, Ba, V, and Cr are known to form nitrides at lower temperatures, and

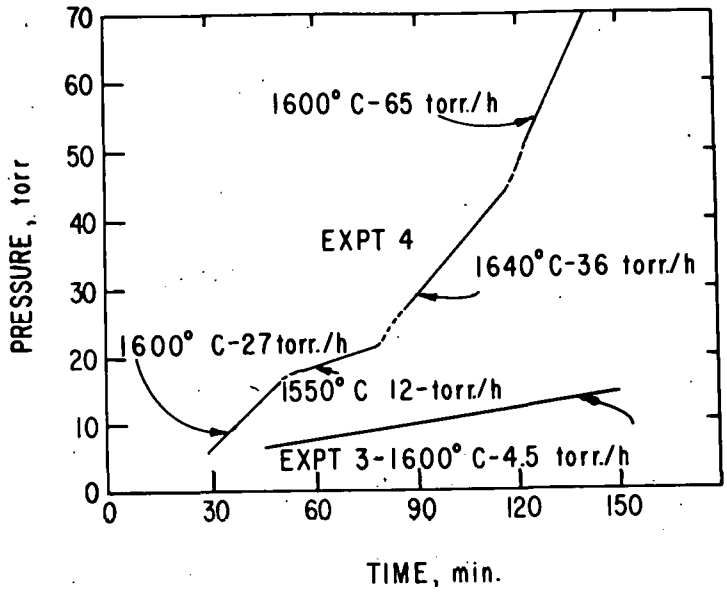

Fig. 31. CO Pressure vs. Time for the Carbothermic Reduction of UO_2 in Tin in the Presence of Graphite. Cobalt was added as a catalyst in experiment 4 to increase the rate of reaction.

this affinity for nitrogen might promote nitrogen solubility in the melt at 1900 K, even though they are not expected to form nitrides at this temperature.

In a series of experiments (experiments 8-13), we explored the effect of potential catalysts on nitriding rate under stagnant nitrogen. We used a mixture of Cr, V, and Ca on the first try (exp. 8) and found an approximately threefold increase in nitriding rate in comparison with the earlier uncatalyzed run with static nitrogen. Nitrogen uptake was complete in 1.2 h; with an additional hour of exposure, there was no further change in nitrogen pressure. The amount of nitrogen uptake, however, was in excess of the amount required to form UN. We concluded that vanadium as well as uranium had nitrided under these conditions. The material balance was then confirmed to within 2-3%, which is within the uncertainty of the nitrogen pressure and volume measurement. In the remaining catalysis experiments, we attempted to identify the metals catalyzing the nitriding reaction. We firmly established that calcium is an effective catalyst (1.3 h for complete reaction), while chromium and vanadium are not. Barium did not appear to catalyze the reaction, but results were not clear-cut since in the experiment with barium (11), most of the uranium had already been nitrided and so uranium was present at a substantially reduced activity. We conclude from these preliminary experiments that the nitriding reaction can be catalyzed by at least one catalyst (calcium) to obtain essentially complete conversion (within 2-3%) of uranium to UN.

Table 28. Uranium Nitriding in Molten Tin (Reaction vessel was pressurized with N_2)

Sample Composition: 50 g Sn, 9 g U
Reaction Temperature: 1900 K
Nitrogen Pressure: 0.9 atm

Exp.	Catalyst	Run Duration, h	Uranium Nitriding Rate, %/h	Remarks
5	None	4	—	U nitriding rate obscured by nitriding of ZrO_2 insulation. Carbon wool was used as insulation in later runs.
6	None	2.6	26	Reference rate for uncatalyzed reaction.
7	None	2	—	N_2 bubbled through melt at 10 cm^3/min for 1 h. Sample, held in stagnant N_2 for an additional hour, showed a pressure rise (denitriding?).
8	1 g Cr, 1 g V, 2 g Ca	1.2	80	Catalyst was effective. Complete nitriding of both uranium and vanadium.
9	1 g Cr	1.6	30	Chromium is not an effective catalyst.
10	1 g Cr, 1 g V	1	20	Add-on to experiment 9. Catalyst is not effective. Nitriding rate is corrected to reflect nitriding of V. If only U is nitriding, rate is 40%/h.
11	1 g Cr, 1 g V, 1 g Ba	1	20	Add-on to melts from experiments 9 and 10. Barium shows no significant catalytic effect here, but note that the uranium activity was low because most of the uranium had been nitrided in experiments 9 and 10.
12	1 g Ca	2	75	Calcium is an effective catalyst. Reaction went to completion in 1.3 h.
13	2 g Ca	1	—	An additional gram of calcium was added to melt from experiment 12. No further nitrogen uptake was noted.

We also conducted an experiment (7) in which we bubbled an excess of nitrogen through the uncatalyzed melt for one hour and then held the sample under stagnant nitrogen for an additional hour. We believe that the uranium nitrided completely during the flow phase since no additional nitrogen uptake occurred during the stagnant phase. Puzzling, however, was a slight gradual pressure rise during the stagnant phase. It seems unlikely that any UN could have denitrided. In any event, combining a metallic catalyst with a nitrogen sweep system should promote reaction even further in a commercial plant.

(3) Nitriding of Th/U Mixtures in Tin

We have begun experimentation to explore the separation of thorium from uranium by preferentially nitriding out ThN from Th/U mixtures dissolved in molten tin. Nitriding seems to be a reasonable approach for separation, considering that ThN is substantially more stable than UN (i.e., ΔH°_{f298} = -90.6 kcal/mol for ThN compared with -70.4 kcal/mol for UN [KORDIS]). We made two runs. The first run was made to establish the conditions under which uranium does not nitride. We used a composition of 50 g Sn, 1 g U, and 1 g Ca (Ca was included as a catalyst) at 1900 K under stagnant nitrogen. A sequence of nitrogen pressures was used, namely, 304 torr, 432 torr, 507 torr, 608 torr, and 704 torr, and the pressure versus time curves were observed for 30 min at each input pressure setting. Within the accuracy of the capacitance pressure manometer used to record the pressure, no nitrogen uptake was observed under any of these conditions. If as much as 6% of the uranium present had nitrided, it is believed it would have been detected. It was especially surprising that nitriding did not occur at the highest pressure (704 torr), since in our earlier work in which we had started with higher uranium contents [see Section (2) above], the reaction essentially went to completion. Work by others [ANDERSON] indicated a threshold reaction pressure of 486 torr at 1840 K.

In the second experiment, we added 9 g of thorium to the mixture of 50 g Sn, 1 g U, and 1 g Ca from the earlier experiment, and nitrided under 395 torr nitrogen for 2 h at 1880 K. The nitriding rate for the thorium was found to be 6%/h. We conclude that thorium will nitride in molten tin under conditions where uranium will not, although the reaction rate was low in the first experiment conducted here.

(4) Nitriding of U/Pu Mixtures in Tin

Equipment assembly to permit high-temperature investigation of the precipitation of uranium-plutonium nitride from a tin solvent is nearing completion. This work will be performed in existing plutonium foundry facilities by installing new components in the existing alpha-contaminated equipment. To simplify installation, we have constructed a simple mock-up of the existing system so that experimental equipment can be assembled prior to committing it to a "hot" system. The mock-up and the first experimental test assembly are essentially complete. Initially, the tests will utilize approximately 80% U-19% Pu as the mock spent fuel with a small amount of calcium catalyst to promote nitridation and will be run in

a stagnant nitrogen atmosphere. We are also in the process of developing methods for analyzing the results. We expect to isolate the nitride precipitate from the melt by reheating the charge to a few hundred degrees above the melting point of tin and then either filtering or using a centrifuge for the separation.

d. Plans for the Next Quarter

The major technical goals for the coming quarter are to evaluate the separation factors for U/Pu and Th/U mock fuels in the nitriding step. We also expect to begin studies on the separation of fission products from actinides.

9. Engineering Support for the PDPM Program
(K. M. Myles, E. D. Creamer, and O. C. Linhart)

The objective of this work is to assist the PDPM Program management in evaluating the proliferation resistance, process equipment designs, conceptual process scoping designs, and materials applications of all other work in the program. This assistance will be provided by reviewing various reports, participating in the technical information exchange meetings, utilizing other appropriate means of interaction with others in the program, and performing exploratory experimental engineering projects.

Several engineering aspects of the zinc distillation process were studied. Calculations showed that the rate at which the molten metal solvent can be transferred from the decladding vessel is only minimally affected by the presence of restrictors placed in the line to control the quantity of entrained fuel particles. From an analysis of the literature, it was concluded that the amount of unrecoverable uranium collecting on the sidewalls of the zinc still pot is best controlled either by preventing the formation of zinc vapor bubbles in the melt or by redissolving the uranium in a zinc wash.

Data from various mass transfer operations (e.g., dissolution) were examined, and correlations were sought using dimensionless numbers such as the Sherwood number and Reynolds number. Extrapolations of existing correlations tentatively fit liquid metal-fuel pellet data. The correlations predict that alternative means of agitation to impeller mixing, such as pulsed columns, can be effective in mass transfer operations. These dimensionless correlations also may permit predictions for scale-up from results of small-scale laboratory experiments, provided that the necessary variables have been measured.

II. ENCAPSULATION OF RADIOACTIVE WASTE IN METAL

(L. J. Jardine, K. F. Flynn, W. J. Mecham, and R. H. Pelto)

The major objective of this program is to identify the advantages and disadvantages of encapsulating solidified radioactive waste forms in a metal matrix. The net attributes of metal encapsulation, if any, are to be identified by comparisons of waste form properties and fabrication methods with those of other well-developed solidification alternatives--i.e., calcination and vitrification in the special case of high-level radioactive wastes.

Laboratory-scale investigations are in progress specifically aimed at generating data required to further assess probable or unresolved problem areas. Experimental studies during this report period have focused upon the determination of leach rates of simulated waste forms and the development of a casting method to encapsulate glass bead and ceramic simulated-waste forms in lead. A study aimed at assessing the impact resistance of metal-encapsulated waste forms in comparison to glass waste forms has continued during this period.

A. Leach Rates of Simulated Radioactive Waste Materials

1. Introduction

Leach rate studies of materials under consideration for the disposal of high-level radioactive waste (HLW) are being advanced. These studies are part of a continuing program directed toward establishing the integrity of radioactive waste material against dispersal from terminal repositories by hydraulic means. Neutron activation analysis (NAA)* techniques [STEINDLER-1978A, FLYNN] have been used exclusively in measuring leaching. During this report period, time sequential studies of the leach rate of two metal-matrix composite waste forms and two highly leach-resistant glass forms (neutron-activated Pyrex and PNL 76-68) have progressed. Additional information on these studies can be found in previous reports in this series [STEINDLER-1977, 1978A, 1978B, 1978C, 1978D, and 1979].

2. Experimental Procedures, Results and Discussion

a. Leaching of Borosilicate Glass

Leach rate studies using Pyrex (borosilicate) glass beads (0.4-cm) have been undertaken. About 150 g of these beads were neutron-activated in the isotope tray of the Argonne National Laboratory (ANL) CP-5 research reactor for 24 h to a neutron fluence (n/cm^2) of about 5×10^{17}. The irradiated beads were allowed to cool for several weeks to allow the short-lived activated species (e.g., ^{24}Na) to decay. After this cooling period, 30 beads (3.85 g) were gamma counted, using a lithium-drifted germanium (GeLi) detector.

---

*In NAA, leaching of radioactive isotopes is determined by measuring their concentrations in simulated waste before leaching and in the leachant after leaching.

The principal radioactivities remaining were ^{124}Sb (about 10^9 dpm/g) and ^{134}Cs (about 10^5 dpm/g). The ^{124}Sb was by far the most abundant radioactivity present; hence, results based on this species are considered the most reliable. In all cases where data were based on the less intense ^{134}Cs, the gamma rays were sufficiently above background so that their determination was unambiguous. Nevertheless, uncertainties (errors) in the data based on ^{134}Cs determinations are significantly larger, perhaps by an order of magnitude, than those in the data based on ^{124}Sb determinations.

Leach rates of the Pyrex (borosilicate) glass were determined for three physical configurations. These were: (1) pulverized beads (4.2 g), using a conventional Soxhlet apparatus (refluxed distilled water, pH 7.3); (2) unaltered beads (69 g), using 25°C quiescent distilled water (pH 5.8); and (3) a cylindrical lead matrix composite (3 cm in diameter by 5 cm long) consisting of 68 g of beads (close-packed) cast in about 230 g of lead (beads exposed at the outermost surface) leached by 25°C quiescent distilled water (pH 5.8). These three configurations are similar to those used in previous studies of sintered waste form granules [STEINDLER-1979].

The specific surface areas (m^2/g) of the unaltered and pulverized beads were determined both by calculation (assuming that the beads are impervious spheres) and by BET measurements using krypton gas as the sorbent [STEINDLER-1978D]. These surface area determinations are summarized in Table 29. The BET-measured surface areas are higher by an order of magnitude than the areas calculated from geometrical shapes.

Table 29. Specific Surface Areas (cm^2/g) for Pyrex Glass

Method	Unaltered Beads	Pulverized Beads
BET	7.0E1	1.1E3
Geometric[a]	3.9E0	1.0E2

[a]Areas were calculated assuming impervious spheres. For the pulverized form, mechanical sieving into six fractions was used to determine the particle size [STEINDLER-1978D].

Incremental leach rates for the unaltered beads are compared with those for the pulverized beads (powder) in Table 30. The data for the unaltered beads are based on 58 days of leaching 69 g of material, whereas data for the pulverized beads are based on 75 days of leaching 4.2 g of material. The fraction of the indicated isotope leached per day has been converted to the mass equivalent leach rate (g/cm^2d), using the specific surface area determined by geometrical calculation, as well as the specific surface area determined by BET measurements (Table 29).

Table 30 shows that the fraction leached per day for the pulverized glass (from both Sb and Cs measurements) is more than two orders of magnitude (i.e., a factor of about 130) greater than that for the unaltered

Table 30. Leach Rates for Pyrex (Borosilicate) Glass

	^{124}Sb		^{134}Cs	
	Beads	Powder	Beads	Powder
Fraction/day	1.0E-6	1.4E-4	8.0E-5	1.0E-2
g/cm^2d (geom)[a]	2.6E-7	1.4E-6	2.1E-5	1.0E-4
g/cm^2d (BET)[a]	1.4E-8	1.3E-7	1.1E-6	9.1E-6

[a]Geometric and BET surface areas as given in Table 29.

beads. Surface area determinations (both calculated and BET) indicate only a factor of about twenty increase in the surface areas for the pulverized form compared to the unaltered form. The leach rates for the pulverized form, normalized to constant specific surface area, are about a factor of five greater than leach rates for beads when geometric areas are used and are about a factor of ten greater when BET surface areas are used (Table 30). Some uncertainty (perhaps a factor of 2) exists because of deviations from spherical shapes assumed for pulverized forms. Results were also affected by leaching of the pulverized form in a Soxhlet extractor, in which the leachant temperature was somewhat above the temperature (room temperature) used for leaching the unaltered beads. Also, the Soxhlet leachant is devoid of leached ions and has a more nearly neutral pH (i.e., 7.3 as compared with 5.8). The effects of these variables are currently being determined.

The incremental leach rate from Pyrex glass, as measured with cesium, seems to be about two orders of magnitude greater than that measured with antimony (Table 30). This difference is independent of the physical form of the solid matrix and hence indicates the possibility that the kinetics and/or leaching mechanism for these two chemically dissimilar elements are significantly different. Future studies involving other elements, as well as kinetic studies of these elements, may shed light on this phenomenon.

The leach rates for a metal(lead)-encapsulated composite with no protective metal envelope* are compared with those for the unaltered beads in Table 31. Sequential leach tests using 300 mL of 25°C quiescent distilled water (pH 5.8) over a period of 160 days have been made. These tests indicate that (particularly as measured with cesium) the fraction leached from the beads differed by significantly less than an order of magnitude from the fraction leached from the metal-encapsulated composite. (These results are in agreement with the results obtained for more porous sintered waste pellets reported previously [STEINDLER-1979].) The fraction of cesium leached was the same, within experimental uncertainty (i.e., within about a factor of 2), for

*The composite contained 68 g of neutron-irradiated Pyrex beads (4-mm beads) and was 5 cm long with a 3-cm diameter. This composite was prepared during the previous report period.

Table 31. Incremental Leach Rates (fraction leached/day) for Glass Beads and for Metal Composites of Glass Beads with No Protective Envelopes

	1st Leach	2nd Leach	3rd Leach	4th Leach	5th Leach
	(7.8)[a] (7.8)[b] (3.9)[c]	(13)[a] (20.8)[b] (14.3)[c]	(37)[a] (57.8)[b] (39.3)[c]	(49)[a] (106.8)[b] (82.3)[c]	(54)[a] (160.8)[b] (133.8)[c]
^{124}Sb Beads	5.2E-6	7.4E-7	2.4E-7	2.3E-7	5.3E-8
^{124}Sb Composite	1.6E-6	3.1E-7	4.7E-8	1.9E-8	d
^{134}Cs Beads	2.4E-4	1.9E-4	6.1E-6	1.8E-5	5.0E-6
^{134}Cs Composite	d	d	1.4E-5	1.8E-5	3.6E-6

[a]Duration (days) of each leach test.

[b]Cumulative duration (days) of leaching.

[c]The sum of the median time (days) of this leach test and the cumulative time of leaching preceding this leach.

[d]These data were not resolved from the gamma spectra.

the composite as for the unencapsulated beads. These preliminary results indicate that at least for the more leachable cesium ions, the surface area of the glass beads in the metal composite exposed to leaching is essentially the same as the surface area of the unencapsulated beads. Differences in the linear expansions of lead and glass, combined with the composite fabrication technique used, could result in voids or channels between the lead matrix and the glass beads. These voids would allow leachant to permeate the matrix. More accurate determinations of the relative fractions leached from beads and composites will be necessary in order to quantify these comparisons. Again, as in the case of the data reported in Table 30, cesium seems to be leached about two orders of magnitude faster than antimony.

A sample of lead from the casting was assayed for cesium and antimony to see if any of these elements had leached into the metal during the casting operation. The results of this assay indicated that less than 1 part in 10^3 of the cesium and less than 1 part in 10^5 of the antimony were extracted into the molten metal.

The antimony incremental leach rate data from Table 45 can be evaluated as a function of time. For example, the data for the beads and the composite can each be fit on a log-log plot by a straight line with the equation:

$$L = at^n \qquad (1)$$

where L = leach rate, t = time, a = constant, and n = slope. The data, if plotted, give two lines with the same slope (i.e., approximately -1.2) but with a factor of about four difference in absolute magnitude. Diffusion theory would predict a $t^{-1/2}$ dependence for the incremental leach rate [CRANK], i.e.,

$$L = at^{-1/2} \tag{2}$$

Another possibility is dissolution from the surface of a homogeneous waste form, which would result in an incremental leach rate that is independent of time since it is reasonable to assume that the dissolution rate under these circumstances would be constant. Neither of these idealized hypotheses can be substantiated by the data of Table 31 since the initial leach rates decrease with time with a slope of approximately -1.2. Since only a small fraction of the total radioisotopes were leached during the time interval, it might be assumed that the material is being leached from a thin surface layer. Further work is in progress to collect additional data to define this phenomenon more exactly and to interpret its effect on long-term storage of radioactive wastes in geologic repositories.

b. Leaching of Sintered PW-7a Granules

Leach rate measurements are being continued for a composite waste form with no protective envelope consisting of 54 g of close-packed sintered porous waste granules* (0.4-cm-dia spheroids) cast as a cylindrical ingot (3-cm diameter by 5 cm) in 230 g of lead [STEINDLER-1979]. These tests are done with 25°C quiescent distilled water (pH 5.8) as the leachant. The porous SWF granules used in this study have a relatively low leach resistance (e.g., the cesium initial leach rate is about 1E-2 g/cm^2d [STEINDLER-1979]). Eleven sequential leach tests over a period of about 290 days have been completed. The results of these tests (part of which were presented in [STEINDLER-1979]), are summarized in Table 32. Plots of the incremental leach rate (fraction/day) as a function of time for four representative radioisotopes (^{152}Eu, ^{134}Cs, ^{124}Sb, and ^{141}Ce) are in Fig. 32. Although the leach rates for these four radioisotopes vary by four orders of magnitude, the time dependence of the incremental leach rate is approximately the same for all four elements within experimental error. In fact, all eight isotopes identified in Table 32 exhibit similar behavior. Initial leach rates (i.e., data accumulated during the first 10 days of leaching) for these composite waste forms are subject to uncertainty with respect to time correlation since, in all probability, equilibrium between the solid and liquid had not yet been realized.

A reference line having a $t^{-1/2}$ dependence as predicted by diffusion theory (see above) has been included in Fig. 32 to allow comparison. However, as can be seen from Fig. 32, the leach rate for this waste

*This nonoptimized sintered waste from (SWF) material was obtained from Battelle Pacific Northwest Laboratories (PNL) in the form of granules for the purpose of testing the NAA method. The granules were prepared with a disk pelletizer by agglomerating 85 wt % PW-7a [BONNER] spray calcine and 15 wt % glass frit, followed by sintering for 1 h at 1000°C.

Table 32. Sequential Leach Tests for PW-7a Waste Form in 284-g Lead Ingot (25°C quiescent distilled water)

Isotope Analyzed	Leach Rate, fraction leached/day										
	1st	2nd	3rd	4th	5th	6th	7th	8th	9th	10th	11th
	(2.9 d)[a]	(10.2 d)[a]	(6.8 d)[a]	(13.8 d)[a]	(17.0 d)[a]	(21.0 d)[a]	(32.0 d)[a]	(37.2 d)[a]	(48.9 d)[a]	(49.1 d)[a]	(54.1 d)[a]
	(2.9 d)[b]	(13.1 d)[b]	(19.9 d)[b]	(33.7 d)[b]	(50.7 d)[b]	(71.7 d)[b]	(103.7 d)[b]	(140.9 d)[b]	(189.8 d)[b]	(238.9 d)[b]	(292.5 d)[b]
	(1.5 d)[c]	(8.0 d)[c]	(16.5 d)[c]	(26.8 d)[c]	(42.2 d)[c]	(61.2 d)[c]	(87.7 d)[c]	(122.3 d)[c]	(168.9 d)[c]	(214.4 d)[c]	(265.4 d)[c]
^{51}Cr	3.7 E-2	1.5 E-2	7.1 E-3	5.4 E-3	d	4.4 E-3	3.0 E-3	2.0 E-3	1.3 E-3	1.0 E-3	8.8 E-4
^{60}Co	6.1 E-7	1.5 E-6	7.4 E-7	6.5 E-8	2.9 E-8	2.1 E-8	4.3 E-8	1.7 E-7	6.5 E-8	4.9 E-8	6.3 E-8
^{65}Zn	6.6 E-6	5.9 E-6	4.2 E-6	2.3 E-7	7.8 E-8	9.7 E-7	1.7 E-7	7.8 E-7	1.4 E-7	1.8 E-7	7.3 E-8
^{75}Se	6.2 E-3	2.0 E-3	1.2 E-3	7.3 E-4	4.8 E-4	3.8 E-4	2.5 E-4	1.4 E-4	7.5 E-5	2.6 E-5	7.4 E-6
^{124}Sb	1.6 E-5	5.5 E-6	4.2 E-6	3.0 E-6	8.9 E-7	1.4 E-6	9.0 E-7	3.4 E-7	6.1 E-7	1.1 E-6	2.2 E-7
^{134}Cs	1.0 E-2	3.4 E-3	1.8 E-3	1.2 E-3	1.4 E-3	6.1 E-4	4.0 E-4	2.5 E-4	1.9 E-4	7.7 E-5	3.8 E-5
^{141}Ce	d	2.7 E-6	1.2 E-6	5.4 E-7	1.1 E-7	2.3 E-7	5.7 E-8	d	d	d	d
^{152}Eu	1.1 E-7	3.3 E-7	5.2 E-7	2.3 E-7	1.6 E-7	1.6 E-7	8.5 E-8	6.5 E-8	8.6 E-8	2.0 E-8	2.1 E-8

[a]Duration (days) for each sequential leach test.

[b]Cumulative duration of leaching.

[c]The sum of the median time (days) of each leach test and the cumulative time of leaching preceding the leach test.

[d]These data were not resolved from the gamma spectra.

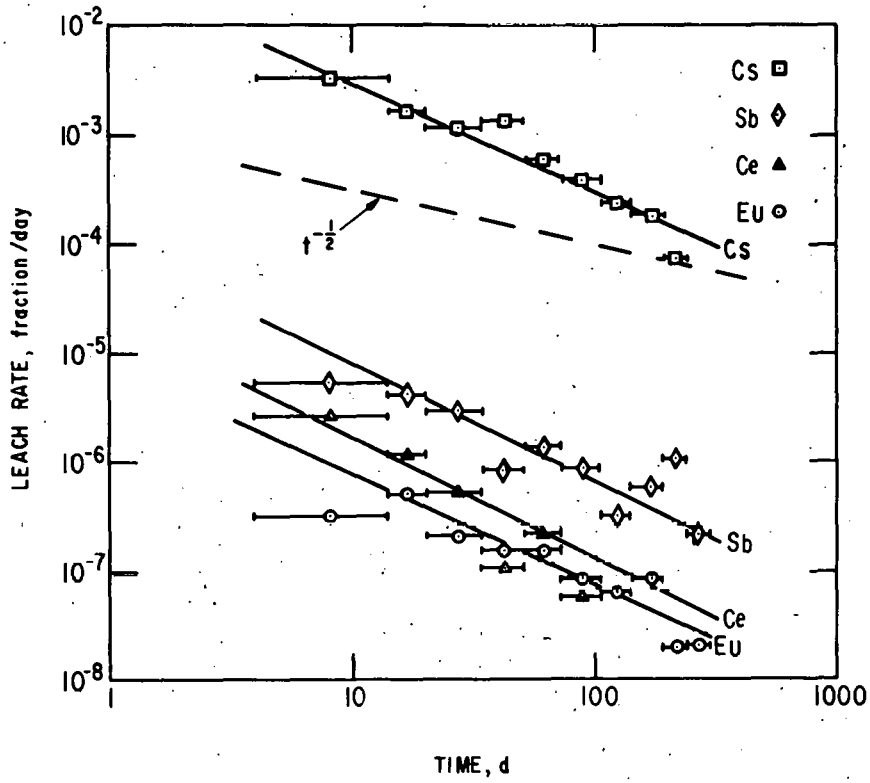

Fig. 32. The Time Dependence of the Fraction Leached per Day from a Small Laboratory-Scale Composite of Porous Sintered Waste Granules Encapsulated in a Lead Matrix with No Protective Lead Envelope

composite (as is the case for Pyrex bead ingots) decreases much faster than would be predicted by simple diffusion theory. In fact, the slope is approximately -1 (i.e., leach rate linearly decreasing with time). As is stated above, dissolution from the surface of a homogeneous waste form should result in an incremental leach rate that is independent of time. These preliminary results indicate that leaching from this waste composite is neither entirely diffusion controlled nor dependent on dissolution from the surface. Leaching is probably dependent on relative solubilities of the various phases present in this heterogeneous waste form.

The leach rates for this waste form (i.e., SWF beads in a lead matrix) decreased to reasonably low values during the 290 days of this experiment.

c. Leaching of Simulated High-Level Waste Glass

Leaching from a simulated high-level waste (HLW) glass obtained from Battelle Pacific Northwest Laboratories (PNL) and identified as PNL-glass [STEINDLER-1978D, McELROY-1977A] has been continuing for about

240 days. The leaching medium is 25°C quiescent distilled water. Seven sequential leach tests were made during the 240-day time interval. Incremental leach rates, based on the fractions of specific radioisotopes leached and converted to a grams-per-square centimeter-per-day basis, have been determined for ten radioisotopes. These measurements were also based on the neutron activation technique previously described [STEINDLER-1978A and 1978D]. The results are tabulated in Table 33.

The incremental leach rates are relatively independent of the radioisotopes measured (i.e., they agree within about an order of magnitude) and have a very weak time dependence. Because of the very low leach rates associated with this waste form and the small size (0.5 g) of the sample used, the technique was pushed to its limits in these determinations. These leach tests are continuing in order to more definitely establish the time dependence of the leach rate.

3. Conclusions

The neutron activation analysis (NAA) technique has been applied to leach rate studies, using Pyrex (boroslicate) glass. Sufficient quantities of antimony and cesium are present in this glass to make possible the determination of leach rates as low as $10^{-8}g/cm^2d$.

Measurements of leach rates of pulverized and intact glass beads indicate that pulverizing the waste form may significantly affect its leaching characteristics. These results are consistent with previous observations based on a more porous waste form [STEINDLER-1979].

Comparisons of the measured leach rates for Pyrex beads with those for a composite consisting of Pyrex beads in a lead matrix with no protective envelope) indicate that there was little if any decrease in the leach rate for the composite form. Hence, incorporating Pyrex beads into a lead matrix ingot using the fabrication technique applied here had little effect on reducing the surface area exposed to the leaching media. The effects of other fabrication techniques are being examined.

Surface areas for Pyrex glass measured by BET gas (krypton) sorption techniques were about one order of magnitude larger than surface areas calculated assuming solid spheres. Leach rates based on geometrically calculated surface areas generate conservative (i.e., upper limit) estimates. Hence, the use of calculated surface areas rather than those measured by gas sorption (BET) is recommended when converting experimentally measured fractions leached to area-normalized leach rates.

Table 33. Incremental Leach Rates for PNL-Glass[a] in 25°C Quiescent Distilled Water (Sequential Tests)

Isotope Analyzed	Leach Rate, g/cm^2d[b]						
	1st	2nd	3rd	4th	5th	6th	7th
	(5.8 d)[c]	(21.0 d)[c]	(32.0 d)[c]	(29.1 d)[c]	(48.9 d)[c]	(49.0 d)[c]	(54.1 d)[c]
	(5.8 d)[d]	(26.8 d)[d]	(58.8 d)[d]	(87.9 d)[d]	(136.8 d)[d]	(185.8 d)[d]	(239.9 d)[d]
	(2.9 d)[e]	(16.3 d)[e]	(42.8 d)[e]	(73.4 d)[e]	(112.4 d)[e]	(161.3 d)[e]	(212.9 d)[e]
^{51}Cr	1.9 E-5	3.0 E-7	4.2 E-7	f	f	f	f
^{60}Co	4.8 E-5	1.4 E-6	1.2 E-6	4.1 E-6	1.2 E-7	1.2 E-7	5.2 E-7
^{65}Zn	5.4 E-5	8.7 E-7	6.5 E-7	1.8 E-7	1.5 E-8	1.5 E-8	3.5 E-7
^{85}Sr	5.8 E-5	1.1 E-6	9.6 E-7	1.5 E-6	4.6 E-7	1.3 E-6	2.1 E-6
^{95}Zr	4.5 E-7	1.1 E-7	1.0 E-7	f	f	f	f
^{134}Cs	7.8 E-7	2.9 E-7	6.1 E-7	4.4 E-7	5.2 E-8	1.3 E-7	4.2 E-7
^{141}Ce	6.0 E-7	7.1 E-8	1.2 E-7	1.2 E-7	f	f	f
^{152}Eu	5.1 E-7	6.5 E-8	8.4 E-8	3.1 E-8	1.7 E-9	2.7 E-9	3.5 E-7
^{237}U	1.5 E-7	f	f	f	f	f	f
^{239}Np	1.5 E-6	f	f	f	f	f	f

[a] Composition 76-68 as defined in [McELROY-1977A]. The initial sample weight was 0.47 g and the initial surface area (calculated) was 2.3 cm^2 (apparent geometric surface).

[b] These units of grams per square centimeter·day (g/cm^2d) represent the gram equivalents that would have been leached had the entire matrix leached at the same rate as the specific isotope listed.

[c] Duration (in days) of each sequential leach test.

[d] Cumulative duration of leaching.

[e] The sum of the median time (days) of each leach test and the cumulative time of leaching preceding the leach test.

[f] These isotopes were not resolvable from the gamma spectrum because of radioactive decay.

4. Planned Work

Expansion of the leach rate studies to include other leaching media as well as other temperatures are necessary and are in progress. Tests wherein the temperature, pH, and salinity of the leaching media are varied will establish the effects of these variables on the leaching characteristics of proposed waste forms.

B. Metal Encapsulation Techniques

1. Introduction

The objective of this task is to assess and to develop concepts and laboratory techniques for encapsulating solid waste forms in a continuous metal matrix. A reference metal encapsulation concept is discussed.

2. Encapsulation Method

Metallic lead alloys are the current reference encapsulation metals at Argonne National Laboratory (ANL). The techniques for encapsulating solid wastes examined by Eurochemic, Battelle Pacific Northwest Laboratories (PNL), and Allied Chemical at Idaho Nuclear Engineering Laboratory (INEL) have been reviewed previously [JARDINE, STEINDLER-1978B]. A later report [LAMP] summarizes the casting work at INEL. Preparation of small laboratory-scale castings with lead, aluminum, and copper alloys at ANL has been summarized in a quarterly progress report [STEINDLER-1978B]. From this technical data base and a concept outlined by workers at Eurochemical [DETILLEUX], a reference method has been defined for encapsulating solid wastes in a lead alloy matrix.

Figure 33 illustrates the concept. The reference waste canister shown is essentially a doubled-walled container constructed of two concentric cylinders ("outer canister" and "inner retainer" in Fig. 33). This type of canister design is also important to the casting or encapsulation step, as outlined below. Although lead is given as the reference alloy in this text, the method may be applied to other alloys. Other alloys would likely require higher process temperatures and different canister materials than those used for lead.

As shown in Fig. 33, the inner solid retainer has three penetrations (openings). (If a mesh retainer were used, the openings would not be necessary.) The lower penetration is covered by a wire mesh screen that retains the solid waste granules, pellets, fragments, etc. within the inner retainer before molten lead is introduced into the canister. One upper penetration of the inner retainer can be connected to a tube that allows filling with solid waste granules and purging of the canister with an inert gas. Effluent gas escapes through the lower penetration. In the other upper penetration of the inner canister a fusible metal plug (e.g., lead) may be placed which may be sealed sufficiently so that purge gas will escape through the annulus between the two concentric cylinders (Fig. 33) and the inner retainer. The fusible seal is destroyed during the canister lead charging

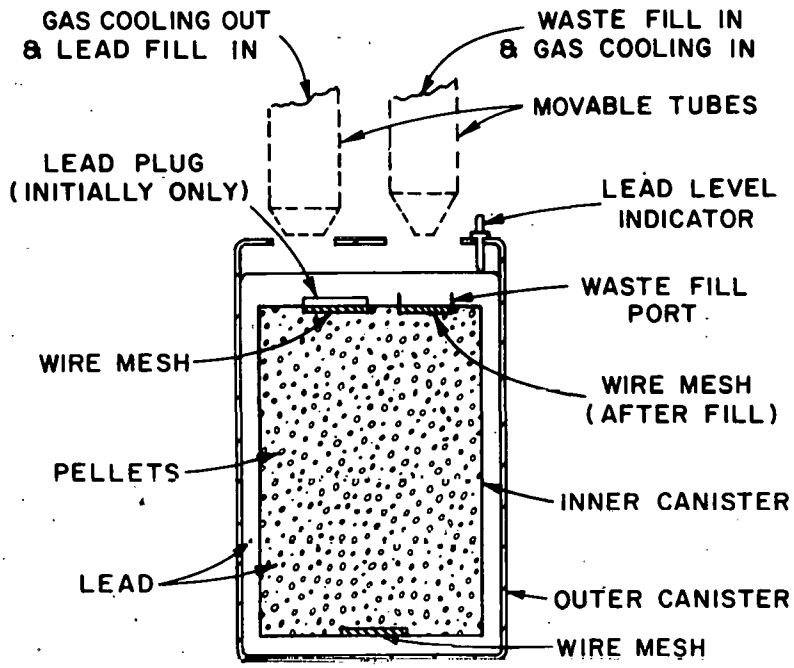

Fig. 33. Conceptual Canister Design for Metal Encapsulation of Waste in Lead

operation and thus becomes a second point where lead may enter the inner retainer. (Only one access is actually required for the encapsulation process.) Access is important for ensuring a supply of lead to the inner canister during solidification, when the lead shrinks. When proper zone cooling is employed, this additional source of lead prevents a large depression or void (i.e., a cooling "pipe") from forming in the top of the casting.

The encapsulation process consists of first filling the inner canister or retainer with solid waste granules (e.g., stabilized calcine, glass beads, incinerator ash, pellets, etc.). Then a wire mesh is placed over the top openings so that waste granules do not escape during the lead-filling operations. If cooling is required prior to the actual encapsulation process or as an additional safety factor, inert-gas purge can be accomplished through the lead-fill and waste-fill tubes (Fig. 33).

Either liquid or solid lead is then added (from a storage hopper located outside the hot cell) to the heated annulus region between the walls of the two canisters. Molten lead flows downward, enters the inner container through the lower penetration, and rises in the inner container to fill the spaces between the waste granules. The operation is done at ambient pressures. Gases are vented through one of the openings in the outer canister. Avoidance of large voids or "pipes" due to contraction of lead on cooling is accomplished by maintaining an excess of liquid lead in the upper portion of the canister while simultaneously the entire canister is gradually cooled, commencing at the bottom. Thus, as shrinkage occurs, molten lead is available to fill the volume. In the annulus of the cast ingot is a protective

envelope of metallic lead, free of waste granules, and also isolating the waste granules from exterior events and the environment. The resulting canned "ingot" is then ready for final sealing and/or characterization testing. This technique has been demonstrated in our laboratory. Initial experiments are described in the next section.

Also note that two major requirements of solid waste forms for encapsulation in a canister (Fig. 33) are (1) that they be chemically compatible with the molten and solid metallic phase and (2) that there are void spaces of adequate size between the solid waste particles to allow filling with metal. If these two constraints remain as the only major constraints on solid waste forms and no others are uncovered in future work, the casting technology just described for encapsulation in lead should be rather insensitive to the type of solid waste and the encapsulation concept may be applicable to many solid waste forms. For example, metal encapsulation seems technically feasible and potentially beneficial for pellets, fragments, etc., of incinerated TRU wastes; glass beads (or marbles or chips) of either high-level or TRU incinerator ash wastes; or fractionated CsCl and SrF_2 wastes as currently separated from the Hanford defense waste [JACKSON] or in some other form. However, final judgment must be withheld until waste form packaging and handling criteria are developed.

3. Experimental Results and Discussion

Experiments were performed to demonstrate the technical feasibility of making lead metal-matrix castings based on the reference concept just discussed. The experimental castings were 24 in. long and 3 1/8 in. in diameter. This is about one-fourth to one-fifth the scale of a full-size specimen often assumed for glass monoliths. In previous ANL studies, castings about 4 in. long and about 1 1/2 in. in diameter were examined as described in a previous quarterly report [STEINDLER-1978B]. Previous tests indicated that cooling rates of castings would have to be controlled to prevent axial voids (i.e., cooling "pipes") due to shrinkage or contraction of the metal (e.g., lead) as it solidifies. Thus, a concept of zone-cooling entire castings was also examined.

Canisters (which also served as primary crucibles for the experiment) were each fabricated by silver-brazing a pipe cap onto the end of a 24-in. length of 3 1/8-in.-OD (0.109-in. wall thickness) copper pipe. Copper was selected for ease of construction and may not be suitable as a final canister material. In a similar manner, 18 1/2-in. lengths of 2-in.-ID (0.083-in. wall thickness) copper pipe were used to fabricate vessels for holding the simulated waste form (alumina or Pyrex glass beads) in the interior of the assembly (Fig. 33). This interior vessel was designed to hold the simulated wastes in position away from the outer canister wall while allowing molten lead to flow freely into it through both ends. Note that this interior retainer could be replaced with a wire mesh screen although then the gas cooling option previously described would not work as described. Wire mesh was silver-brazed into the two innermost pipe caps to retain Al_2O_3 pellets or glass beads. The upper pipe cap of the inner canister was also fitted with a brazed 1/2-in.-dia copper tube through which simulated wastes were introduced. This tube was also used to hold the inner vessel in place during the casting operation.

The simulated wastes used were activated alumina pellets in one experiment and 6-mm Pyrex glass beads in the other. Alumina pellets with diameters ranging from about 3.25 to about 7.0 mm were used. Prior to casting, the pellets and beads were dried for about three days in a vacuum oven (29 in. H_2O and 150°C). Significant amounts of moisture were driven off from the Al_2O_3 pellets in this drying process.

For the casting operation, the outermost crucible wall was fitted with three thermocouples. The assembly of two concentric canisters was then mounted on a heavy-duty scissor jack under a clamshell tube furnace. The jack allowed lowering of the entire casting from the bottom of the furnace at a rate permitting zone-cooling to be investigated.

The simulated inner waste vessel was filled with either Al_2O_3 granules or Pyrex glass beads and positioned inside the 3 1/8-in. crucible. The inner vessel was braced to prevent shifting or floating. Then the crucible was placed under an argon purge and heated to the casting temperature (about 400°C) for about 30 min. The lead shot (about 3 to 5-mm dia) used in the casting was premelted and skimmed of its oxide prior to being used to cast simulated waste. When a crucible reached the casting temperature, the lead was poured into the annulus region.

The molten lead was then cooled by lowering the crucible out of the bottom of the hot furnace in small (about 25%) increments over a period of about two hours. This was done to maintain a molten reservoir of lead above the lead solidifying in the bottom of the crucible. Thus, as shrinkage occurred, additional molten lead was always available as make-up material.

Nondestructive ultrasonic testing, performed* on the finished lead-Al_2O_3 casting, was concluded to have only limited applicability as a possible quality assurance technique since the ultrasonic waves would be reflected somewhat similarly from either voids in the casting or similated waste Al_2O_3. Ultrasonics can, however, show whether or not metallic bonding has occurred between the lead and the canister. This might be useful information in relation to heat transfer from the waste canister. For example, good metallic bonding was found to have occurred in several localized places in the canister.

Sectioning† of each of the two castings into two 24-in.-long halves revealed that the castings had no significant voids. Figure 34 shows photographs of an Al_2O_3 pellet-lead composite and a glass bead-lead composite. The lead-to-crucible interface also had no visible gaps. It was observed that the level of lead after cooling in the crucible was about 1 in. lower than the fill level when at about 400°C. This supports the notion that most of the voids caused by the solidifying lead were eliminated because molten lead had been supplied from upper regions of the casting.

---

*Tests were done by R. Massow and M. Kovar of the Quality Assurance Division.

†Done by John Bos of Central Shops.

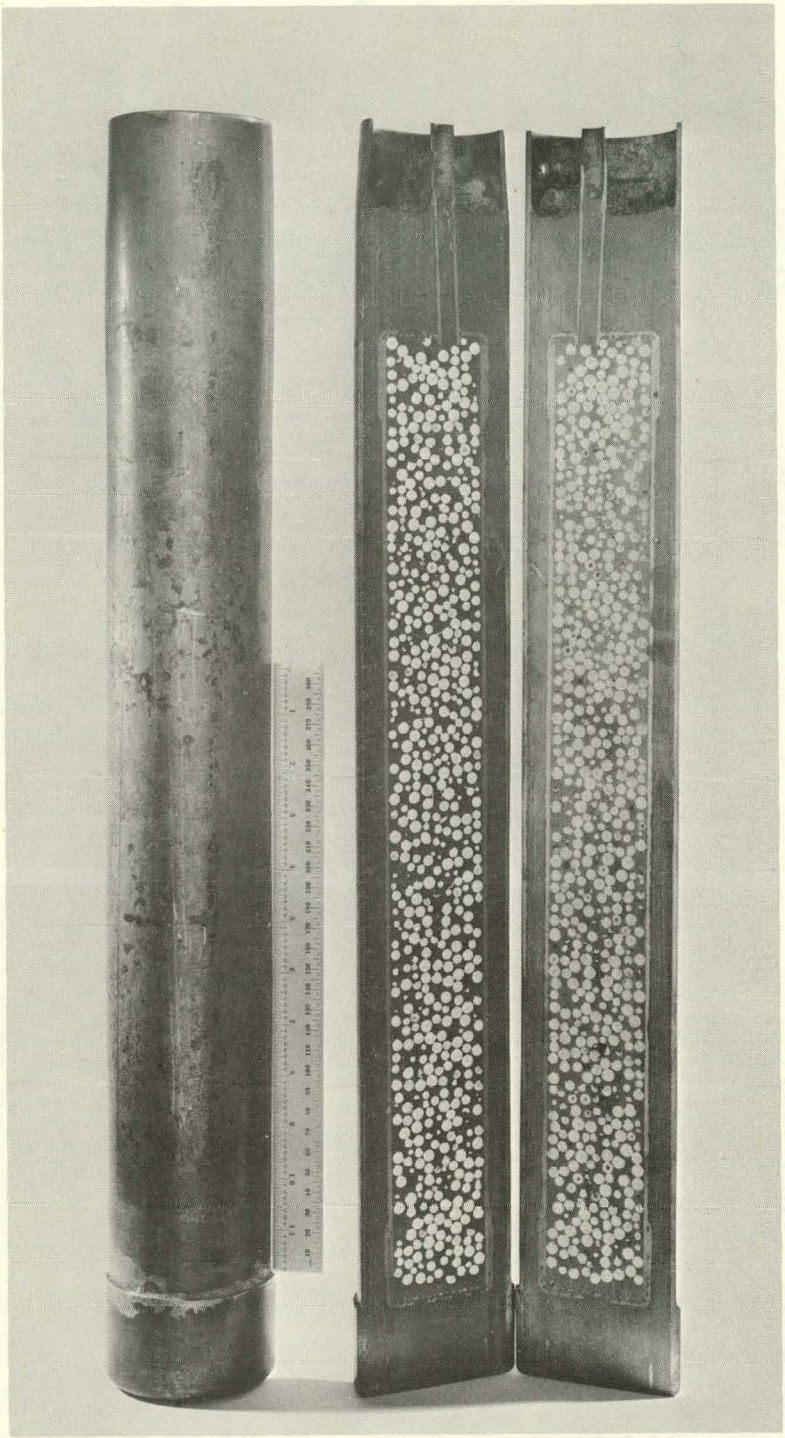

Fig. 34. Photographs of Sectioned Castings (Composites) of Lead-Encapsulated Pellets.

A: Sectioned Casting of a Canister of Simulated Waste Pellets (Al_2O_3) Encapsulated in Lead with Intrinsic Protective Envelope.
ANL Neg. No. 308-79-638

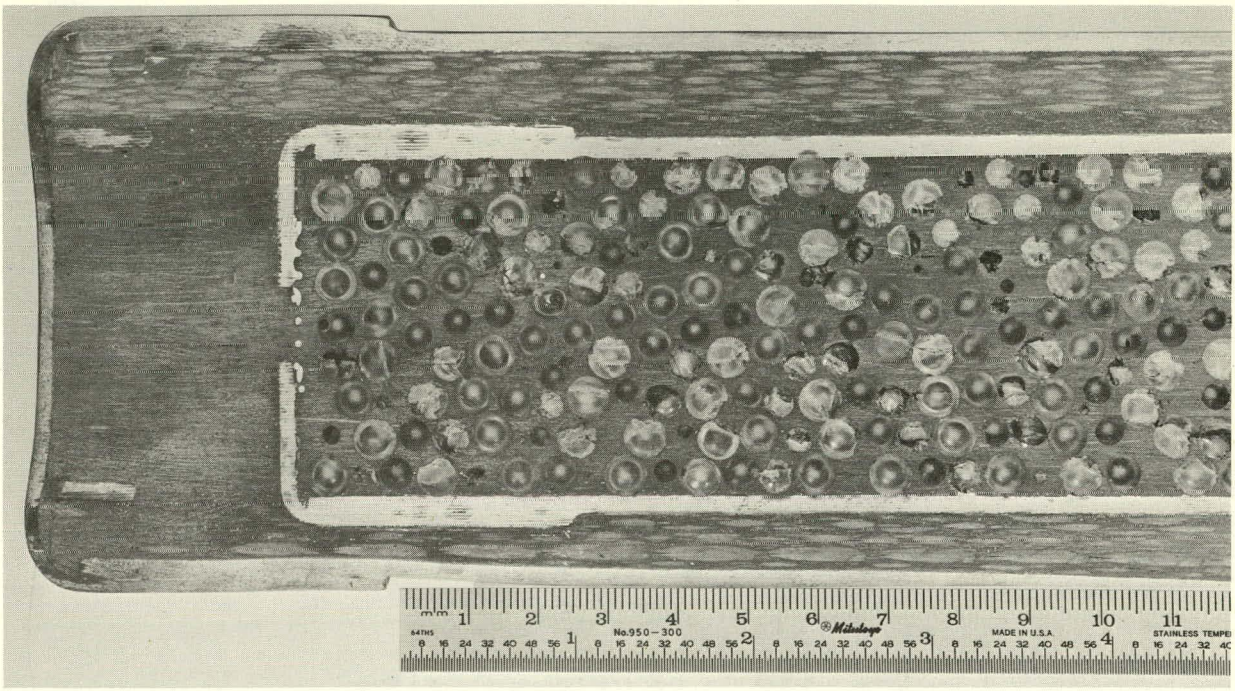

Fig. 34B. Close-Up View of a Sectioned Casting of 6-mm Glass Beads Encapsulated in a Lead Matrix with its Protective Envelope. Cracking of the glass beads occurred during sectioning. ANL Neg. No. 308-79-635

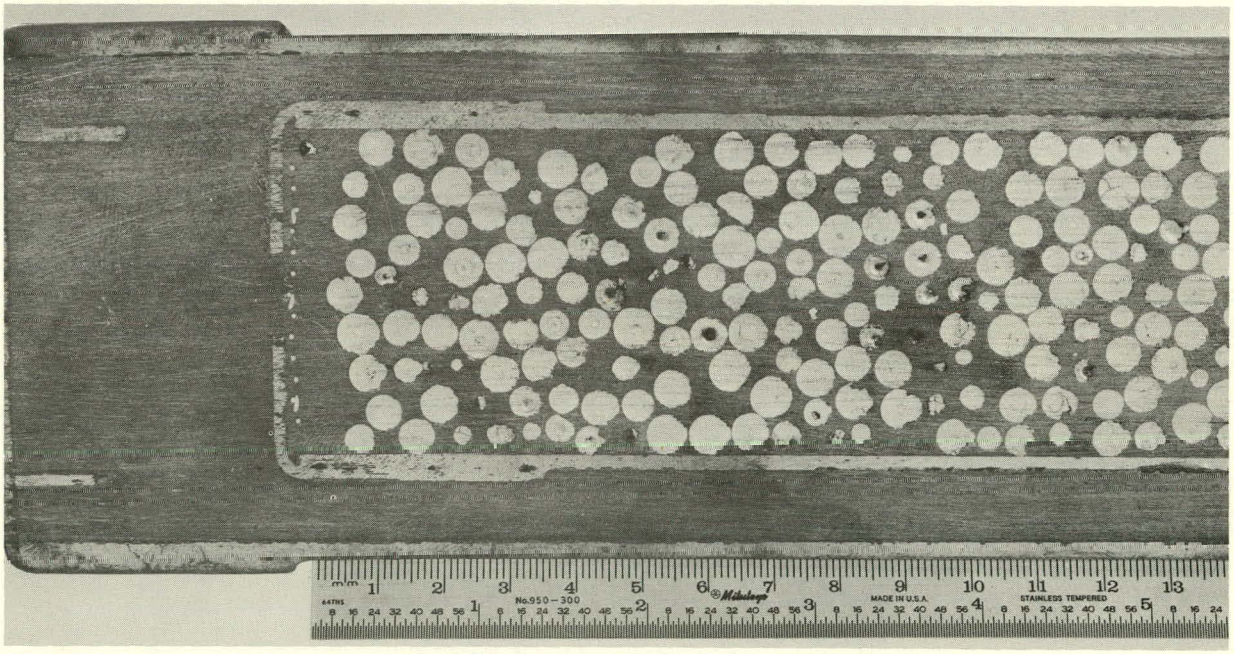

Fig. 34C. Close-Up View of the Sectioned Casting of Al_2O_3 Pellets Encapsulated in a Lead Matrix with its Protective Envelope. ANL Neg. No. 308-79-637

4. Conclusions

These tests have produced metal-encapsulated simulated waste forms free of large shrinkage voids. The concept was demonstrated on a 3 1/8-in.-OD by 24-in.-long scale for both a simulated ceramic waste form (Al_2O_3) and glass beads. Cooling pipes that might have been caused by metal shrinkage were prevented by using a zone-cooling technique. This casting technique is likely to be applicable to a range of solid wastes other than the two forms tested to date and appears to be amenable to processes performed remotely in hot cells. Further work is in progress.

C. Comparative Evaluation of Impact Resistance of Metal-Matrix Waste Forms

1. Introduction

Resistance of solid radioactive waste forms to dispersion by mechanical impacts during in-plant storage and transportation is likely to be a property of great concern. A study has been initiated to analyze and evaluate the effects of mechanical impacts on reference metal-matrix waste forms. The effects of primary concern are those bearing on release and dispersion of waste to the environment, including the degree of resistance to groundwater leaching. The objective of this effort is to develop sufficient information on impact resistance so that decisions can be made (by others) regarding either the need or the effort required for mechanical impact demonstrations of metal-encapsulated waste forms and for comparison with other waste forms, particularly glass.

This is the second report on impact resistance of waste forms. Emphasis in this period was placed on systematic analysis of information in the literature reviewed and summarized in [STEINDLER-1979]. From this analysis, further inferences were drawn from the literature reviewed, and generalizations were made as to the way materials deform under impact--that is, the way impact energy interacts with the properties and configurations of materials of various kinds. In particular, the partitioning of energy determines the distribution of deformations in composite bodies consisting of both brittle and ductile materials. Generalization of empirical data is aided by knowledge of the solid state structure of the materials involved. A summary of relevant information in the literature, briefly recapitulated in section 2 below, will serve as an introduction to further analysis and generalizations that are mentioned here and presented in detail in sections 3-5 below.

2. Recapitulation of Literature Review

As reported previously [STEINDLER-1979], design principles and properties of lead and steel relevant to impact deformation have been summarized in reports on the impact behavior of shipping casks made of lead and steel. Impact deformation of these ductile materials was correlated with the input kinetic energy of the impact. Deformations were measured by the displacement volume $\Delta V(m^3)$ of the configuration change of plastic flow, which

takes place under a dynamic flow stress,* σ_D (Pascal, Pa) characteristic of each material constituent. For kinetic energy derived from free fall of a body of mass M(kg) a distance H(m) under normal gravity, g (9.8 m/s^2), the velocity u(m/s) of impact supplies a kinetic energy 1/2 Mu^2 (J), such that for a given material:

$$gMH = 1/2\ Mu^2 \qquad (1)$$

$$= \sigma_D \Delta V$$

This relation is to be interpreted as the impact force applied to a portion of the external surface of the body. The deformation takes place as a displacement volume, ΔV, in the vicinity of the impact surface. The magnitude of ΔV depends on the configuration, the material, and the total energy available. For a composite body of two ductile materials, M in Eq. 1 is the sum of the masses, and the two $\sigma_D \Delta V$ terms are used--one for each material.

In the reports cited in the literature survey, the utility of Eq. 1 was established by experimental impacts validating calculations. The reference values of σ_D were 6.90×10^7 Pa (10,000 psi) for lead and 3.45×10^8 Pa (50,000 psi) for mild steel [STEINDLER-1979].

A major result of these tests was the absence of significant strain-rate effects in realistic impacts (principally for highway conditions). The type and magnitude of plastic deformation were found to depend only on the total energy of impact and not on the speed with which the load stresses were applied. This result provides a great simplification in the generalization of impact effects and permits the use of small-scale models for impact measurements, according to principles of dimensional analysis previously reported. This result is also supported by basic information on the relation of solid state structure to the modes of deformation (discussed below).

The literature reviewed previously that pertains to the deformation of brittle material also showed that impact energy is correlated with the total surface area of the fractured cylindrical glass specimens. This result is consistent with energy dependence and with insensitivity to strain rate for brittle fracture and is supported by general knowledge of solid-state structure described below. If the surface area generated is expressed by $\Delta S(m^2)$ and if the energy-surface correlation is expressed by the ratio K_F (J/m^2), then the energy of brittle deformation can be expressed as

$$gMH = 1/2\ Mu^2 \qquad (2)$$

$$= K_F \Delta S$$

For brittle materials, deformation (fracture) is not localized [STEINDLER-1979].

---

*Energy absorbed per unit volume of material displaced in plastic deformation.

The impact deformation of a composite body of brittle and ductile material can be summarized by the energy equation

$$gMH = 1/2\ Mu^2$$

$$= \sigma_D \Delta V + K_F \Delta S$$

where σ_D is the dynamic flow stress of the ductile material and K_F is the energy coefficient per unit surface energy in brittle fracture.

3. Solid-State Structure Related to Deformation

Certain classifications among the features of basic deformation processes are useful in relating specific solid-state structures to modes of deformation [McCLINTOCK, KINGERY, HOFMANN]:

1. Structural types of material deformed.
   a. crystalline (e.g., metal)
   b. noncrystalline (e.g., vitreous)
2. Modes of deformation (above elastic limit)
   a. brittle fracture
   b. nonbrittle deformation (ductile or plastic flow)
3. Models of atomic mobility in deformation
   a. atomic dislocation in planes of crystal lattice (plastic flow or fracture)
   b. atomic mobility from thermal energy levels (viscous flow)
4. Time periods of deformation
   a. impacts (time period < 1 s)
   b. quasistatic load tests (10 s < time period < 10 h)
   c. long-term loading (creep tests) (time: 10^3 h, 10^4 h, or larger)

The common classification of materials of interest is: metals, ceramics (i.e., crystalline waste forms), and glasses. Metals are crystalline and ductile, ceramics are crystalline and brittle, and glasses are noncrystalline and brittle.

At elevated temperatures, glasses manifest their noncrystalline structure by having no definite melting point and by deforming in viscous flow, rather than by fracture. On the other hand, crystalline materials are inherently rigid (nonviscous) at all temperatures well below their melting points, due to their regular atomic crystal lattices. At sufficiently high temperatures, even in crystalline materials, the atomic mobility increases due to high thermal energy levels, and various phenomena take place, such as atomic diffusion (sintering and annealing) and creep (viscous flow).

Viscous flow is not dependent on the crystal lattice (with its definite bonding energies) but is a rate process involving a stress gradient as a driving force and a rate constant reflecting the internal resistance to flow in the material. This resistance to viscous flow is measured by the property defined as viscosity, which is a strong function of temperature. The energy consumed in viscous flow will depend on the rate of deformation, and this rate-dependent deformation is different from plastic flow of common metals.

At room temperature, the viscosity of glass is so high that deformation in the viscous-flow mode is too slow to relieve stresses formed--even in quite slow rates of loading; therefore, the glass deforms in the brittle mode, by fracture and fragmentation.

Crystalline materials, on the other hand, deform by breaking bonds in the crystal lattice; this process is energy-dependent and not time-dependent, consistent with Eq. 1. For ductile materials, the atomic bonds re-form at new locations. No plastic deformation and no energy absorption occurs when the stress is below the threshold stress expressed by σ_D in Eq. 1. When stress reaches the level of σ_D, plastic flow will continue (if space permits) indefinitely until the energy supply is used up. It is possible that the total impact energy input does not go into deformation energy $\sigma_D \Delta V$ but that some fraction goes into other modes of energy dissipation, e.g., various kinds of heat-producing friction.

In impacts, the time period for deformation is so short that rate-dependent modes of deformation are not important, such as viscous flow, creep, or even work-hardening effects relative to static yield stresses.

In brittle crystalline materials, atomic bonds are broken but do not re-form as in ductile materials. Therefore fracture results from stress above the elastic limit. At low temperatures, glass behaves similarly. The elastic deformation of ductile materials (metals) and of brittle materials (glass and ceramics) is energy-dependent and not rate-dependent.

The above discussion is preparatory for more quantitative analysis of deformation behavior with respect to properties of materials over a range of deformation conditions and configurations, to allow some generalization about the effect of size and the effect of substitution of materials. Specifically, calculational models of deformation and of threshold stresses are needed to express and predict the partitioning of deformation energy in the impacting of composite bodies.

4. Threshold Compressive Stress in Deformation: The Relation to Elastic Properties

The quantitative relations of energy in ductile and brittle deformation are presented in Eqs. 1 and 2, which in general require empirical determination of the energy factors, σ_D and K_F. In this report section, the amount of threshold compressive stress for inelastic deformation is approximated from relations of commonly measured elastic tensile properties of materials which in turn have been developed from simple calculational models, using idealized conditions of uniform stress in cylindrical geometry.

The basis of these simplified calculational models is that the load is applied to a body over time, and the initial buildup of stress is in the elastic range. Elastic energy is stored in the material. Finally, stresses build up to the point where the elastic limit of tensile stress is exceeded somewhere in the body, and deformation occurs, discharging the stored elastic energy in either ductile or brittle deformation. Of course, the inelastic deformation may continue if there is sufficient energy input. It should be noted, however, that in the case of brittle fracture, the original geometry is considerably altered by the initial fragmentation of the body.

For any material, the one-dimensional relation of elastic stress, and strain, $\frac{\Delta L}{L}$, is given in terms of the elastic modulus, E; this can be stated in differential form as:

$$d\sigma = \frac{dL}{L} \tag{3}$$

The maximum elastic tensile strain, $\Delta L_y/L$, is that at the yield (or fracture) stress, σ_y:

$$\frac{\sigma_y}{E} = \frac{\Delta L_y}{L} \tag{4}$$

For a typical glass, $\frac{\sigma_y}{E} = \frac{\Delta L_y}{L}$

$$= \frac{10{,}000}{10 \times 10^6}$$

$$= 1 \times 10^{-3}$$

For lead, $\frac{\sigma_y}{E} = \frac{\Delta L_y}{L}$

$$= \frac{2500}{2 \times 10^6}$$

$$= 1.25 \times 10^{-3}$$

For a cylinder of axial length L and diameter D, the application of elastic stress in the axial direction σ_A (either tensile or compressive stress) involves elastic energy, W_E, which can be stated in differential terms as

$$dW_E = \frac{\pi D^2 L \sigma_A}{4} \frac{dL}{L} \tag{5}$$

Equation 5 can be integrated directly for constant average stress $\bar{\sigma}_A$ and constant D and L:

$$W_E = V \sigma_A \Delta L, \tag{6}$$

where V is the constant cylindrical volume $\left(\frac{\pi D^2 L}{4}\right)$.

An alternative form of Eq. 6 comes from the use of Eq. 3:

$$W_E = V \int_0^{\sigma_A} \sigma d\sigma \tag{7}$$

$$= \frac{V \sigma_A^2}{2E}$$

Equation 7 relates elastic energy to axial stress.

In general, the cross-sectional area, $\frac{\pi D^2}{4}$, is not constant over L elastic deformation. Poisson's ratio,* μ, states that:

$$\frac{dD}{D} = - \mu \frac{dL}{L} \tag{8}$$

The value of μ for typical glass is 0.20; for lead, $\mu = 0.42$. We have seen in connection with maximum tensile (yield) strain $\frac{\Delta L_y}{L}$ in Eq. 4 above, that

*Poisson's ratio is the ratio: the resultant transverse strain divided by the applied longitudinal strain, under elastic conditions.

$\frac{\Delta L_y}{L}$ has a maximum of about 1×10^{-3} and hence the variation of the cross-sectional area $\frac{\pi D^2}{4}$ is so small that the use of a constant cross-sectional area and volume is justified for the interaction in Eq. 7.

In the deformation of a cylinder by the application of axial compressive stress, the axial length is shortened and the diameter is increased. In the elastic range, this relation is expressed in differential terms by Poisson's ratio, μ, as given in Eq. 8. In cylindrical geometry, the differential circumferential strain, $\frac{dC}{C}$, is equal to the differential diametral strain, $\frac{dD}{D}$, and the tensile yield point is first reached by this expansion near the circumference. The elastic tensile stress, σ_T, in the circumference is given by

$$\sigma_T = E\frac{\Delta C}{C} \tag{9}$$

$$= E\,\frac{\Delta D}{D}$$

The axial compressive stress, σ_A, is related to Eq. 9 by Eq. 3 and Eq. 8 and gives for yield stress, $\sigma_T = \sigma_y$:

$$\sigma_A = \frac{1}{\mu}\,\sigma_y \tag{10}$$

Equation 10 gives the general relation of threshold compressive axial stress to tensile yield stress in cylinders.

This axial stress for inelastic deformation can be given for lead and for glass by substituting the appropriate values (stated above) such that for lead, $\sigma_A = \frac{2500}{0.42} = 6000$ psi, and for glass, $\sigma_A = \frac{10{,}000}{0.20} = 50{,}000$ psi. The above relations were derived for static load data, but since impact deformation is primarily energy-dependent and not rate-dependent, the static-load measurements are also reasonable approximations for impacts. These calculated values for σ_A are in the range of empirical values for the dynamic flowstress of lead and are only slightly below empirical values of the compressive fracture stress of glass specimens [WALLACE].

For plastic deformation, we may compare the plastic work, W_p, which is equal to $\sigma_D \Delta V$ in Eq. 1, with the elastic work W_E in Eq. 7. When evaluation of W_E is made for the axial stress equal to the dynamic flow stress, σ_D, we have:

$$\frac{W_E}{W_P} = \frac{\sigma_D}{2E(\Delta V/V)}$$

For the stated properties of lead, this equation becomes

$$\frac{W_E}{W_P} = \frac{2.5 \times 10^{-3}}{\Delta V/V}$$

That is, plastic energy is larger than elastic energy when the volume displacement of deformation is greater than about 1/4% of the original volume. In cask impact tests, volumetric deformations of 1 to 10% were observed, indicating that elastic energy is typically small compared with energy absorbed in plastic deformation [SHAPPERT].

We may estimate the energy requirement for generation of fragmentation surface (i.e., the factor, K_F) from the tensile fracture modulus of glass, i.e., $\sigma_F = 10{,}000$ psi, by calculating the elastic energy in tension, W_E, from Eq. 7, and by equating this energy to the energy to produce fracture, W_F, in Eq. 2, that is,

$$W_E = W_F \tag{11}$$

$$= K_F \Delta S$$

$$= \frac{V\sigma_F^2}{2E}$$

A simple tensile fracture results in a single cleavage of the cross-sectional area $A = \frac{\pi D^2}{4} = V/L$, such that $\Delta S = 2A$, and from Eq. 11:

$$K_F = \frac{L\sigma_F^2}{4E} \tag{12}$$

$$= \left(\frac{V}{A}\right)\left(\frac{\sigma_F^2}{4E}\right)$$

In Eq. 12, A is the cross-sectional area and L is the length through which the tensile stress was applied that resulted in fracture strain. When fracture results from a compressive axial stress on a cylinder, the fracture results from radial strain. For the compressive fracture, the mean cross-sectional area, $\bar{A}$, over the volume, V, can be calculated for the diameter, D, from the ratio $\frac{A}{V} = \frac{1}{D}$ as follows:

$$\bar{A} = \int_0^D \frac{A}{V}\, dV \tag{13}$$

$$= \frac{\pi L}{2} \int_0^D dD$$

$$= \frac{\pi LD}{2}$$

From Eq. 13, $V/\bar{A} = \frac{D}{2}$, and

$$K_F = \frac{D\sigma_F^2}{8E} \tag{14}$$

If we evaluate K_F in Eq. 12 by glass properties and the 1.3-cm diameter of specimens used in SRL tests [WALLACE], we obtain

$$K_F = \frac{(1.3 \times 10^{-2}\text{m})(6.9 \times 10^{7}\text{Pa})^2}{8(6.9 \times 10^{10}\ \text{Pa})} \tag{15}$$

$$= \frac{112\ \text{J}}{\text{m}^2}$$

This calculated value is much less than the impact energy (1.06×10^3 J/m^2) value obtained experimentally at SRL. However, the calculated value is close to that value of 77 J/m^2 obtained in single-impact fracture of Pyrex and quartz specimens [ZELENY]. The high value reported by SRL is based on the assumption of cubical symmetry of glass fragments (which underestimates the true surface) and also included the energy absorbed in deformation of the metal parts of the impact apparatus. Therefore, the calculated value of K_F seems to be in agreement with available experimental measurements.

The ratio of (1) the elastic energy, W_E, stored as defined in Eq. 7 to (2) the energy of brittle fracture, W_F, as defined in Eq. 11 can be expressed as

$$\frac{W_E}{W_F} = \left(\frac{V\sigma_A^2}{2E}\right) \Big/ \left(K_F \Delta S\right) \tag{16}$$

where σ_A is the threshold axial compressive stress for fracture (in Pa) and K_F is the ratio of (1) the input energy (J) that causes fragmentation to (2) the total surface area $\Delta S(\text{m}^2)$. The volume, $V(\text{m}^3)$, and the elastic modulus, E(Pa), are generally known.

In the primary fracture of a solid glass cylinder, the stored elastic energy is the major source of energy for the breaking of atomic bonds and the creating of new surface in fragmentation by impact. If we take $W_F = W_E$ in Eq. 16, we can solve for the ratio of new surface to volume, $\Delta S/V$, of the fragments:

$$\frac{\Delta S}{V} = \frac{\sigma_A^2}{2EK_F} \tag{17}$$

We can calculate $\frac{\Delta S}{V}$ for the quantities in Eq. 17 known in the case of glass: $E = 1.0 \times 10^2$ psi $= 6.9 \times 10^{10}$ Pa; σ_A (as discussed above) = 50,000 psi = 3.45×10^8 Pa; $K_F = 1.12 \times 10^2$ J/m^2 for a single impact of 1.96 J/g [WALLACE]. From these values:

$$\frac{\Delta S}{V} = 7.70 \times 10^3 \text{ m}^{-1} \tag{18}$$

For a single cube or sphere, the ratio of surface to volume is equal to 6/D where D is the diameter or edge length. For glass fragments, however, the observed ratio is 12/D [McELROY-1977B]. Therefore, the mean size, D_M, of the impact fragments represented by $\Delta S/V$ in Eq. 18 can be found, in general, as

$$D_M = 12/(\Delta S/V) \tag{19}$$

or, from the value of $\frac{\Delta S}{V}$ in Eq. 18,

$$D_M \equiv 1600 \text{ μm} \tag{20}$$

Particle-size distributions are discussed in the following subsection.

From the above analysis of primary fragmentation of a small glass cylinder, it is probable that if the mass-mean particle size of impact fracture is less than about 1000 μm, the fragmentation occurred in more than one stage. The primary fragmentation of the glass cylinder would give particles of mean sizes of about 1×10^3 to 3×10^3 μm and secondary fragmentation would occur by subsequent crushing of the primary particles. Multiple stages of fragmentation would be expected to give somewhat lower efficiency of conversion of input energy to new surface, i.e., would give higher values of K_F.

In the above discussion of threshold compressive stress for inelastic deformation, the dynamic flow stress of lead was in the range 5000 to 10,000 psi and the compressive strength of glass in the range of 50,000 to 100,000 psi. Consequently, lead may flow before glass will fracture. Qualitative confirmation of this is provided by a report [McELROY-1977B, p. 27] in which lead and glass were contacted by a standard impact test method (ASTM C 496-64 T). In the test described, a flat pad of metallic lead was placed between (a) the curved side of the glass cylinder to be

tested and (b) the flat "hammer" face of hard steel used to apply the impact force. It was found that the lead was ejected (i.e., rapidly extruded) from between the hammer and the glass specimen. This appears to demonstrate for this select geometry the preferential deformation of lead, predicted by the above analysis.

The extent of protection of the glass by a lead "cushion" in impacts depends on (a) the impact energy, (b) the thickness of lead, and (c) the ability of the configuration to allow lead to flow to the maximum thickness of the lead. The energy relation of Eq. 1 can be written for the self-deformation of the impact of a lead cylinder moving at velocity, u:

$$\frac{\rho u^2}{2} = \sigma_D\left(\frac{\Delta V}{V}\right) \tag{21}$$

At 35.2 m/s (80 mph) before impact and for the properties of lead, ρ = 11,300 kg/m^3 and $\sigma_D = 6.9 \times 10^7$ Pa, we have

$$\frac{\Delta V}{V} = 0.101 \tag{22}$$

indicating that all of the impact energy would be consumed by a fractional displacement of 10% of the volume of the lead. This indicates a high potential for lead as a protective matrix.

5. Relation of Particle Size Distributions to Surface/Volume Ratio

The impact deformation of brittle material results in fragmentation, and the fragmentation product is a collection of particles which is described quantitatively by a total surface area and a particle size distribution. The previous sections have related the energy of brittle fracture to the surface area generated. However, the dispersability of particles depends on the distribution of sizes, especially the mass fraction which has diameters smaller than 10 μm (generally considered the respirable size fraction). In general, both surface area and size fractions are needed for an adequate description.

In the literature review summarized in [STEINDLER-1979], mass fractions of particle sizes were determined by screen analyses, and these data were plotted against size on log-log graphs to give a continuous particle-size distribution function. For a given particle shape, the total surface area, S, of the fragments can be calculated from geometrical relationships, whereby the surface/volume ratio, $\frac{S}{V}$, is related to a mean size, D_M, for the dimensionless shape factor, α.

$$\frac{S}{V} = \frac{\alpha}{D_M} \tag{23}$$

The particle density, ρ, is used to convert volumes to masses in these geometrical relations; actual measurements are in mass fractions rather than volume fraction. For spheres and cubes, $\alpha = 6$.

Screen analyses are not practical for particle sizes smaller than about 20 μm. Also, vibrating screens are subject to losses--particularly losses of the smaller sizes, which may be entrained in air or remain attached to fixed screen surfaces. Liquid methods of particle size analysis are more accurate for smaller particle sizes, but more experimental effort is required. Even small losses of small particles may be significant because of their high surface to volume ratio; small particles also constitute the most dispersible fraction.

Direct measurements of surface area may be made by gas-adsorption methods, e.g., the Brunauer-Emmett-Teller (BET) method. However, for accurate measurement by this method, samples must have rather large specific surface areas. Also, the BET method cannot distinguish between the internal surface area of a porous material and the geometric surface area of particles. (For solid nonporous glass, this is no problem.) In any case, direct measure of surface area does not by itself give information on particle size distribution.

Very commonly, size distribution measurement data are incomplete either with respect to the full range of sizes or with respect to the total surface area. Good size distributions are difficult to determine over a wide range as are surface areas. Also, the accuracy of the methods is in question.

The lognormal probability distribution is a mathematical function with two adjustable parameters and which has been widely used to describe actual particle size distributions by adjusting the two parameters to the data [HERDAN]. The parameters, i.e., the geometric mean diameter, D_g, and the geometric standard deviation σ_g, have physical significance and are especially convenient in graphical analysis and in conversion of distributions from particle masses to particle number, etc. The nature, properties, and uses of the lognormal distribution function are described in detail in standard reference works [DALLAVALLE, HERDAN].

The lognormal function plots as a straight line on lognormal graph paper, with the diameter, D, as the abscissa (on a log scale) and the fraction of the particle population of size smaller than D as the ordinate (a special percentage scale). The 50% fraction locates the geometric mean diameter, D_g, and the slope is a function of the geometric standard deviation σ_g, the magnitude of which is given by the ratio of diameters:

$$\sigma_g = \frac{D(84\% \text{ fraction})}{D(50\% \text{ fraction})} \qquad (24)$$

$$= \frac{D(50\% \text{ fraction})}{D(16\% \text{ fraction})}$$

where, of course, $D_g = D(50\% \text{ fraction})$.

The lognormal parameters are thus determined by any two percentiles. However, it is desirable to have a number of percentiles over a wide range of diameters in order to establish the fit of the distribution, especially for the smaller sizes.

The standard deviation, σ_g, is the same for the size distribution of mass as for the distribution by particle number. Therefore, the plots have the same slope. The geometric means differ:

$$\frac{(D_g)\text{mass distribution}}{(D_g)\text{number distribution}} = e^{3 \ln^2 \sigma_g} \tag{25}$$

The surface to volume ratio, $\frac{S}{V}$, for the entire particle population is given in terms of the parameter, D_g (mass), and σ_g as

$$\frac{S}{V} = \frac{\alpha}{D_g} \sigma_g^{0.5 \ln \sigma_g} \tag{26}$$

In fragmentation tests, the total volume and mass of the original specimen are known, and therefore the total surface of the fragments can be obtained from the $\frac{S}{V}$ ratio in Eq. 26.

Because of the physical significance of σ_g, it frequently occurs that, for similar fragmentation processes, the values of σ_g are similar and differences are primarily reflected in the value of D_g. Accordingly, if the value of σ_g can be assumed, the complete particle-size distribution can be calculated by a direct measurement of surface area, according to Eq. 26. If Eq. 26 is compared with Eq. 23, it can be seen that particles smaller than the mass mean (D_M and D_g) have more surface than do particles larger than the mean.

Appreciation of the lognormal distribution function is used below in a preliminary way to interpret data on impact fragmentation of glass, which is a homogeneous material without grain microstructure. Crystalline materials may fracture into two particle populations, with a smaller-size population corresponding to the grain size. In such a bimodal particle-size distribution, no single lognormal distribution would be appropriate--either two lognormal distributions or an entirely different distribution function would be required.

Particle size distribution data points (from empirical measurements in glass impact tests) are plotted on lognormal probability graph coordinates in Fig. 35. In two of these tests, the surface area was determined from the size data; in two other tests, no surface area was reported. The major test data and calculated results are summarized in Table 34.

As can be seen from Fig. 35, the slopes of straight lines connecting the points are generally parallel, but there is a tendency for the slope to increase with particle size, with values of σ_g ranging from about 3.5 to 4.9. The effect of variations in σ_g is most easily seen from the formula given above in Eq. 26. (The shape factor of 6×10^6 was used for D_g in μm and V in m^3.)

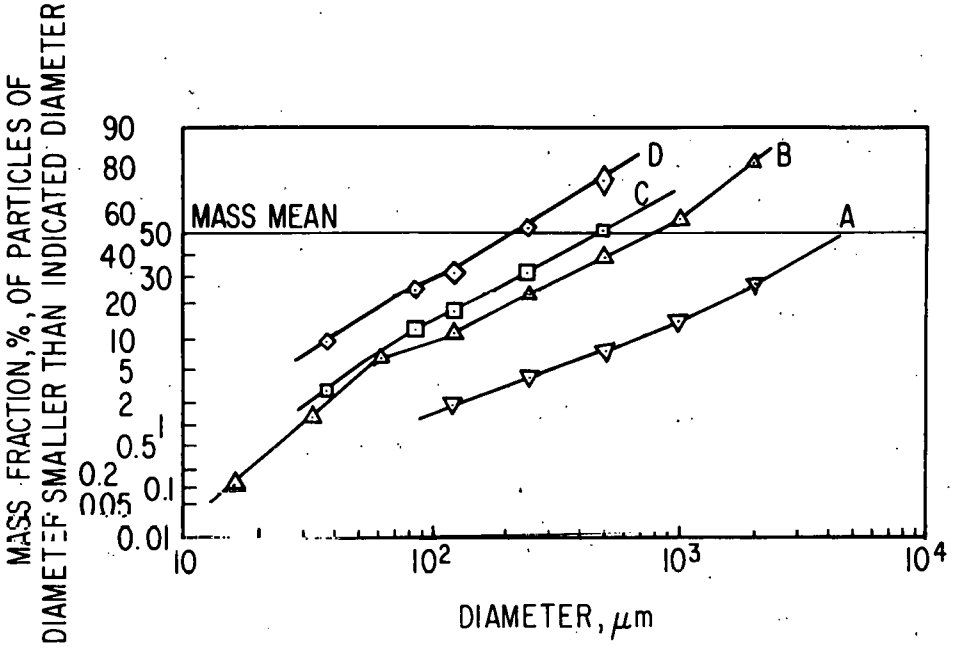

Fig. 35. Lognormal Plots of Particle Size Distributions Resulting from Impact Fractures of Glass Specimens at Various Impact Energies (see Table 34 for legend).

Calculations of surface area shown in Table 34 were made for both $\sigma_g = 3.5$ and for $\sigma_g = 4.9$ to indicate the range of uncertainty in this graphical method. The utility of the lognormal method is shown by the degree of agreement of (1) the energy/surface ratios calculated (column X) and (2) the measured data in column VI. Further refinements would consider more realistic shape factors and the possible decrease in K_p for single impacts rather than repeated crushing of particles formed by the primary impact fracture.

Tests made with very high impact-energy inputs per gram of specimen have no clear relevance to realistic impact effects. If deformations are considered to occur by collision of a moving body with an essentially unyielding barrier, then impact energy can be related to velocity. The impact energy per unit mass, W/M, can be calculated for the velocity u as follows:

$$\frac{W}{M} = \frac{u^2}{2} \tag{27}$$

For some reference velocities, the impact energy input is given below:

Table 34. Impact Fragmentation Calculations Based on the Lognormal Probability Distribution Applied to Test Data on Glass Specimens

I	II	III	IV	V	VI	VII	VIII	IX	X
	Specimen		Reported Values			Graphical Mass Mean	Surface/Vol Ratio,[a] S/V		Calc'd K_F,
Test Index	Mass, g	Density, g/cm^3	$\frac{S}{V}$, m^{-1}	$\frac{J}{g}$	$\frac{J}{m^2}$	D_g, μm	$\sigma=3.5$, m^{-1}	$\sigma=4.9$, m^{-1}	$\frac{J}{m^2}$ [b]
A	10.0[c]	3.0	5.1×10^3	2.0	1.2×10^3	4500	2.6×10^3	3.7×10^3	1.6×10^3
B	10.0[c]	3.0	2.2×10^4	7.8	1.0×10^3	780	1.7×10^4	2.7×10^4	8.6×10^2
C	3.0[d]	2.47	–	9.3	–	490	2.8×10^4	4.2×10^4	1.6×10^3
D	3.0[d]	2.47	–	71.8	–	220	6.6×10^4	1.1×10^5	4.9×10^3

[a] Calculated from the equation $\frac{S}{V} = \frac{\alpha\sigma_g^{0.5 \ln \sigma_g}}{D_g}$.

[b] Calculated for S/V values in $\sigma_g = 4.9$ column.

[c] Special borosilicate glass [WALLACE, p 8].

[d] Soda-lime-silica glass [McELROY-1977B, p. 24] and [ROSS, p. 11]. Apparently this glass is Corning No. 0080 (73 wt % SiO_2, 17 wt % Na_2O, 5 wt % CaO, 4 wt % MgO, 1 wt % Al_2O_3) [HUTCHINS].

velocity			W/M,
mph	ft/s	m/s	J/g
30	44	13.2	0.087
45	66	19.8	0.20
80	117	35.2	0.62
750	1100	330	54

For tests with W/M > 54.4 J/g, the equivalent velocity is higher than MACH 1, the speed of sound in air (330 m/s).

At 80 mph, even if 90% of the mass of the waste package was other than glass and even if all of this energy were absorbed by the glass, it is difficult to conceive of an energy input to the glass greater than 6.2 J/g. Glass and supercalcine specimens have been subjected to impacts of about 30 J/g [McELROY-1977B, p. 43].

III. TRANSPORT PROPERTIES OF NUCLEAR WASTE IN GEOLOGIC MEDIA

(M. G. Seitz, P. G. Rickert,* S. M. Fried,* A. M. Friedman,* Jacqueline Williams,† and M. J. Steindler)

A. Introduction

A method being considered for permanent disposal of radioactive waste generated with nuclear power is to place the waste in a repository deep beneath the surface of the earth. Groundwater infiltrating the repository may leach radionuclides from solidified waste in such repositories and transport them into the fissures or pores of the surrounding geologic formation, where they may react and become immobilized.

In work done previously to evaluate the safety of a waste repository, the movement of radionuclides from a repository was studied using radionuclide leaching and radionuclide migration experiments, with the two types of experiments being run independently of each other [e.g., STEINDLER-1978A, 1978B, SEITZ-1979, RICKERT]. In fact, migration behavior is dependent on solution composition [SEITZ-1978], which is altered by leaching. Therefore, the two processes (leaching and migration) should be treated collectively. The radioactive species leached from a solid waste form would be difficult to characterize and to synthesize in free-standing solutions. We developed an approach, termed leach-migration, to generate these leached species experimentally and to determine their migration characteristics without the need to formulate each species. The initial leach-migration experiments were described in [STEINDLER-1979].

In this report, leach-migration experiments are described, together with conventional infiltration experiments. Both types of experiments were performed to determine how the method of applying a radionuclide to a rock column affects migration.

Also described are filtration and dialysis studies of solutions used in the leach-migration and infiltration experiments. These studies were done in search of an explanation for cesium behavior differing in the leach-migration and the infiltration experiments.

B. Leach-Migration Studies

A leach migration experiment similar to those reported previously [STEINDLER-1979] was performed this quarter. In the leach-migration experiment, 1-mm fragments of a simulated high-level-waste glass were confined in a slow-moving stream of simulated groundwater solution by stainless steel tubing and frits. The glass and simulated groundwater solution were heated by an oven to simulate the elevated temperature that may exist from radioactive decay heating. The simulated groundwater solution (made by reacting distilled water with rock [SEITZ-1979]) flowed around the waste form and leached radionuclides, then carried them to a rock column with which the radionuclides could interact. Other details on the leach migration apparatus are given in the preceding quarterly report [STEINDLER-1979].

---

*Members of the Chemistry Division.

†Member of the Analytical Group of the Chemical Engineering Division.

The leach-migration experiments performed to date were run with columns of solid oolitic limestone (1-cm dia by 3.5-cm long) and a simulated waste glass composed of PW-8A-3 calcine and 76-68 glass [McELROY-1977A]. Limestone was chosen for this study because it is commonly associated with bedded salt and because it forms aquifiers and therefore may be a final pathway for radionuclides to man. The waste glass was irradiated in the CP-5 research reactor at ANL to activate about ten nuclides for study [STEINDLER-1978A]. Radionuclides of interest for geologic storage and having short-lived isotopes in the glass are strontium, zirconium, iodine, cesium, uranium, and neptunium.

1. Leach-Migration Experiment

Earlier experiments, one with 4.87 mg of glass (Expt. 128-89) and the other with 0.35 g of irradiated glass (Expt. 128-95), were discussed in the preceding quarterly report [STEINDLER-1979]. An additional experiment (Expt. 148-1) was done this quarter, using a column of 0.35 g of irradiated glass as the waste form. As in past experiments, the glass was heated to 80°C and leached with a stream of simulated groundwater solution flowing at about 0.07 mL/min. (The simulated groundwater solution had been made by reacting distilled water with granulated limestone.) The solution stream, afer leaving the column of glass, was forced through a limestone column. The solution leaving the column was collected in five fractions totaling 1305 mL of solution. The fractions were evaporated, and the residues (in 10-mL glass vials) were radiochemically analyzed. The limestone column was cut into four segments. The limestone in each piece was dissolved in acid, and the acid and insoluble residue were transferred into a 10-mL vial where they were radiochemically analyzed.

2. Results of the Leach-Migration Experiment

Activities of cesium-134 in the solution fractions from Expt. 148-1 are listed in Table 35, together with the sizes of the fractions and the flow rates at which the fractions were delivered. The activities of cesium in the four segments of the column, as determined from the activity of the 0.605-MeV gamma ray from the decay of cesium-134, are listed in Table 36. From a comparison of the activities on the column (total of 23 c/s from Table 36) and in solutions (total of 1130 c/s from Table 35), about 98% of the cesium leached from the glass was seen to move through the limestone column.

C. Intiltration Experiments With Soluble Cesium

The migration of cesium through oolitic limestone at room temperature was studied by spiking oolitic-limestone groundwater solutions with a solution of cesium chloride and passing the spiked solutions through columns of the solid limestone. Cesium-134 was used and its concentrations in the columns and solutions leaving the columns were analyzed by gamma counting. In the first spike experiment (Expt. 128-56), a small quantity (20 µL) of the radioactive cesium solution was injected into (rather than mixed with) a stream of simulated groundwater solution that was free of radioactive cesium. The simulated groundwater stream then passed through a limestone column. Results of this experiment were summarized in the preceding quarterly report [STEINDLER-1979].

Table 35. Sizes of Solution Fractions, Flow Rates, and Activities Due to Cesium-134 in the Solution Fractions from Expt. 148-1

Solution Fraction	Fraction Size, mL	Measured Average Flow Rate, mL/min	Net Activity,[a] c/s·mL
1	250	0.087	0.78
2	420	0.073	0.87
3	200	0.063	0.92
4	185	0.064	0.87
5	250	0.058	0.89

[a]Activity is for the 0.605-MeV gamma ray from the decay of cesium-134. Background correction was about 0.004 c/s·mL. Uncertainty(σ) from counting statistics is less than 1%. The solutions were dried, and the residues were counted with a NaI crystal.

Table 36. Cesium-134 Activities in the Segments of the Column from Expt. 148-1

Column Segment	Weight of Limestone, g	Net Activity,[a] c/s·g
1	1.13	3.4
2	1.26	2.9
3	1.38	2.9
4	1.63	6.8

[a]Activity is for the 0.605-MeV gamma ray from the decay of cesium-134. Background correction was 1.0 c/s·g. Uncertainty (σ) from counting statistics is about 4%. The limestone was dissolved in acid, transferred with the insoluble residue to a vial, and after the water was evaporated was counted with a NaI crystal.

In the second spike experiment (Expt. 148-22), the cesium chloride solution was mixed with a large volume (2 L) of simulated groundwater solution. The spiked solution was then pumped through a limestone column. The experiments were performed to determine if the different methods of adding cesium to the columns produced different migration behavior for cesium and whether either method produced behavior analogous to that observed for leached cesium.

1. Cesium Delivered to Column in a Small Volume of Solution

In experiment 128-56, in which the radioactive cesium was introduced into the column in a small volume of solution, the aqueous solution was continuously monitored for cesium by an on-line counting system. No radioactive cesium was detected in the 1200 mL of solution that passed through the column. After the experiment was terminated, the column was dried to fix any absorbed cesium and was sectioned to determine the location of the cesium. Cesium activities in the different segments are given in Table 37.

Table 37. Cesium-134 Activities in the Segments of the Limestone Column. Expt. 128-56

Column Segment	Length,[a] cm	Activity in Limestone,[b] c/s·g
1	0.50	7.2
2	0.60	6.8
3	0.45	7.3
4	0.40	6.3
5	0.40	5.6
6	0.50	4.6
7	0.40	5.1

[a] Limestone weighed about 1.61 g/cm of column.

[b] Activity was the 0.605-MeV gamma ray from the decay of cesium-134. The background correction about 0.61 c/s·g. Uncertainty (σ) due to counting statistics is about 3%. The activity measured on the column was more than 50% of the activity used in the experiments. Attenuation of the γ-radiation in the stainless steel column and limestone precluded accurate estimation of the activity on the column in relation to that added in the experiment.

Cesium was carried into the column by the aqueous solution and was detected in all sections. The presence of cesium in the bottom section suggests that some of the cesium was carried through the column by the solution. Possibly activity in solution passed through the column (0.3 c/s·mL) is the minimum activity which would be detected by the counting system); this could account for the 50% of the cesium activity not in the column segments.

2. Cesium Delivered Continuously to Column

Experiment 148-22 was performed by pumping through a column of oolitic limestone, a simulated groundwater solution that had been reacted with oolitic limestone and then mixed with a low concentration of cesium-134. The solution, after passing through the column, was collected in four fractions which were analyzed for cesium activity. The counting data and the fraction sizes for the solutions from the experiment are listed in Table 38. The solution in the first fraction had two-thirds the cesium concentration that the starting solution had. In the second fraction, the cesium concentration was only slightly lower than in the starting solution, and the third and fourth fractions contained as much cesium as did the starting solution. About 90% of the cesium activity that had been delivered to the column passed through the column during the experiment.

Table 38. Counting Data and Fraction Sizes for Solutions Obtained from Experiment 148-22 (groundwater solution containing cesium-134 pumped through a limestone column)

Solution	Fraction Size, mL	Activity in the Solution, c/s·mL[a]
Starting Solution	--	0.31
First Fraction	111.9	0.21
Second Fraction	271.8	0.26
Third Fraction	196.8	0.31
Fourth Fraction	129.6	0.30

[a]Activity is for the 0.605-MeV gamma ray from the decay of cesium-134. The background correction was about 0.20 c/s·mL. Uncertainty (σ) from counting statistics is about 15%.

D. Discussion of Leach Migration and Infiltration Results

None of the results reported here show that cesium migration in oolitic limestone can be predicted by simple exchange models (i.e., cesium was not seen to generate recognizable break-through curves or to move at a well-defined rate relative to the water). Neither the high nor the low partitioning values for cesium between limestone and water measured in the controlled sample program [RELYEA], represent the behavior of cesium observed in these experiments. In both leach-migration and infiltration experiments, some cesium moved through columns with the water front rather than requiring 370 mL or more of solution, as one would predict from measured partitioning values [RELYEA] in excess of 45. Some cesium was strongly bound on the limestone, a result not expected for partitioning values [RELYEA] as low as 2.

The leach-migration and infiltration experiments reported here were initiated because it was suspected that the radionuclides leached from solidified waste might migrate differently from radionuclides formulated in solutions from soluble compounds. Of the many elements monitored in these experiments, only cesium was studied extensively because it is expected to exhibit behavior uncomplicated by changes in valence, complex formation, etc.

Quantitatively, cesium that had been leached from the waste form did behave differently from cesium in solutions formulated from soluble compounds. In leach-migration experiment 148-1, 98% of the cesium moved through the column in about 1305 mL of solution, and in experiment 128-95, 99% of the cesium moved through the column in about 1500 mL [STEINDLER-1979], whereas in the experiment with a small quantity of radioactive solution added (Expt. 128-56), less than 50% of the cesium moved through the column in about 1200 mL of solution. In the experiment in which a large volume of solution that contained cesium was pumped through limestone (Expt. 148-22), about 90% of the cesium moved through the column, a result not unlike that obtained in the leach-migration experiments.

Insufficient data are available to formulate a reliable explanation of the observed results. One likely mechanism is that the fraction of absorbed cesium is strongly dependent on concentration in the range, 10^{-7} to 10^{-10} M cesium. Independent of the mechanism, the results show that cesium behavior differed significantly, depending on the method of applying the cesium to a rock column, which raises questions about experimental methodology. The leach-migration experiments are thought to simulate migration of radionuclides from a breached waste repository more closely than do conventional infiltration methods and may be preferred in evaluating the safety of a waste repository.

E. Cesium Associated with Colloids or Particulate in Solution

In the migration experiments, both cesium leached in a large volume of solution from the waste form and cesium delivered to the column in a large volume of solution were seen to behave differently from cesium delivered to

the column in a small volume of solution. It was postulated that cesium might combine with finely divided residues of the leached glass or with tiny particulate (<0.4 μm) in large volumes of groundwater solution. Combined cesium could move through the rock column, reacting little with the limestone. Alternatively, cesium dissolved in a small volume of solution could be carried immediately to the rock and could react with the rock, rather than suspended matter, and be immobilized.

Solutions obtained from the experiments have been filtered and studied by equilibrium dialysis to determine whether the cesium in any solution was associated with particulate or colloidal material.

1. Solutions Filtered through 0.4 and 0.1 μm Pore-Sized Membrane Filters

Activities of solutions before and after being filtered through 0.4-μm and 0.1-μm-pore membrane filters (Nuclepore polycarbonate membranes) are given in Table 39. Two solutions suspected of having cesium associated with the particulate were filtered: (1) the cesium-containing simulated groundwater solution that was delivered in large volumes to the column and (2) a leachate (obtained from solidified waste glass). The cesium-containing simulated groundwater solution was filtered both before and after it had passed through the column to determine whether, as postulated, the column retained only dissolved cesium, allowing only cesium on particles to pass.

Table 39. Radioanalyses of Solutions Before and After Filtering

Sample	Net Activity of Cesium,[a] c/s·mL		
	Initial Solution	Filtrate Passing Through 0.4-μm-Pore Membrane	Filtrate Passing Through 0.1-μm-Pore Membrane
Cesium-Spiked Groundwater, Expt. 148-22	0.36	0.33	0.34
Groundwater Eluate from Expt. 148-22	0.21	0.23	0.22
Leachate from Simulated Waste	1.40	1.38	1.36

[a]Activity is for the 0.605-MeV gamma ray from the decay of cesium-134. Background correction was about 0.32 c/s·mL. Uncertainty (σ) from counting statistics is about 7%.

The results in Table 39 indicate that little if any cesium in these solutions is associated with 0.1-μm or larger particles.

2. Solutions Subjected to Equilibrium Dialysis

A dialysis membrane permits molecules of low molecular weight to pass through the membrane to solutions on either side while retaining molecules of high molecular weight in one of the solutions. Equilibrium dialysis studies were performed by placing radioactive cesium-bearing solutions inside a dialysis tube and immersing the tube in a solution containing no radioactive cesium. Seamless, regenerated cellulose tubing, 2.7 cm in diameter, obtained from Scientific Products and used in the studies, has a nominal transmission cutoff at a molecular weight of 5000 (a nominal pore size of 0.0014 μm). The light molecules in the solutions were allowed to exchange between the solutions, and the cesium activities in the solutions inside and outside the dialysis tube were measured.

In an experiment, 25 mL of radioactive solution was inside the tube; 100 mL of inert solution outside the tube was stirred with a small, 0.7-cm-long stirring bar. In this configuration, it was found that the solution outside the tubing attained, in 2 h, 82% of the cesium activity that would have been expected if there had been complete mixing with the solution inside the bag. Dialyses were run for at least 6 h to ensure an equilibrium concentration of the transferable cesium in the outer solution (>99% equilibrium concentration).

Results of the equilibrium dialysis studies for four solutions are given in Table 40. In none of the solutions was any measurable amount of cesium retained by the dialysis membrane.

F. Discussion of the Filtration and Dialysis Results

The molecular forms of cesium in the solutions studied cannot be distinguished from the results of the filtrations or dialyses. The dialysis results indicate that cesium was not bound to particles larger than about 0.0014 μm. Although it is still possible that cesium's association with small particles (<0.0014 μm) in some solutions accounts for the behavior of cesium observed in column studies, it is likely that cesium is present as light ions similarly in all solutions. If cesium were combined with suspended material, it would be expected that at least some of the particles would be larger than 0.0014 μm, and that some of the cesium would have been stopped by the dialysis membrane. Therefore, absorption of cesium on suspended particles is no longer suspected of being responsible for the observed behavior, but rather other solution properties of cesium (pH, concentration of cesium or competing ions, etc). The different behavior for cesium may be due to the existence of a nonlinear absorption isotherm in the concentration range spanned by these experiments. Results of this ongoing investigation appear to indicate that the latter is the case.

Table 40. Radioanalyses of Equilibrium Dialysis Experiments

Sample	Net activity of Dialysis Samples,[a] c/s·mL		
	Diluted Sample[b]	Solutions Inside Dialysis Tubing	Solutions Outside Dialysis Tubing
Cesium-Spiked Groundwater, Expt. 148-22	0.07	0.05[c]	0.07[c]
Groundwater Eluate from Expt. 148-22	0.07	0.08[c]	0.06[c]
Leachate from Simulated Waste	0.31	0.28[d]	0.27[d]
Concentrated Cesium Spike, Expt. 128-56	1.42	1.09[e]	1.14[e]

[a] Activity is for the 0.796-MeV gamma ray from the decay of cesium-134. Background correction was about 0.29 c/s·mL.

[b] Activity of the sample diluted by the equilibrating solution was calculated from the measured activity of the initial solution and from the solution volumes after equilibration. Approximately 10% of the solution was lost (by evaporation) in a 20-h period.

[c] Uncertainty (σ) from counting statistics is about 25%.

[d] Uncertainty (σ) from counting statistics is about 9%.

[e] Uncertainty (σ) from counting statistics is about 5%. Less than 7% of the radioactive cesium was found to be adsorbed by the dialysis tubing.

G. Conclusions

The mobility of cesium in limestone was found to depend on how cesium was introduced into groundwater solutions. Cesium leached from a glass waste form was more mobile than was cesium that had been dissolved in a large quantity of groundwater solution. In turn, the latter was more mobile than cesium dissolved in a small volume of solution and added directly to the rock.

None of the solutions investigated by filtration and dialysis studies was found to contain cesium associated with particles larger than 0.0014 μm. Therefore, the cesium behavior observed in the infiltration experiments is apparently not a result of cesium being associated with leaching residues or with rock particles suspended in the solutions.

As yet, there is no reliable explanation of the observed cesium behavior. Independently of the mechanism, the results show that cesium behavior differed significantly, depending on the method of applying the cesium to a rock column. This raises questions about experimental methodology. The leach-migration experiments simulate migration of radionuclides from a breached repository more closely than do conventional infiltration methods and may be preferred for evaluating the safety of a waste repository.

H. Future Directions

Additional leach-migration experiments are planned that may reveal the mechanism leading to the migration behaviors of cesium in limestone differing for different methods of applying cesium to rock columns. Two possibilities will be considered: first, that slight changes in the pH of solution may drastically affect cesium absorption; and secondly, that different concentrations of cesium in the solutions produce different migration behavior due to a nonlinear isotherm for cesium absorption on limestone.

New leach-migration apparatus will be assembled in which actinide-bearing solid waste forms can be studied. Irradiated light water reactor fuel will be considered as a solid waste form to simulate leaching from unreprocessed fuel in a repository.

IV. TRACE-ELEMENT TRANSPORT IN LITHIC MATERIAL BY FLUID FLOW AT HIGH TEMPERATURE

(M. Seitz and R. Couture)

A. Introduction

During the last quarter of 1978, two separate subjects were investigated. In the first, we determined the rates of transport of I^- and Na^+ relative to that of tritiated water in order to determine the effect of the streaming potential on the migration rates of ions through kaolinite columns. Second, adsorption of iodide and iodate by several compounds was studied, and some implications of the results for disposal of radioactive iodine discussed. This work may have practical value in relation to the disposal of iodine-129 from nuclear fuel reprocessing.

B. Ionic Transport Through Kaolinite Columns

In the preceding quarterly report [STEINDLER-1979], we reported our determinations of the Cs^+-Na^+ ion exchange selectivity of the clay mineral, kaolinite [$Al_2Si_2O_5(OH)_4$], from 25 to 210°C at trace concentrations of Cs^+. In these determinations, made by fluid flow experiments through columns, it was assumed that the rate of transport of a solute relative to that of the solvent is equal to the fraction of the solute in solution (i.e., the relative rate of transport equals one minus the fraction sorbed). However, that assumption does not take into account the effect of the streaming potential. The charge on a mineral surface must be balanced by an opposite charge in the interstitial solution. If the solution is pumped through the column, maintaining neutrality of the effluent solution requires that anions and cations move through the columns at different rates under the influence of the streaming potential. For the usual situation in which the mineral surface is negatively charged, anions must be transported faster than cations. At progressively increasing ionic strengths, the surface charge decreases because of adsorption of ions and the electrostatic effect on ionic transport decreases.

In the experiments described in the preceding quarterly report [STEINDLER-1979], we worked with solutions of moderate ionic strength (0.1M) and with kaolinite, which has a modest ion-exchange capacity. Therefore, we expected the electrostatic effect to be small. The effluent solution was observed to have the same concentration of $NaHCO_3$ as the influent solution (within 0.5%), which is supporting evidence, but not proof of this contention.

In order to better evaluate the electrostatic effect, small spikes of radioactive I^-, Na^+, and tritiated water in 0.1M $NaHCO_3$ solution were injected into kaolinite columns in successive experiments. The solutions were collected in a fraction collector and were analyzed for radioactivity to determine the migration velocity of the radioactive material.

The tritiated water was used to monitor the column performance. The electrostatic effect on I^- should be fairly similar in magnitude to that on Cs^+ because both are large, singly-charged ions which are only slightly hydrated. Thus, they ought to have similar ionic mobilities in an electric field. Na^+ was also used as a test of the migration velocity theory

because in $NaHCO_3$ solutions, its migration velocity should be easily predictable from the ion-exchange capacity of the column. Since Na^+ is the only bound cation, the fraction bound to the column is easily determined. Na^+ is highly hydrated compared to Cs^+ and should therefore have a large hydrated radius and a low mobility in an electric field. Therefore, the effect of the streaming potential on migration velocity should be smaller than that for Cs^+.

1. Results

The results of the elution experiments are shown in Figs. 36 and 37. As expected, I^- was eluted about 15% faster than tritiated water. If I^- does not interact chemically with the column, this gives the magnitude of the streaming potential effect. Na^+ was eluted about 30% faster than expected from the ion-exchange capacity of the kaolinite. Duplicate experiments gave

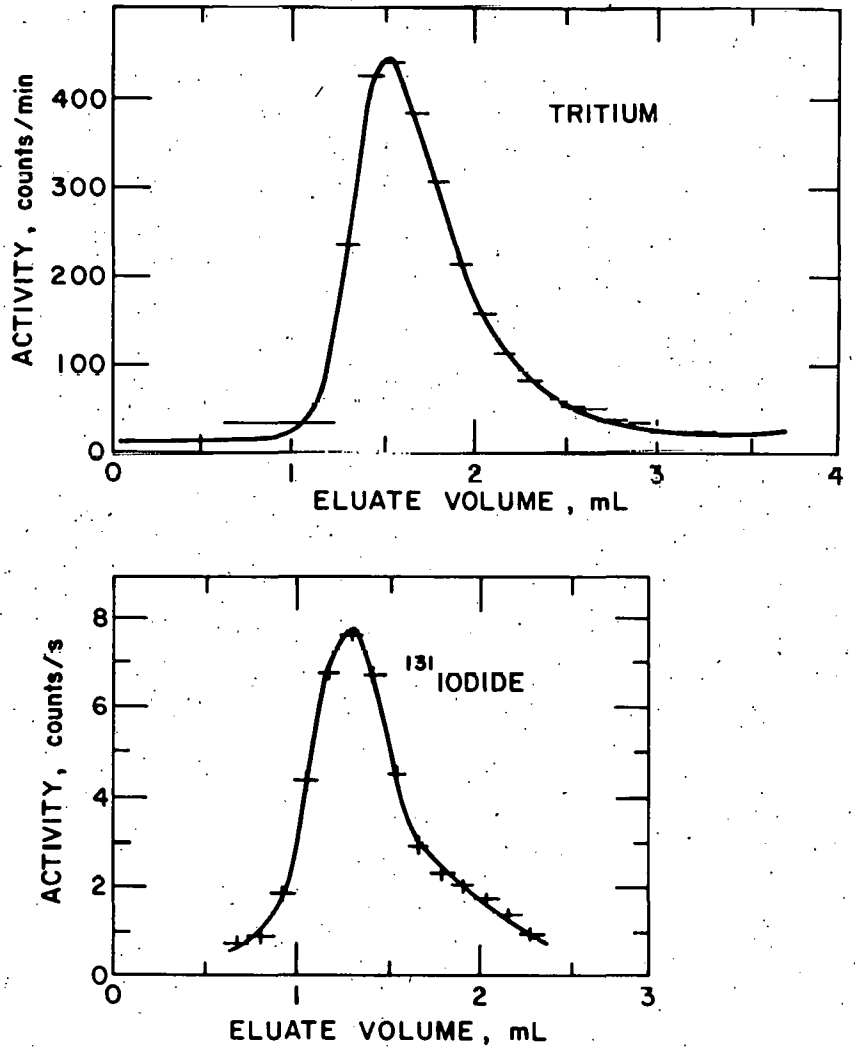

Fig. 36. Tritium and Iodide Elution Curves--Kaolinite Column 7

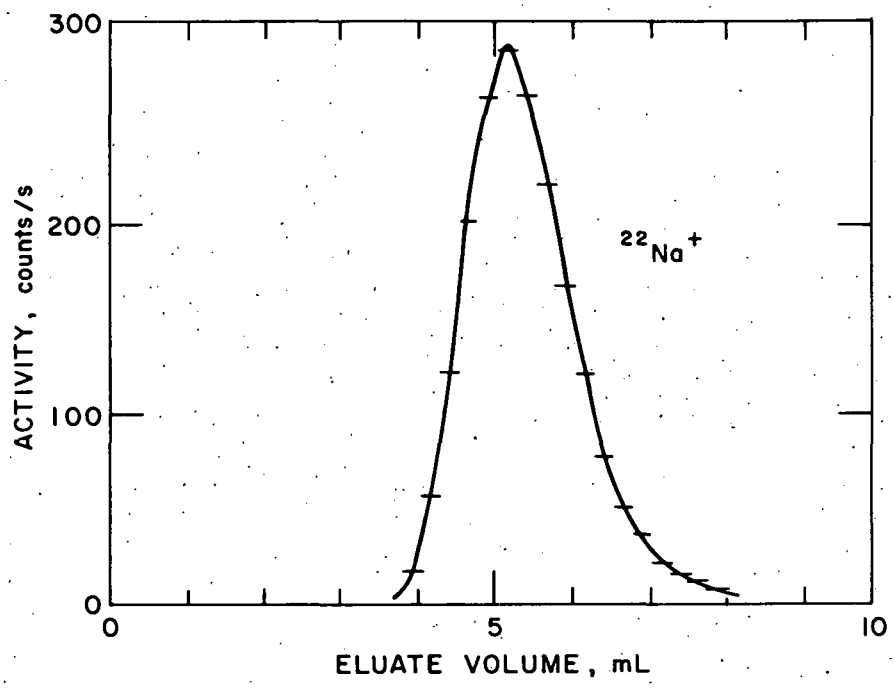

Fig. 37. $^{23}Na^+$ Elution Curve in 0.1M $NaHCO_3$

peak elution volumes of 5.1 mL and about 5.2 mL. Therefore, the problem may be an error in the determination of ion-exchange capacity. The ion-exchange capacity is important because selectivity coefficients and ion-exchange constants are scaled to this value in our method of determination. The results do not indicate a large electrostatic effect on Na^+ migration.

2. Discussion

At room temperature, the error in our measurements of Cs-Na selectivity coefficients should be approximately 15%. We are now performing the same experiments at elevated temperatures.

The peak widths are interesting. The peak widths at half height divided by the respective peak elution volumes are: for water, 0.26 and for Na^+, 0.32. The difference between these values is not significant. (The peak widths were determined from the sharper leading edge. The peaks are slightly asymmetrical because of compaction and the consequent formation of a liquid-filled void at the top of the kaolinite column.) Thus, both peaks have essentially the same shape. This is evidence that the broadening of the peaks (on the sharper edge) is due entirely to dispersion in liquid path length and velocity, and not to slow reaction kinetics.

C. Adsorption of Dissolved Iodide and Iodate on Kaolinite and Selected Oxides

1. The Disposal Problem

Disposal of power-reactor-produced iodine-129, which has a 17 million-year half life, poses a significant problem. Many geological formations have measurable cation-exchange capacity but little or no anion-exchange capacity. Therefore, the anions of iodine are not expected to interact substantially with ordinary rocks or sediments. Iodine does not form compounds that are insoluble in groundwaters. Therefore, it is difficult to guarantee that only insignificant amounts of iodine-129 will be leached from a geologic radioactive waste repository and enter the biosphere.

Nothing in the literature we have seen indicates that any rocks or sediments except sulfide ores would present a significant sorptive barrier to the migration of radioactive iodine. It is known that sulfide ores sorb iodide and perhaps iodate [STRICKERT]. Sulfide ores could be used to sorb small quantities of iodide in the vicinity of a repository. However, this may be a very expensive solution to the problem--especially since the sorptive capacity of sulfide minerals is likely to be very small.

Our experimental results suggest a probable solution to the problem. We discovered and reported in earlier quarterly reports [STEINDLER-1978C, 1979D] that at least two dissolved iodine species were strongly retained by kaolinite columns in aqueous fluid flow experiments. It was also reported that neither iodide nor iodate is adsorbed by kaolinite in significant quantities, and so the interaction of dissolved iodine with kaolinite columns is probably due to interaction with iron oxide impurities in the apparatus or to interaction of I_2, HOI, or periodate (IO_4^-) with kaolinite [STEINDLER-1979]. In order to determine which substances adsorb iodide and iodate, work has been done on the adsorption of iodide and iodate on hematite (Fe_2O_3), $Fe(OH)_3$, kaolinite, $Al(OH)_3$, Al_2O_3, and MgO. Also, the isotherm for adsorption of iodate on hematite in KIO_3 solutions has been determined, and the possible uses and implications of this information discussed.

2. Preparation of Iodide and Iodate

A solution of $Na^{131}I$ in 0.1M NaOH was obtained. NaI carrier was added, and iodide was oxidized to I_2 with HNO_2 and extracted into CCl_4. The I_2 was then extracted into 0.1M $NaHSO_3$ as NaI. Previously, this procedure was found (by paper chromatography) to yield pure iodide.

Iodate was prepared by adding carrier and oxidizing the iodide with 5% NaClO in 0.1M NaOH. This method was expected to yield periodate, but examination by paper chromatography of one sample following the sorption experiment showed only iodate, as explained later. Since there was some question as to whether periodate might be reduced to iodate by the chromatography paper, preparation was repeated with nonradioactive iodine at a

larger concentration of 0.0033M. The results agreed with results obtained on reagent grade KIO_3 at the same concentration. Therefore, the iodine was assumed to be in the iodate form. (Paper chromatography was carried out on Whatman No. 1 paper with 60:40 i-propanol:1.5M NH_3.)

3. Nature of the Adsorbents

The kaolinite [$Al_2Si_2O_5(OH)_4$] is a commercially prepared natural kaolinite (Hydrite R from Georgia Kaolin Co.); particles have a mean spherical equivalent diameter of 0.8 μm. It was washed several times with H_2O, then with 0.001M $NaHCO_3$, then with H_2O. The water was removed with a pipette after centrifuging. The clay was then dried, and the lumps were broken with a mortar and pestle to produce a fine powder.

One sample was treated as above, except that the sequence of treatment was: washing with H_2O several times, with H_2O + excess Br_2, with H_2O, with 0.001M $NaHCO_3$, and then with H_2O. This sample is referred to below as "oxidized" kaolinite. It was hoped that the oxidation would oxidize any residual reducing agents that might be present in the clay.

Reagent grade samples of MgO, Al_2O_3, $Al(OH)_3$, and Fe_2O_3 were used. The Fe_2O_3 is moderately well crystallized hematite with a fairly uniform particle diameter of about 0.25 μm.

4. Procedures

In one set of experiments (results in Table 41), weighed quantities of solid adsorber were each mixed with 3 mL of 0.001M $NaHCO_3$ or H_2O in test tubes. Spikes of the iodine species were added, and the samples were mixed again. The samples were rotated overnight. The solutions were sampled and centrifuged, then analyzed by counting for ^{131}I. One solution was analyzed for iodine species by paper chromatography.

The isotherm for adsorption of KIO_3 on hematite was determined by a similar method. Weighed quantities of Fe_2O_3 were dispersed in distilled water, and various amounts of dilute KIO_3 solution were added. The samples were mixed and rotated for several hours, then filtered through polycarbonate membrane filters. The filtrates were analyzed for IO_3^- by reaction with 0.01M NaI + 0.005M H_2SO_4 followed by titration of the resulting I_2 with a standardized thiosulfate solution, using a soluble starch indicator.

5. Results

The results of the first experiment are shown in Table 41. Generally, less than 5% of the iodide was adsorbed. The solid to solution ratios were 0.3 g/mL. Sorption of about 20% of the iodate on kaolinite is indicated. This may be due to analytical error, since the accuracy of the determination of iodate was not very good. Sorption on the test tubes is another possibility.

Table 41. Adsorption of Iodide and Iodate by Solids

Adsorber	Initial I Concentration, M	pH	Fraction in Solution
Iodide in 0.001M $NaHCO_3$/0.0006-0.003M $NaHSO_3$ solution			
Fe_2O_3	0.1×10^{-6}	6.6	0.71
Fe_2O_3	0.02×10^{-6}	6.8	0.95
$Al(OH)_3$	0.1×10^{-6}	8.3	0.95
MgO	0.1×10^{-6}	9.9	>0.56
Al_2O_3	0.1×10^{-6}	9.2	>0.90
Kaolinite	0.1×10^{-6}	3.92	0.99
Kaolinite	0.02×10^{-6}	5.69	0.95

Adsorber	Initial Iodate Concentration, M	pH	Fraction in Solution	Final Species
Iodate in 0.0014-0.007M NaClO/0.001M $NaHCO_3$ solution except where otherwise indicated				
Fe_2O_3	9.7×10^{-6}	6.9	<0.00008	
Fe_2O_3	1.9×10^{-6}	7.0	(0.020)	
Fe_2O_3	9.7×10^{-6}	6.7[a]	<0.0001[a]	
"Oxidized" kaolinite	9.7×10^{-6}	4.1	0.8	IO_3^-
"Oxidized" kaolinite	$<1.9 \times 10^{-6}$	5.2	0.81	

[a]No $NaHCO_3$ added.

Iodate is strongly adsorbed by Fe_2O_3 in millimolar $NaHCO_3$ solutions. Adsorption ranged from 98% to 99.99%! The lower value (98%) may be an error caused by incomplete mixing in the test tube; 99.99% adsorption is probably the more reliable value. The solid to liquid ratios were 0.31-0.34 g/mL.

The isotherm (at room temperature) for adsorption of iodate on hematite in KIO_3 solutions is shown in Fig. 38. Evidently, the hematite has a small anion-exchange capacity--less than 1.5×10^{-5} mol/g (Fig. 38). At iodate concentrations substantially above this value, relatively small fractions of the iodate can be adsorbed. At small concentrations, the curve is very steep, indicating that large fractions can be adsorbed.

One piece of indirect evidence confirms the suggestion that the surface of the hematite is saturated at loadings exceeding 1.3×10^{-5} mol/g.

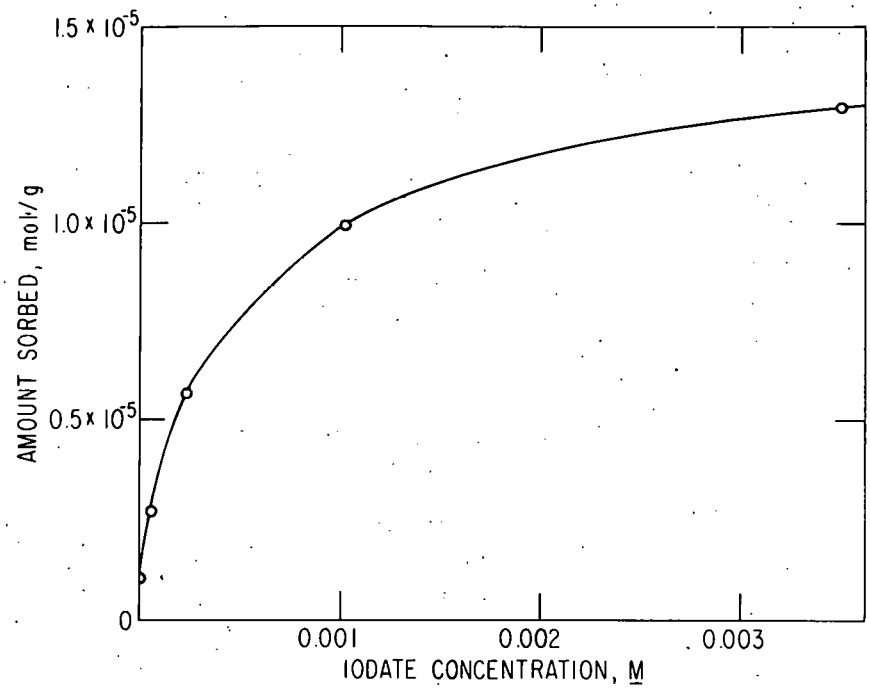

Fig. 38. Isotherm for Adsorption of Iodate on Hematite (Fe_2O_3) in KIO_3 Solutions at Room Temperature

Flocculation was observed in two samples. At an iodate concentration of 3.4×10^{-3}M, corresponding to a loading of 1.3×10^{-5} mol/g, flocculation was virtually complete; at a concentration of 1.1×10^{-3}M, flocculation was incomplete; at lower concentrations, no flocculation was observed. Flocculation presumably represents the point at which the surface charge is neutralized so that the particles no longer repel each other. Neutralization of the surface charge is presumably accomplished by adsorption of exchangeable ions, and so it is probably not accidental that surface charge neutralization and saturation of the ion-exchange sites occur at about the same concentration.

In order to test whether other iron oxides adsorb iodate, an attempt was made to coprecipitate iodate with $Fe(OH)_3$. Iodate was prepared by mixing 0.25 mL $Na^{131}I$ in 0.1M NaOH with 0.5 mL 0.0001M NaI and 0.5 mL of 5% NaClO. This was aged overnight. Then, 0.1 mL of this solution was added to 0.1 mL of 0.1M $FeCl_3$, followed by 5 mL of water. At least 57% of the activity was removed from solution within a few minutes. (Since some colloidal material was left in the solution during counting, 57% is a lower limit.) In a similar experiment with iodide, virtually no iodide was coprecipitated (less than 6% at the 95% confidence level). Subsequent oxidation of the iodide with NaClO caused sorption of iodate. Therefore, iodate can coprecipitate or sorb on previously formed $Fe(OH)_3$, but iodide cannot.

6. Discussion

In the reprocessing of radioactive waste, it is convenient to handle iodine in oxidized form, as iodate. Iodate can be precipitated in any of several salts, of which $Ba(IO_3)_2$ is among the least soluble. Precipitation of $Ba(IO_3)_2$ and mixing with Portland cement has been proposed as a method of preparing a waste form that has a moderately low leach rate [MORGAN]. This waste form would ensure isolation from the biosphere only if it were kept dry. Water moving past such a waste form would carry with it some of the iodine. It is estimated that a drum of concrete containing 15% iodine as $Ba(IO_3)_2$ would lose one-third of the iodine by leaching for 2500 to 25 million years [MORGAN]. Since ^{129}I has a 17 million-year half life, encapsulation in concrete should not be regarded as a complete solution of this waste disposal problem, and use of a secondary barrier is highly desirable.

Since iodate can be sorbed by hematite (Fe_2O_3) or by $Fe(OH)_3$, it is very likely that iodate can be sorbed by goethite (FeOOH) as well. The sorption mechanism may be related to the formation of $Fe-IO_3$ bonds on the mineral surface. $Fe(IO_3)$ is only slightly soluble.

Goethite (FeOOH) and hematite (Fe_2O_3) are the most common iron oxides at the earth's surface. Thus, natural iron oxides in an oxidized geologic formation might be expected to sorb iodine-129 leached from a radioactive waste repository.

Iron oxide packed around waste containers is another secondary barrier worth considering. If only small amounts of iodate are leached from a repository in which iron oxide is a barrier, the concentration of iodate in groundwater might be brought to very low concentrations. Shortly after intrusion of water into a repository, the iodate concentration in the water might approach the value determined by the solubility of $Ba(IO_3)_2$, i.e., 1.6×10^{-4}M at 0°C (Fig. 39). However, a layer of Fe_2O_3 would adsorb an appreciable fraction of the iodate released, and the iodate concentration would decrease greatly at increasing distances from the concrete. The sorption capacity of hematite is small, but adequate for a repository. If a sorption capacity of 10^{-5} mol/g is assumed, processing 1500 tons of fuel/year (which would contain a total of 170 g of ^{127}I (stable) and ^{129}I per ton) would require at least 200 metric tons of Fe_2O_3 per year. From Fig. 38 the dissolved iodate concentration in a water-saturated system would be 1×10^{-3}M. If the Fe_2O_3 should be packed to 50% porosity and the iodate distributed evenly throughout the Fe_2O_3, about 98% of the iodate would be adsorbed. If not all of the iodine was in solution because the leach rate was low, a much larger percentage of the iodine in solution could be adsorbed. Thus, iron oxide could make a very effective barrier to the migration of iodate.

Interference by competing ions might cause a problem. The adsorption of iodate in the presence of salts other than $NaHCO_3$ has not been determined, and so it would be prudent to determine the adsorption isotherm in various groundwater solutions.

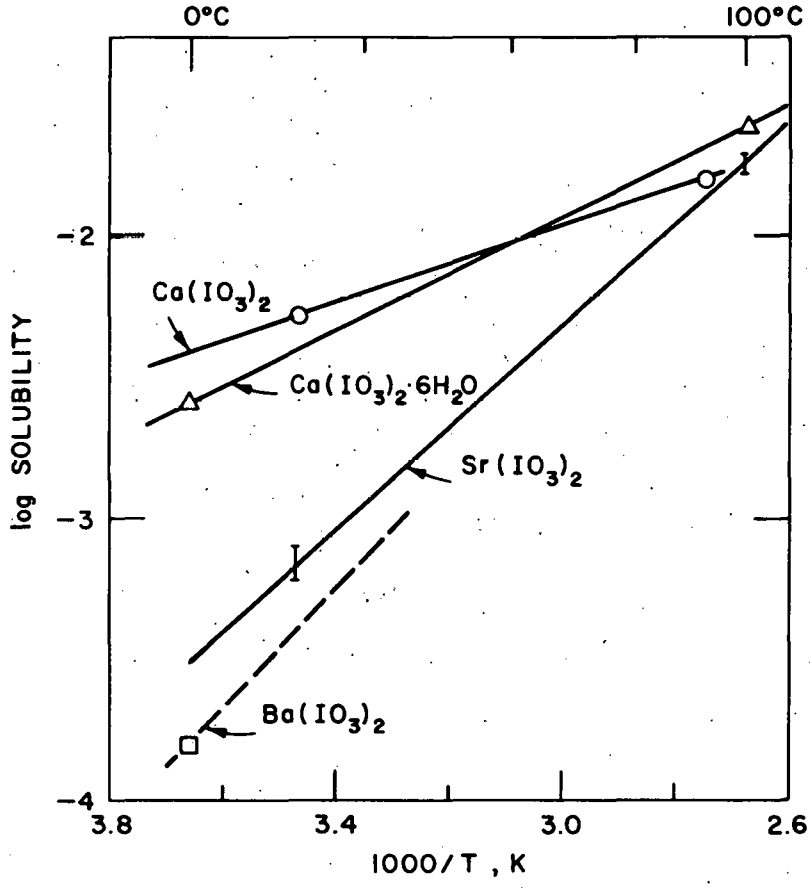

Fig. 39. Solubility of Some Alkaline Earth Iodates. Source of data: R. C. Weast, Ed., Handbook of Chemistry and Physics, 52nd Ed., CRC Press, West Palm Beach, Florida.

The best location for a repository would be an environment which is incapable of reducing iodate to iodide. A desert ferruginous soil zone above the water table would meet the requirements for an oxidizing, relatively dry environment. There would be the additional advantage that natural iron oxides in the soil would also sorb iodate.

The requirement for an oxidizing environment would limit but not necessarily preclude the use of stainless steel or other ferrous metal in a repository. In an anaerobic environment, iron would reduce iodate to iodide, which is not strongly sorbed on iron oxides or on common silicate minerals.

The presence of sulfate in groundwater would be detrimental. Sulfate would react with $Ba(IO_3)_2$, causing $BaSO_4$ to precipitate and liberating iodate. This problem limits the type of rock or sediment which can be used for a repository. For example, exposed marine beds may have unsuitably high dissolved-sulfate concentrations.

Burial of concrete that contains $Ba(IO_3)_2$ in ocean sediments has been proposed [MORGAN]. This method has some attractions. An overburden of a few meters of sediment would be quite effective as a barrier to diffusion into the water column. Iodate is probably stable in oxidized sediments, and red clay, with its free iron oxides, might adsorb significant quantities of iodate. However, reaction of $Ba(IO_3)_2$ with sea water to form $BaSO_4$, $Sr(IO_3)_2$, $Ca(IO_3)_2 \cdot 6H_2O$, and possibly $Ca(IO_3)_2$ would certainly complicate the analysis and might be a pathway for iodine to enter the seawater. Even so, the oceans have a large reservoir of nonradioactive iodine to dilute the waste [MORGAN].

An alternative strategy for disposal would be to coprecipitate iodate with some other ion in a calcium or barium salt or in $Fe(OH)_3$. The dissolved iodate concentration in equilibrium with such precipitates might be lower than that in equilibrium with $Ba(IO_3)_2$. Even in the event of recrystallization of the waste, the resulting dissolved iodate concentration would be low. Recrystallization reactions can be written as follows:

$$Fe(OH)_3 \cdot xFe(IO_3)_3 \rightarrow Fe(OH)_3 + xFe(IO_3)_3$$

$$BaX \cdot zBa(IO_3)_2 \rightarrow BaX + zBa(IO_3)_2$$

The products would be relatively insoluble.

REFERENCES

Ackermann

R. J. Ackermann and E. G. Rauh, J. Phys. Chem. 73, 769 (1969).

Ader

Milton Ader, private communication.

Amecke

B. Amecke, Contributions to the Reprocessing of Thorium-Uranium Nuclear Fuels with the Salt Transport Method, Dissertation, Technical University of Carolo-Wilhelmina at Braunschweig, ANL-TRANS-1141 (1975).

Anderson

R. N. Anderson and N. A. D. Parlee, Metall. Trans. 2, 1599 (1971).

Barletta

R. E. Barletta, private communication.

Bates

J. K. Bates, private communication (October 1978).

Bauer

R. H. Bauer, private communication to R. G. Sachs, Oct. 24, 1978.

Benedict

G. E. Benedict, K. M. Harmon, G. Jansen, Jr., L. K. Mudge, and F. A. Scott, Production of Reactor Fuel Oxides from Molten Chloride Salt Solutions, HW-SA-2915 (July 1963).

Bonner

W. F. Bonner, H. T. Blair, and L. S. Romero, Spray Solidification of Nuclear Waste, Battelle Pacific Northwest Laboratories Report BNWL-2059 (August 1976).

Chase-1974

M. W. Chase et al., JANAF Thermochemical Tables, 1974 Supplement, J. Phys. Chem. Ref. Data 3(2), 311-480 (1974).

Chase-1975

M. W. Chase et al., JANAF Thermochemical Tables, 1975 Supplement, J. Phys. Chem. Ref. Data 4(1), 1-176 (1975).

Cooper

T. D. Cooper, USAF Materials Lab., Investigation of Tantalum and Tantalum Alloys, ASD-TDR-62-594, Part II (May 1963).

Crank

J. Crank, The Mathematics of Diffusion, Oxford University Press, New York (1956).

Dallavalle

J. M. Dallavalle, Micromeritics, 2nd Ed., Pitman Publishing Co., New York (1948).

Detilleux

E. Detilleux, H. Eschrich, and J. van Geel, The MINERVA Process, European Company for the Chemical Processing of Irradiated Fuels Report ETA-294 (July 1978).

Federov

P. I. Federov and V. V. Tsimbalist, Russ. J. Inorg. Chem. 9(7) 908 (1964).

Flynn

K. F. Flynn, L. J. Jardine, and M. J. Steindler, Method for Determining Leach Rates of Simulated Radioactive Waste Forms, ACS Symposium Series 100, 115 (1979).

Friedman

H. L. Friedman and H. Taube, J. Am. Chem. Soc. 72, 2236 (1950).

Gibson

A. R. Gibson and J. H. Buddery in Extraction and Refining of the Rarer Metals, The Institution of Mining and Metallurgy, London, p. 63 (1957).

Glassner

Alvin Glassner, The Thermochemical Properties of the Oxides, Fluorides, and Chlorides to 2500°K, Argonne National Laboratory Report ANL-5750.

Grimes

W. R. Grimes, J. H. Shaffer, R. A. Strehlow, W. T. Ward, and G. M. Watson, Radioisotopes as Tracers for Reactions in Molten Fluoride Media, Radioisotopes in Physical Science and Industry, IAEA, 1962.

Hachmeister

K. Hachmeister, Z. Anorg. Allg. Chem. 109, 170 (1920).

Hammer

W. J. Hammer, M. S. Malmberg, and B. Rubin, Theoretical Electromotive Forces for Cells Containing a Single Solid or Molten Chloride Electrolyte, J. Electrochem. Soc. 103, 8-16 (1956).

Hammond

R. P. Hammond, Ph.D. Thesis, University of Chicago (1947).

Herdan

G. Herdan, Small Particle Statistics, Elsevier Publishing Co., New York (1953).

Hofmann

Wilhelm Hofmann, Lead and Lead Alloys, Springer-Verlag, New York (1970).

Honig

R. E. Honig, RCA Laboratory, Princeton, N. J. (September 1962).

Hutchins

J. R. Hutchins and R. V. Harrington, Glass, Encyclopedia of Chemical Technology, Vol. 10, pp. 533-604, John Wiley & Sons, New York (1966).

Jackson

R. R. Jackson, Hanford Waste Encapsulation: Strontium and Cesium, Nucl. Technol. 32, 10 (1977).

Jardine

L. J. Jardine and M. J. Steindler, A Review of Metal-Matrix Encapsulation of Solidified Radioactive High-Level Waste, Argonne National Laboratory Report ANL-78-19 (May 1978).

Johnson-1960

I. Johnson and A. E. Martin, personal communication (1960).

Johnson-1962

I. Johnson, Argonne National Laboratory, private communication (1962).

Johnson-1965

I. Johnson and I. G. Dillon, The Solubilities of Metals in Liquid Zinc, Argonne National Laboratory Report ANL-7083 (November 1965).

Johnson-1967

I. Johnson, Partition of Metals Between Liquid Metal Solutions and Fused Salts, Applications of Fundamental Thermodynamics to Metallurgical Processes, G. K. Fitterer, Ed., Gordon and Breach Science Publ., New York (1967).

Johnson-1969

T. R. Johnson, F. G. Teats, and R. D. Pierce, A Method for the Purification of Molten Chloride Salts, Argonne National Laboratory Report ANL-7603 (August 1969).

Kendall

J. Kendall, E. D. Crittenden, and H. K. Miller, J. Am. Chem. Soc. 45, 976 (1923).

Kingery

W. D. Kingery, Introduction to Ceramics, John Wiley & Sons, New York (1966).

Klemm

W. Klemm, E. Clausen, and H. Jacobi, Z. Anorg. Chem. 200, 378 (1931); see also W. Klemm and E. Tanake, ibid., p. 354.

Klopp

W. D. Klopp, A Review of Chromium, Molybdenum, and Tungsten Alloys, J. Less Common Met. 42, 261-278 (1975).

Knighton-1969A

J. B. Knighton, I. Johnson, and R. K. Steunenburg, Uranium Purification by the Process of Salt Transport, Argonne National Laboratory Report ANL-7524 (March 1969).

Knighton-1969B

J. B. Knighton, I. Johnson, and R. K. Steunenburg, Symposium on Reprocessing of Nuclear Fuels, Nuclear Metallurgy, 15, 337, Conf. 690801 (August 1969).

Knoch

W. Knoch, Argonne National Laboratory, private communication.

Kordis

J. Kordis and K. A. Gingerich, J. Nucl. Mater. 66, 197 (1977).

Kraus

C. A. Kraus and F. E. Toonder, Proc. Nat. Acad. Sci. 19, 292 (1930).

Lamp

K. M. Lamp, Final Report: Development of a Metal Matrix for Incorporating High-Level Commercial Waste, Idaho Nuclear Engineering Laboratory Report ICP-1144 (March 1978).

Laughlin-1975A

W. C. Laughlin and N. W. Gregory, Inorg. Chem. 14, 1263 (1975).

Laughlin-1975B

W. C. Laughlin and N. W. Gregory, J. Chem. Eng. Data 20, 137 (1975).

Lawroski

S. Lawroski et al., Chemical Engineering Division Summary Report, October-December, 1962, Argonne National Laboratory Report ANL-6648 (May 1963).

Martin-1959

A. E. Martin, personal communication (1959).

Martin-1961

A. E. Martin, J. B. Knighton, and H. M. Feder, Solubilities in Liquid Zinc-Zr, Nb, Mo, Pd, and Th, J. Chem. Eng. Data 6(4), 596-599 (1961).

McClintock

F. A. McClintock and A. S. Argon, Mechanical Behavior of Materials, Addison-Wesley Publishing, Reading, Mass. (1966).

McElroy-1977A

J. L. McElroy, Quarterly Progress Report, Research and Development Activities, Waste Fixation Program, Oct-Dec 1976, Battelle Pacific Northwest Laboratories Report PNL-2264 (November 1977).

McElroy-1977B

J. L. McElroy, Quarterly Progress Report Research and Development Activities, Waste Fixation Program, January through March 1977, PNL-2265 (November 1977).

Morgan

M. T. Morgan, J. G. Moore, H. E. Devaney, G. C. Rogers, C. Williams, and E. Newman, The Disposal of Iodine-129. Materials Res. Soc. Symposium, Nov-Dec 1978, G. J. McCarthy, Chairman, pp. 38-39.

Mulford

R. N. R. Mulford, Proc. Symp., Vienna, IAEA, P. 231 (1965).

Myles

K. M. Myles, Argonne National Laboratory, private communication.

Nesmeyanov

An. N. Nesmeyanov, Vapor Pressures of the Elements, Academic Press, New York (1963).

Oetting

F. L. Oetting, The Chemical Thermodynamic Properties of Plutonium Compounds, Chem. Rev. 67, 261-97 (1967).

ORNL

Oak Ridge National Laboratory, Aqueous Processing of LMFBR Fuels - Technical Assessment and Experimental Progam Definition, ORNL-4436 (June 1970).

Rand

M. H. Rand and O. Kubaschewski, The Thermodynamic Properties of Uranium Compounds, Oliver and Boyd, Edinburgh, Scotland (1963).

Raseman

C. J. Raseman, H. Sussking, G. Farber, W. E. McNulty, and F. J. Salzano, Engineering Experience at Brookhaven National Laboratory in Handling Fused Chloride Salts, BNL-627(T-192) (June 1960).

Relyea

J. F. Relyea, Controlled-Sample Program Results, Waste Isolation Safety Assessment Program, Seattle, Washington (1978).

Rickert

P. G. Rickert, R. G. Strickert, and M. G. Seitz, Nuclide Migration in Fractured or Porous Rock, Radioactive Waste in Geologic Storage, S. Fried, Ed., Symposium Series 100, American Chemical Society, Washington, D.C., pp. 167-189 (1979).

Ross

W. A. Ross et al., Annual Report on the Characterization of High-Level Waste Glasses, Pacific Northwest Laboratories Report PNL-2625 (June 1978).

Seitz-1978

M. G. Seitz, P. G. Rickert, S. M. Fried, A. M. Friedman, and M. J. Steindler, Nuclear-Waste Migration in Geologic Media, Annual Report, Contractors' Meeting, Waste Isolation Safety Assessment Program, Seattle, Washington (1978).

Seitz-1979

M. G. Seitz, P. G. Rickert, S. M. Fried, A. M. Friedman, and M. J. Steindler, Migratory Properties of Some Nuclear Waste Elements in Geologic Media, Nucl. Technol. 44, 284-296 (1979).

Shaffer

J. H. Shaffer, Preparation and Handling of Salt Mixtures for the Molten Salt Reactor Experiments, ORNL-4616 (January 1971).

Shappert

L. B. Shappert et al., A Guide for the Design, Fabrication and Operation of Shipping Casks for Nuclear Applications, Oak Ridge National Laboratory Report ORNL-NSIC-68 (February 1970).

Sharma

R. A. Sharma and I. Johnson, J. Am. Ceram. Soc. 52(11), 613 (1969).

Smith-1978A

Duane H. Smith et al., Molten Salt Processes Applied to Ceramic Fuels, 2nd PDPM Information Exchange Meeting, Argonne National Laboratory, Nov. 8, 1978.

Smith-1978B

Duane H. Smith and H. F. McDuffie, An Examination of the Proliferation Resistance of 'Pyro-CIVEX' Flowsheet (memorandum to O. O. Yarbro) ORNL (Oct. 10, 1978).

Smith-1978C

Duane H. Smith and H. F. McDuffie, A. Literature Review of Selected Methods of Molten Salt Reprocessing of Ceramic Fuels, ORNL (September 1978) (draft).

Sood

S. O. Sood and A. U. Hariharan, Chlorination Volatility Separation of Thorium and Uranium, Nuclear and Radiation Chemistry Symposium, Poona, India, March 6 to 9, 1967.

Steindler-1977

M. J. Steindler et al., Chemical Engineering Division Fuel Cycle Programs, October-December 1976, Argonne National Laboratory Report ANL-77-36.

Steindler-1978A

M. J. Steindler et al., Chemical Engineering Division Fuel Cycle Programs Quarterly Progress Report, January-September 1977, Argonne National Laboratory Report ANL-78-11.

Steindler-1978B

M. J. Steindler et al., Chemical Engineering Division Fuel Cycle Programs Quarterly Progress Report, October-December 1977, Argonne National Laboratory Report ANL-78-37.

Steindler-1978C

M. J. Steindler et al., Chemical Engineering Division Fuel Cycle Programs Progress Report, January-March 1978, Argonne National Laboratory Report ANL-78-68 (April 1979).

Steindler-1978D

M. J. Steindler et al., Chemical Engineering Division Fuel Cycle Programs Quarterly Progress Report, April-June 1978, Argonne National Laboratory Report ANL-78-76.

Steindler-1979

M. J. Steindler et al., Chemical Engineering Division Fuel Cycle Section Quarterly Progress Report, July-September 1978, Argonne National Laboratory Report ANL-79-6.

Sterlin

Ya. M. Sterlin and V. V. Artamonov, Sov. At. Energy 22(6), 473 (1967).

Strickert

R. Strickert, A. M. Friedman, and S. Fried, The Sorption of Technetium and Iodine Radioisotopes by Various Minerals (abstract), Trans. Am. Nucl. Soc. 28, 365-366 (1978).

Stull

D. R. Stull and H. Prophet, JANAF Thermochemical Tables, NSRDS-NBS-37 (1971).

Teitel

R. J. Teitel, J. E. Luderer, and T. M. Henderson, Study of Nonaqueous Reprocessing Methods, Final Progress Report on ANL Contract No. 31-109-38-4693, ANL-K78-4693-1 (Nov. 17, 1978).

Thamer

B. J. Thamer and G. E. Meadows in Phase Diagrams of Nuclear Reactor Materials, R. Thoma, Ed., ORNL-2548, p. 94 (1959).

Vander Wall

E. M. Vander Wall, H. T. Hahn, and D. L. Bauer, Salt Phase Chlorination of Reactor Fuels II, IDO-14525 (October 1960).

Vogel

R. C. Vogel et al., Chemical Engineering Division Annual Report 1968, Argonne National Laboratory Report ANL-7575, pp. 22-24 (April 1969).

Wade

W. Z. Wade, and T. Wolf, UCRL-50403, p. 9.

Wallace

R. M. Wallace and J. A. Kelley, An Impact Test for Solid Waste Forms, Savannah River Laboratory Report DP-1400 (March 1976).

Webster

D. S. Webster et al., Chemical Engineering Division, ANL, Fuel Cycle Technology Quarterly Report, April May June 1970, Argonne National Laboratory Report ANL-7735.

Wenz

D. A. Wenz, I. Johnson, and R. D. Wolson, J. Chem. Eng. Data 14(2), 252 (1969).

Wicks

C. E. Wicks and F. E. Block, Thermodynamic Properties of 65 Elements - Their Oxides, Halides, Carbides and Nitrides, Bureau of Mines Bull. 605 (1963).

Winsch

I. O. Winsch, K. R. Tobias, R. D. Pierce, and L. Burris, Jr., Sampling of Liquid Metals, Argonne National Laboratory Report ANL-7088 (September 1965).

Yamamoto

A. S. Yamamoto and W. Rostoker, Trans. Am. Soc. Met. 50, 1090 (1957).

Zeleny

R. A. Zeleny and E. L. Piret, Dissipation of Energy in Single Particle Crushing, Ind. Eng. Chem. Process Des. Dev. 1(1), 37 (January 1962).

Distribution for ANL-79-29

Internal:

W. E. Massey
M. Ader
J. K. Bates
L. Burris
F. A. Cafasso
T. F. Cannon
R. A. Couture
E. J. Croke
P. R. Fields
K. F. Flynn
S. Fried
A. M. Friedman
D. R. T. Frost
T. J. Gerding
D. R. Hamrin
J. E. Harmon
L. J. Jardine
J. H. Kittel (2)
V. M. Kolba
M. Krumpelt
B. J. Kullen
R. A. Leonard
W. J. Mecham
A. Melton
K. M. Myles
M. V. Nevitt
R. H. Pelto
W. B. Seefeldt
M. G. Seitz
M. Seliga
J. Simmons
M. J. Steindler (10)
L. E. Trevorrow
S. Vogler
D. S. Webster
A. A. Ziegler
A. B. Krisciunas
ANL Contract File
ANL Libraries (4)
TIS Files (6)

External:

DOE-TIC, for distribution per UC-70 (314)
Manager, Chicago Operations and Regional Office, DOE
Chief, Office of Patent Counsel, DOE-CORO
S. A. Mann, DOE-CORO
Argonne Universities Association:
President
C. B. Alcock, U. Toronto
J. T. Banchero, U. Notre Dame
P. W. Gilles, U. Kansas
R. I. Newman, Fripp Island, S. C.
S. W. Ahrends, Oak Ridge Operations Office, USDOE (2)
T. W. Ambrose, Battelle Pacific Northwest Lab.
C. K. Anderson, Combustion Engineering
R. E. Barletta, Brookhaven National Lab.
G. S. Barney, Rockwell Hanford Operations
Battelle-Columbus Labs.
R. C. Baxter, Allied-General Nuclear Services
B. C. Blanke, USDOE-DA, Miamisburg, O.
E. Bondietti, Oak Ridge National Lab.
D. Bowersox, Los Alamos Scientific Lab.
M. G. Britton, Corning Glass Works
C. L. Brown, Battelle Pacific Northwest Lab.
R. Brown, Allied Chemical Corp., Idaho Falls
L. L. Burger, Battelle Pacific Northwest Lab.
D. Camp, Lawrence Livermore Lab.
D. O. Campbell, Oak Ridge National Lab.
W. Carbiener, Battelle-Columbus Labs.
W. T. Cave, Mound Lab.
B. H. Cherry, GPU Services Corp.
E. D. Clayton, Battelle Pacific Northwest Lab.
J. M. Cleveland, U. S. Geological Survey, Lakewood, Colo.
F. E. Coffman, USDOE-MFE
J. J. Cohen, Lawrence Livermore Lab.
Commonwealth Edison, Vice Chairman, Chicago
C. R. Cooley, Office of Nuclear Waste Management, USDOE

J. L. Crandall, Savannah River Lab.
M. C. Cullingford, Nuclear Regulatory Commission
R. Cunningham, USNRC, Nuclear Materials Safety & Safeguards
G. H. Daly, Waste Technology Branch, USDOE (2)
J. C. Dempsey, Office of Nuclear Waste Management, USDOE
B. R. Dickey, Allied Chemical Corp., Idaho Falls
J. E. Dieckhoner, Div. Waste Products, USDOE
J. Dietz, Los Alamos Scientific Lab.
R. L. Dillon, Battelle Pacific Northwest Lab.
R. G. Dosch, Sandia Labs., Albuquerque
G. H. Dyer, Bechtel Corp.
Eastern Environmental Radiation Lab., HEW
G. Eichholz, Georgia Inst. Technology
O. J. Elgert, Richland Operations Office, USDOE (2)
B. Erdal, Los Alamos Scientific Lab.
E. D. Erickson, Rocky Flats Plant
D. Ferguson, Oak Ridge National Lab.
Foster Wheeler Corporation, Library (HQAP)
C. W. Francis, Oak Ridge National Lab.
R. G. Gavin, Savannah River Lab. (3)
R. G. Geier, Rockwell Hanford Operations, Richland
General Electric Co., San Jose (DOE)
E. S. Goldberg, Savannah River Operations Office, USDOE
S. Goldsmith, Battelle Pacific Northwest Lab.
J. P. Hamric, Idaho Operations Office, USDOE
S. G. Harbinson, San Francisco Operations Office, USDOE
M. Harwell, Battelle Pacific Northwest Lab.
C. A. Heath, Div. Waste Isolation, USDOE
J. L. Heffter, NOAA, Silver Spring
L. L. Hench, U. Florida
T. B. Hindman, Jr., USDOE-SR
B. F. Judson, General Electric Co., San Jose
S. V. Kaye, Oak Ridge National Lab.
G. R. Keepin, Los Alamos Scientific Lab.
R. G. Kepler, Sandia Labs., Albuquerque
C. J. Kershner, Mound Lab.
F. J. Kiernan, Aerojet Energy Conversion Co., Washington
J. F. Kircher, Battelle-Columbus Labs.
K. Kraus, Oak Ridge, Tenn.
S. J. Lambert, Sandia Labs., Albuquerque
G. Lehmkul, Rocky Flats Plant
S. Levine, USNRC, Div. of Reactor Safety Research
W. H. Lewis, Nuclear Fuel Services, Rockville
R. C. Liikala, Battelle Pacific Northwest Lab.
J. L. Liverman, Deputy Asst. Secy. for Environment, USDOE
Los Alamos Scientific Lab., Director
A. L. Lotts, Oak Ridge National Lab.
R. Y. Lowrey, Albuquerque Operations Office, USDOE (2)
L. Machta, NOAA, Silver Spring
R. Maher, Savannah River Plant
J. C. Mailen, Oak Ridge National Lab.
W. J. Maraman, Los Alamos Scientific Lab.

A. B. Martin, Rockwell International, Canoga Park (2)
M. L. Matthews, Nuclear Power Development, USDOE
D. J. McGoff, Waste Technology Branch, USDOE
D. L. McIntosh, Savannah River Lab.
W. H. McVey, USDOE-NPD
R. E. Meyer, Oak Ridge National Lab.
S. Meyers, Office of Nuclear Waste Mgmt., USDOE
R. B. Minogue, USNRC, Office of Standards Development
J. Mishima, Battelle Pacific Northwest Lab.
NASA, John F. Kennedy Space Center
Ronald D. Nelson, Battelle Pacific Northwest Lab. (3)
I. Neretnieks, Lawrence Berkeley Lab.
Y. Ng, Lawrence Livermore Lab.
G. K. Oertel, Div. Waste Products, USDOE
R. D. Oldenkamp, Atomics International
D. A. Orth, Savannah River Plant
B. Paige, Allied Chemical Corp., Idaho Falls
H. Palmour III, North Carolina State U.
J. H. Pashley, Oak Ridge Gaseous Diffusion Plant
A. M. Platt, Battelle Pacific Northwest Lab. (3)
H. Postma, Oak Ridge National Lab.
C. A. Preskitt, IRT Corp., San Diego
J. J. Reilly, Brookhaven National Lab.
J. F. Relyea, Battelle Pacific Northwest Lab.
L. M. Richards, Atlantic Richfield Co., Los Angeles
G. L. Ritter, Exxon Nuclear Corp., Richland
D. M. Rohrer, Los Alamos Scientific Lab.
R. Romatowski, Office of Nuclear Waste Mgmt., USDOE
H. E. Roser, USDOE, Albuquerque Operations Office
R. Roy, Pennsylvania State U.
K. J. Schneider, Battelle Pacific Northwest Lab.
R. L. Seale, U. Arizona
T. A. Sellers, Sandia Labs.
J. Serne, Battelle Pacific Northwest Lab.
B. Silva, Lawrence Berkeley Lab.
A. Squire, Hanford Engineering Development Lab.
J. A. Stiegler, Sandia Labs.
S. Stoller, The S. M. Stoller Corp.
K. Street, Lawrence Livermore Lab.
G. Stukenbroeker, NL Industries, Wilmington, Del.
J. L. Swanson, Battelle Pacific Northwest Lab.
J. Tewhey, Lawrence Livermore Lab. (3)
USDOE Div. of Nuclear Power Development, Nuclear Fuel Cycle Programs Br.
USDOE Office of Basic Energy Sciences
USDOE Div. of RRT, Engineering
USDOE Div. of RRT, Technology
USDOE Idaho Operations Office
USDOE New Brunswick Laboratory
USDOE San Francisco Operations Office
USDOE Southern California Energy Office
H. H. Van Tuyl, Battelle Pacific Northwest Lab.
V. C. A. Vaughn, Oak Ridge National Lab.
E. E. Voiland, General Electric Co., Morris, Ill.
B. L. Vondra, Oak Ridge National Lab.

R. D. Walton, Jr., Office of Nuclear Waste Mgmt., USDOE
C. D. Watson, Oak Ridge National Lab.
L. L. Wendell, Battelle Pacific Northwest Lab.
J. B. Whitsett, Idaho Operations Office, USDOE
W. J. Wilcox, Oak Ridge Gaseous Diffusion Plant
A. K. Williams, Allied-General Nuclear Services, Barnwell
R. O. Williams, Rocky Flats Plant
D. D. Wodrich, Rockwell Hanford Operations
J. E. Yanoski, Office of Nuclear Energy Programs, USDOE
D. Zeigler, Rocky Flats Plant
Arizona, U. of, Dept. of Nucl. Engineering
A. H. Emmons, U. Missouri
H. S. Isbin, U. Minnesota
W. R. Kimel, U. Missouri
Maine Univ., Prof. in charge of Chem. Engr. Lib.
Marquette U., Dept. of Chemistry
Michigan Technological U., Library
D. W. Moeller, Kresge Ctr. for Environmental Health, Boston
G. Murphy, Iowa State U.
H. Rosson, U. Kansas
L. Schwendiman, Pacific Northwest Lab.
E. R. Stansberry, Purdue U.
B. S. Swanson, Illinois Inst. Technology
B. W. Wilkinson, Michigan State U.
W. E. Wilson, Washington State U.
W. F. Witzig, Pennsylvania State U.